U.S. DEPARTMENT OF COMMERCE
National Technical Information Service

PB-285 981

A Study of Horizontal Visibility, Atmospheric Vertical Optical Properties and Solar Isolation at Stanton, North Dakota

Martin Marietta Aerospace, Denver, CO. Denver Div.

Prepared for

Environmental Protection Agency, Denver, CO

Nov 77

PB 285 981
EPA-908/1-77-005

A STUDY OF HORIZONTAL VISIBILITY, ATMOSPHERIC VERTICAL OPTICAL PROPERTIES, & SOLAR INSOLATION AT STANTON, NORTH DAKOTA

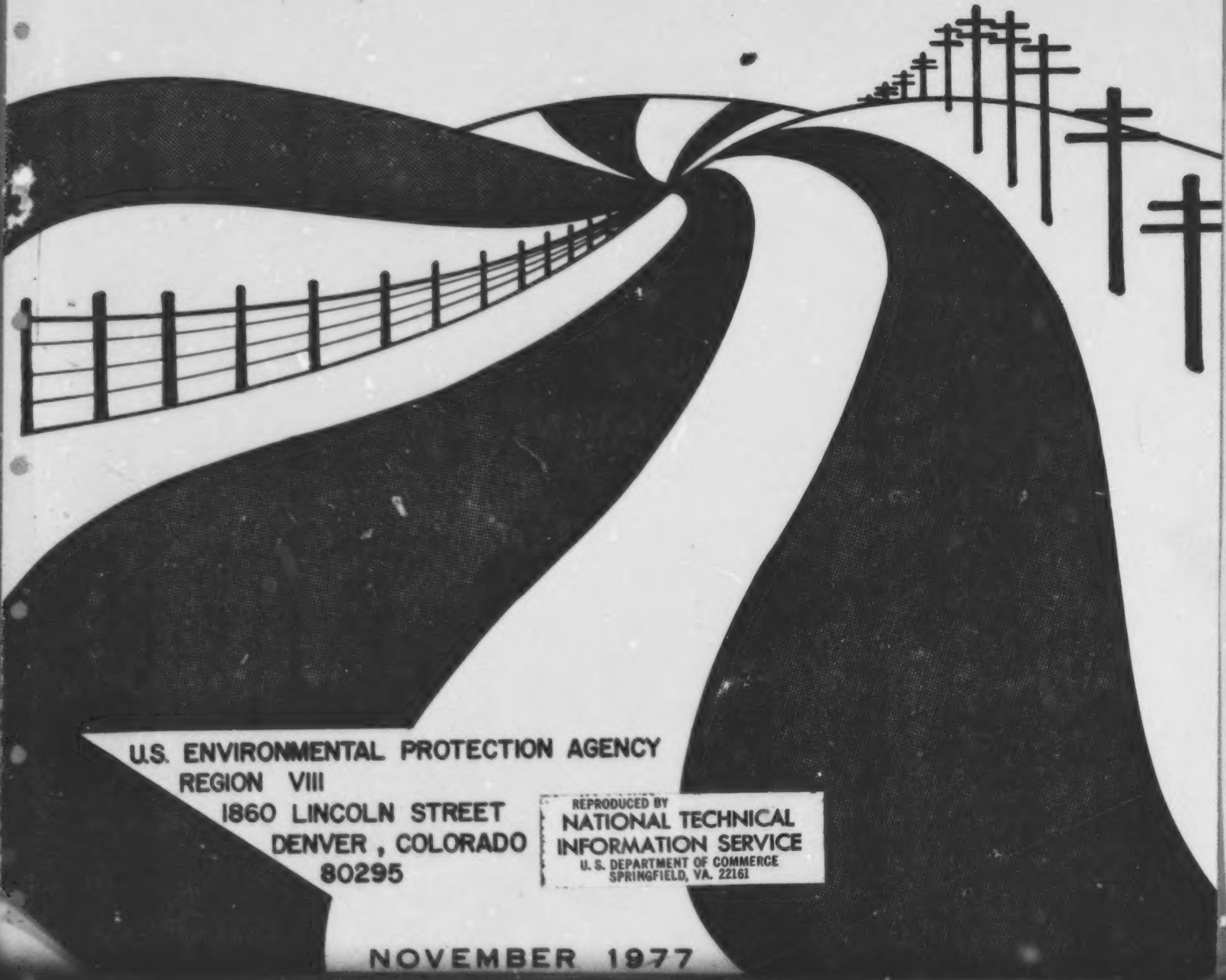

U.S. ENVIRONMENTAL PROTECTION AGENCY
REGION VIII
1860 LINCOLN STREET
DENVER, COLORADO
80295

REPRODUCED BY
NATIONAL TECHNICAL
INFORMATION SERVICE
U.S. DEPARTMENT OF COMMERCE
SPRINGFIELD, VA. 22161

NOVEMBER 1977

TECHNICAL REPORT DATA
(Please read Instructions on the reverse before completing)

1. REPORT NO.
EPA-908-1/77-005

2.

3. RECIPIENT'S ACCESSION NO.
PB285981

4. TITLE AND SUBTITLE
A Study of Horizontal Visibility, Atmospheric Vertical Optical Properties and Solar Insolation at Stanton, North Dakota

5. REPORT DATE

6. PERFORMING ORGANIZATION CODE

7. AUTHOR(S)
Roland L. Hulstrom

8. PERFORMING ORGANIZATION REPORT NO.

9. PERFORMING ORGANIZATION NAME AND ADDRESS
MARTIN MARIETTA CORPORATION
Denver Division
Post Office Box 179
Denver, Colorado 80201

10. PROGRAM ELEMENT NO.

11. CONTRACT/GRANT NO.

12. SPONSORING AGENCY NAME AND ADDRESS
U. S. Environmental Protection Agency, Region VIII
Office of Energy Activities
1860 Lincoln Street
Denver, Colorado 80295

13. TYPE OF REPORT AND PERIOD COVERED

14. SPONSORING AGENCY CODE
908/00

15. SUPPLEMENTARY NOTES

16. ABSTRACT

A study to establish methods for the acquisition of baseline data for horizontal visibility and vertical optical air quality is described. The study was performed for the U. S. Environmental Protection Agency, Region VIII.

The site was Stanton, North Dakota, which is located in an area where extensive development of fossil fuel energy is anticipated. The baseline measurements consisted of horizontal visibility along three views, solar radiation and vertical atmospheric spectral attenuation coefficients. Basic meteorological data were also taken. These baseline data were established for the months of April, July, and October, 1976, and January, 1977. The methods used, results, conclusions and recommendations are presented.

17. KEY WORDS AND DOCUMENT ANALYSIS

a. DESCRIPTORS	b. IDENTIFIERS/OPEN ENDED TERMS	c. COSATI Field/Group
Visibility Air Quality Solar Insolation Atmospheric Attenuation Visual Range	Visibility Air Quality	

18. DISTRIBUTION STATEMENT
Release Unlimited

19. SECURITY CLASS *(This Report)*
Unclassified

20. SECURITY CLASS *(This page)*
Unclassified

21. NO. OF PAGES
175

22. PRICE
A08 - A01

EPA Form 2220-1 (Rev. 4-77) PREVIOUS EDITION IS OBSOLETE

EPA-908/1-77-005

FINAL REPORT

A STUDY OF HORIZONTAL VISIBILITY, ATMOSPHERIC VERTICAL OPTICAL PROPERTIES AND SOLAR ISOLATION AT STANTON, NORTH DAKOTA

by

ROLAND L. HULSTROM*

Program Manager

Martin Marietta Corporation
Denver Division
Denver, Colorado

Contract No. 68-01-3567

DAVID B. JOSEPH

Project Officer

U. S. ENVIRONMENTAL PROTECTION AGENCY
REGION VIII
Office of Energy Activities
1860 Lincoln Street
Denver, Colorado 80295

November, 1977

* Now with the Solar Energy Research Institute,
Golden, Colorado 80401

ia

DISCLAIMER

This report has been reviewed by Region VIII of the U. S. Environmental Protection Agency, and approved for publication. Approval does not signify that the contents necessarily reflect views and policies of the U. S. Environmental Protection Agency, nor does mention of trade names of commercial products constitute endorsement or recommendation for use.

This report is available from the National Technical Information Service, Springfield, Virginia 22161. A limited number of copies are also available by contacting Ms. Betty Thalhofer, U. S. Environmental Protection Agency, Region VIII, 1860 Lincoln Street, Denver, Colorado 80295.

ABSTRACT

A study to establish methods for the acquisition of baseline data for horizontal visibility and vertical optical air quality is described. The study was performed for the Environmental Protection Agency, Region VIII. The site was Stanton, North Dakota, which is located in an area where extensive development of fossil fuel energy is anticipated. The baseline measurements consisted of horizontal visibility along three views, solar radiation and vertical atmospheric spectral attenuation coefficients. Basic meteorological data were also taken. These baseline data were established for the months of April, July, and October, 1976, and January, 1977. The methods used, results, conclusions and recommendations are presented.

FORWARD

The work described herein was performed at the Denver Division of the Martin Marietta Corporation, under EPA Contract No. 68-01-3567, entitled "A Study to Provide For the Acquisition of Baseline Visibility Measurements at Stanton, North Dakota". The work was performed during the period from February 1976 to November 1977.

The Martin Marietta Program Manager and Technical Director was Mr. Roland L. Hulstrom, who has since taken a position with the Solar Energy Research Institute, Golden, Colorado. The E.P.A., Region VIII, Project Officer was Mr. David Joseph. Detailed review and comments were supplied by Mr. David Joseph, Mr. Terry Thoem, Mr. Donald Henderson, of E. P. A. Region VIII; and Mr. Lloyd Oldham of Martin Marietta Corporation. Mr. Samuel Rensser and Mr. William Miles were responsible for on-site data collection.

TABLE OF CONTENTS

Page No.

Disclaimer ii

Abstract iii

Forward iv

1. Introduction 1

2. Summary, Conclusions, and Recommendations 3

3. Basic Concepts of Vertical and Horizontal Optical Air Quality 13

4. Horizontal Visibility 18

4.1 Techniques/Instrumentation 18

4.2 April Horizontal Visibility 27

4.3 July Horizontal Visibility 28

4.4 October Horizontal Visibility 28

4.5 January Horizontal Visibility 29

4.6 Seasonal Horizontal Visibility Comparisons 29

5. Atmospheric Vertical Optical Attenuation 49

5.1 Techniques/Instrumentation Used 49

5.2 April Optical Attenuation 55

5.3 July Optical Attenuation 56

5.4 October Optical Attenuation 57

5.5 January Optical Attenuation 58

5.6 Seasonal Optical Attenuation Comparisons 59

6. Incident Solar Irradiance 81

6.1 Techniques/Instrumentation Used 81

6.2 April Solar Irradiance 82

6.3 July Solar Irradiance 84

6.4 October Solar Irradiance 85

6.5 January Solar Irradiance 86

6.6 Seasonal Solar Irradiance Comparisons 87

7. Sky Appearance 119

7.1 Techniques/Instrumentation Used 119

7.2 April Sky Appearance 119

7.3 July Sky Appearance 119

TABLE OF CONTENTS (Continued)

Page No.

7.4 October Sky Appearance 119
7.5 January Sky Appearance 119
7.6 Seasonal Sky Appearance Comparisons. 122
8. Meteorology 123
8.1 Techniques/Instrumentation Used. 123
8.2 April Meteorology. 124
8.3 July Meteorology 125
8.4 October Meteorology. 125
8.5 January Meteorology. 126
8.6 Seasonal Comparisons 126
9. Satellite Imagery 159
9.1 Techniques/Instrumentation Used. 159
9.2 April Satellite Imagery. 159
9.3 July Satellite Imagery 159
9.4 October Satellite Imagery. 159
9.5 January Satellite Imagery. 160
9.6 Seasonal Satellite Imagery Comparisons 160
10. Comparison of Horizontal with Vertical Optical Attenuation and Solar Irradiance. 162
10.1 Horizontal Visibility Versus Vertical Optical Aerosol Attenuation at 0.500 um 162
10.2 Horizontal Visibility Versus Ratio of Diffuse to Total Solar Irradiance. 163
Appendix. 164

1. INTRODUCTION

Recently, a growing awareness of the possibility of man-made air pollution degrading horizontal visibility led the Congress of the United States to amend the Clean Air Act. Part of these new amendments, Sec. 169A.(a)(3)(A), calls for a study and report to Congress to include recommended methods for identifying, characterizing, determining, quantifying and measuring visibility impairment in Federal pristine areas, such as national parks. The purpose of the study reported herein was to establish methods of measuring horizontal visibility, plus methods for measuring the vertical atmospheric optical air quality, and for quantifying the solar insolation environment. The purpose of this study also included the actual establishing of the baseline horizontal visibility, vertical optical air quality, and solar insolation at Stanton, North Dakota. This site was chosen because it is located in an area where extensive development of coal reserves is likely to take place in the near future. Therefore, establishing the current baseline conditions is necessary in order to determine the future impairment due to the development and utilization of the area's coal resources.

The Stanton, North Dakota area map is shown in Figure 1. The measurements at this site included horizontal visibility, atmospheric vertical optical attenuation (vertical optical air quality), incident solar insolation, ambient air pressure, temperature, relative humidity, wind direction, wind speed, vertical water vapor content, and relative dust concentration. Data was collected on site for four periods of time which were indicative of each season. The first data collection period was from April 5 to May 1, 1976; the second was from July 12 to August 7, 1976; the third was from October 4 to 30, 1976; and the fourth was from January 13 to February 19, 1977. During each data collection period, a total of

Reproduced from
best available copy.

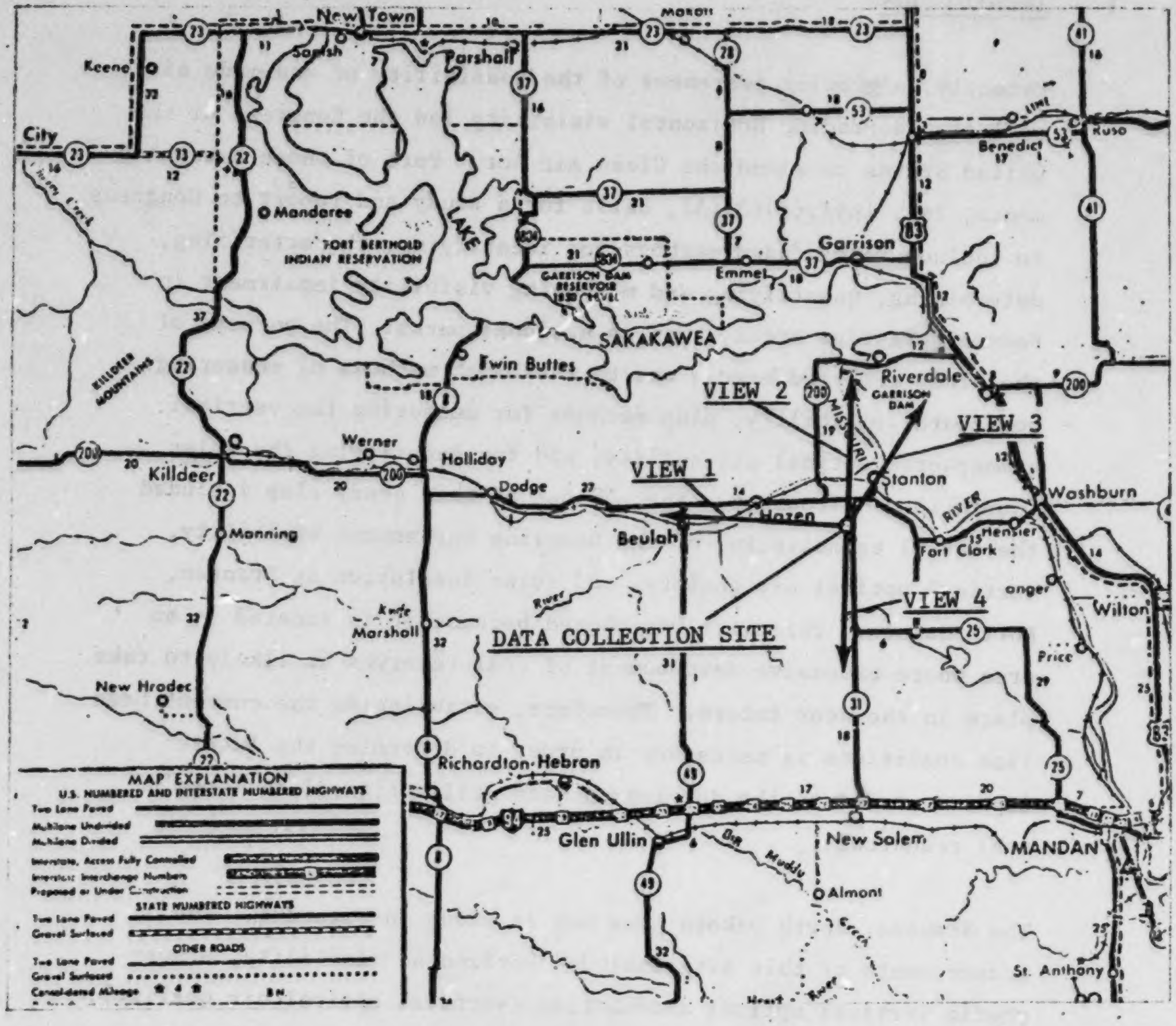
VIEW 1
VIEW 2
VIEW 3
VIEW 4
DATA COLLECTION SITE
New Town
Parshall
Keene
City
Sanish
Mandaree
FORT BERTHOLD INDIAN RESERVATION
LAKE
SAKAKAWEA
GARRISON DAM RESERVOIR
Garrison
Emmet
Benedict
Ruso
Twin Buttes
Riverdale
GARRISON DAM
MISSOURI
RIVER
KILLDEER MOUNTAINS
Killdeer
Werner
Halliday
Dodge
Hazen
Beulah
Stanton
Washburn
Hensler
Fort Clark
Manning
Knife River
Marshall
New Hradec
Wilton
Price
Richardton
Hebron
Glen Ullin
New Salem
MANDAN
Almont
St. Anthony
Heart River
MAP EXPLANATION
U.S. NUMBERED AND INTERSTATE NUMBERED HIGHWAYS
Two Lane Paved
Multilane Undivided
Multilane Divided
Interstate, Access Fully Controlled
Interstate Interchange Numbers
Proposed or Under Construction
STATE NUMBERED HIGHWAYS
Two Lane Paved
Gravel Surfaced
OTHER ROADS
Two Lane Paved
Gravel Surfaced
Consolidated Mileage

FIGURE 1

STANTON, NORTH DAKOTA AREA MAP -- VISIBILITY VIEWS DEFINITION

- -

24 days of data were collected. For each day, data was collected on an hourly basis from approximately 0800 to 1600 Local Standard Time (Central). In addition to these data, the North Dakota Department of Health collected data consisting of SO_2, NO_x, total suspended particulates, particle size distribution, ozone and sulfation rates,

at various sites near the Stanton site. A list of these measurements and their locations is given in Table 1 of Appendix A.

The following sections will present: (1) the basic concepts concerning horizontal visibility, vertical optical air quality, solar insolation, and their inter-relationships; (2) the techniques and instruments used to make each measurement; (3) the results of the measurements; and (4) the summary and conclusions of this study.

2. SUMMARY, CONCLUSIONS, AND RECOMMENDATIONS

Various methods were established and used to quantitatively define both the vertical (optical attenuation) and horizontal (visibility) optical air quality at Stanton, North Dakota. These same methods can be used to make similar determinations of optical air quality at other geographical sites, and are thereby employed to determine baseline conditions and the impact of man-made pollution on horizontal visibility and vertical optical air quality. In order to determine the impact of man-made pollution on horizontal visibility and vertical optical air quality in Federal pristine areas, baseline studies similar to the Stanton, North Dakota study have to be performed in order to establish the natural conditions and the variations under natural conditions.

The vertical atmospheric optical air quality measurements consisted of the atmospheric spectral (0.380, 0.440, 0.500, 0.640, and 0.880 um) and broadband (0.30 - 2.8 um) attenuation coefficients. Vertical atmospheric optical air quality also included the broadband (0.30 - 2.8 um) direct, total, diffuse, and ratio of diffuse to total solar insolation as functions of relative air mass. The spectral attenuation coefficients consisted of both the total attenuation, which includes attenuation due to molecular scattering, aerosol scattering, and ozone absorption; and the attenuation due to only aerosols. The horizontal atmospheric optical air quality measurements consisted of visibility determined by a measurement of contrast reduction of an object versus the background sky. The contrast reduction was determined by the photographic method. Meteorological measurements consisted of temperature, pressure, relative humidity, wind speed, wind direction, precipitable water vapor, relative dust concentration and all-sky cloud photography. The general sky appearance and color was documented with color photography. The ground-based measurements were complimented with LANDSAT 1 and 2 satellite imagery to determine if it could readily locate and determine the source of smoke plumes.

The results and analyses of the horizontal visibility and meteorological data indicated the following:

1) For any given season/month the horizontal visibility can be quite variable, depending on viewing direction, and time of day.
2) Marked day to day variations in visibility occur for all seasons/months. These variations are relatively similar for all views.
3) Variations in horizontal visibility occur on a seasonal/monthly basis. When the average hourly overall horizontal visibility for each month, for cloud free conditions, was compared it was determined that July had the greatest visibility, followed by October, April, and January. The daily, average, overall view (average of three views), considering both cloud free and cloud present (clouds behind target) conditions for April is 34.0 miles for July is 39.9 miles, for October is 32.2 miles, and for January it is 27.2 miles. If only cloud free conditions are considered the corresponding values are 34.9, 42.1, 38.9, and 32.3 miles, respectively. If only cloud present conditions are considered the values are 33.4, 38.3, 26.9, and 24.9 miles, respectively. Hence, the derived visibility is also dependent upon the sky conditions, with cloud present conditions having somewhat lower visibilities.

The results and analyses of the vertical optical attenuation coefficients indicated hourly, daily, and monthly variations. However, the variations are not necessarily similar for all wavelengths. The days having the highest overall attenuation also displayed a negative slope attenuation versus wavelength curve. This type of attenuation versus wavelength simply means that the shorter wavelengths display greater attenuation than the longer wavelengths. It has been shown that such a negative slope distribution is characteristic of a dominance of the smaller atmospheric particles/aerosols. Hence, the days having high attenuation were caused by the presence of small particles. Conversely, days having low attenuation values were characterized by a positive slope attenuation vs wavelength curve; thereby indicating a lack of the smaller particles. It was not within the scope of this study to perform attenuation versus particle size distribution analyses in order to infer the corresponding size distributions. However, it is generally known that particles in the 0.1 to 1.0 um size range account for the scattering of sunlight. The results of this study, indication of positive and negative attenuation versus wavelength slopes, points out the importance of taking multispectral vertical optical attenuation data. The five wavelengths (0.380, 0.440, 0.500, 0.640, and 0.880 um) considered in this study provide what is considered to be a minimum number of wavelengths. A single wavelength or two wavelength determination would not be sufficient to define the slope and characteristic of the attenuation versus wavelength curve. The old two channel (0.380 and 0.500 um) Volz photometer is considered to be insufficient.

The average hourly broadband (0.3 to 2.8 um) attenuation coefficient was examined for all seasons/months. It was determined that July had the greatest atmospheric attenuation, followed by April, October and January. The hourly broadband attenuation coefficient for July ranged between 0.265 - 0.370, for April it was 0.245 - 0.315, for October it was 0.148 - 0.215, and for January it was 0.105 - 0.160. Hence, it can be seen that quite significant variations in broadband atmospheric attenuation occur throughout the year/seasons. However, this broadband attenuation is due to both atmospheric scattering (molecules and aerosols) and absorption (mainly water vapor). In order to isolate the attenuation due to aerosols, the 0.640 um narrow band was analyzed for each season/month. The results showed July to have the highest attenuation/aerosols (0.105 - 0.155), followed by April (0.113 - 0.120), October (0.055 - 0.075) and January (0.021 - 0.043). These narrow band aerosol attenuation results agree with the broadband attenuation results, in terms of the relative clarity of the vertical atmosphere from season to season. However, recalling the horizontal visibility results mentioned previously, the vertical atmospheric air quality results do not indicate the same results concerning clarity as the horizontal visibility results. The horizontal atmospheric clarity was greatest in July, followed by October, April and January. The vertical atmospheric clarity was greatest in January, followed by October, April and July. The relative horizontal and vertical atmospheric clarity results agree for October and April, but they are exactly opposite concerning January and July. The horizontal clarity was greatest during July, while the vertical clarity was the least during July. This is due to the fact that the vertical and horizontal atmospheric conditions can be quite different and are not necessarily relatable. For example, a strong temperature inversion near the surface can trap aerosols near the surface, resulting in poor horizontal visibility/clarity; however, the temperature inversion is so shallow that the overall vertical atmospheric clarity can actually be quite good. This situation may exist quite often in the winter season. These results indicate the need for measuring both the horizontal and vertical atmospheric optical air quality.

The analysis of broadband 0.3 to 2.8 um, solar insolation data consisted of seasonal/monthly plots of direct, diffuse, total, and ratio of diffuse to total insolation versus relative air mass. The direct solar insolation versus relative air mass plots were able to delineate clear days, hazy days, and cloud present conditions. By plotting all direct solar insolation measurements versus relative air mass, a hypothetical clearest baseline day was established. This was performed for each season/month, which indicated that January was the clearest vertically, followed by October, July, and April. It is interesting to note that this ranking of vertical clarity is slightly different than that derived, as shown previously, by averaging the broadband attenuation coefficient. This simply indicates the difference between averaging and taking the extreme clarity. Plots of the diffuse and ratio of diffuse to total solar insolation versus relative air mass were also able to delineate atmospheric vertical clarity. However, the influence of clouds on the diffuse insolation make it a less usable indication of clarity, as compared to the direct insolation. As with the direct insolation, a hypothetical clearest day baseline was established for the diffuse and ratio of diffuse to total insolation by considering the lowest values at any given relative air mass. By analyzing such plots, it was shown that the slope of the ratio of diffuse to total insolation versus relative air mass is directly proportional to the broadband optical attenuation coefficient. By considering the slope of such plots, the variable impact of ground albedo on the diffuse insolation was eliminated. One of the most interesting results was obtained by plotting the total insolation versus relative air mass for all months. This plot revealed that despite a widely differing atmospheric clarity (as defined by the direct insolation versus relative air mass plots), the amount of total insolation remains nearly constant for a given relative air mass. The only exception is for January, when snow cover results in higher values of total insolation at a given relative air mass, due to reflection and back-scattering toward the ground. This constant relationship of total insolation versus relative air mass indicates that when the direct beam is attenuated (by scattering), the diffuse sky insolation increases an amount which compensates for the loss in direct insolation. In this manner the total (direct + diffuse) remains constant. This total versus relative air mass represents one of the more important baselines, because it is indicative of the radiation balance of the atmosphere and ground. This is related to the nature of the atmospheric aerosols/particles from the standpoint of their ability to scatter sunlight, and therefore, increase the diffuse insolation to make up for the loss of direct insolation. If the atmospheric aerosols/particles were changed to a man-made soot type aerosol, they would tend to absorb the sunlight, and therefore, not contribute to the diffuse component, which would result in a lower amount of total insolation at a given relative air mass. This would result in less energy input to the ground and would result in a modification of the heat balance. This would result in a direct impact of the man-made air pollution on the natural state. Hence, the total insolation versus relative air mass should be established in Federal Class I areas and subsequently monitored to determine any impact.

The sky appearance from photos indicated smog conditions were apparent during two days in April, during five days in July, during one day in October, and during two days in January. In April, the smog was sited to the northeast; in October, it was sited to the north; and in January, it was sited to the north and east. Obviously, the smog is to the north of the Stanton site, which corresponds to the Knife and Missouri River valleys which contain several sources of air pollution (see Figure A-1 in the Appendix).

The meteorological results showed that January was the coldest month having an average temperature (during the hours from 0800 to 1600 LST) of -9.62°C, followed by October with 5.81°C, April with 12.7°C, and July having the warmest temperature of 25.7°C. January had the highest relative humidity - average of 78.9%, followed by October, 53.1%, April, 47.7%, and July, 38.6%. However, in terms of average total vertical precipitable water vapor, January had the lowest value of 0.35 cm, followed by April, 0.55 cm, October, 0.65 cm, and July, 1.35 cm.

The satellite imagery analyses showed that a smoke plume, from a large coal fired power plant near Stanton, could be easily detected by simply doing a 7X enlargement of the original LANDSAT positive transparency. The smoke plume source, width, length, and altitude above terrain can be determined. A qualitative assessment of the smoke plume opacity can be determined by comparison of the multispectral images. The shortcoming of the LANDSAT satellite images is the fact that it passes over the same ground location only once every 18 days. Therefore, the frequency of sampling is poor. For the month of January, Jan. 19, a large smoke plume was detected, which originated from the plants at Stanton. This plume was 7 miles long, 0.4 miles wide, and was 850 feet above terrain. The plume appeared to be very opaque.

Various correlation analyses were performed in order to determine any relationship between horizontal and vertical atmospheric optical air quality. Such relationships would depend on the vertical structure of the atmosphere in terms of the altitude distribution of aerosols and water vapor. Hence, such a relationship could be quite variable, depending on the atmospheric vertical structure. The horizontal visibility, for an overall view, was compared to the vertical optical attenuation coefficient for a wavelength of 0.500 µm. For all months, an inverse correlation was found indicating low aerosol vertical attenuation when high visibility is present. However, the degree of correlation varied with the season/month. For the month of April, a correlation coefficient (a value of 1.0 indicates a perfect correlation) of 0.38 was obtained; for July a value of 0.56 was obtained; for October a value of 0.51 was obtained; and for January a correlation coefficient of 0.45 was obtained. These values of correlation are not considered to be very high; but they are high enough to indicate a definite correlation of good vertical atmospheric clarity with good horizontal atmospheric clarity. The correlation is not high enough, however, to be able to measure only the horizontal atmospheric clarity and infer the vertical clarity.

A second correlation analysis was performed to determine any correlation between horizontal visibility and the ratio of diffuse to total solar insolation. For all months, an inverse correlation was obtained, which indicates that low values of the ratio of diffuse to total insolation are associated with high visibilities. This correlation is highly dependent upon season however. For the month of April a correlation coefficient of 0.27 was obtained, for July a correlation of 0.24 was obtained; for October a correlation of 0.82 was obtained, and for January a correlation of 0.81 was obtained. The wide range of correlation is interesting and perplexing. It could be due to the particular sky conditions, in terms of clouds present. In other words, clouds present can significantly affect the diffuse insolation while not affecting the horizontal visibility. Because cloud cover can be so variable, the correlation between the ratio of diffuse to total insolation and horizontal visibility can be quite variable.

Several analyses of data for both vertical and horizontal atmospheric optical air quality were generated. The question arises concerning what data, analyses, and methods should be used as baselines to quantitatively define existing, natural conditions in Federal Class I air quality areas. The following are the recommended measurements and baselines.

A. Horizontal Optical Air Quality

1. Average hourly visibility for several views (3), for each season (minimum of one month), for cloud free and cloud present conditions.
2. Average hourly visibility for an overall view (average of all views), for each season (minimum of one month), for cloud free and cloud present conditions.
3. A plot of the percentage of days having an average daily overall view visibility above a given level. This curve should be analyzed, as shown in Section 4.6, to determine the index of visibility quality.

B. Vertical Optical Air Quality

1. For all clear days of each season (minimum of one month) plots of spectral aerosol attenuation coefficient versus wavelength. The spectral points should be a minimum of 0.380, 0.440, 0.500, 0.640, and 0.880 μm.
2. For each month, plot of the average hourly optical attentuation coefficient at 0.640 μm and the broadband, 0.3 to 2.8 μm, attenuation coefficient.
3. Plots of the direct broadband solar insolation and the ratio of diffuse to total insolation versus relative air mass for each season (minimum of one month), for the hypothetical clearest conditions, as derived in Section 6.6.
4. A plot of total insolation versus relative air mass for each season (minimum of one month), and for the entire year (each season).

The above data analyses are considered to be a minimum that is required to establish the baseline conditions of horizontal and vertical optical air quality. If possible, they should be expanded to include analyses of the broadband visible (0.30 to 0.700 μm) and broadband near infrared, (0.70 to 2.8 μm) solar insolation, as described in items 2., 3., and 4. under vertical optical air quality. By doing this the effects of aerosols (0.30 to 0.70 μm) can be separated from the effects of water vapor absorption (0.70 to 2.8 μm). This can be done by simply using an RG-8 Schott filter on the pyrheliometer (direct beam measurement) and the pyranometer (total insolation measurement). This was done at Stanton, but the scope of this study would not allow the analysis of the additional data. It is recommended that the Stanton data be additionally analyzed for the 0.30 to 0.70 and 0.70 to 2.8 μm baselines.

It is generally known that relative humidity can significantly affect visibility, especially for relative humidities above 70%. In order to separate the effects of natural relative humidity on visibility from the affects of man-made pollution on visibility, it is recommended that the horizontal visibility data be stratified in terms of relative humidity. The regions of relative humidity stratification should be determined from past experiments (if possible) and future specifically designed experiments and studies.

Finally, it is recommended that a detailed study be undertaken in order to quantify the relationships between the human eye visibility, photographic visibility, and photopic-photometric visibility. All three of these visibilities are currently being pursued and analyzed by various agencies and institutions. In order to properly respond to the amended Clean Air Act, the term "visibility" and its proper measurement has to be specifically designated. An experiment is called for, where measurements of all three visibilities are performed and compared.

3. BASIC CONCEPTS OF VERTICAL AND HORIZONTAL OPTICAL AIR QUALITY

This section is provided as a general discussion of vertical and horizontal optical air quality, and the reasons for measuring the parameters that were measured in the Stanton, North Dakota baseline study. The detailed techniques and instrumentation used for defining vertical and horizontal optical air quality are presented in later sections.

A general illustration of the applicable interactions of sunlight with the atmosphere are illustrated in Figure 2. The direct solar beam, I, is attenuated by the atmosphere due to the processes of scattering and absorption. The attenuation due to scattering is made up of that due to molecular scattering and that due to aerosols. The sunlight that is scattered from the direct beam is back-scattered out of the atmosphere and is also downward scattered and eventually reaches the ground. This downward scattered sunlight makes up the skylight, S. The scattering due to molecules is a very marked function of wavelength, $1/(\lambda^4)$, such that the shorter wavelengths are scattered much more severely than the longer wavelengths. This selective scattering, due to molecules, results in the blue skylight. Aerosols scatter sunlight less wavelength selective than do molecules. The exact wavelength dependence of aerosol scattering depends on their size distribution, index of refraction, and albedo; however, natural aerosols have been shown to scatter sunlight according to a $1/(\lambda^{1.3})$ manner. Since the molecular atmosphere is relatively constant, variations in attenuation of sunlight due to scattering are caused by variations in the nature and amount of aerosols. The attenuation of the direct beam due to absorption is highly wavelength dependent because of the absorption bands of the various atmospheric constituents. However, over the 0.30 to 2.8 µm solar spectrum, water vapor accounts for nearly all of the attenuation due to absorption. This absorption occurs in the 0.70 to 2.8 µm region. Because atmospheric water

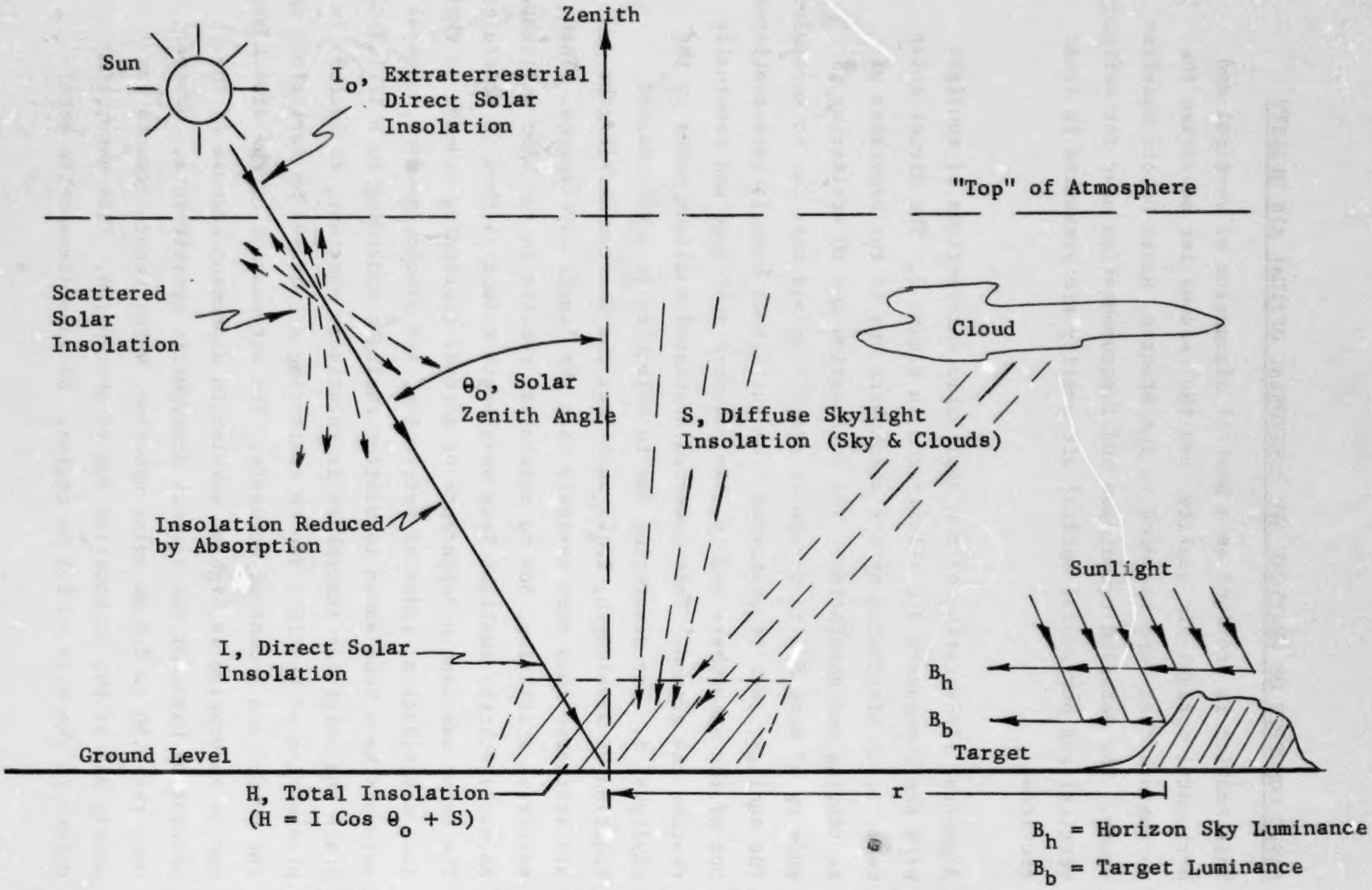
Zenith
Sun
I_o, Extraterrestrial Direct Solar Insolation
"Top" of Atmosphere
Scattered Solar Insolation
Cloud
θ_o, Solar Zenith Angle
S, Diffuse Skylight Insolation (Sky & Clouds)
Insolation Reduced by Absorption
Sunlight
I, Direct Solar Insolation
B_h
B_b
Target
Ground Level
H, Total Insolation
$(H = I \cos \theta_o + S)$
r
B_h = Horizon Sky Luminance
B_b = Target Luminance

FIGURE 2 - INTERACTION OF SUNLIGHT WITH ATMOSPHERE

vapor is quite variable, the attenuation of sunlight in the 0.70 to 2.8 μm region can be quite variable. Hence, the variable nature of atmospheric attenuation of sunlight is because of aerosols in the visible portion of the spectrum (0.30 - 0.70 um); and because of water vapor in the near infrared region (0.70 - 2.8 um).

Mathematically, the atmospheric attenuation of sunlight can be expressed as follows.

$$I = I_o e^{-\tau \sec \theta_o} \quad (1)$$

where I is the intensity of the direct solar beam at ground level, I_o is the extraterrestrial intensity ("Solar Constant"), sec θ_o is the relative path length of the beam through the atmosphere (known as the relative air mass) and τ is the total optical attenuation coefficient of the atmosphere. The total optical attenuation coefficient is made up of the components as follows,

$$\tau = \tau_m + \tau_a + \tau_{H_2O} + \tau_{O_3} + \tau_{CO_2} \quad (2)$$

where τ_m is due to molecules, τ_a is due to aerosols, τ_{H_2O} is due to water vapor, τ_{O_3} is due to ozone, and τ_{CO_2} is due to carbon dioxide. As pointed out previously, τ_a and τ_{H_2O} are the most significant and are also the most variable. The atmospheric optical attenuation coefficient and the components, shown in equation 2, are the vertical attenuation coefficients. These vertical attenuation coefficients are related to horizontal coefficients at various levels (altitudes) in the atmosphere by

$$\tau = \int_{z_o}^{\infty} \beta \, dz \quad (3)$$

$$\tau_m = \int_{z_o}^{\infty} \beta_m \, dz \quad (4)$$

$$\tau_a = \int_{z_o}^{z} \beta_a \, dz \quad (5)$$

$$\tau_{H_2O} = \int_{z_o}^{z} \beta_{H_2O} \, dz \quad (6)$$

$$\tau_{O_3} = \int_{z_o}^{z} \beta_{O_3} \, dz \quad (7)$$

$$\tau_{CO_2} = \int_{z_o}^{z} \beta_{CO_2} \, dz \quad (8)$$

where z_o is the surface altitude, z is altitude above the surface, and β, β_m, β_a, are the corresponding horizontal attenuation coefficients at various altitudes.

The diffuse skylight is a complex function of τ_m, τ_a, $\sec\theta_o$, ground albedo, and the geometry between the direct beam and the aerosols and the molecules. However, in a general sense, the diffuse skylight is dependent upon τ_a and sec θ_o (relative air mass). As τ_a increases and sec θ_o increases the greater amount of sunlight is scattered from the direct beam.

The total amount of insolation at the surface, H, is the sum of the direct insolation on a horizontal surface, $I\cos\theta_o$, and the diffuse skylight, S. Hence,

$$H = I\cos\theta_o + S \tag{9}$$

where the solar insolation components, I and S, are determined by the vertical optical properties.

In the lower atmosphere, near the surface, the horizontal optical air quality parameter is the horizongal visibility, Figure 2. The horizontal visibility, V, is approximated by:

$$V = \frac{3.912}{\beta_s(o)} \tag{10}$$

where $\beta_s(o)$ is the near surface scattering attenuation coefficient, which is given by

$$\beta_s(o) = \beta_m(o) + \beta_a(o) \tag{11}$$

where $\beta_m(o)$ and $\beta_a(o)$ are the molecular and aerosol components. The relationship between the vertical optical air quality and the horizontal optical air quality is shown when equations 4 & 5 are compared to equations 10 & 11. As can be seen the vertical optical attenuation coefficients are simply the integral of the optical attenuation coefficients as a function of altitude. The horizontal, near surface, optical properties represents one increment of the integral. Therefore, the vertical and horizontal optical air quality are not directly related and represent distinct properties of the atmosphere.

In order to define the vertical and horizontal optical air quality, the parameters to be measured would be the various optical attenuation coefficients, as defined previously. The most important parameter, in terms of detecting any man-made pollution effects, would be the aerosol attenuation coefficients. Therefore, the result of changes in the aerosol component should also be determined by the impact on the solar insolation components. The measurements at Stanton, North Dakota were designed to establish a baseline for the vertical and horizontal optical air quality. To do this the following measurements were selected:

A. Vertical optical attenuation coefficients at various wavelengths and over the entire solar spectrum.
B. Direct, diffuse, and total solar insolation.
C. Horizontal optical air quality - visibility.

4. HORIZONTAL VISIBILITY

4.1 Techniques/Instrumentation - A photographic technique was used used to measure horizontal visibility. The basis of this technique has been described by Middleton (Ref. 1). This technique involves photographing a distant, black, object on the horizon then measuring the contrast between the object and its background sky. If the luminance of the black object is B_b, and the luminance of the horizon sky is B_h, then (as shown in Ref. 1, page 63)

$$B_b = B_h (1 - e^{-br}) \tag{12}$$

where b is the horizontal attenuation coefficient, due to scattering, and r is the range to the object. The meteorological visual range, V, is related to the attenuation coefficient by the approximation (see Ref.1 p. 105)

$$V = 3.912/b \tag{13}$$

If the distant object and horizon sky are photographed, the resultant film exposures produced by the horizon sky, E_h, and distant object, E_b, are

$$E_b = B_b \times t \tag{14}$$

$$E_h = B_h \times t \tag{15}$$

where t is the exposure time (camera shutter speed). Because the camera shutter speed is identical for each exposure, it is obvious that

$$\frac{E_b}{E_h} = \frac{B_b}{B_h} \tag{16}$$

Combining equations 12 and 13, the ratio E_b/E_h is related to meteorological visual range, V, by,

$$V = -r \times 3.912/\ln(1-E_b/E_h) \tag{17}$$

Ref. 1: W. E. Knowles Middleton; Vision Through the Atmosphere, University of Toronto Press, 1952.

where the units of V (miles, kilometers, etc) are the same as used for r, hence; by using photography to determine the quantity E_b/E_h, and knowing the distance to the target, r, the meteorological range can be measured. This method/technique, is based upon Koschmieder's theory, as discussed in Ref. 1, having the following assumptions:

(1) The atmosphere is considered as a turbid medium, containing a large number of small particles.

(2) Each element of volume contains a very large number of particles, each of a smaller order of magnitude then the element itself.

(3) The scattering action of each particle is independent of the presence of all the others; i.e., multiple scattering is neglected.

(4) The light scattered from an element of volume will be considered as coming from a point source of which the intensity is proportional to the number of particles.

(5) Light rays will be considered as rectilinear, that is to say atmospheric refraction will be neglected.

(6) All parts of the atmosphere in the horizontal plane are equally illuminated.

(7) The coefficient of attenuation by scattering, b, is constant in a horizontal plane, in particular near the surface of the earth.

(8) The curvature of the earth is neglected, and its surface is considered as plane, horizontal, and diffusely reflecting.

(9) The linear dimensions of the whole observed object are small in comparison to its distance from the observer.

(10) As stated previously, the object is assumed to be black.

Of these assumptions, No's 6, 7, and 10 are the ones that will be most likely violated in the real/actual case. The assumption that all parts of the atmosphere are equally illuminated is subject to violation due to cloud cover changes. In addition, if clouds exist behind the target they will cause an erroneous value of E_h to be measured. Hence the presence of clouds can cause erroneous results. The assumption that the scattering attenuation coefficient is constant in the horizontal plane is subject to violation because of localized anomalies such as smoke plumes, dusty roads, open coal pit operations, or any other localized source of particulates. The assumption that the object is black is probably the most serious violation. Totally black objects/targets simply do not exist in the real situation. If sunlight is reflected from the target, an erroneous value for E_b is obtained. It is interesting to note that if sunlight is reflected by the target, the resultant calculated meteorological range will be low. This is because the luminance originating from the target is interpreted as additional luminance due to additional particles and forward scattering; and therefore, a lower meteorological range. On the other hand, if a cloud is present behind the target, and has a greater luminance than the cloud free atmosphere, an erroneously high value of B_h will be obtained which will result in erroneously high values for meteorological range. Hence, in the real situation, these errors may tend to offset each other. The magnitude of the error introduced by reflected luminance from the object is determined by the object's albedo and the amount of incident sunlight. The amount of incident sunlight is determined by the sun angle to the objects surface and atmospheric attenuation and cloud cover. Similarly, the amount of error introduced by clouds behind the target is dependent upon the incident sunlight on the cloud and the cloud albedo.

In terms of absolute accuracy of meteorological visual range, as pointed out in the above discussion, the photographic method/technique (or any other technique that relies on the measurement of a distant target luminance versus the background sky luminance) cannot be considered as highly accurate. However, in terms of a relative indicator of visibility for a given set of conditions, it is valid because the basic measurement is of the luminance ratio between the target and the background sky. This ratio is certainly an indicator of visibility because the luminance of the target will be a function of the luminance produced by the scattering of light by particulates between the receiver and target. The luminance level of this scattered light is a function of the number, size and characteristics of particulates, assuming negligible absorption by the particulates. The set of conditions includes such items as target albedo, sun angles (time of day, year), cloud cover, etc. For a given time of year and day, sun angles are obviously constant; and, if no marked changes occur that change the target, the target albedo will most likely be fairly constant. The most likely variable will be cloud cover. For this reason, in the following reported results, cloud free conditions and cloudy conditions were reported separately.

It should be pointed out that meteorological range, as determined photographically, is not identical to visibility as perceived by a human observer. The main differences are because they are both wavelength sensitive and the detection of the ratio of E_b/E_h is in one case determined by a densitometer and in the other case determined by the eye. The wavelength sensitivity arises from the fact that the attenuation coefficient, b, is wavelength dependent; therefore, as shown in Equation 13, visibility will be wavelength dependent. Since the photographic film (Panotomic X, B&W) and the eye do not respond identically to all wavelengths, a basic difference exists between the photographically determined meteorological range and the eye visibility. Another basic difference exists due to the sensitivity of the eye to a small difference between E_b and E_h versus the comparitive response of a densitometer. However, despite these differences, a good correlation should exist between the photographically determined meteorological range and the human eye determined visibility, because they are both sensitive to the relationship between E_b and E_h. The instrumentation used for photographically determining meteorological range, hereafter referred to as visibility, consisted of an eight inch diameter/aperture reflective, telescopic, 2000 m.m. focal length lens (Celestron 8); and, a Honeywell Pentax Spotmatic 35 mm camera shown in Figure 3.

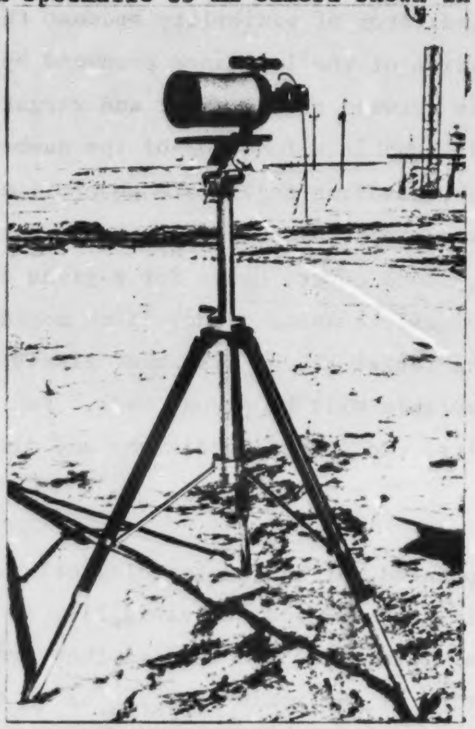

FIGURE 3 - HORIZONTAL VISIBILITY DATA COLLECTION CAMERA SYSTEM

The film used was Kodak Panotomic X B&W. The densitometer used was a MacBeth Model TD 404 Diffuse Densitometer.

The particular film processing included the use of calibrated step-wedges (21 steps) on each roll of film. This produced a film density versus log exposure (D log E) curve for each roll of film. This was performed both before and after the field mission. This produced curves by which measured film densities of the target, D_b, and horizon sky, D_h, could be converted to the corresponding exposures, E_b and E_h.

An example of such a curve is shown in Figure 4. The critical relationship necessary in order to perform such a conversion is that the relationship between film density and the log E be linear, at least over that range of exposures produced by the target and sky luminance. As shown in Figure 4 the D log E relationship is linear over the desired range of density. This was accomplished by experimentation with the film development time. It was determined that by using Kodak D19 developer and a developing time of 7 minutes, a linear relationship was achieved.

The field data collection consisted of photographing three views, as shown in Figure 1, every hour from 0800 to 1600. The horizontal visibility, using the 2000 mm lens system, was determined for views/targets towards 1, 2, and 3. Target No. 1 (see Figure 5) is an open coal pit dump, having a fairly low albedo (~ 20%), approximately 15 miles from the measurement site. Target No. 2 (see Figure 6) is a hillside, having a soil and grass cover, located approximately 15 miles from the site. Target No. 3 (see Figure 7) is a hillside, having a similar cover as No. 2, located approximately 16 miles from the site. View No. 4 (see Figure 8) was taken with a 200 mm lens for sky appearance documentation only.

The baseline horizontal visibility parameters established were as follows:

(1) Average hourly visibility for three views
(2) Average hourly visibility for overall view (average of 3 views)
(3) Average daily visibility for three views
(4) Average daily visibility for overall view.

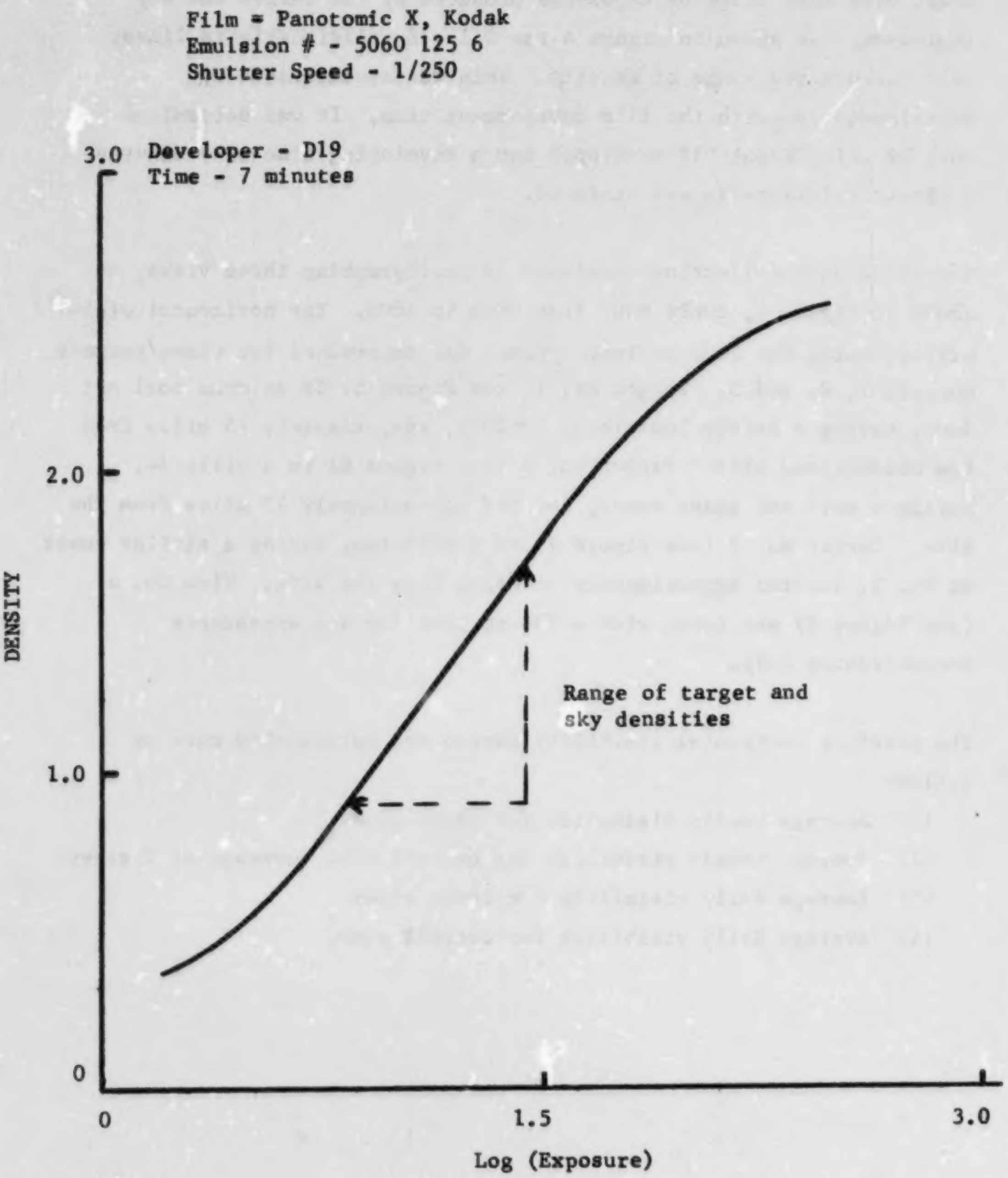

Figure 4 - D LOG E CALIBRATION CURVE FOR RELATING FILM DENSITY TO RESULTANT EXPOSURE

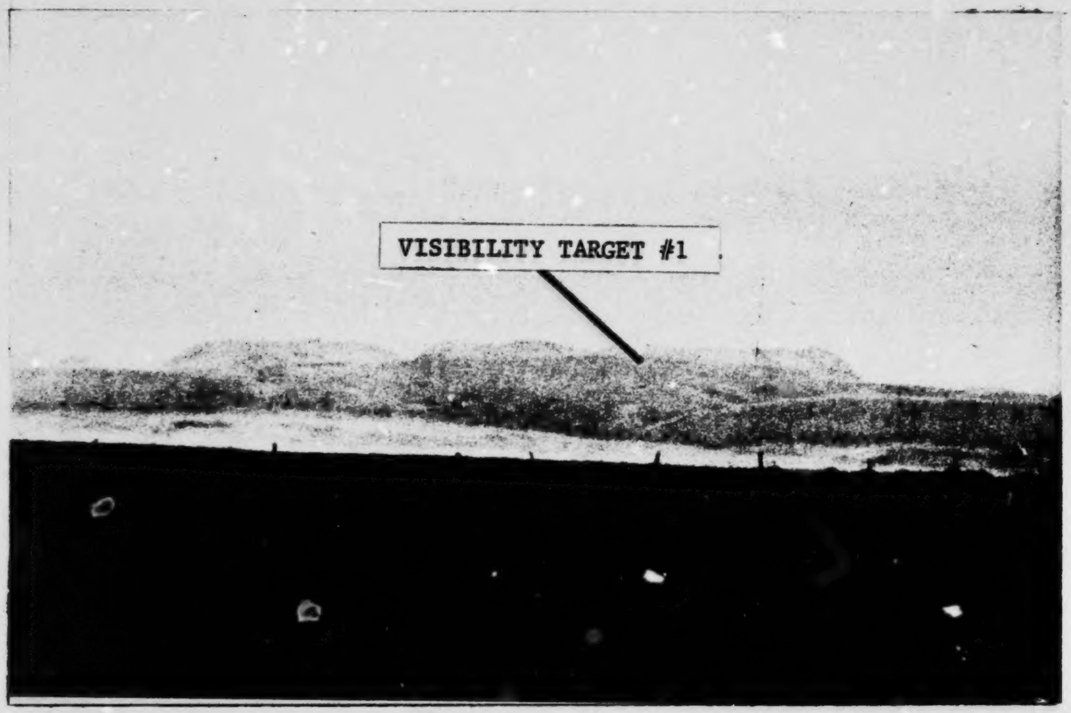
VISIBILITY TARGET #1

FIGURE 5 - TARGET #1 - VIEWED THROUGH 2000 mm LENS

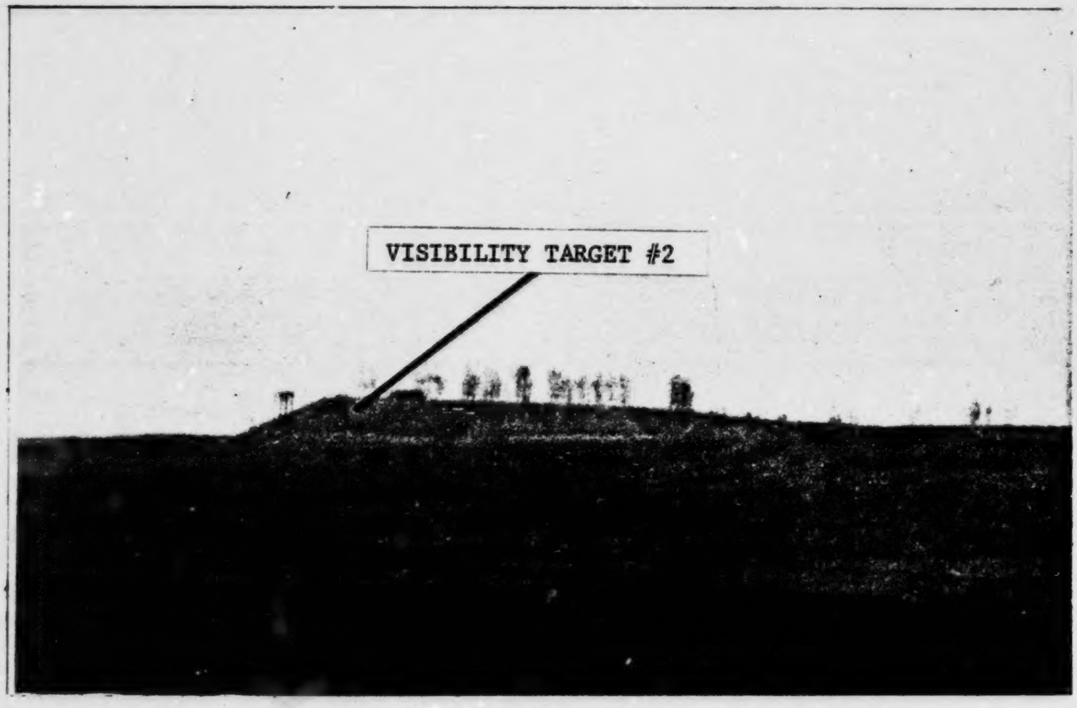
VISIBILITY TARGET #2

FIGURE 6 - TARGET #2 - VIEWED THROUGH 2000 mm LENS

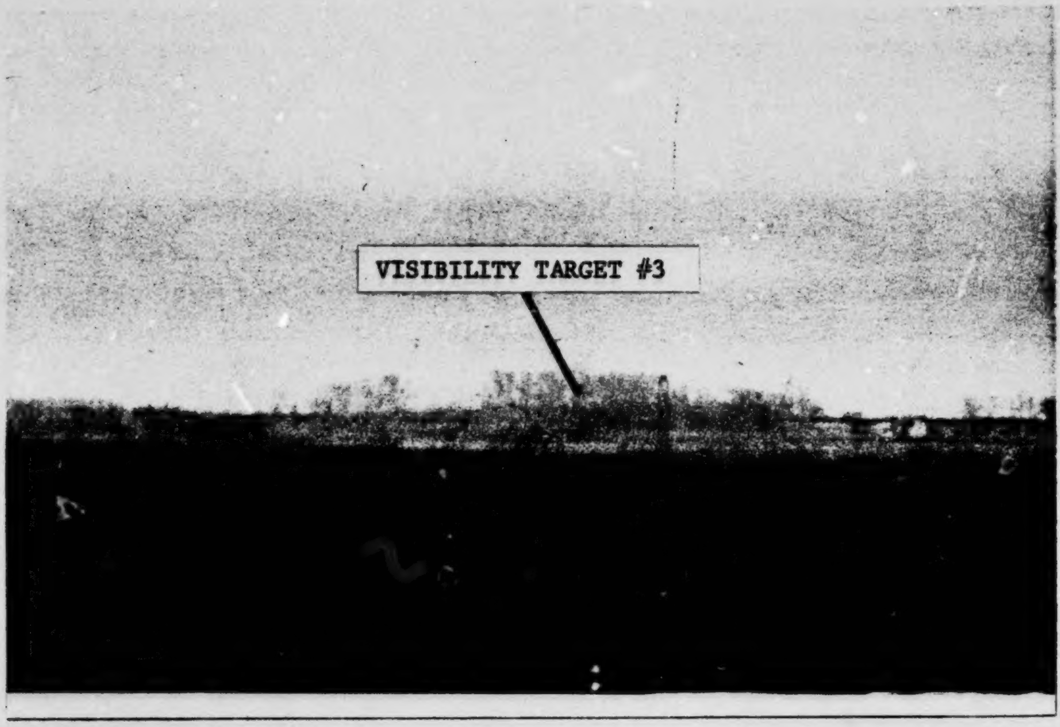
VISIBILITY TARGET #3

FIGURE 7 - TARGET #3 - VIEWED THROUGH 2000 mm LENS

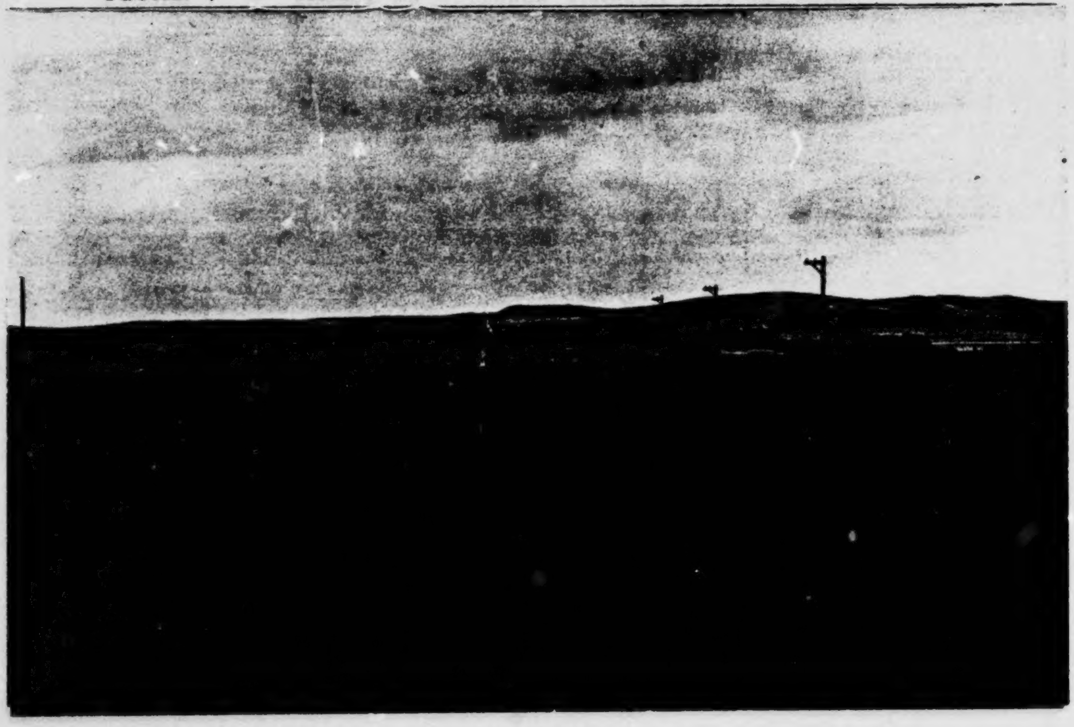

FIGURE 8 - VIEW #4 - SKY APPEARANCE VIEW - 200 mm LENS

4.2 April Horizontal Visibility - The results for the April data collection mission are shown in Figures 9, 10, 11, and 12. They consist of the average hourly visibility for three views, the average hourly visibility for an overall view, the average daily visibility for three views, and the average daily visibility for an overall view. In all cases, the cloud free and cloud present conditions are designated separately because of the previously mentioned influences of clouds. The cloud present conditions refer to a condition when clouds were on the horizon, behind the target. As Figures 9 and 10 point out, both the hourly and daily visibility is dependent upon the view. This is true for both cloud free and cloud present conditions. The hourly dependence of view 1 exhibits a general increase, for both cloud free and cloud present conditions, in visibility throughout the day. This increase is from approximately 25 miles in the early morning hours to approximately 43 miles in the late afternoon. The hourly dependence of view 2 exhibits a much smaller, compared to view 1, fluctuation for both cloud free and cloud present conditions. The view 2 visibility is fairly consistant throughout the day, having a visibility of approximately 25 to 30 miles. The hourly dependence of view 3 exhibits a difference between the cloud free and cloud present conditions, especially for the morning hours. The reason for this is not known, possibly it is due to a sun angle/illuminance effect, i.e., target 3 is sunlit in the morning and shaded in the afternoon. The average daily visibility for the three views, Figure 11, exhibits day-to-day variations. In general, view 2 exhibits less visibility than views 1 and 3. All views tend to exhibit similar day-to-day variations. The hourly dependence for the overall view, Figure 10, displays a general increase in visibility, for both cloud free and cloud present conditions, throughout the day. The morning visibility is approximately 30 miles and the afternoon values approach 40 miles. The overall view daily visibility, Figure 12, exhibits day-to-day variations ranging from 20 miles (mist-rain) to 41 miles. In addition, any specific day can display a wide range of visibility.

4.3 July Horizontal Visibility - The results for the July data collection mission are shown in Figure 13, 14, 15, and 16. As concluded from the April data, both the hourly and daily visibility is dependent upon the particular view. View 1 displays a general increase in visibility throughout the day. Views 2 and 3 display a relatively consistant visibility throughout the day. For cloud free conditions, view 1 has visibilities ranging from 35 miles in the morning to 55 miles in the afternoon. View 2 displays visibilities of approximately 40 miles. View 3 displays visibilities ranging from about 40 miles to a maximum of 48 miles at noon. As with the April results, View 2 displays lower visibilities than views 1 and three. The average daily visibilities for the three views, Figure 15, shows similar day-to-day variations for all views, with View 2 having the lowest visibility. The overall view shows a fairly consistant hourly dependence, Figure 14, ranging from 39 to 47 miles. The overall view daily visibility, Figure 16, shows day-to-day variations, with a maximum of 63 miles and a minimum of 25 miles.

4.4 October Horizontal Visibility - The October data collection mission results are shown in Figures 17, 18, 19, and 20. The plots for the hourly and daily visibilities for the three views again demonstrate the dependence of visibility upon the view, hour, and day. View 1 again exhibits a general increase in visibility throughout the day. Views 2 and 3 again exhibit a relative constant visibility throughout the day. View 3 also exhibits less visibility than views 1 and 2. The daily average visibility for 3 views and the overall view daily average visibility, Figures 19 and 20, exhibit large day-to-day changes. These day-to-day changes are reflected in a similar manner for all views. The average hourly visibility for an overall view, Figure 18, shows a very weak dependence upon time of day. In addition, the cloud present conditions have lower visibilities than the cloud free conditions. However, the time dependence is similar for both conditions.

4.5 January Horizontal Visibility - The January data collection mission results are shown in Figures 21, 22, 23, and 24. The January results exhibit features that have been pointed out for the April, July and October data.

4.6 Seasonal Horizontal Visibility Comparisons - A comparison of the daily average visibility, for an overall view, is shown in Figure 25, for all the seasonal months. As can be seen, July exhibits the greatest visibility, followed by October, April, and January. However, an absolute comparison is dependent upon time of day. July and October display increasing visibilities throughout the day, while April and January display a relatively constant visibility throughout the day. In addition, an absolute visibility comparison between the various seasonal months is complicated by the fact that the targets were not the ideal black target, therefore, it is possible that there exist variations due to sun angle and changing target albedo. The target albedo was observed to be fairly low ($\approx .2$) and consistent for the months of April, July, and October, however the target was snow covered during January. However, it was possible to locate "dark" areas on each of the targets for January, thereby greatly reducing the adverse effects of snow cover. Shown in Figure 26 is another type of seasonal visibility comparison. The percent of days, out of the total number of days measured, that a given daily average visibility, plotted on the x axis is exceeded is shown for each of the seasonal months. Using this type of comparison, it is concluded that July had the best visibility, January had the worst visibility, and April/October had different characteristics. April had a greater number of days with visibilities greater than 15 to 35 miles; whereas, October had a greater number of days with visibilities between 35 to 50 miles. It is obvious, from Figure 26, that the overall visibilities at Stanton, North Dakota do not exceed 50 miles except for a very minimal portion of time. The 15 mile lower limit is established by the distance to the targets. There are several ways by which to interpret the results shown in Figure 26, in order to assign an overall quantitative index to the visibility for each season. One possible method is to establish the 50% level for each season. This level would indicate what visibility was exceeded over 50% of the days. For January this level is about 25-30 miles; for April this level is about 35 miles; for October this level is about 35 miles; and for July this level is 40 miles. However, as exhibited by the October and April data, this type of interpretation may not truly represent the overall visibility quality. In order to do this some sort of integral evaluation is needed over all levels of visibilities. This can be achieved by essentially integrating each of the curves shown in Figure 26 by taking the mid-point value of percent in each of five-mile increments from 15 to 50 miles. This mid-point value is then multiplied by the increment, five miles, to obtain the area under the curve; then all increments (seven) are totaled to obtain the area under each curve. This area can then be divided by 100 to give a convenient number index of visibility quality for each seasonal month. When this is done the visibility quality index for January is 12.40, for April is 18.9, for July is 24.95, and for October is 17.95. These numbers indicate the large difference (a factor of 2) in visibility quality between January and July, and the similarity of April and October. When these relative rankings are compared with the overall view average hourly data, shown in Figure 25, it can be seen that this type of data would indicate that July, October, April, and January was the proper ranking. This disagreement in ranking is because the data shown in Figure 25 is for both clouds present and cloud free conditions. Both types of analysis are useful for establishing the baseline visibility quality. Further analyses could be performed on each individual view.

Fig. 9 Average Hourly Visibility for Three Views

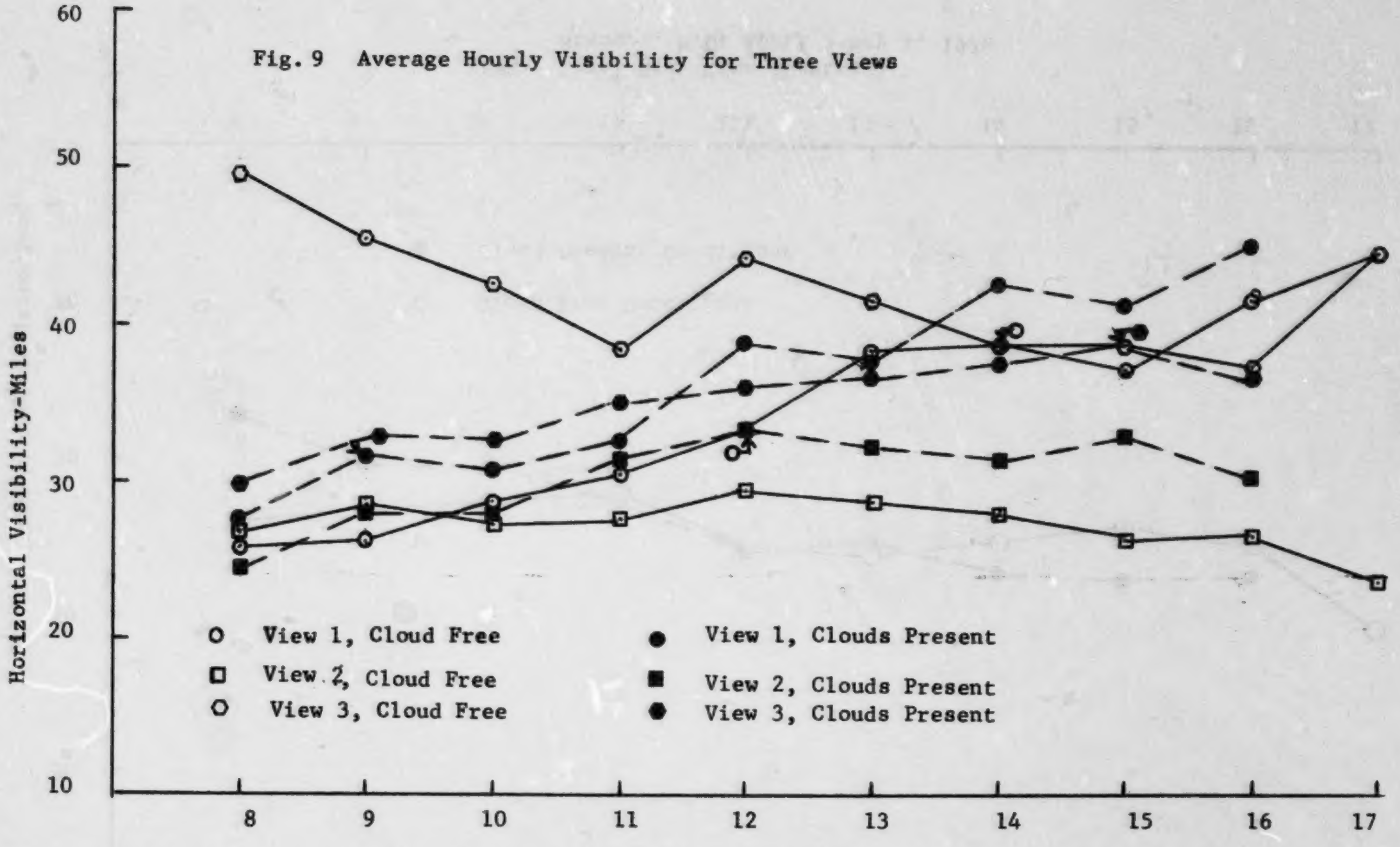

TIME - Local Std. Time (Central)
Stanton, N.D., April 5-May 1, 1976

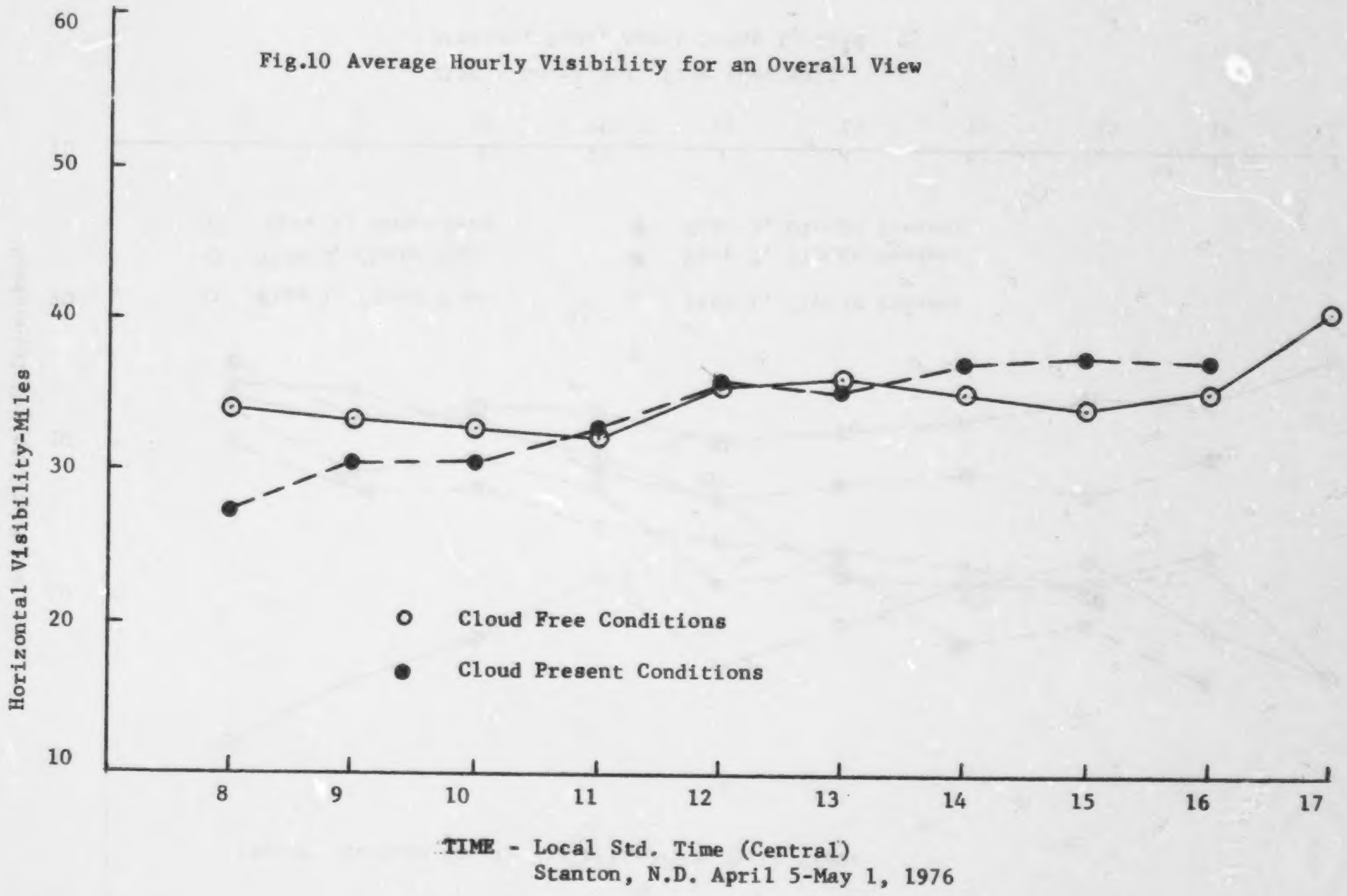

Fig.10 Average Hourly Visibility for an Overall View

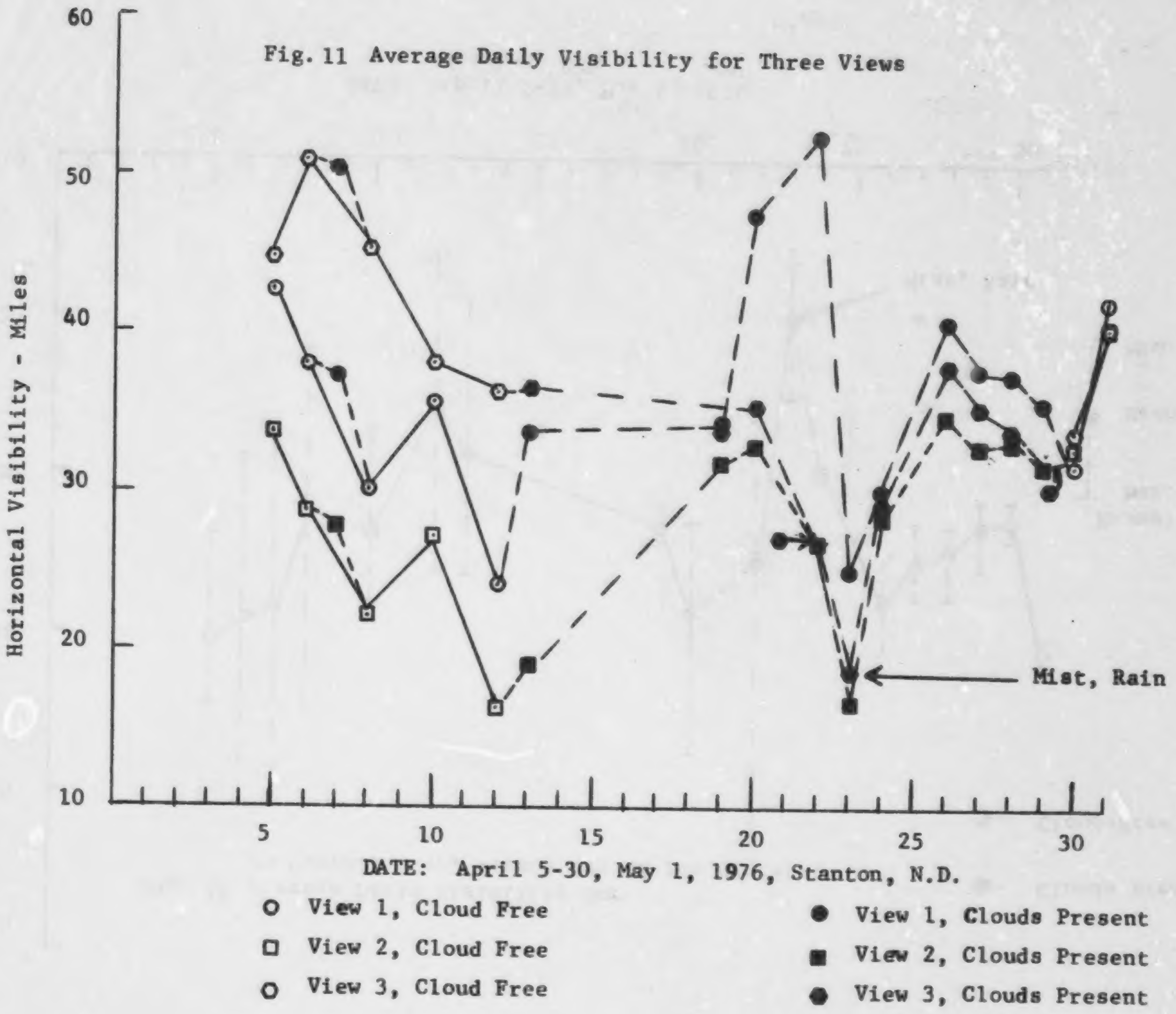

Fig. 11 Average Daily Visibility for Three Views

Fig. 12 Average Daily Visibility for an Overall View, Versus Day of the Month

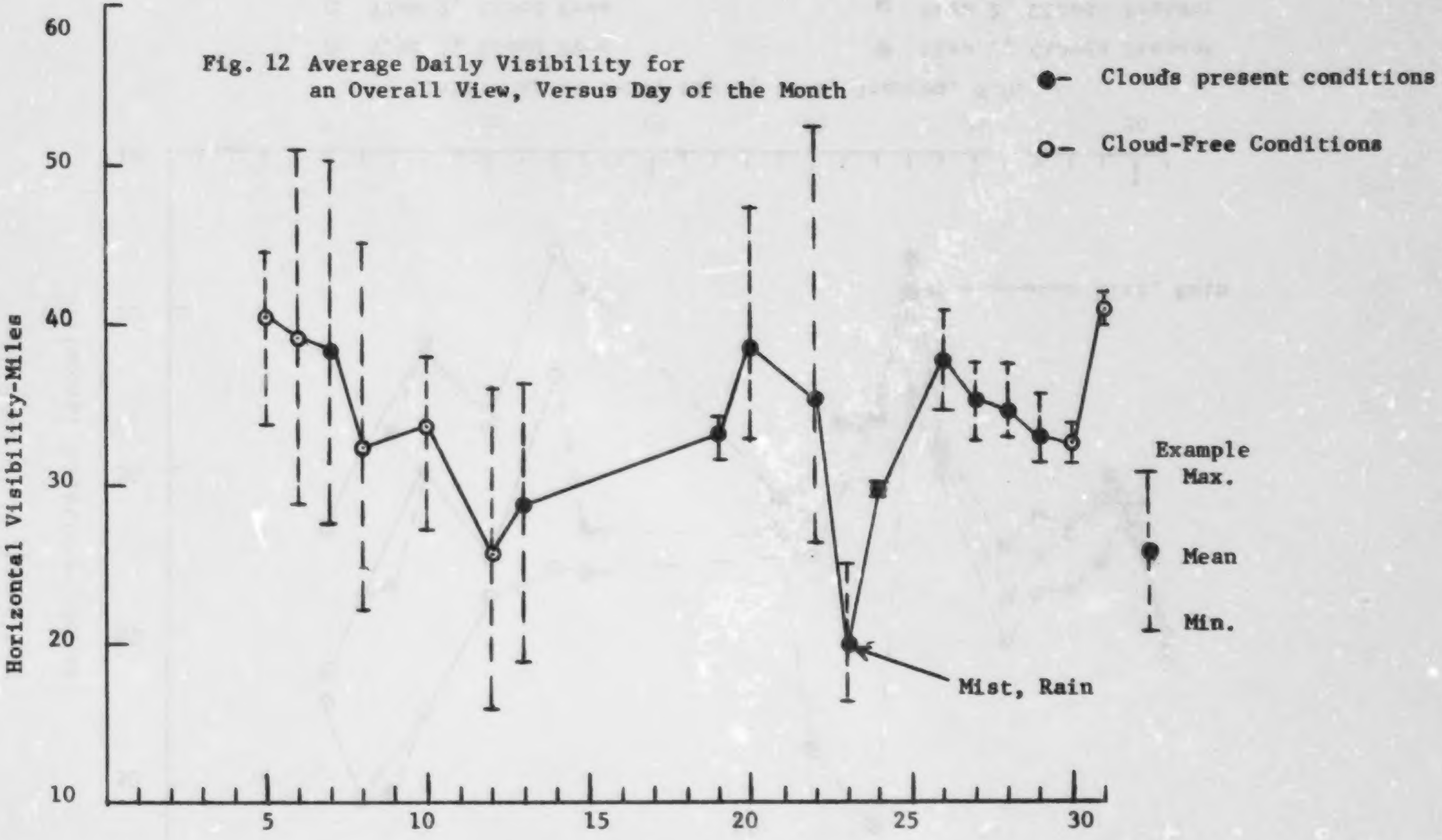

DATE: April 5-30, May 1, 1976
Stanton, N.D.

FIG. 13 AVERAGE HOURLY VISIBILITY FOR THREE VIEWS

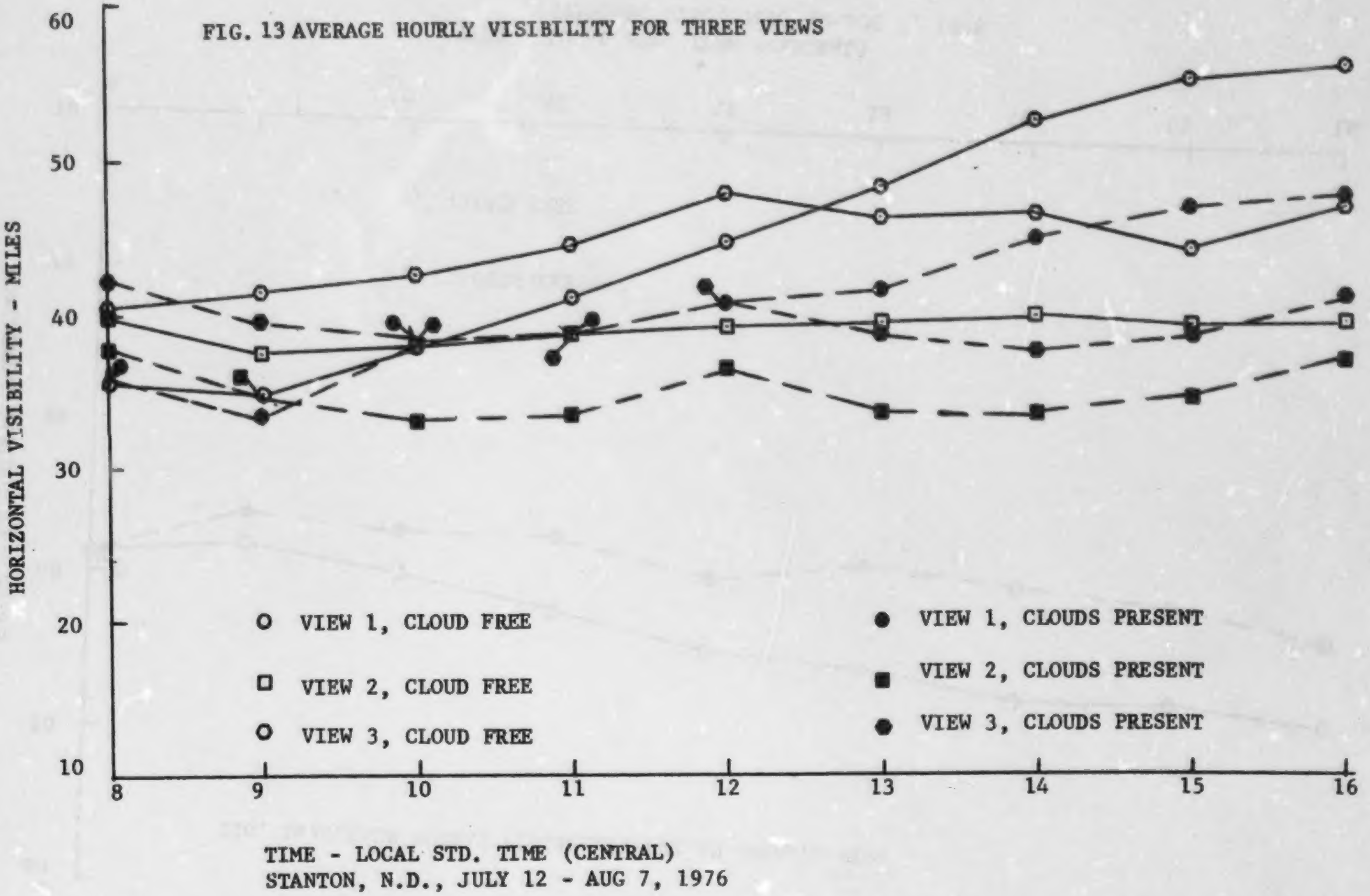

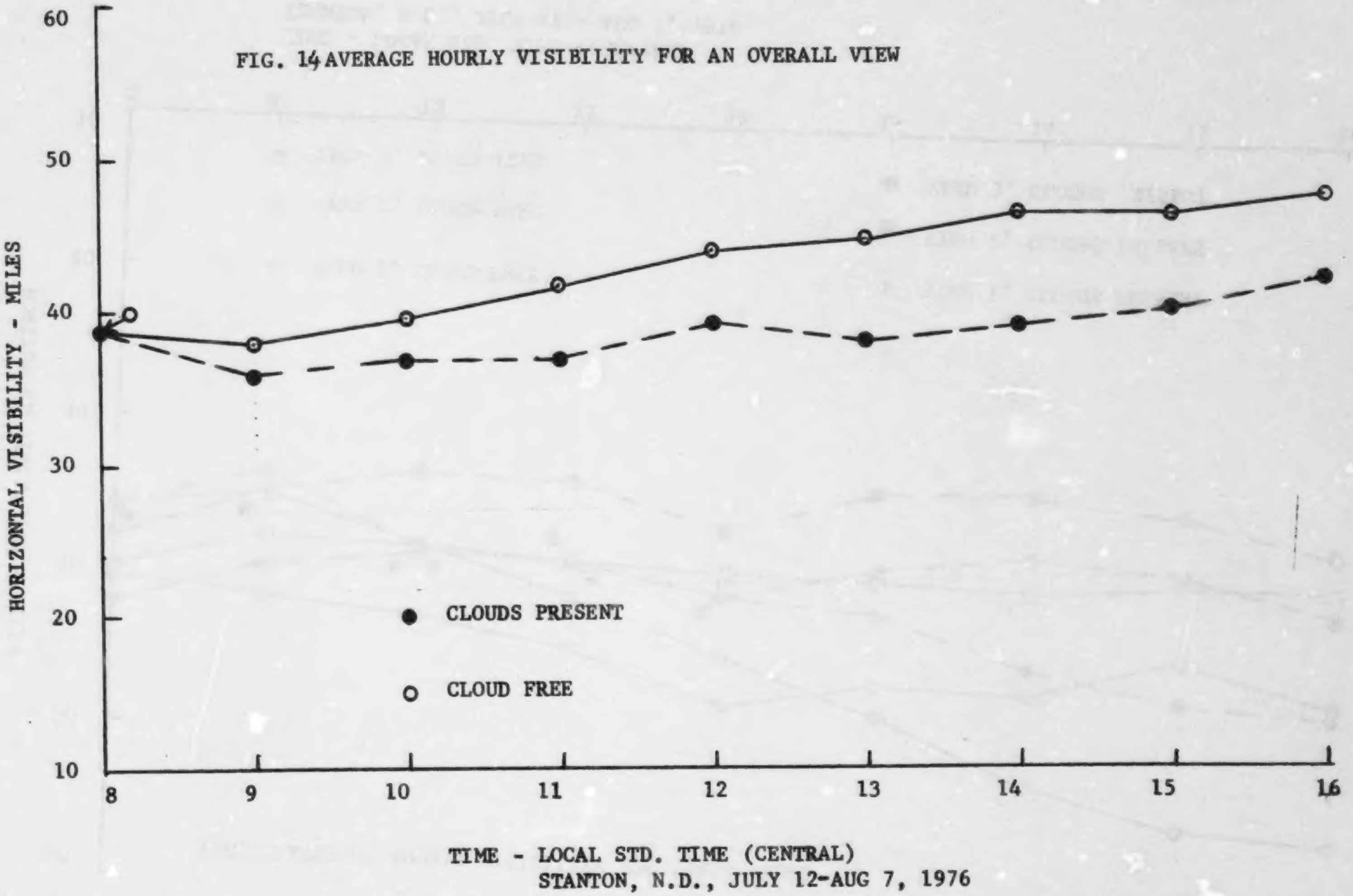
FIG. 14 AVERAGE HOURLY VISIBILITY FOR AN OVERALL VIEW

FIG. 15 AVERAGE DAILY VISIBILITY FOR THREE VIEWS

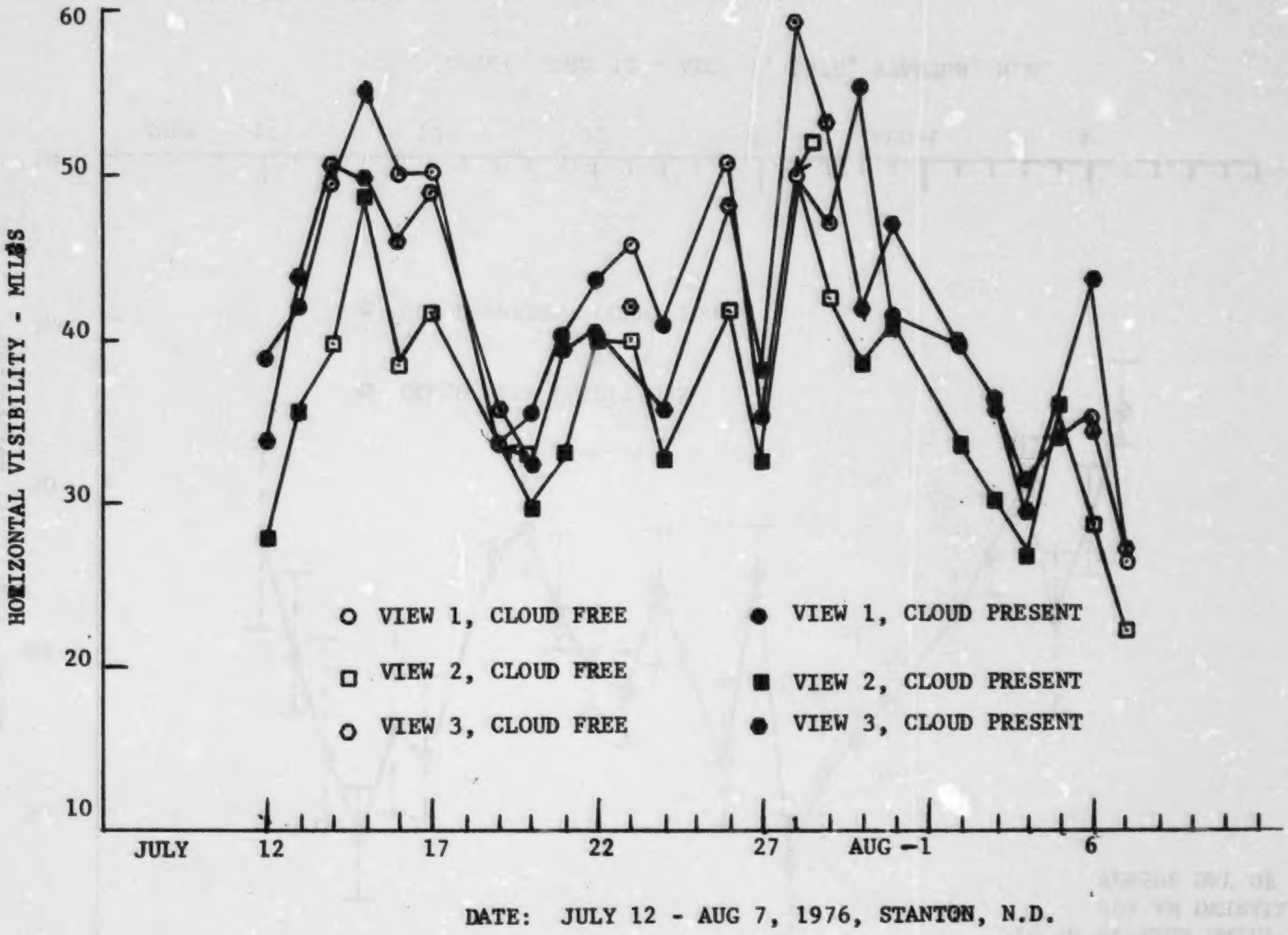

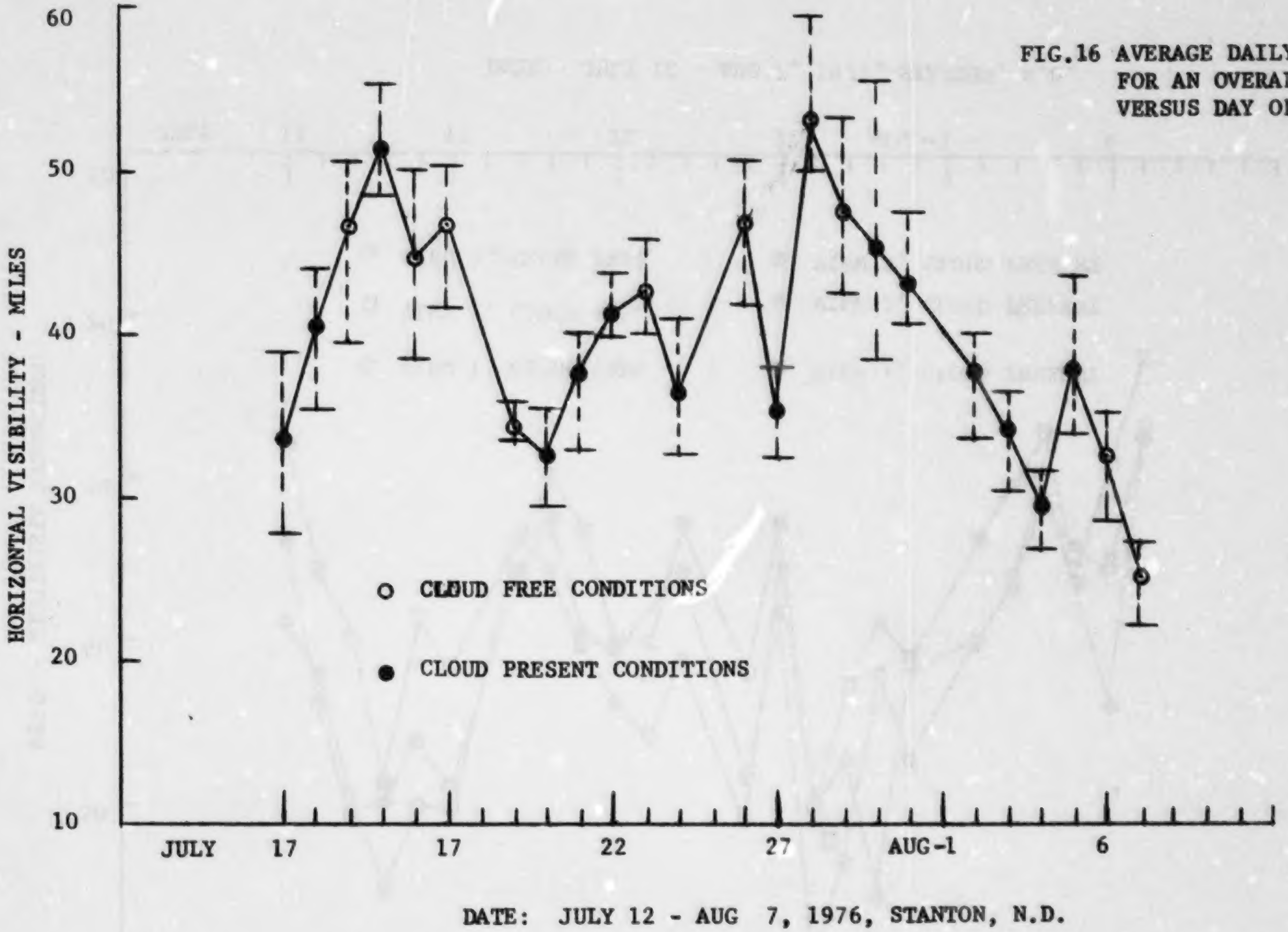

FIG.16 AVERAGE DAILY VISIBILITY
FOR AN OVERALL VIEW,
VERSUS DAY OF THE MONTH

FIG. 17 AVERAGE HOURLY VISIBILITY FOR THREE VIEWS

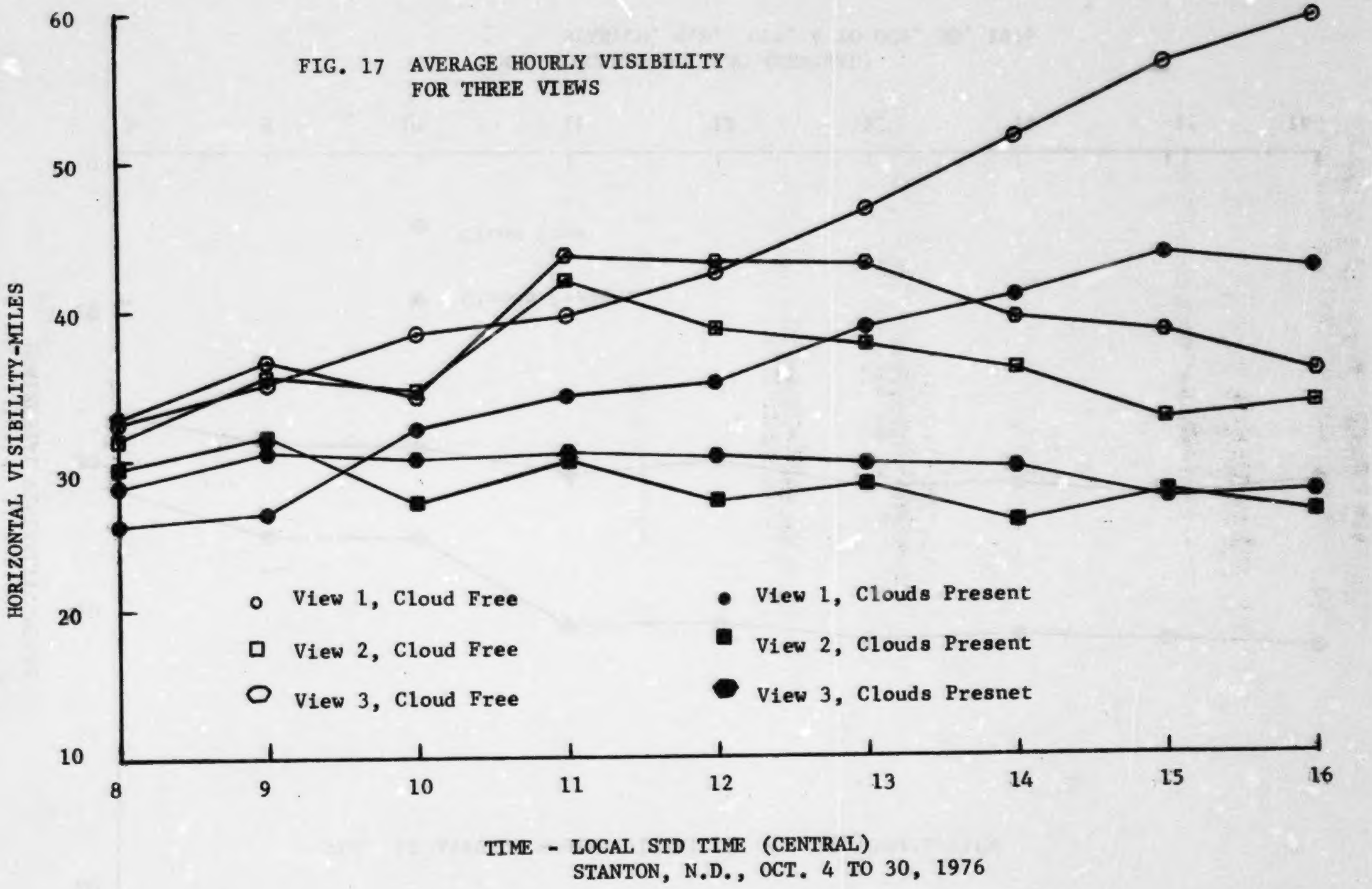

STANTON, N.D., OCT. 4 TO 30, 1976

FIG. 18 AVERAGE HOURLY VISIBILITY FOR AN OVERALL VIEW

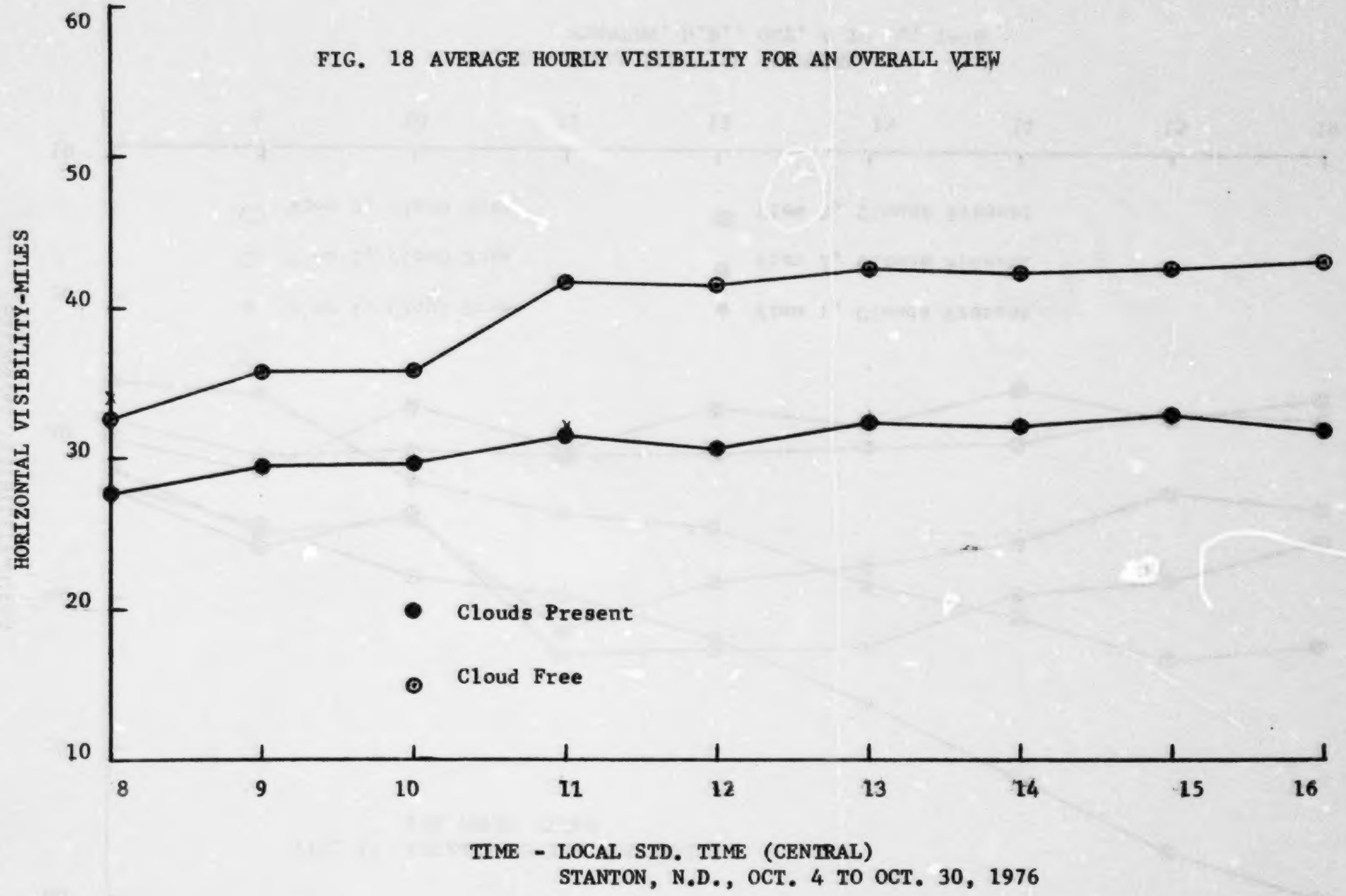

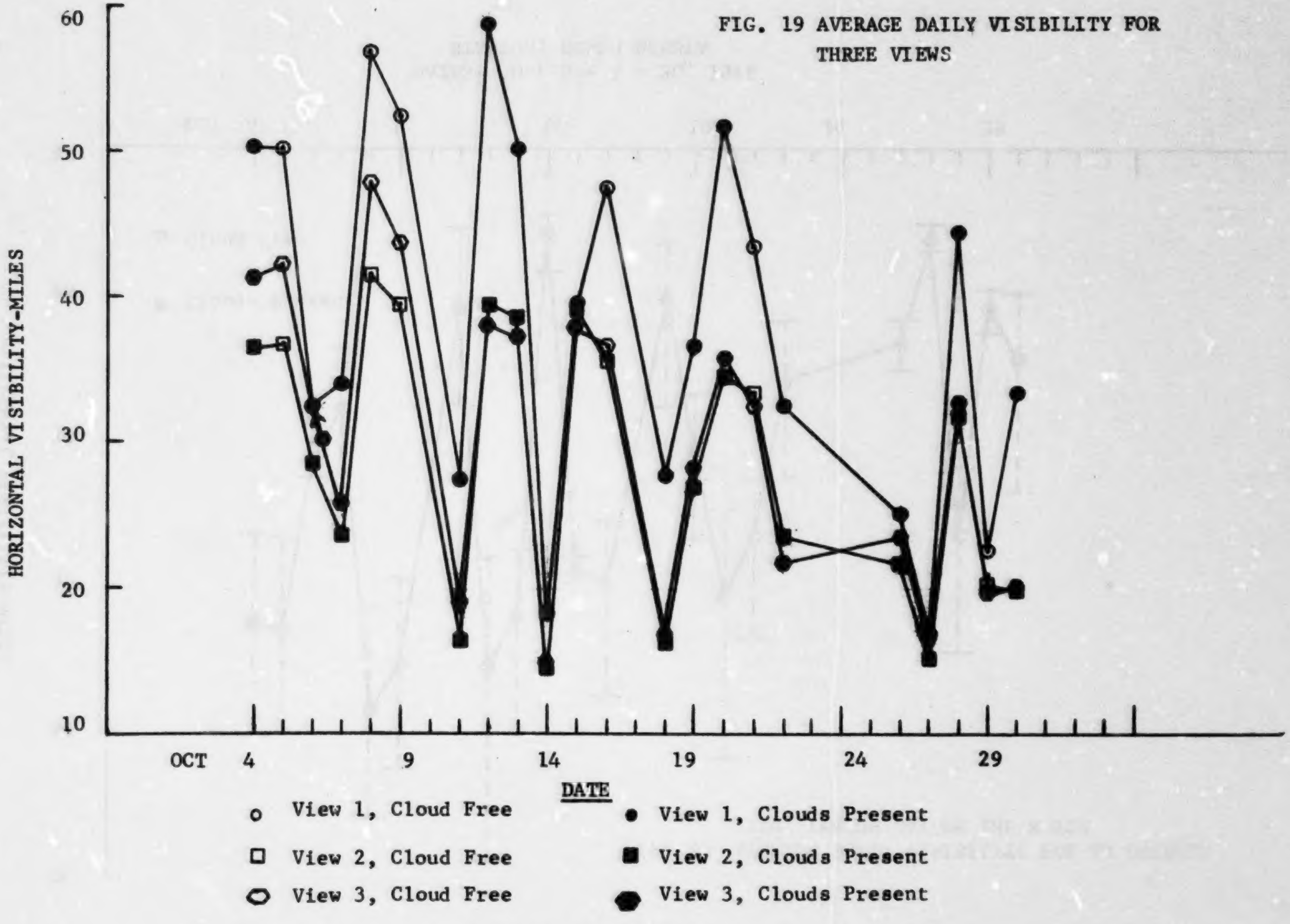

FIG. 19 AVERAGE DAILY VISIBILITY FOR THREE VIEWS

STANTON, N.D., 1976

FIG. 20 AVERAGE DAILY VISIBILITY FOR AN OVERALL VIEW, VERSUS DAY OF THE MONTH

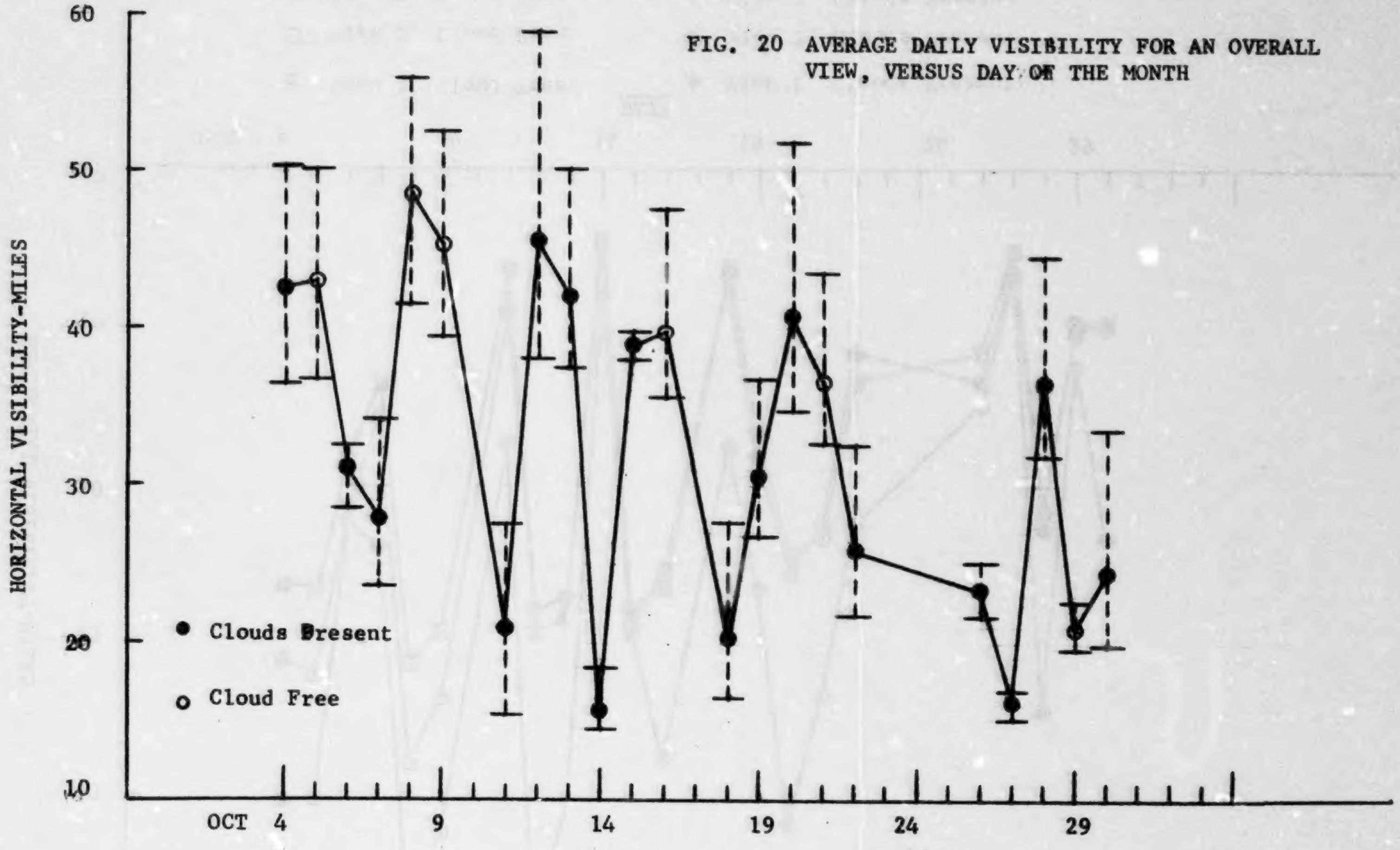

DATES: October 4 - 30, 1976
STANTON, NORTH DAKOTA

FIG. 21 AVERAGE HOURLY VISIBILITY FOR THREE VIEWS

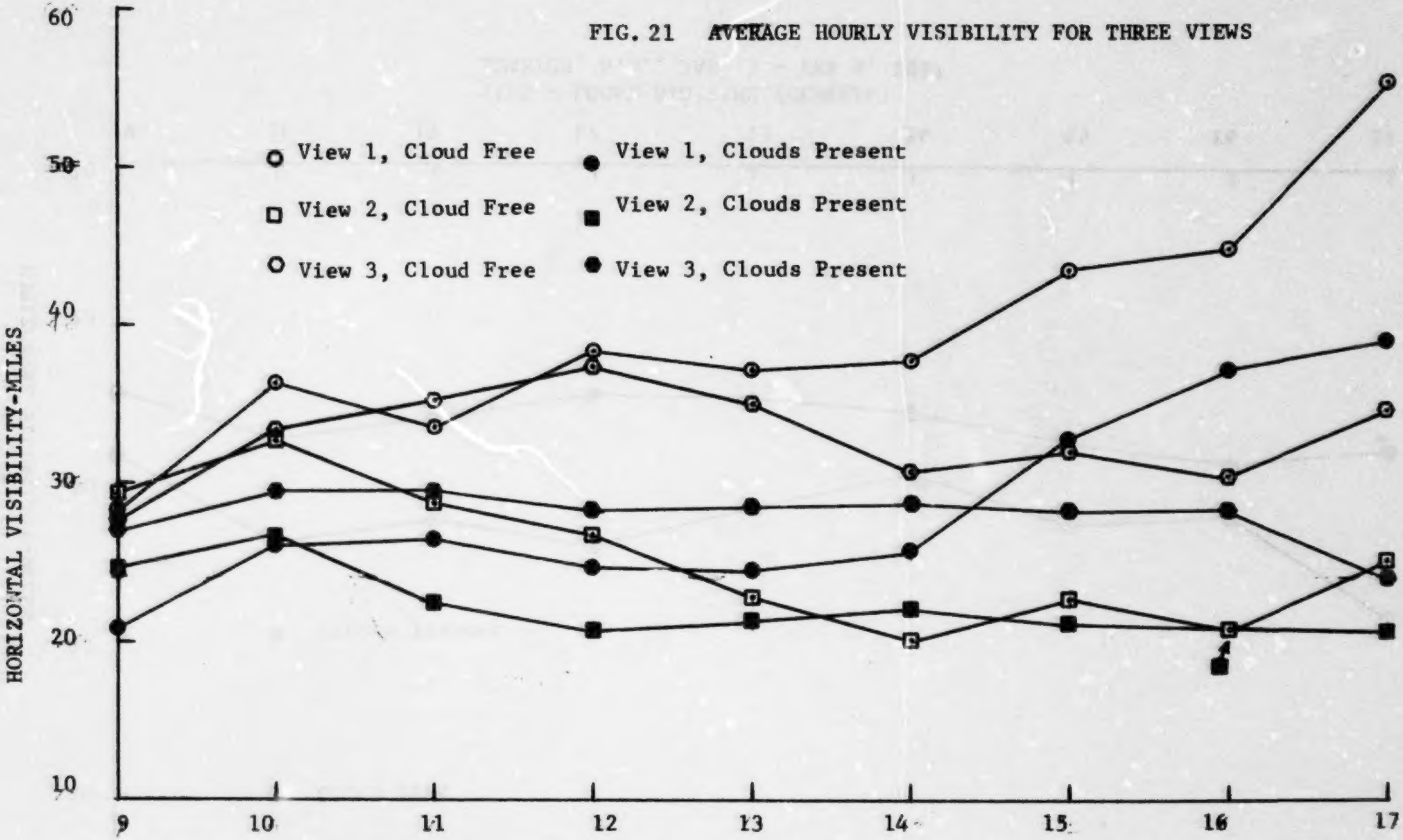

STANTON, N.D., JAN 13 - FEB 9, 1977

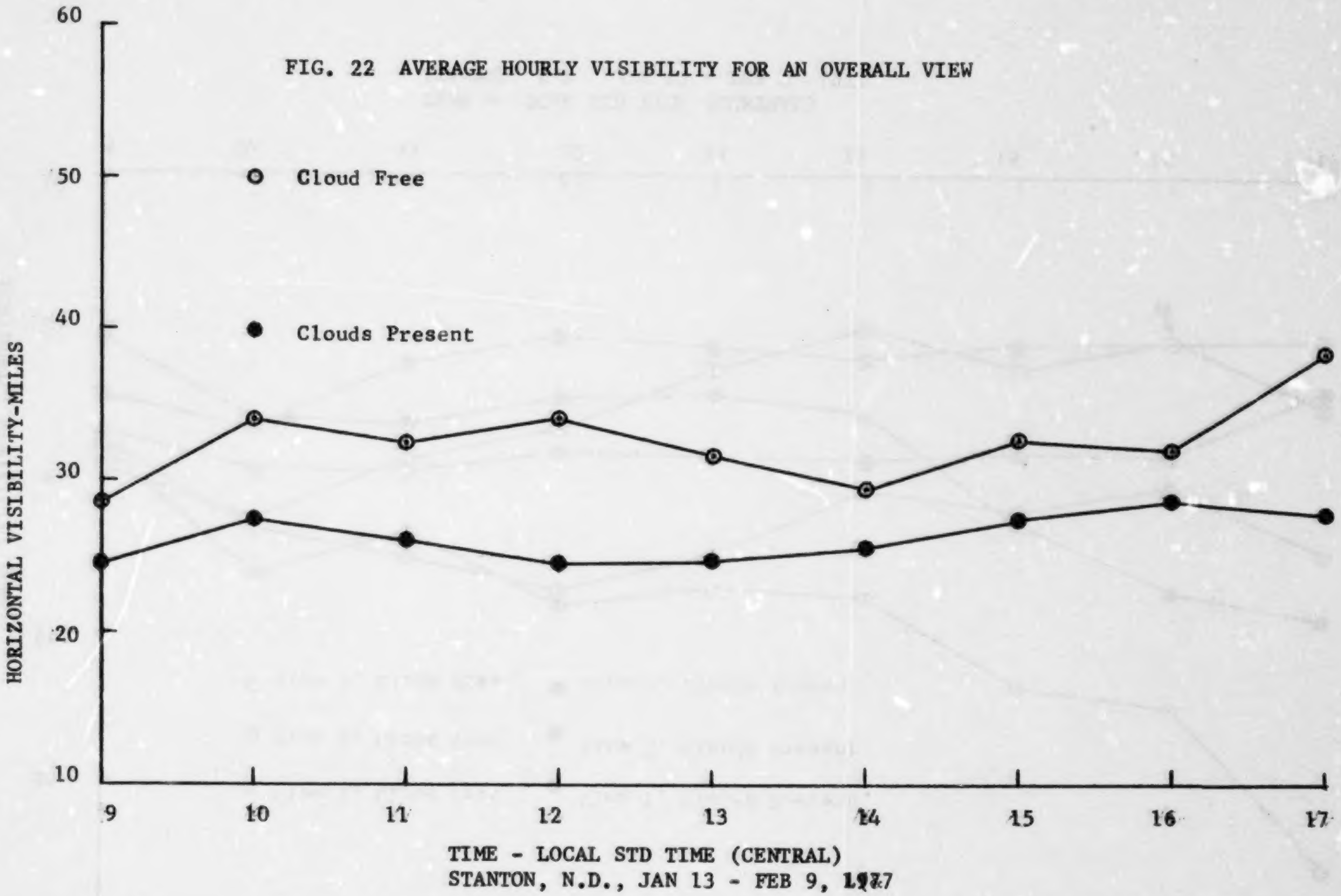
FIG. 22 AVERAGE HOURLY VISIBILITY FOR AN OVERALL VIEW

FIG. 23 AVERAGE DAILY VISIBILITY FOR THREE VIEWS

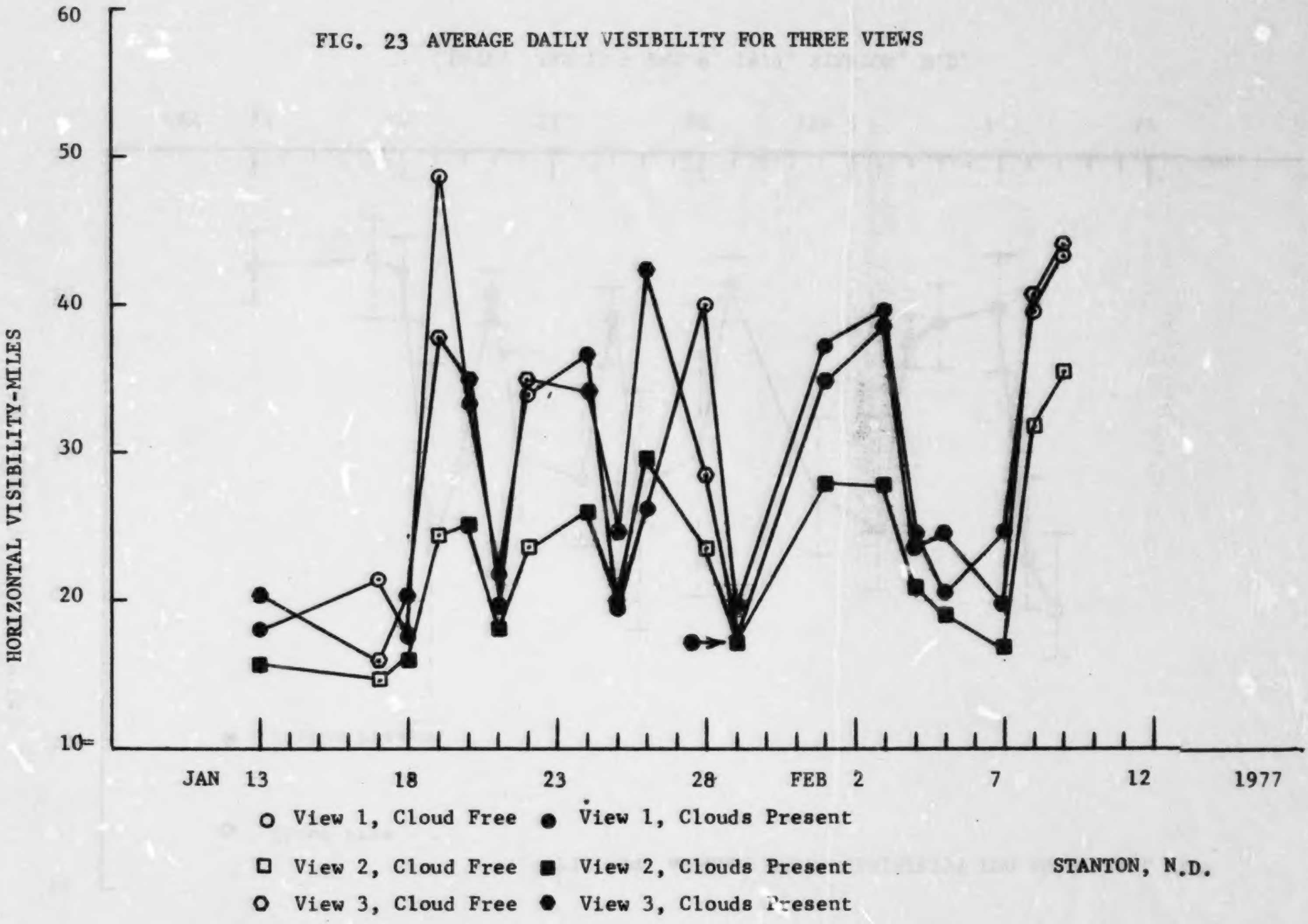

STANTON, N.D.

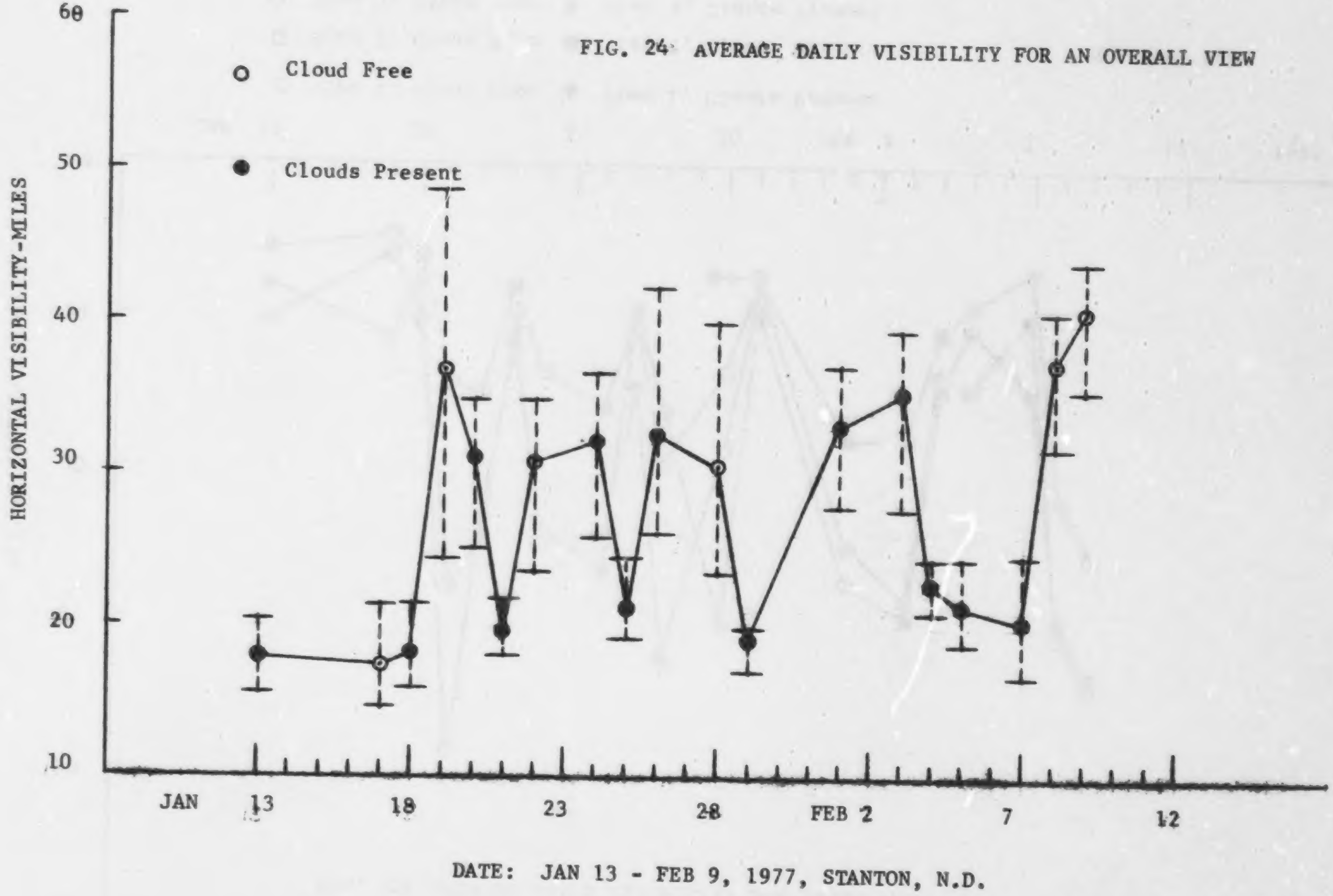

FIG. 24 AVERAGE DAILY VISIBILITY FOR AN OVERALL VIEW

FIG. 25 AVERAGE HOURLY VISIBILITY FOR AN OVERALL VIEW, FOR JULY, OCTOBER, APRIL, AND JANUARY, STANTON, N.D., 1976-77

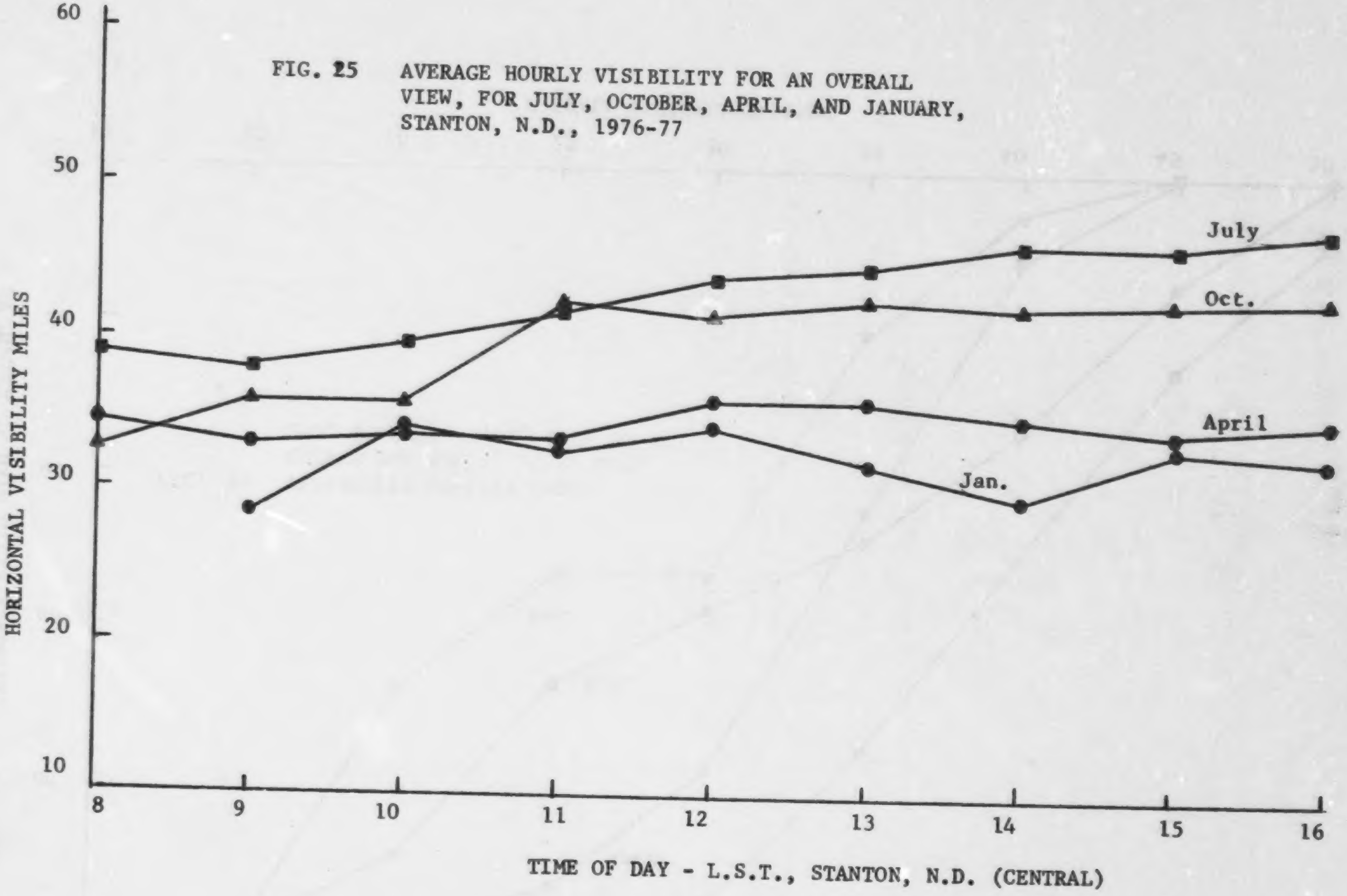

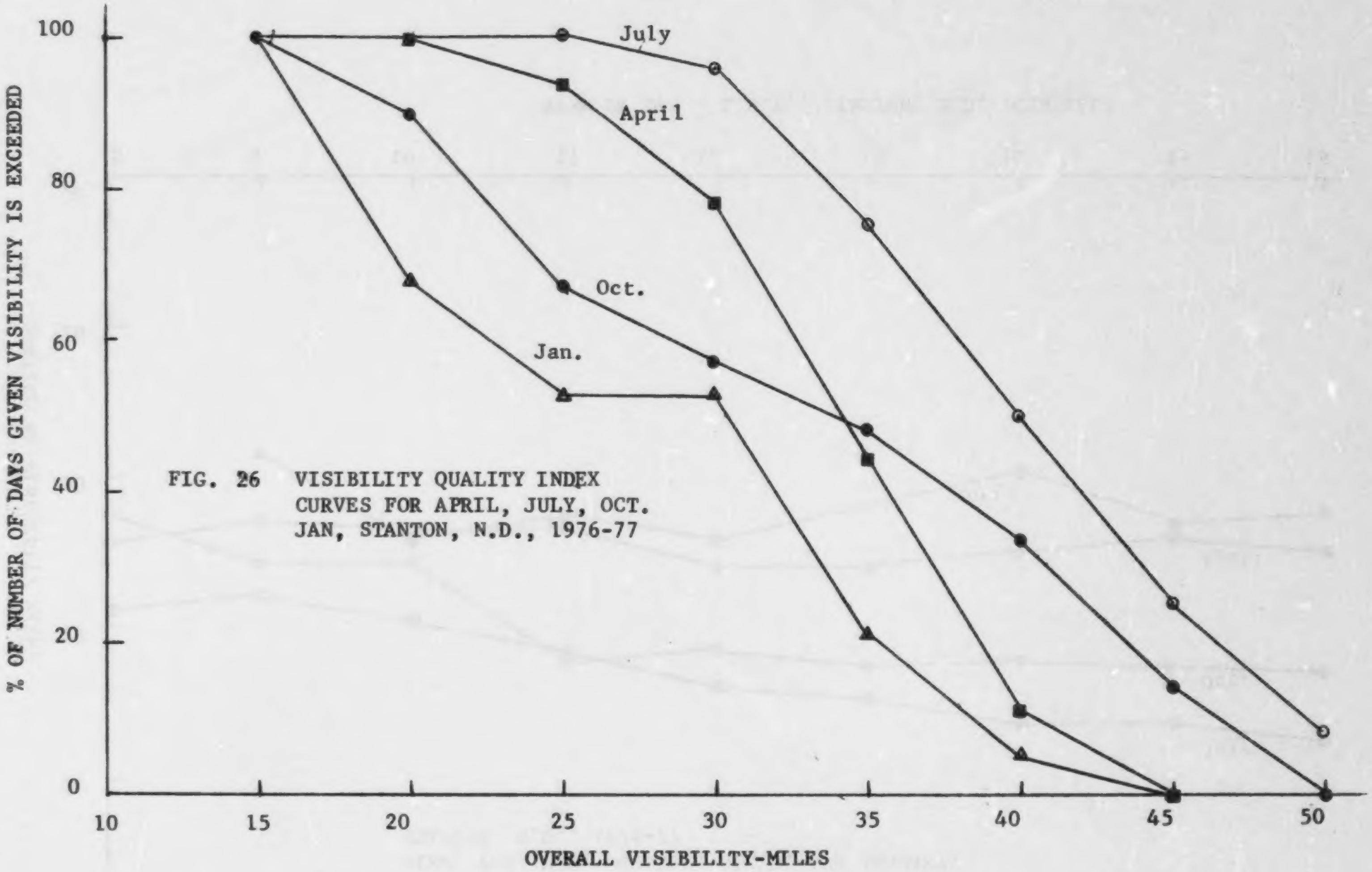

FIG. 26 VISIBILITY QUALITY INDEX CURVES FOR APRIL, JULY, OCT. JAN, STANTON, N.D., 1976-77

5. Atmospheric Vertical Optical Attenuation

5.1 Techniques/Instrumentation Used - The basic technique used to determine optical attenuation coefficients was that of solar photometers/radiometry and Beer's/Lambert's law. This relationship between solar photometer/radiometer measurements and the atmospheric optical attenuation coefficient is as follows:

$$M = M_o e^{-\tau m} \qquad (18)$$

where M is the meter reading/intensity of the direct (collimated) solar beam at the bottom of the atmosphere, M_o is the meter reading/intensity at the "top" of the atmosphere, m is the relative air mass, and τ is the optical attenuation coefficient. Hence, the optical attenuation coefficient may be derived by

$$\tau = -(\ln M/M_o)/m \qquad (19)$$

where M is the measured quantity. The relative air mass may be calculated by $\sec\theta_o$, where θ_o is the solar zenith angle (see Figure 2), for zenith angles from 0 to 60^o (air masses of 1.00 to 2.00). For greater zenith angles, atmospheric refraction has to be considered by the following expressions:

If $2.0 < \sec\theta_o < 3.0$

$$m = \sec\theta_o - 3.93 \times 10^{-4} \sec\theta_o{}^{3.65}\, p/p_o \qquad (20)$$

If $3.0 < \sec\theta_o < 15.0$

$$m = \sec\theta_o - 8.6 \times 10^{-4} \sec\theta_o{}^{2.96}\, p/p_o \qquad (21)$$

where p = site pressure, p_o = sea level pressure.

The solar zenith angle may be calculated by the well known equation:

$$\cos\theta_o = \sin\phi \sin\delta + \cos\phi \cos\delta \cos(t) \tag{22}$$

where ϕ is the site latitude, δ is the solar declination, and t is the solar hour angle. A computer program incorporating all these parameters was used to calculate θ_o for any given time of day at Stanton, N.D. Obviously, the quantity M_o cannot be determined directly. Instead, M_o is determined by performing measurements of M versus air mass (times of day), and using this data to extrapolate to zero air mass to determine M_o, as illustrated in Figure 27.

The optical attenuation coefficient given in Equation No. 18 is defined as the total optical attenuation coefficient, τ. It is made up of optical attenuation coefficients due to molecular scattering, τ_m, aerosol scattering, τ_a, and gaseous absorption, τ_{ab}. Hence,

$$\tau = \tau_m + \tau_a + \tau_{ab} \tag{23}$$

where τ_{ab} is also made up of components due to water vapor, ozone, carbon dioxide, etc, depending upon the wavelength region being considered.

The specific optical attenuation coefficients addressed for Stanton, N.D., were the total and the aerosol coefficients. The total attenuation coefficient was determined as discussed previously (Equation 18), and the aerosol attenuation coefficient was determined by

$$\tau_a = \tau - \tau_m - \tau_{O_3} \tag{24}$$

where $\tau(O_3)$ was determined by models given by Elterman* along with τ_m. The specific wavelengths considered were 0.380, 0.440, 0.500,

---

*Ref. 2: Elterman, 1970, "Vertical-attenuation Model with 8 Surface Meteorological Ranges 2 to 13" AFCRL-70-0200, 31 ERP No. 318

FIG. 27 EXAMPLE OF PLOTS TO DETERMINE EXTRATERRESTRIAL METER READING OF PHOTOMETER/RADIOMETER

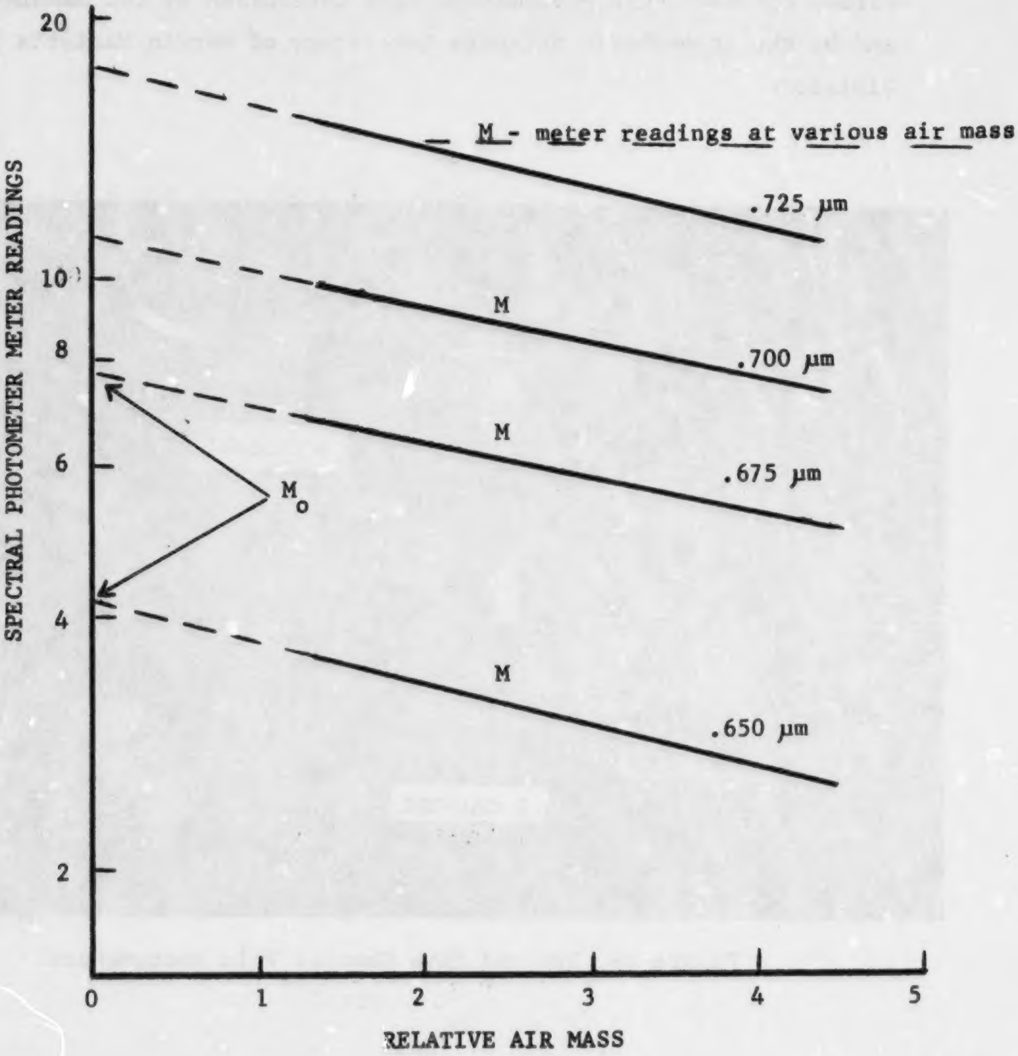

0.640, and 0.880 μm. These wavelengths are those of the 2 channel and 5 channel Volz photometers (see Figure 28). The 2 channel Volz photometer wavelengths are 0.380 and 0.500 μm. The 5 channel Volz photometer wavelengths are 0.440, 0.500, 0.640, 0.880, and 0.940 um. The fifth channel of Volz 5 channel photometer (0.940 um) is the center of a water vapor absorption band and is used, as discussed later, to derive total atmospheric water vapor content. The M_o values for both Volz photometers were determined by the manufacturer and by the Atmospheric Sciences Laboratory of Martin Marietta Denver Division.

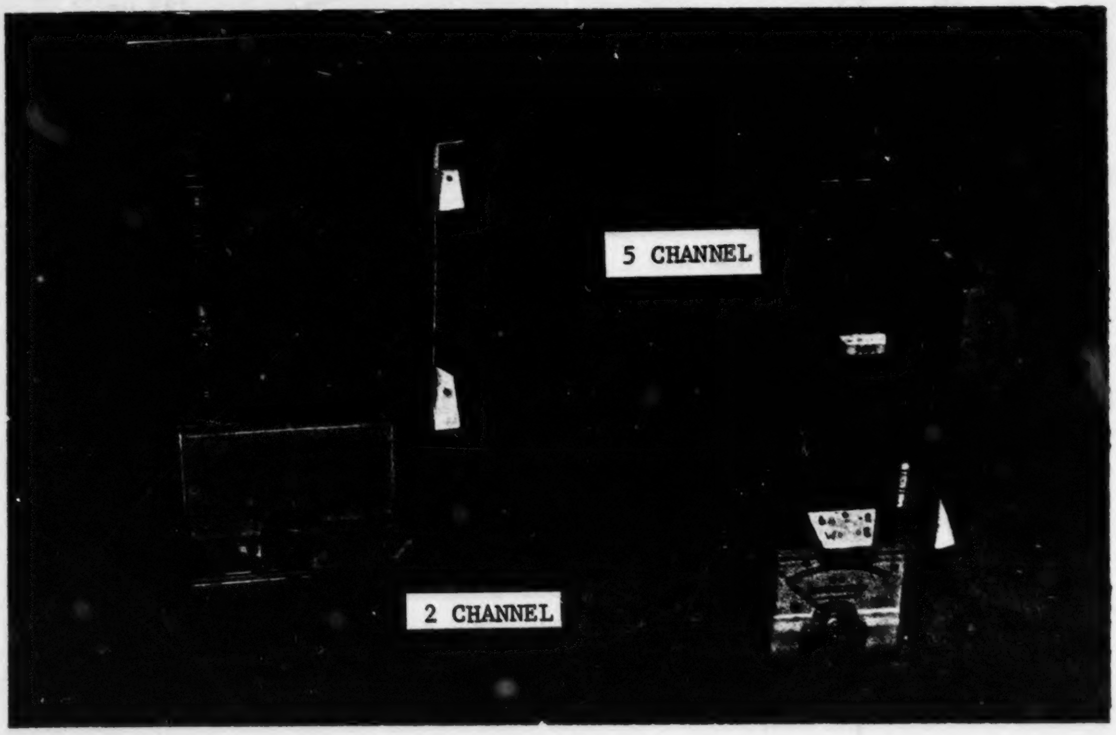

Figure 28 Two and Five Channel Volz Photometers

In addition to the Volz spectral photometry determinations of the optical attenuation coefficients, a broadband absolute radiometer was used to measure the 0.30 to 2.8 μm region. This radiometer (see Figure 29) is manufactured by Eppley labs and has a 5.5° field of view. It was used to measure the direct solar beam. The field setup of the instruments discussed above is shown in Figure 30.

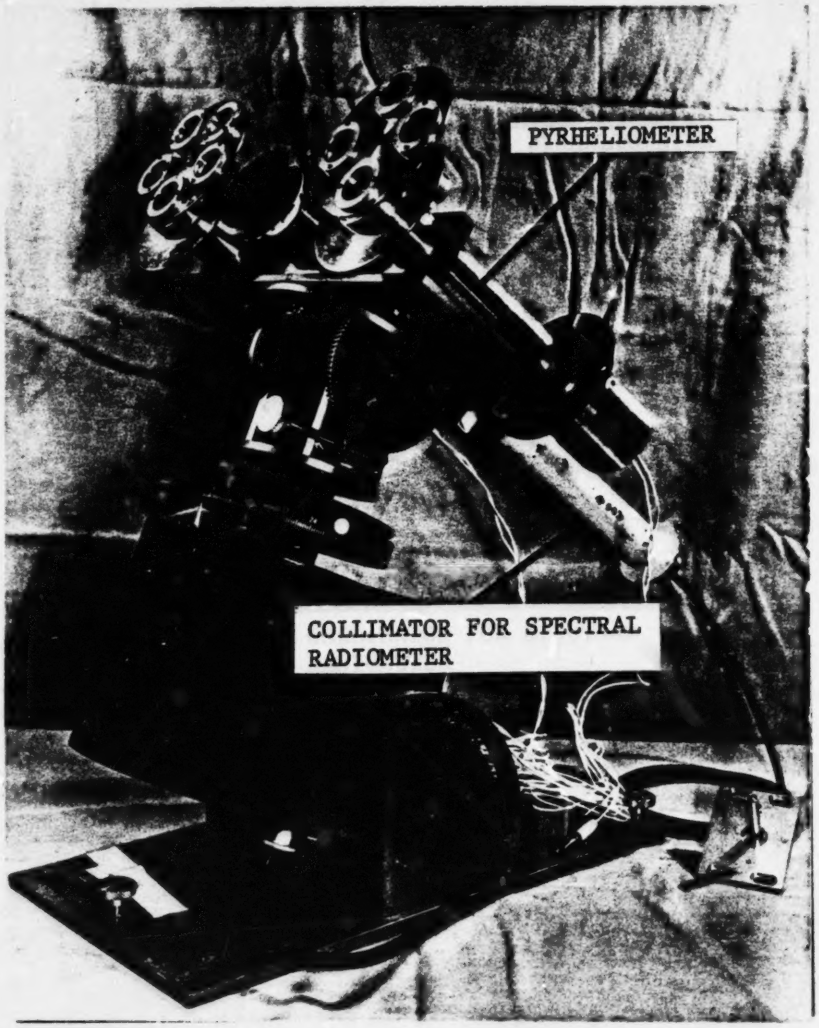
PYRHELIOMETER
COLLIMATOR FOR SPECTRAL RADIOMETER

Figure 29 Eppley Pyrheliometers and Collimator for Spectral Radiometer

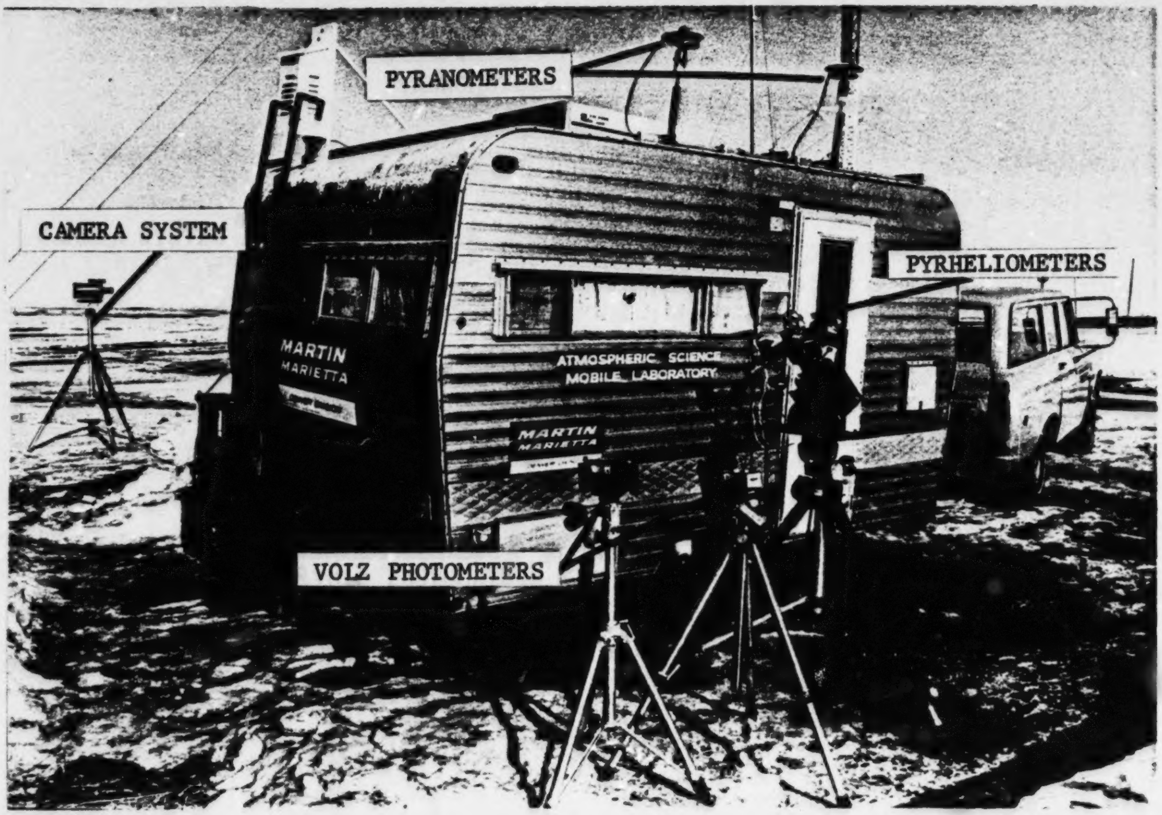
PYRANOMETERS
CAMERA SYSTEM
PYRHELIOMETERS
MARTIN MARIETTA
ATMOSPHERIC SCIENCE MOBILE LABORATORY
MARTIN MARIETTA
VOLZ PHOTOMETERS

Figure 30 Field Setup of Total Data Collection System

Because absolute solar intensities are used in this case, the M_o and M terms given in Equation No. 18 are replaced by I_o and I; where I_o is the absolute extraterrestral solar irradiance ("Solar constant"), and I is the absolute measured solar irradiance.

The baseline vertical atmospheric optical attenuation coefficients established were as follows:

(1) Daily average optical attenuation coefficients for the wavelengths of 0.380, 0.440, 0.500, 0.640, 0.880, and 0.30 to 2.8 micrometers.

(2) Daily average aerosol optical attenuation coefficients versus wavelengths for the wavelengths of 0.380, 0.440, 0.500, 0.640 and 0.880 micrometers.

(3) Average hourly aerosol optical attenuation coefficient at 0.640 mircometers.

(4) Average hourly broadband - 0.30 to 2.8 micrometers - optical attenuation coefficient.

5.2 April Optical Attenuation - The optical attenuation results for April are presented in Figures 31, 32, 33, 34 and 35. The daily average total optical attenuation coefficients, shown in Figure 31, represent three days - April 5, 6 and 8 - of cloud free condition, and two days - April 10 and 12 - of cloud present conditions. The remainder of the data collection days were overcast, allowing no direct solar measurements. Cloud free conditions represent days that had little or no clouds in any part of the sky; whereas, cloud present conditions represent days when there were clouds present in a significant portion of the sky. However, all measurements were made when the solar disc was not visibly obscured by clouds. As can be seen in Figure 31, the various days exhibit somewhat different optical attenuation at all wavelengths; and all wavelengths exhibit the same relative attenuation for the various days. The fact that the 380 micrometer channel has the greatest attenuation, with the 0.440, 0.500, 0.640 and 0.880 following, is due to the wavelength selective scattering by molecules (Rayleigh) and aerosols (Mie). The 0.3 to 2.8 micrometer band is a broadband that experiences attenuation due to both molecular and aerosol scattering but also includes the well known strong attenuation due to water vapor absorption in the near infrared wavelengths, 0.7 to 2.8 μm. Therefore, this band cannot be directly compared to the narrow bands, where molecular and aerosol scattering dominate. As discussed in section 5.1, the molecular scattering component may be subtracted, along with the ozone absorption component, to yield the optical attenuation due to atmosphere aerosols.

This aerosol optical attenuation coefficient is most indicative of the atmospheric clarity. The daily average aerosol optical attenuation coefficient is shown in Figure 33. It can be seen that the cloud present conditions result in a significantly higher attenuation, especially in the shorter wavelengths. This higher attenuation is most likely due to the presence of thin portions of clouds, especially cirrus clouds, that obscure the solar disc. The cloud free conditions display similar aerosol optical attenuation, on the order of 0.11. The average hourly aerosol attenuation at 0.640 μm is shown in Figure 34. No readily apparent hourly dependence exists, with a representative value of about 0.11. The average hourly broadband optical attenuation is shown in Figure 35. This parameter displays a slight hourly dependence, with the maximum occurring near the middle of the day. The values range from 0.22 to 0.34.

5.3 July Optical Attenuation - The July optical attenuation results are shown in Figures 36, 37, 38, 39 and 40. As compared to April, July had a greater number of sunny days which allowed many more determinations of optical coefficients, shown in Figure 36, which show some day-to-day variations for all wavelengths. The designation of partly cloudy signifies a day where clouds were present but did not obscure the solar disc. The designation of cloudy signifies a day where clouds were present and did, at times, obscure the solar disc. The greatest optical attenuations for clear days occurred on July 12 and Aug. 7. The daily average aerosol optical attenuation coefficient results shown in Figure 37, show noticeable daily fluctuations. For example, at the .380 μm wavelength, the clear days exhibit variations between

0.30 to 0.18. In addition, it can be seen that the various wavelengths do not necessarily "track" each other from day-to-day. The reason for this is shown in Figure 38. The wavelength dependence of the aerosol optical attenuation coefficient, as shown in Figure 38, exhibits changes from day-to-day. For example, the Aug. 7 data indicates what is known as a "negative" slope wavelength dependence. This type of wavelength dependence is caused by a dominance of small particles. The July 17 results indicate a "positive" slope wavelength response, which is indicative of a dominance of larger particles. From Figure 38, it can be seen that July 16, 17, 23 and 26 were similar days having low optical attenuation and a dominance of larger particles. On the other hand, Aug. 6 and 7 displayed higher optical attenuation with a dominance of small particles. The average hourly aerosol optical attenuation, for 0.640 μm, results, shown in Figure 39, display a slight hourly dependence with the maximum occurring from noon to afternoon. In addition, large variations can occur for any given hour. For example, at 1600 hours, the variation can be from 0.105 to 0.230 (a factor of 2.2). The average hourly broadband optical attenuation coefficient results, shown in Figure 40, display a similar hourly dependence, with maximums occurring in the noon-afternoon period.

5.4 October Optical Attenuation - The optical attenuation coefficient results for October are shown in Figures 41, 42, 43 and 44. A total of seven (7) days of measurements were acquired. Of these seven days, no day was completely clear. Cirrus clouds were a very common occurrence, however, as mentioned previously, measurements were made only when the solar disc appeared to be free of any cloud obscuration. The daily average total optical attenuation results, shown in Figure 41, display day-to-day variations. The degree of these variations is dependent upon wavelength. For example, the 0.440 μm data show much more marked daily variations than the 0.880 μm data. The reason for this is shown in Figure 42. As with the July data, it can be seen that "negative" slope/small particle and "positive" slope/large particle were present. As shown in Figure 42, this results in large differences in aerosol optical attenuation at the shorter wavelengths, and smaller differences at the longer wavelengths. For example, at 0.440 μm there exists a difference of 0.035 - 0.163 between Oct. 8 and Oct. 21, respectively; whereas, for 0.880 μm, there exists a difference of 0.07 - 0.11. This points out the need for measuring the aerosol optical attenuation at several wavelengths, over a range from short to long, to adequately define the attenuation properties. The average hourly aerosol optical attenuation coefficient, at 0.640 μm, results are shown in Figure 43. These results indicate a very minimal hourly dependence for aerosol attenuation. However, as with the July results, any particular hour may have a wide range of attenuation. Similar results are shown, Figure 44, for the average hourly broadband attenuation coefficient.

5.5 January Optical Attenuation - The January optical attenuation results are shown in Figures 45, 46, 47, 48 and 49. The daily average total optical attenuation, Figure 45, and the daily average aerosol optical attenuation, Figure 46, display daily fluctuation. This is especially true for the days of January 17 and 19. As can be seen, January 17 was a much more turbid day as compared to January 19. The daily average aerosol attenuation coefficient versus wavelength results, shown in Figure 47, show that all days except the 17th had a "positive" slope/large particle characteristic. The 17th was much more turbid and had a "negative" slope/small particle character. The average hourly aerosol optical attenuation coefficient, at 0.640 μm, results, Figure 48, show little hourly dependence but wide ranges of values for any given hour. The corresponding broadband results, Figure 49, show a slight decrease toward the late afternoon.

5.6 Seasonal Optical Attenuation Comparisons - The seasonal comparisons consist of the broadband optical attenuation coefficient, Figure 50, and the aerosol optical attenuation coefficient at 0.640 μm, Figure 51. As pointed out previously, the aerosol optical attenuation coefficient is dependent upon wavelength, with the greatest sensitivity at the shorter wavelengths. The 0.640 μm wavelength was chosen to be compromise between the short and long wavelengths. The average hourly broadband optical attenuations coefficient, Figure 50, shows that July had the highest vertical attenuation, followed by April, October, and January having the lowest attenuation. The 0.640 μm results, Figure 51, also display this seasonal ranking of vertical attenuation. The range between July and January, for both the broadband and 0.640 μm wavelengths, is quite large. For the broadband wavelength, July displays a typical value of 0.37 (at noon), compared to a value of 0.16 (at noon) for January. For the 0.640 μm band, July displays a typical value of 0.155 (at noon), compared to a value of 0.04 (at noon) for January. A comparison of the wavelength dependence of the aerosol optical attenuation coefficient at all months reveals that when conditions are such that the aerosol optical attenuation is low, "positive" slope/large particle distribution are also present. This indicates that small particles cause the overall attenuation to fluctuate from day-to-day. When the aerosol attenuation is high, the wavelength dependence of the attenuation indicates a "negative" slope/small particle characteristic. The various days are quite markedly defined by their wavelength dependence of the aerosol attenuation coefficient.

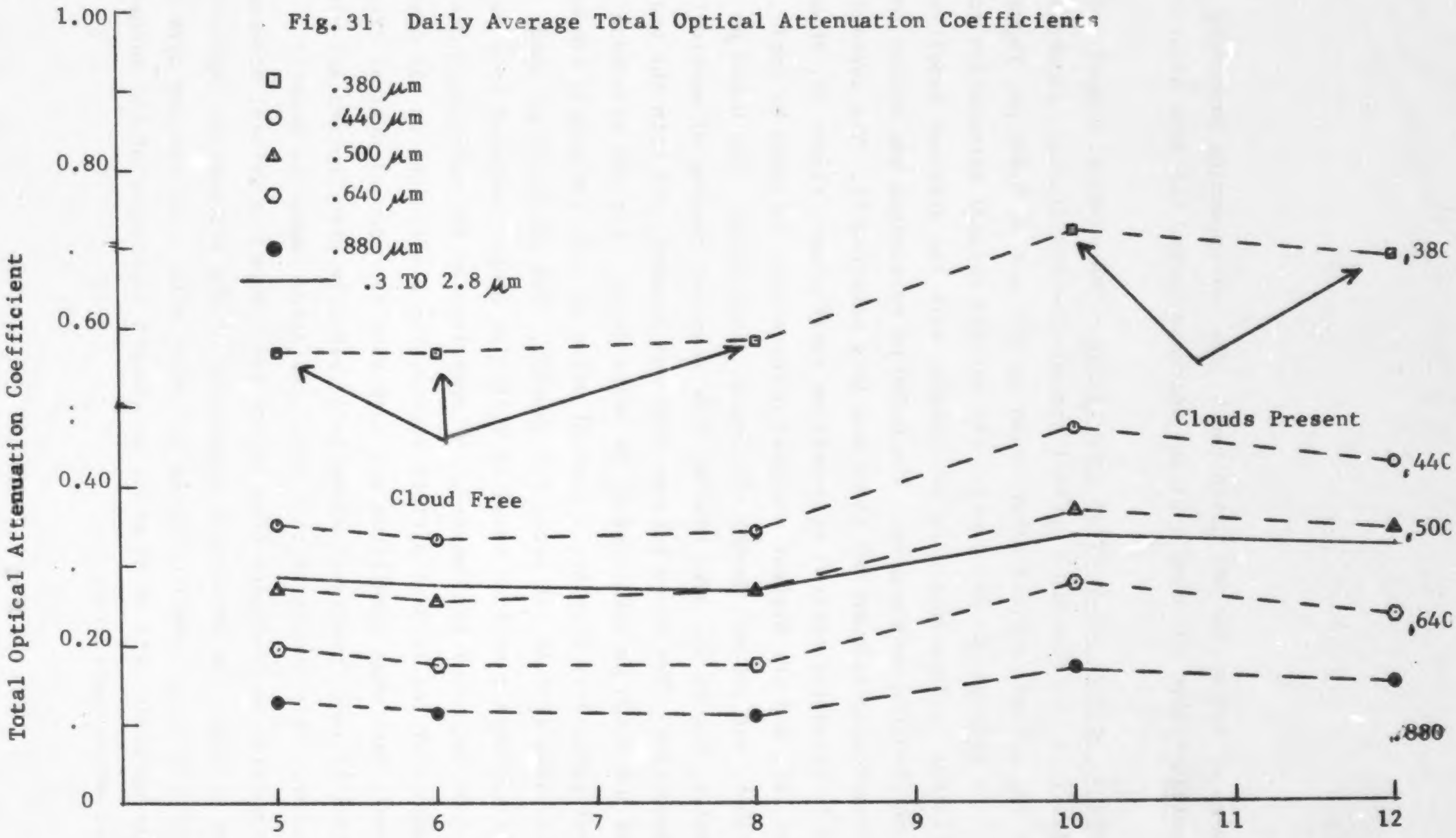

Fig. 31 Daily Average Total Optical Attenuation Coefficients

Date: April, 1976

Stanton, N.D.

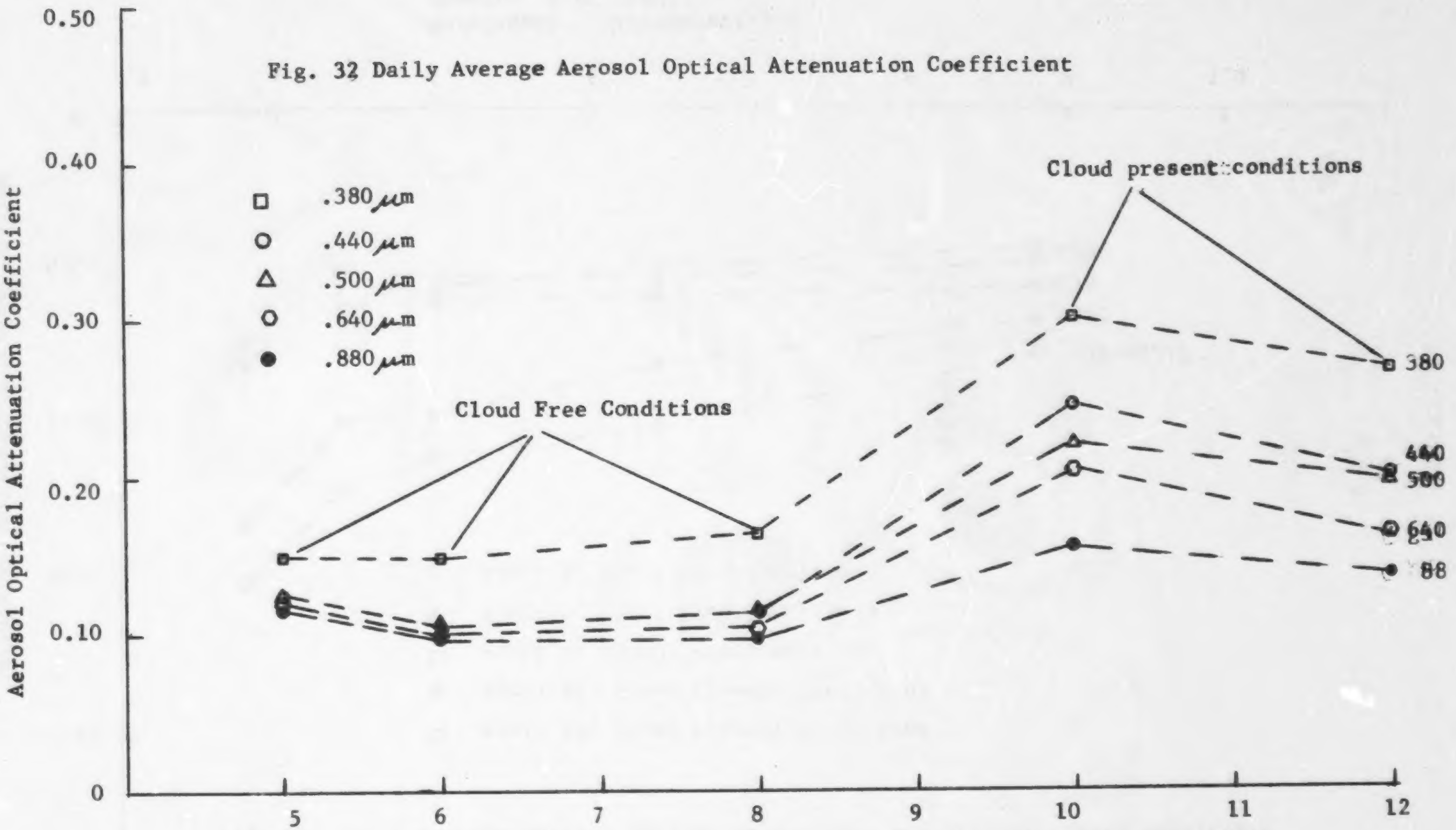

Fig. 32 Daily Average Aerosol Optical Attenuation Coefficient

Fig: 33 Daily Average Aerosol Optical Attenuation Coefficient Versus Wavelength

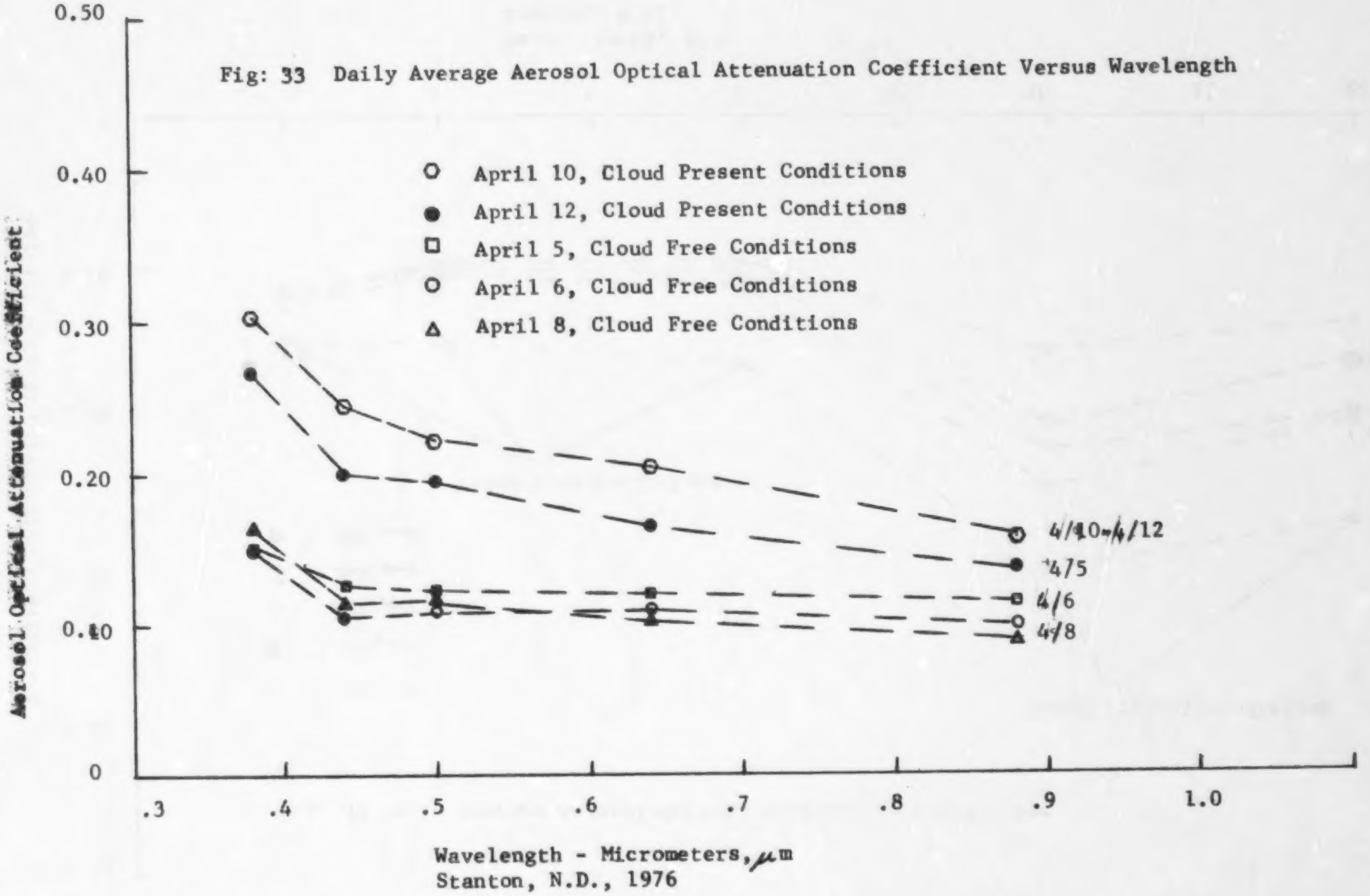

Fig. 34 Average Hourly Aerosol Optical Attenuation Coefficient for .640 μm.

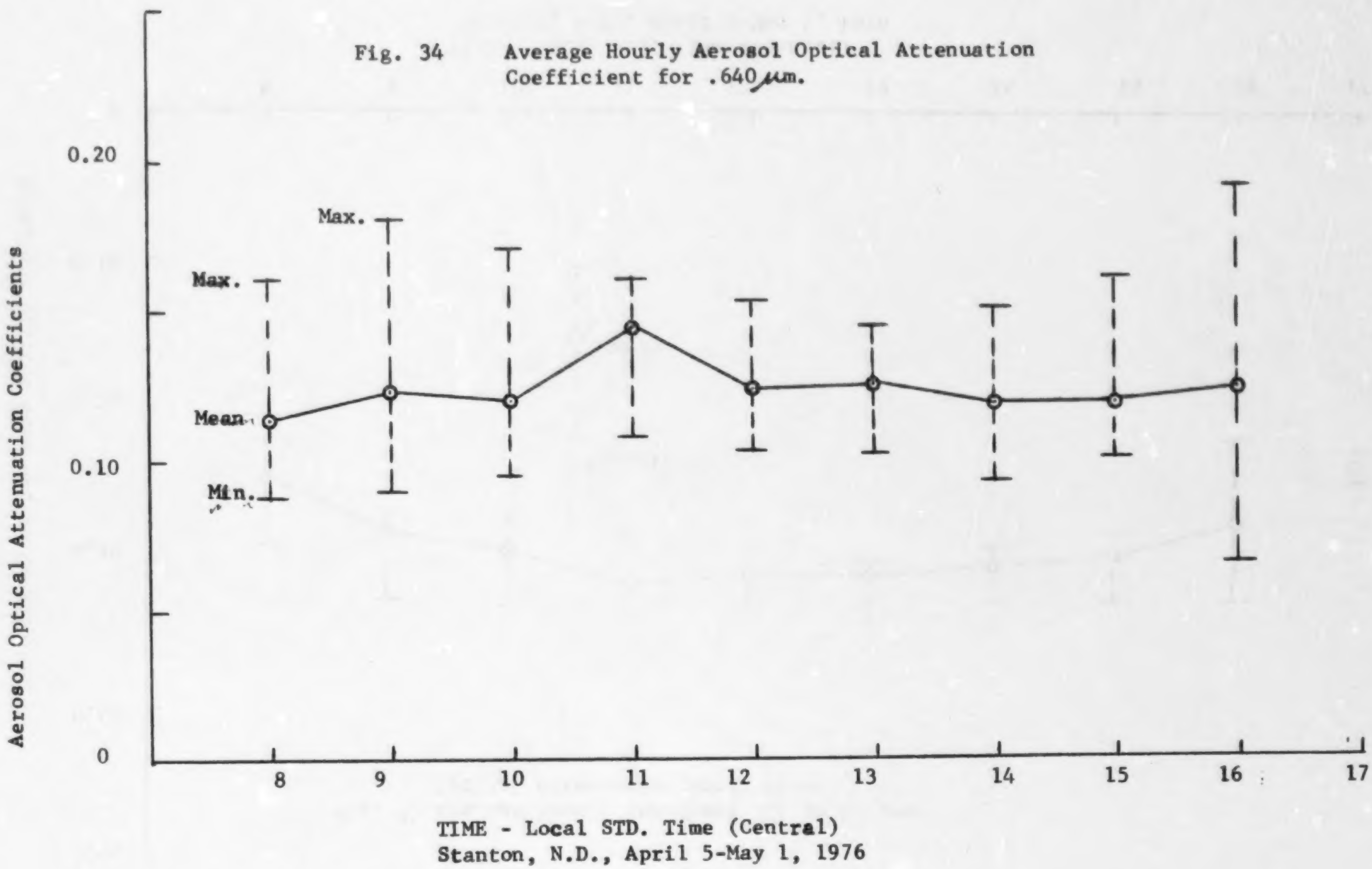

Fig. 35 Average Hourly Broadband (.3 to 2.8μm) Optical Attenuation Coefficient

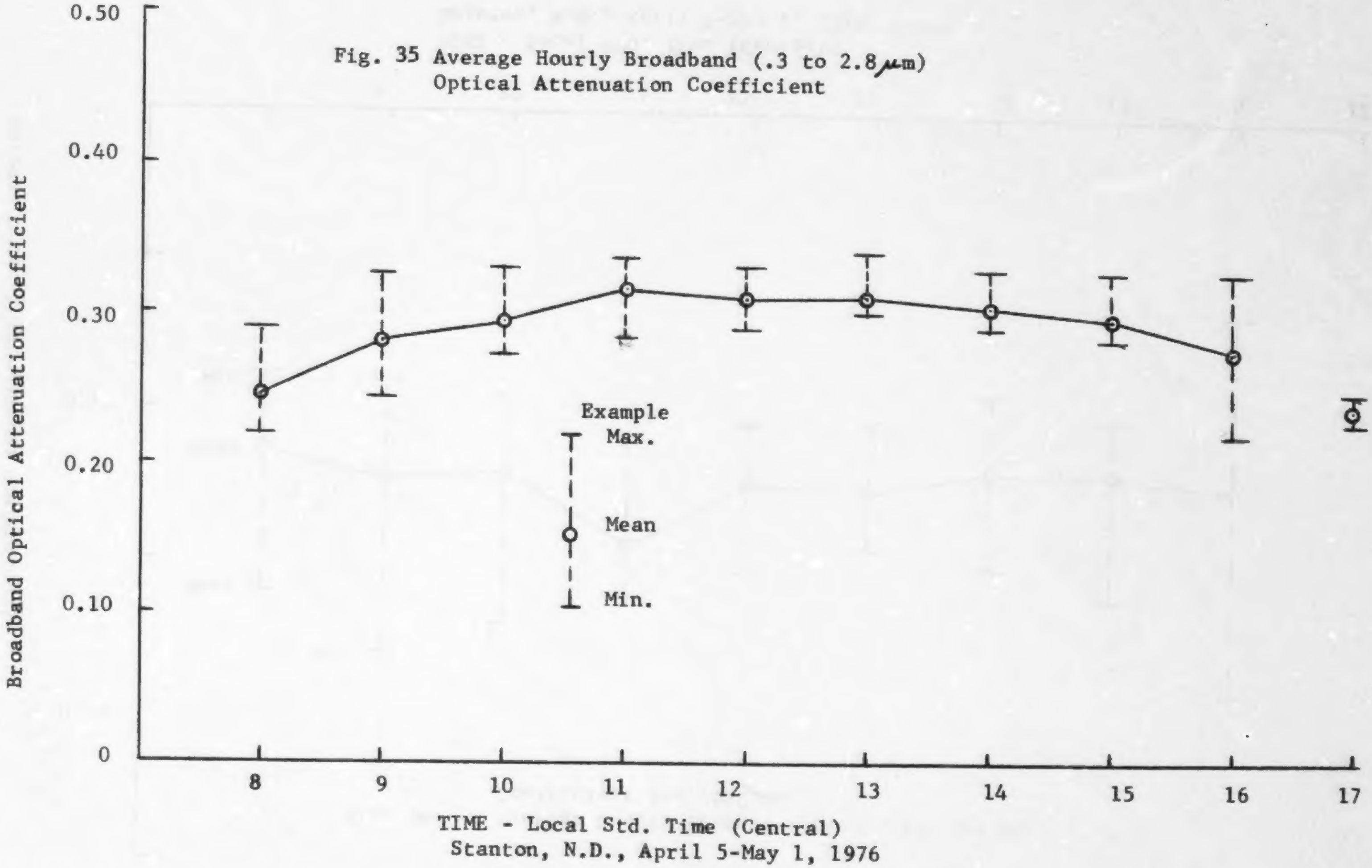

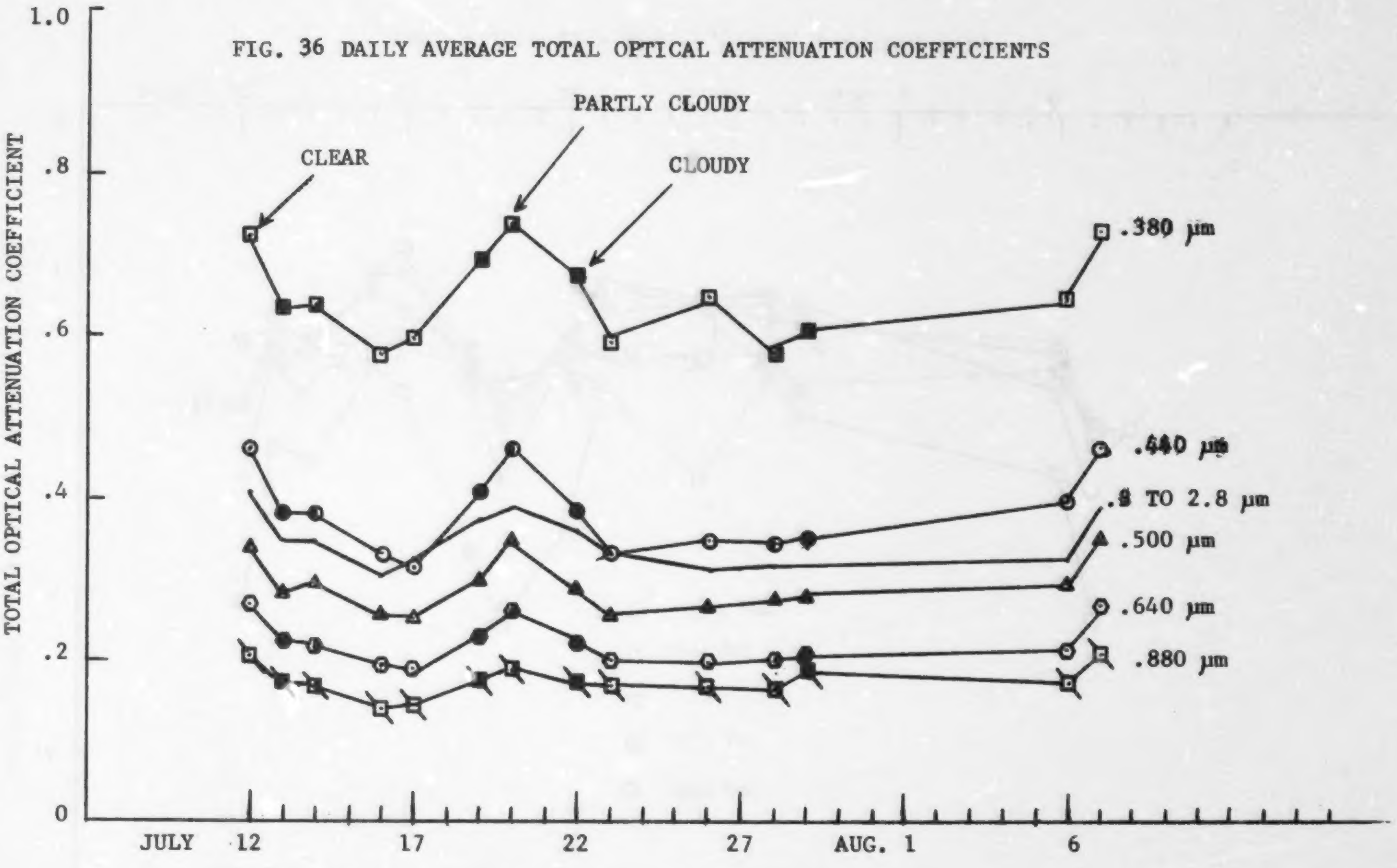

FIG. 36 DAILY AVERAGE TOTAL OPTICAL ATTENUATION COEFFICIENTS

DATE: JULY 12 - AUG. 17, 1976 STANTON, N.D.

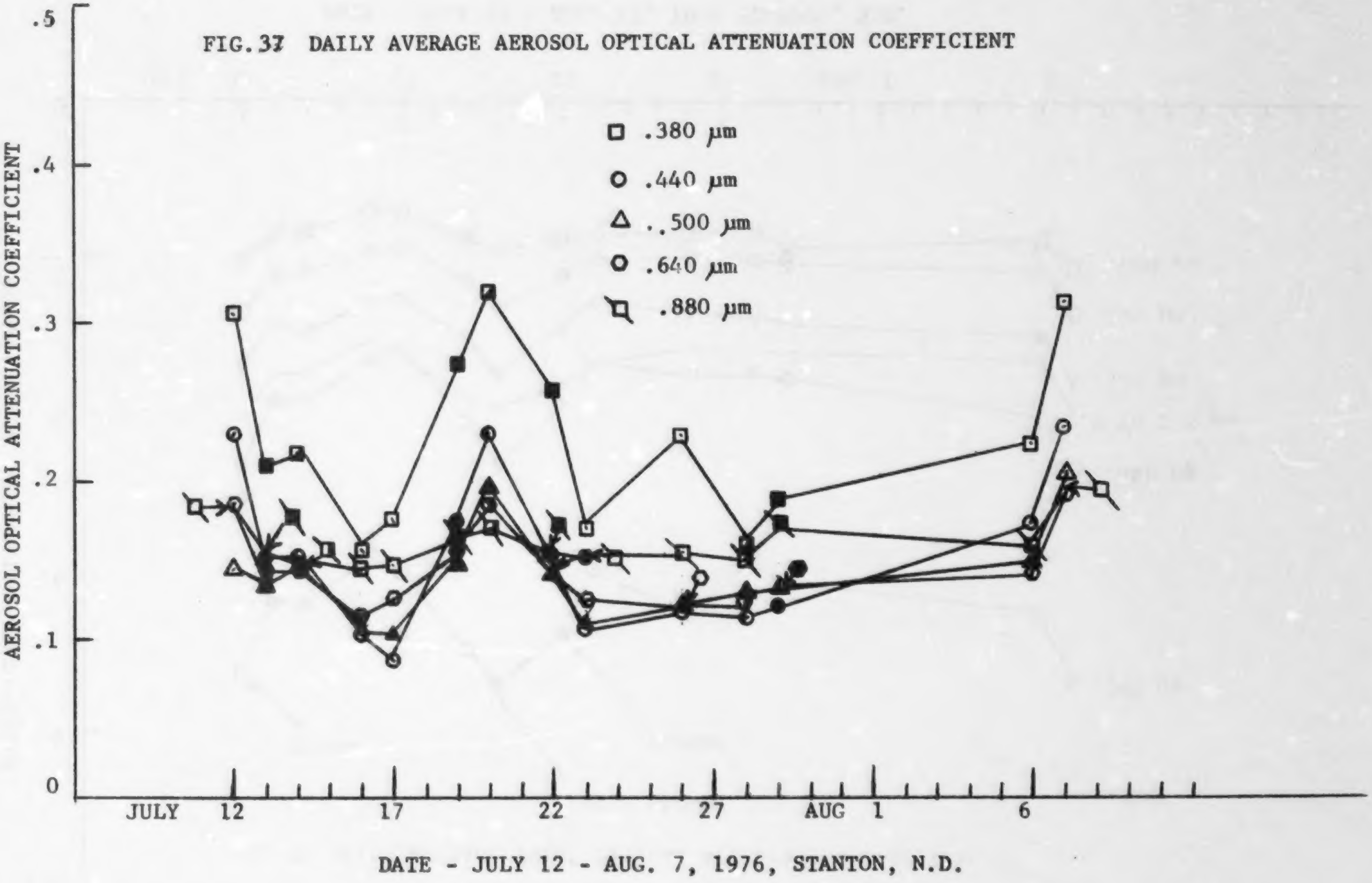

FIG.37 DAILY AVERAGE AEROSOL OPTICAL ATTENUATION COEFFICIENT

FIG. 38 DAILY AVERAGE AEROSOL OPTICAL ATTENUATION COEFFICIENT VERSUS WAVELENGTH

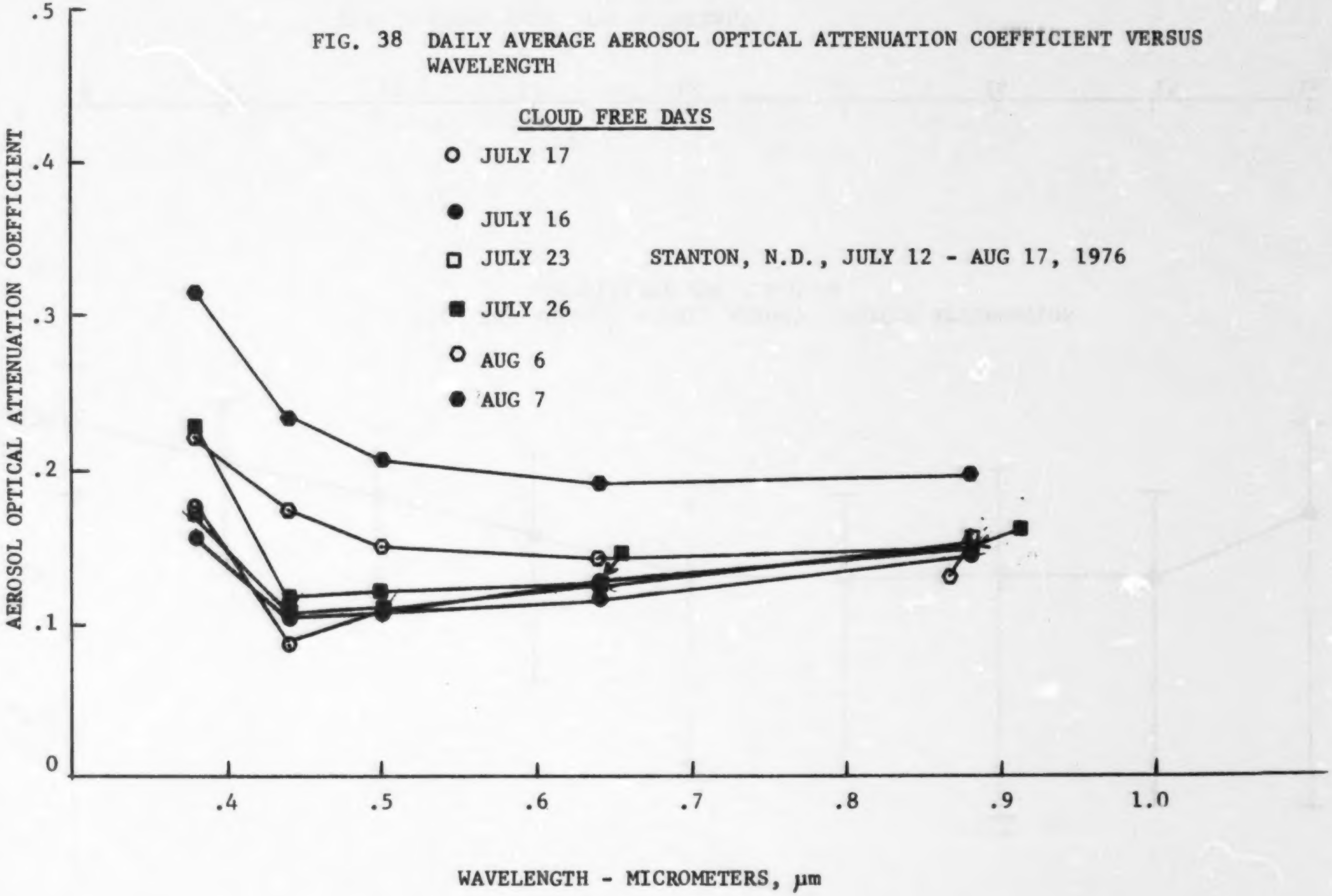

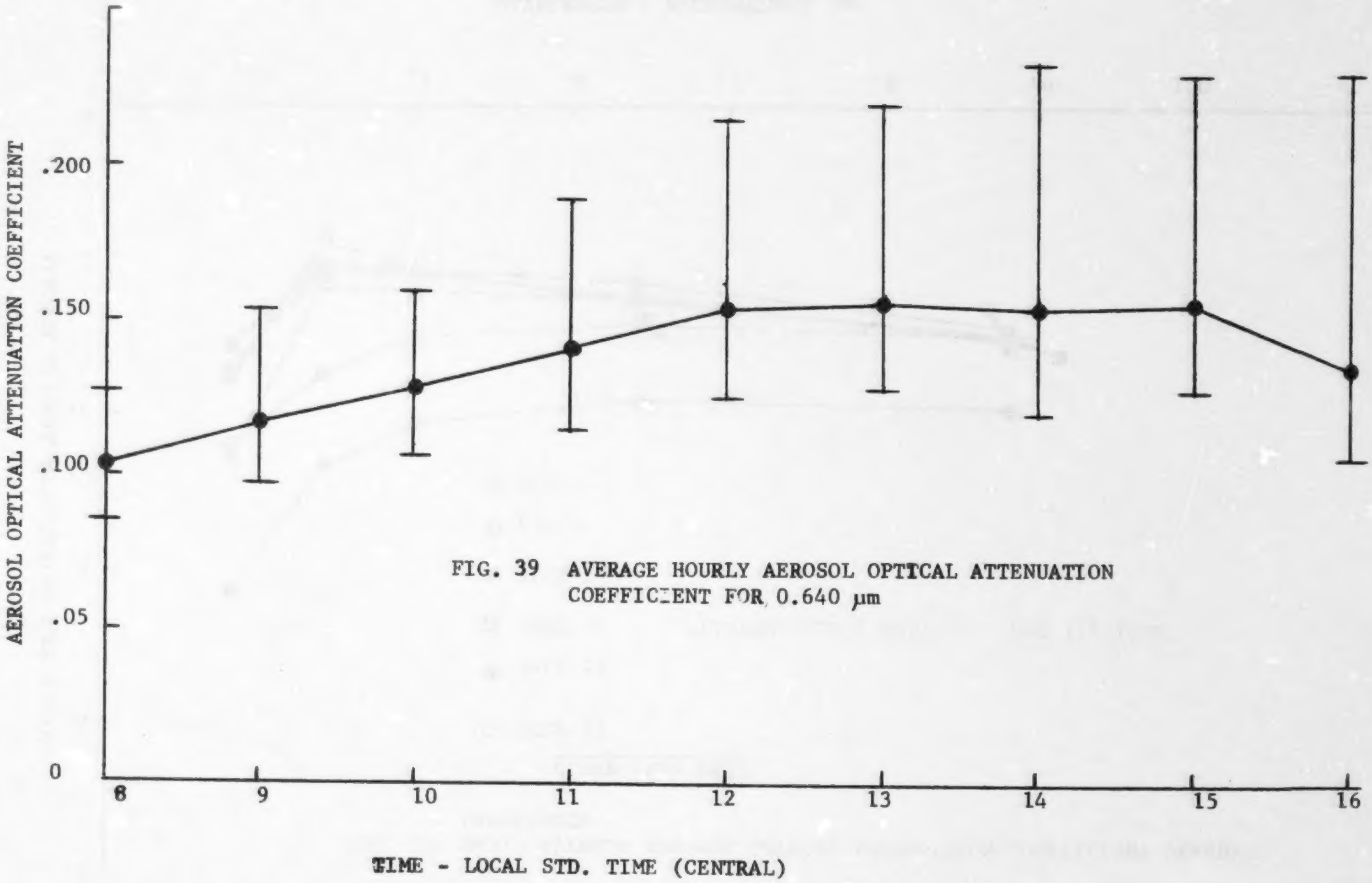

FIG. 39 AVERAGE HOURLY AEROSOL OPTICAL ATTENUATION COEFFICIENT FOR 0.640 μm

STANTON, N.D., JULY 12 - AUG. 7, 1976

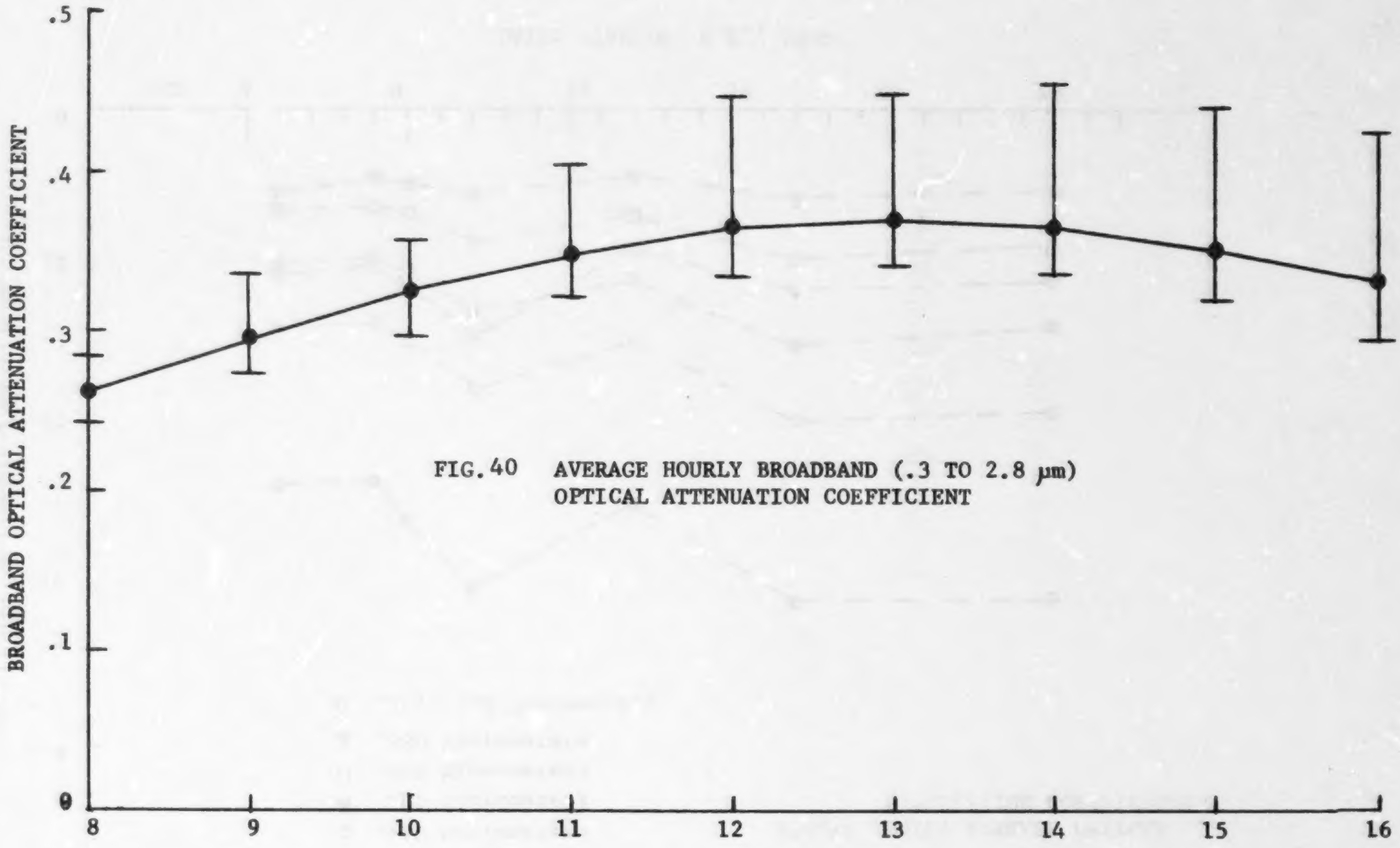

FIG. 40 AVERAGE HOURLY BROADBAND (.3 TO 2.8 μm) OPTICAL ATTENUATION COEFFICIENT

TIME - LOCAL STD. TIME (CENTRAL)
STANTON, N.D., JULY 12 - AUG 7, 1976

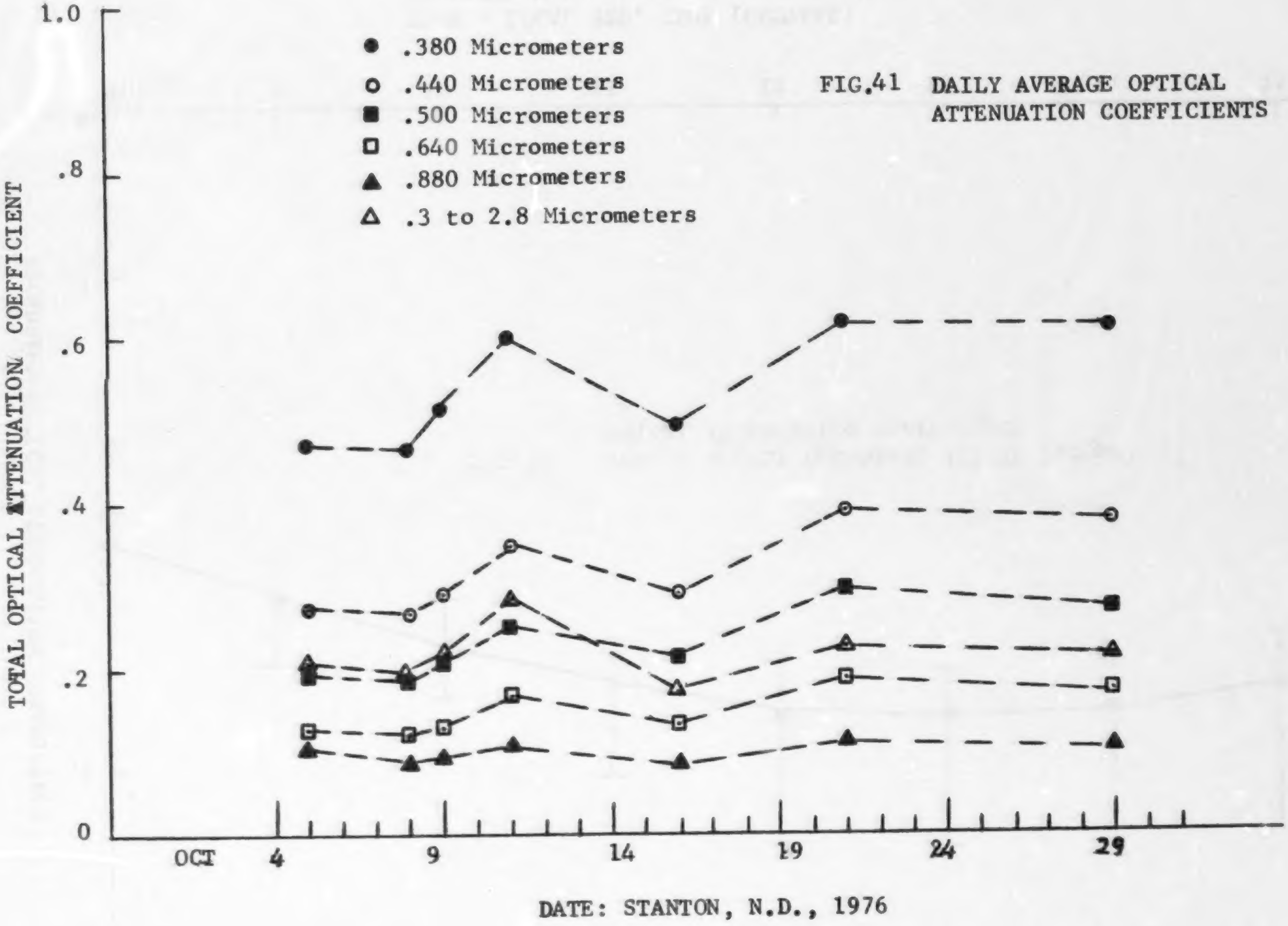

FIG.41 DAILY AVERAGE OPTICAL ATTENUATION COEFFICIENTS

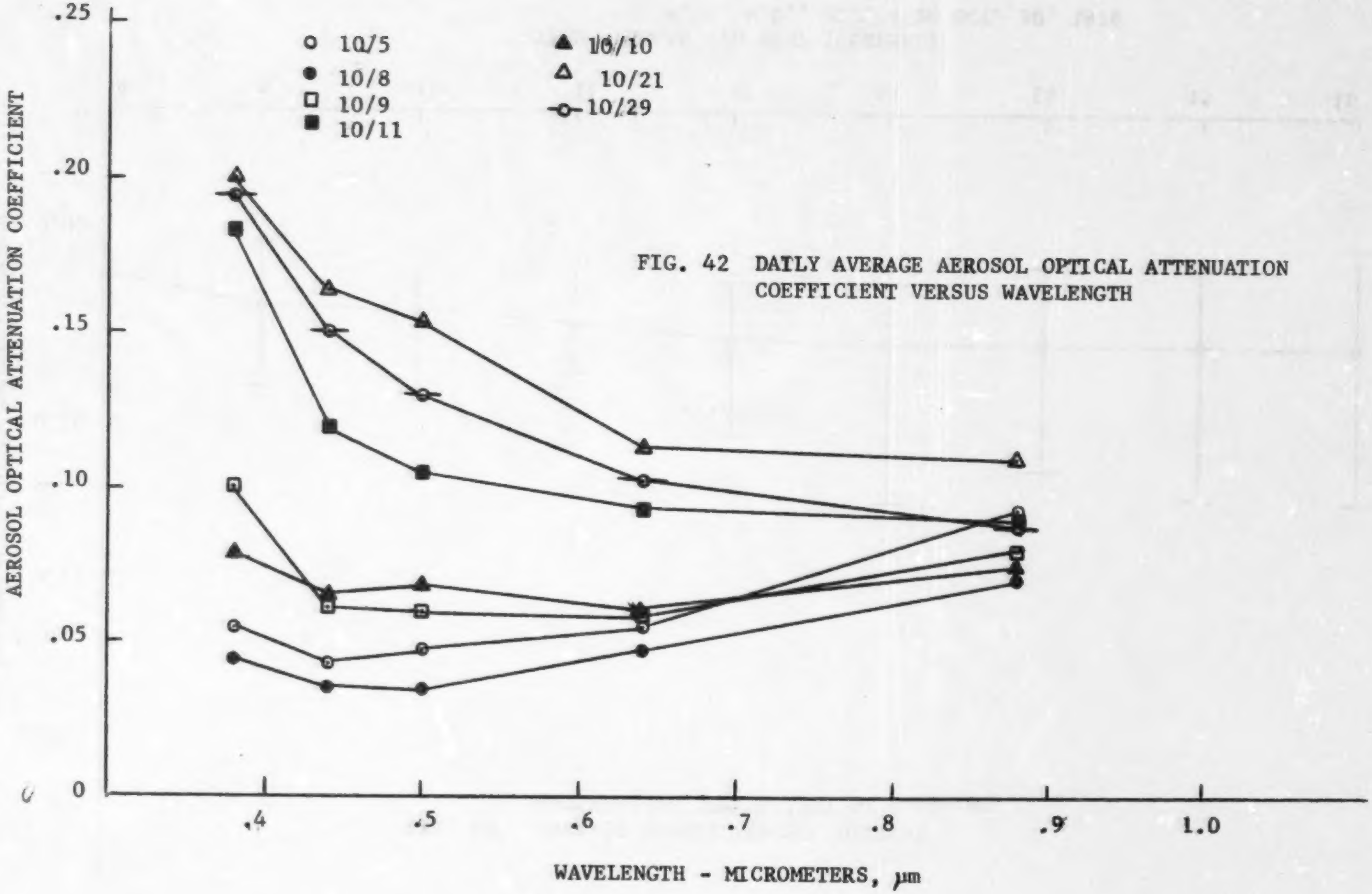

FIG. 42 DAILY AVERAGE AEROSOL OPTICAL ATTENUATION COEFFICIENT VERSUS WAVELENGTH

FIG. 43 AVERAGE HOURLY AEROSOL OPTICAL ATTENUATION COEFFICIENT AT 0.640 μm

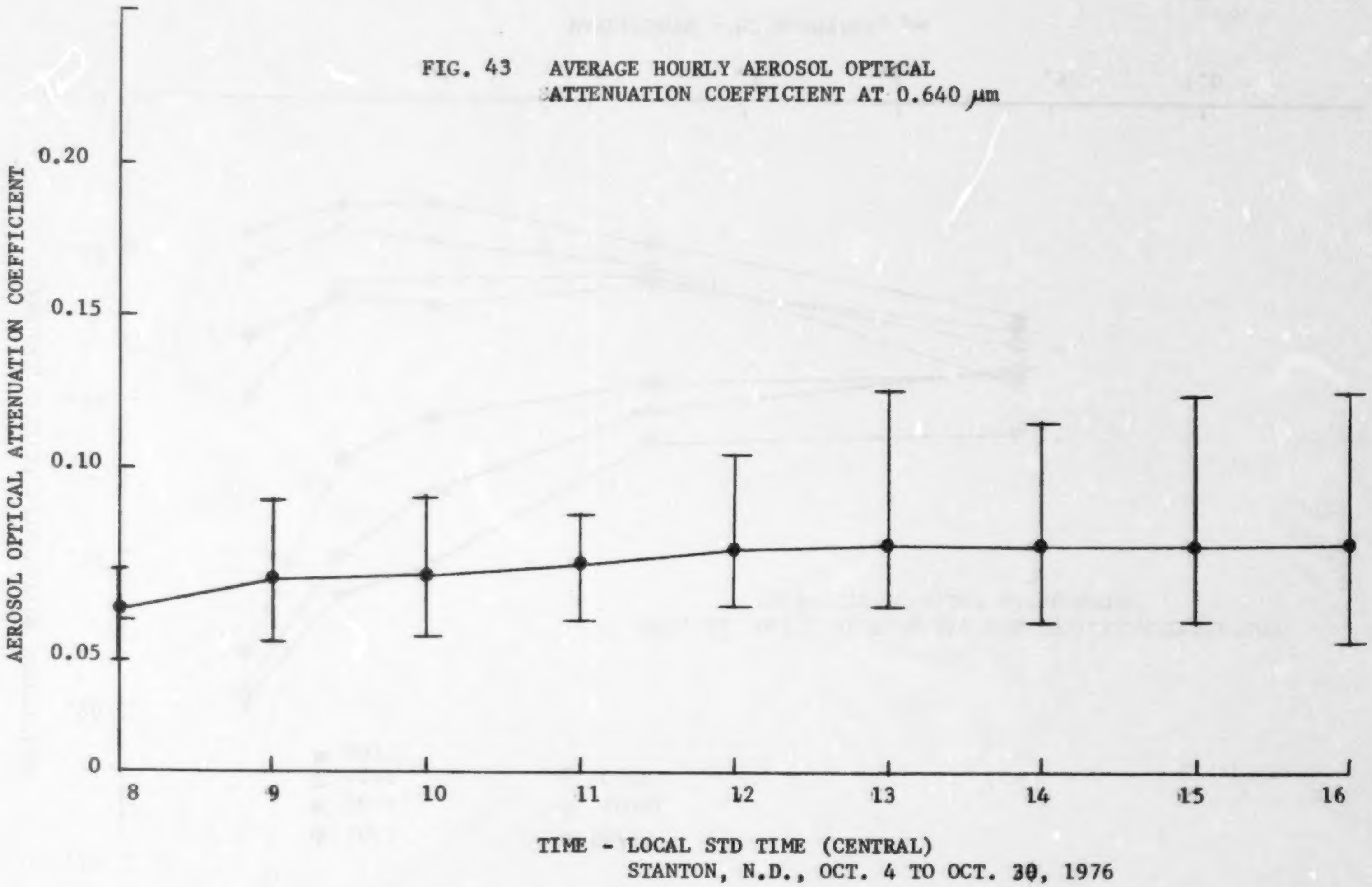

STANTON, N.D., OCT. 4 TO OCT. 30, 1976

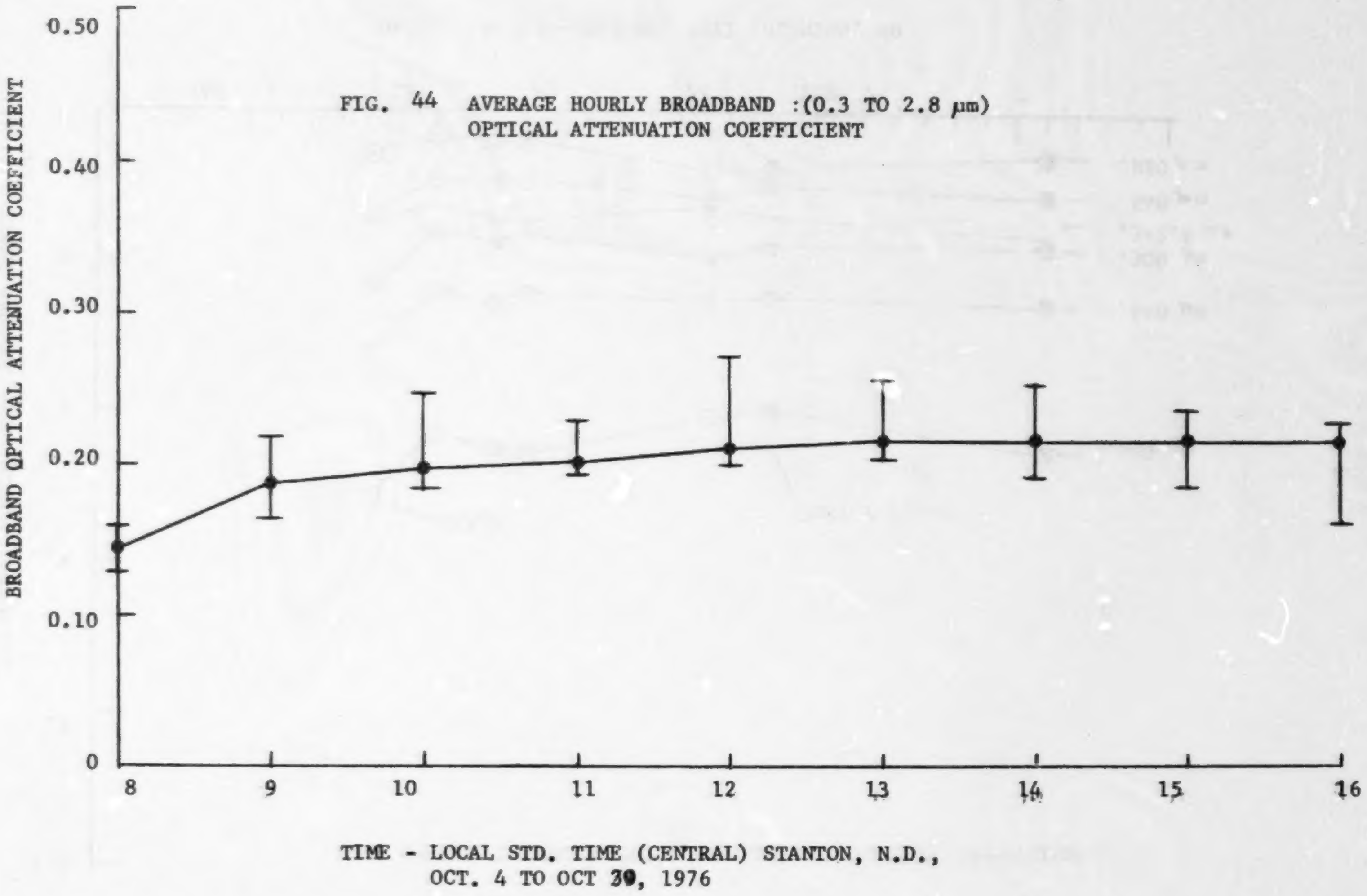

FIG. 44 AVERAGE HOURLY BROADBAND :(0.3 TO 2.8 μm) OPTICAL ATTENUATION COEFFICIENT

FIG. 45 DAILY AVERAGE TOTAL OPTICAL ATTENUATION COEFFICIENTS

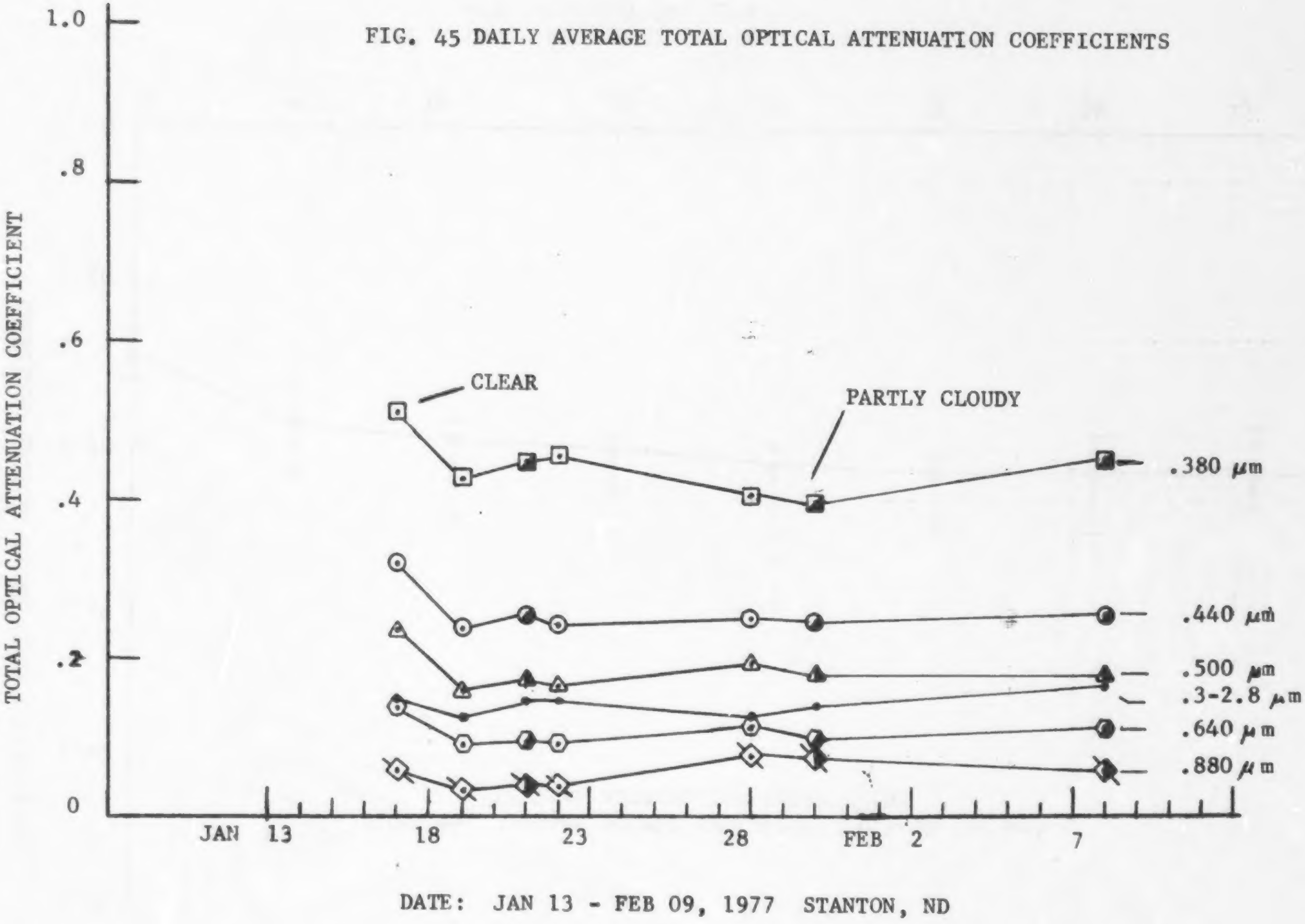

FIG. 46 DAILY AVERAGE AEROSOL OPTICAL ATTENUATION COEFFICIENT

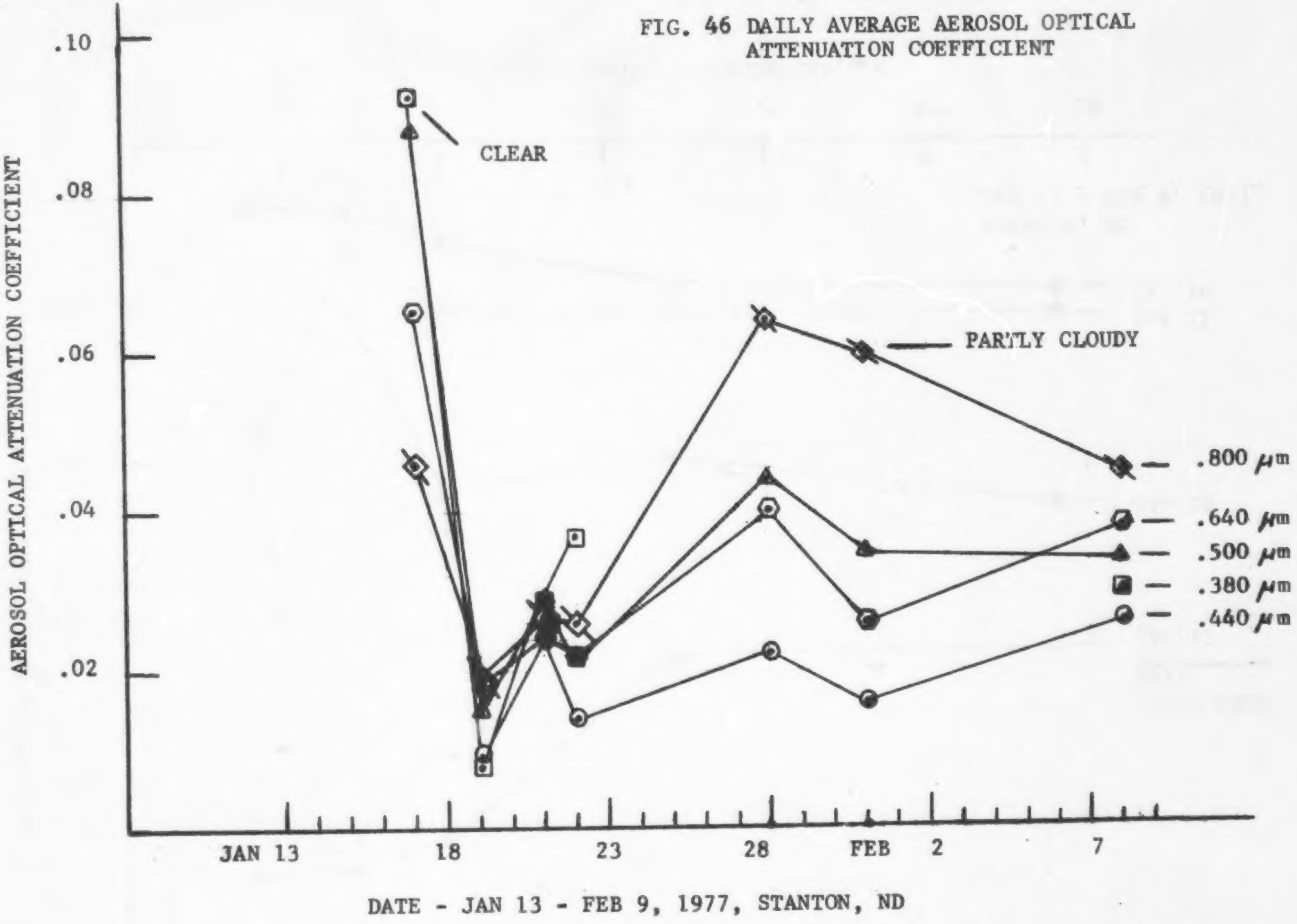

FIG. 47 DAILY AVERAGE AEROSOL ATTENUATION COEFFICIENT VERSUS WAVELENGTH

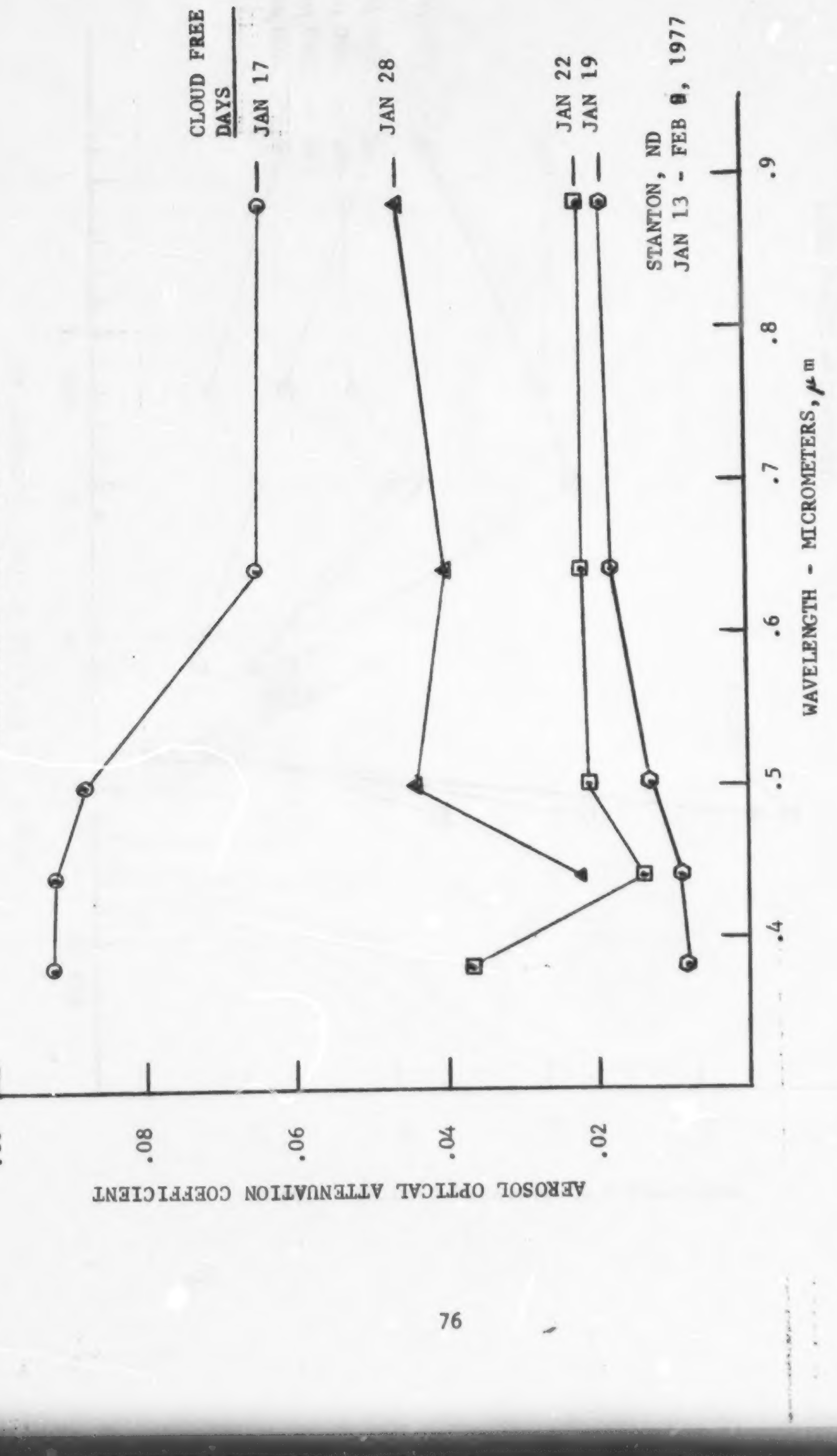

FIG. 48 AVERAGE HOURLY AEROSOL OPTICAL ATTENUATION COEFFICIENT FOR CLEAR DAYS AT 0.640 μm

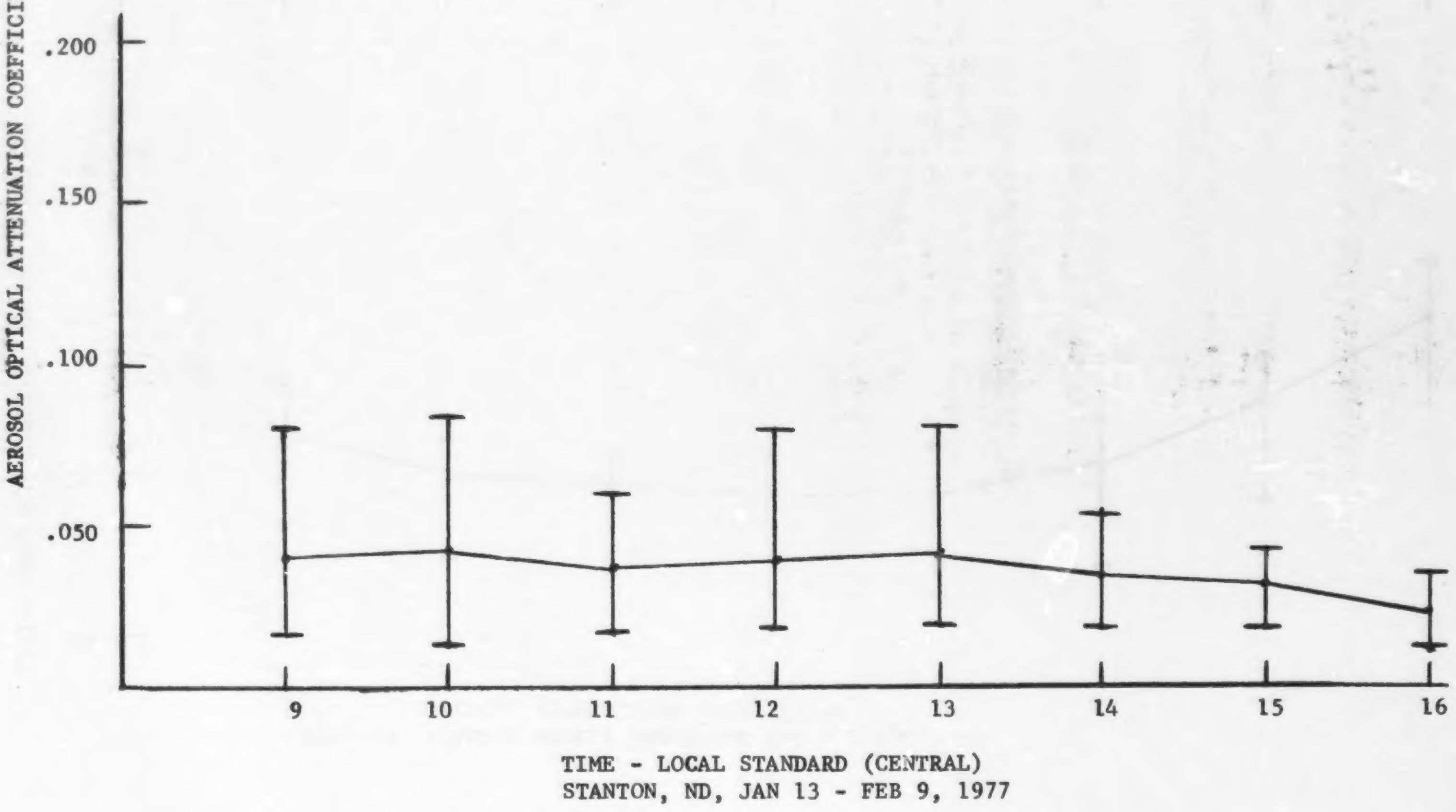

FIG. 49 AVERAGE HOURLY BROADBAND (.3 - 2.8μm)
OPTICAL ATTENUATION COEFFICIENT

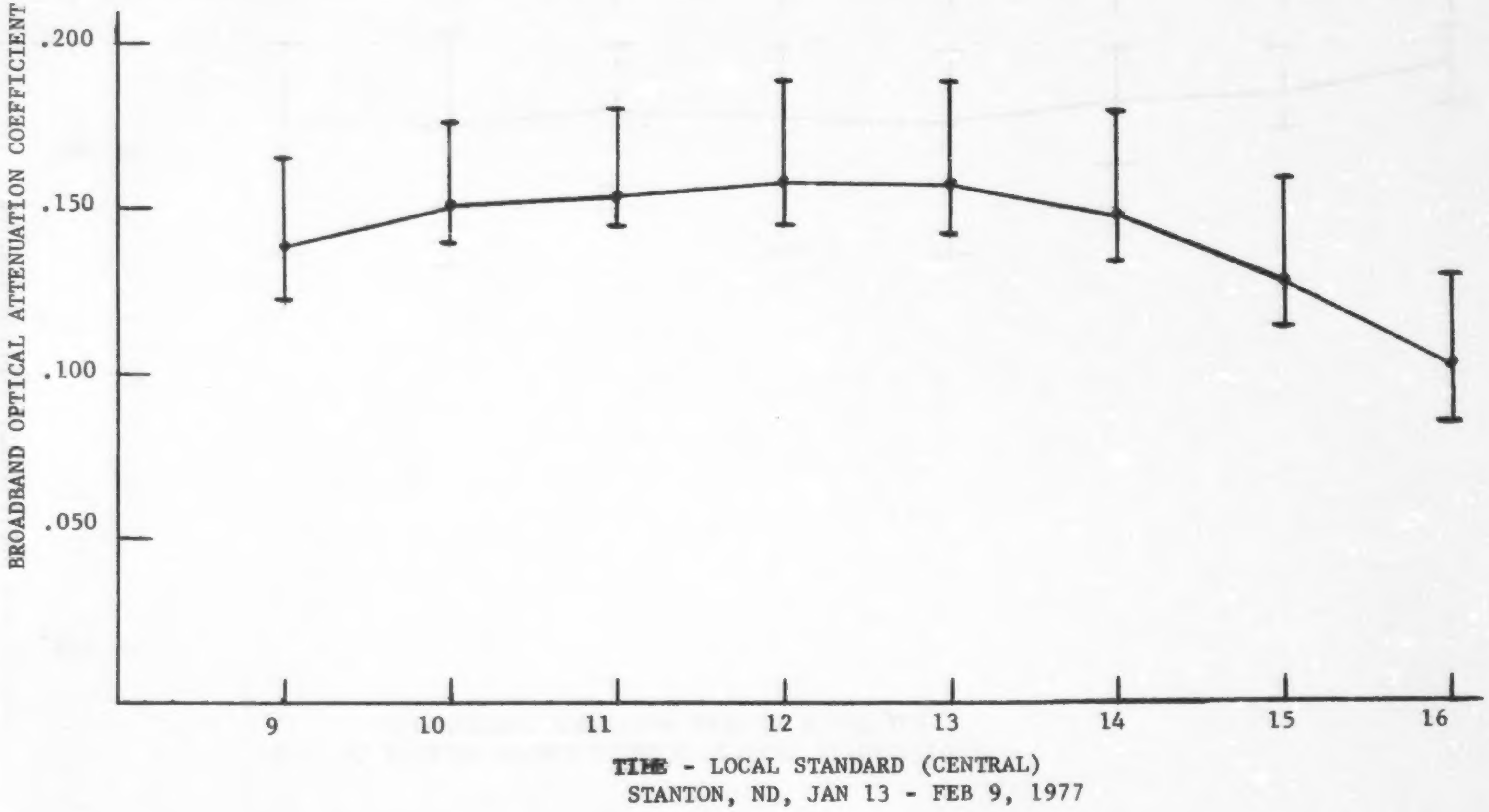

FIG. 50 COMPARISON OF HOURLY AVERAGE BROADBAND (.3 to 2.8 µm) ATTENUATION FOR APRIL, JULY, OCT., JAN, STANTON, N.D., 1976-77

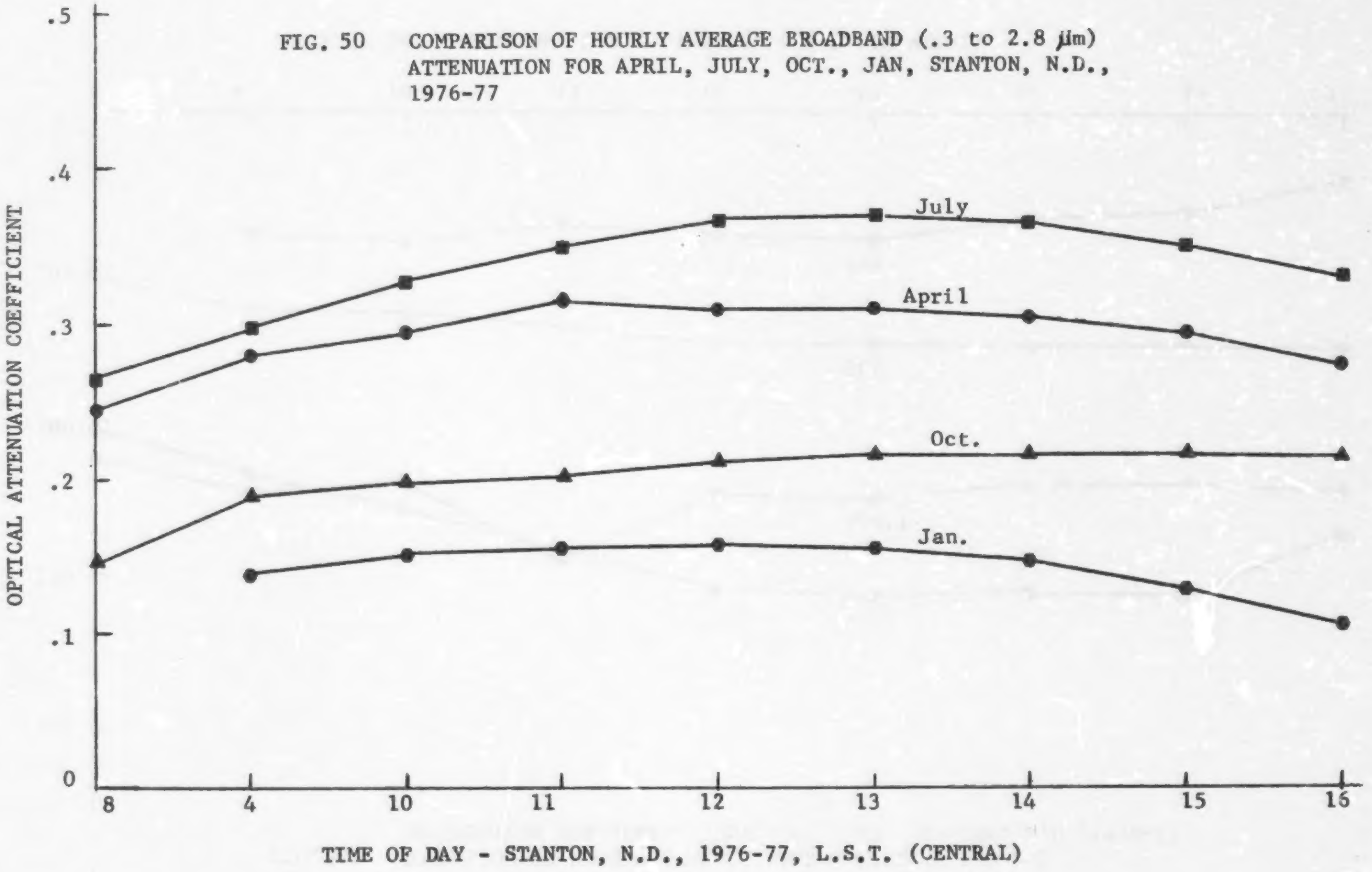

FIG. 51 COMPAISON OF HOURLY AVERAGE NARROW-BAND (0.640 μm) ATTENUATION FOR APRIL, JULY, OCT, JAN, STANTON, N.D., 1976-77

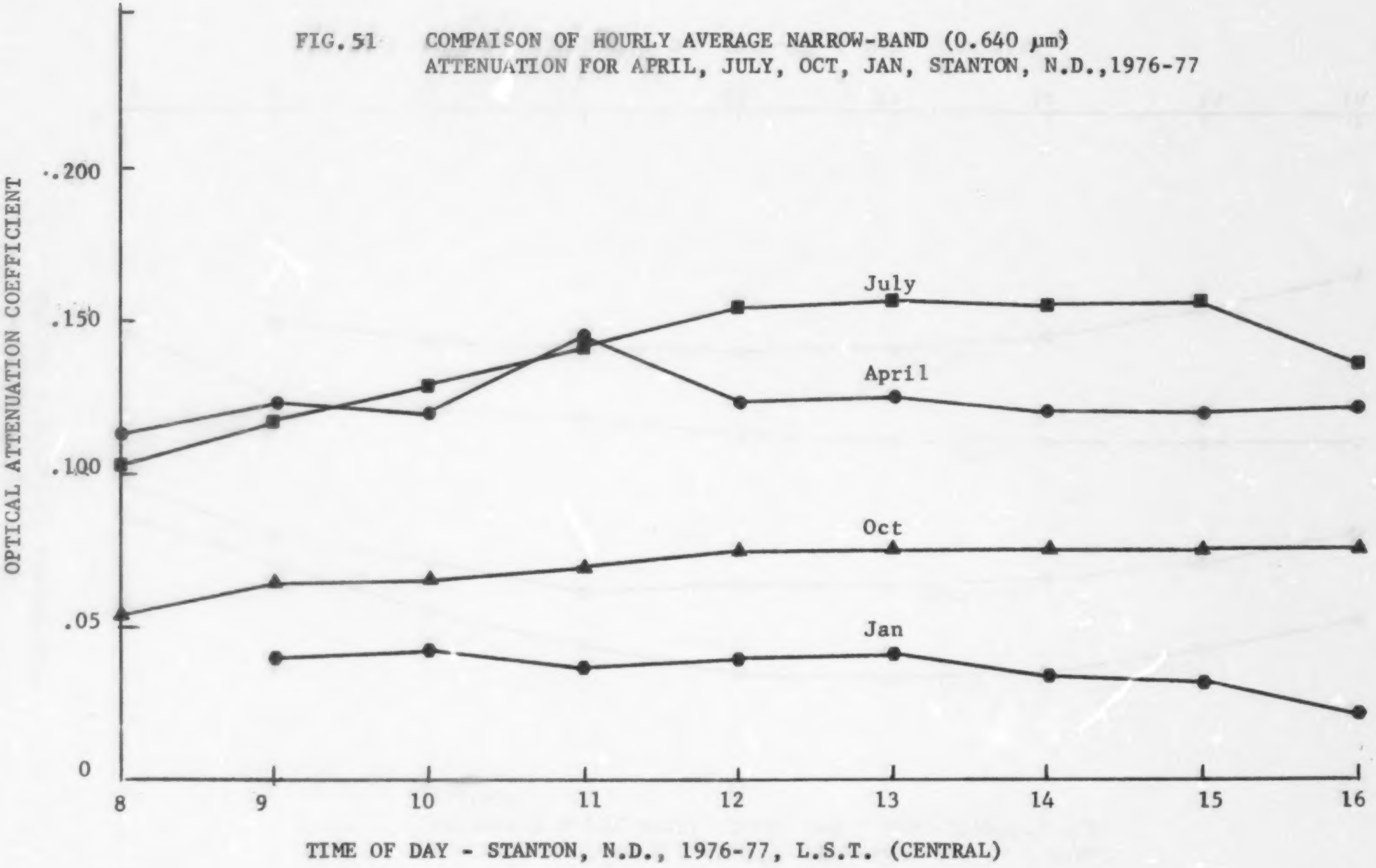

6. INCIDENT SOLAR IRRADIANCE

6.1 Techniques/Instrumentation Used - The absolute quantities of solar irradiance measured consisted of the normal incident direct solar beam, I, and the total (180^o, global) incident solar irradiance on a horizontal surface, H. The wavelength region measured encompasses 99% of the available solar energy and is the 0.3 to 2.8 μm broadband region. The two quantities measured are related by

$$H = I \cos\theta_o + S \tag{25}$$

where S is the diffuse sky irradiance.

The specific baseline parameters established were the absolute quantities of direct, total, and diffuse solar irradiance versus relative air mass, and the ratio of the diffuse to total solar irradiance. For a given solar zenith angle, θ_o, the relative air mass, m, these parameters are determined by the atmospheric optical air quality. In the case of the diffuse irradiance some dependence exists concerning ground albedo; but, for a given season/condition, this dependence should be relatively constant.

The instrumentation used consisted of an Eppley pyrheliometer (see Figure 29) for measuring the direct solar beam and an Eppley pyranometer for measuring the total solar irradiance. The pyranometers are shown in Figure 52. The field location of the pyranometers is shown in Figure 30.

The baseline absolute solar irradiance parameters established were as follows:

(1) Broadband--0.30 to 2.8 micrometer - direct solar irradiance versus relative air mass.
(2) Diffuse broadband solar irradiance versus relative air mass.
(3) Total Broadband horizontal solar irradiance versus relative air mass.

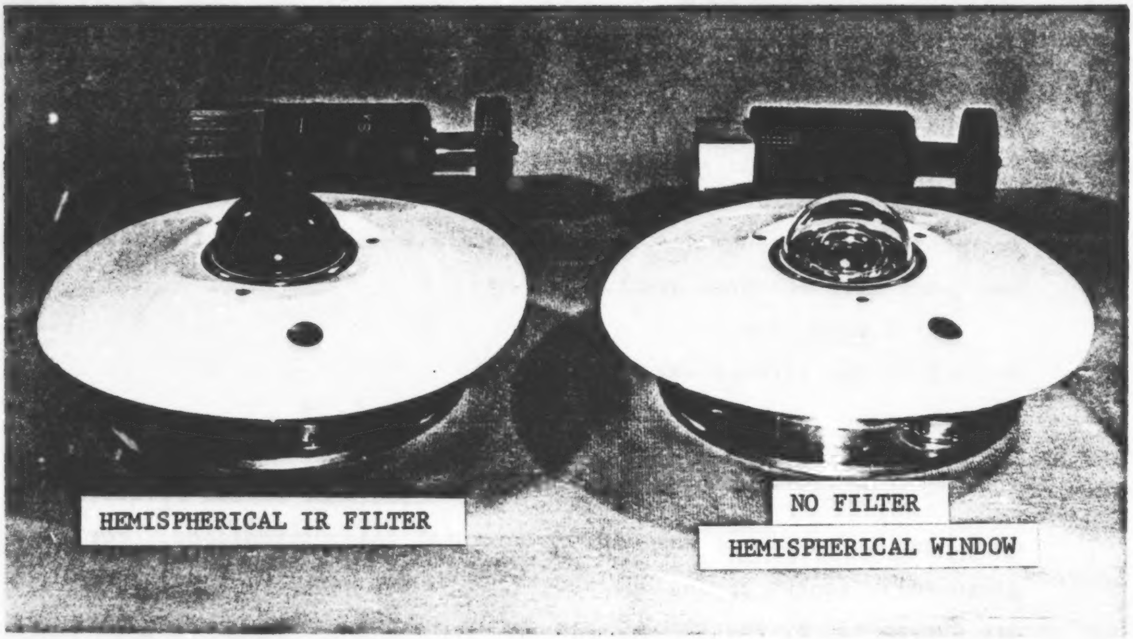

Figure 52 Eppley Pyranometers

(4) Ratio of broadband diffuse to total solar irradiance.

(5) Average daily ratio of broadband diffuse to total solar irradiance.

(6) Average hourly broadband ratio of diffuse to total solar irradiance.

6.2 April Solar Irradiance - The results for the April solar irradiance are shown in Figures 53, 54, 55, 56, 57 and 58. The results for the direct solar beam irradiance versus relative air mass, Figure 53, display a baseline for cloud free and cloud present conditions. The clarity of the atmosphere, optical attenuation for the .3 to 2.8 μm band, controls this baseline. Therefore this baseline is indicative of vertical atmospheric optical air quality. As can be seen, the presence of cirrus clouds significantly reduce the baseline. This is indicative of the sensitivity of the measurements as compared to the human eye observations, because the ground-based observer could not detect any obscuration of the solar disc. Shown in Figure 54 is the baseline for the diffuse sky, solar irradiance versus relative air mass. Again, baselines for cloud present and cloud free conditions were evident. Note that the diffuse sky irradiance is significantly lower for the clear conditions because of less scattering of the direct solar beam. The results for the total solar irradiance versus relative air mass, shown in Figure 55, show the interesting phenomenon of a single total versus relative air mass baseline despite the atmospheric condition. This can be explained by recalling that although the cloud conditions reduced the direct solar beam, they increased the diffuse sky component. This evidently results in the constant baseline shown in Figure 55. Such a baseline is important because it defines the solar heat input to the ground, under the natural conditions. These natural conditions are defined by the characteristics of the aerosols and cloud particles. If these particles significantly absorbed the solar irradiance, instead of scattering into the diffuse sky component, the diffuse irradiance component would not raise the total irradiance to the level shown for the natural baseline, Figure 55. Hence, if any man-made aerosols that have a low surface albedo are injected into the atmosphere, the total solar irradiance versus relative air mass baseline would be altered. The baseline would most likely shift downward, indicating a reduction in total solar irradiance, at a given relative air mass. Shown in Figure 56 is the ratio of diffuse to total solar irradiance versus relative air mass. As can be seen, this baseline is also indicative of clear and cloud present conditions. The average daily ratio of diffuse to total solar irradiance, shown in Figure 57, displays variations between the clear (April 5,6,8) and cloud present days (April 10 and 12). The average hourly broadband ratio of diffuse to total solar irradiance, shown in Figure 58, displays a dependence upon time of day, having a minimum near noon and maximums in the early morning and late afternoon. This is due to the dependence on relative air mass, shown in Figure 56. At low relative air masses the ratio of diffuse to total solar irradiance is a minimum because the path length, traveled by the solar beam, is a minimum, and the total solar irradiance is a maximum. The shorter path lengths result in a lower amount of diffuse sky irradiance because of a lower amount of direct solar irradiance scattered from the beam. The lower relative air masses correspond to higher total solar irradiance because they are indicative of higher sun angles (elevation) which result in a greater amount of direct solar irradiance on the horizontal surface.

6.3 July Solar Irradiance - The July solar irradiance results are shown in Figures 59, 60, 61, 62, 63 and 64. The broadband direct solar irradiance versus relative air mass, Figure 59, distinctly identify very clear conditions, July 16, hazy conditions on August 6 and extremely hazy conditions for August 7. The marked effects of haze on the direct solar irradiance versus relative air mass is obvious. This points out the usefulness of the direct solar irradiance versus relative air mass as a quantitative identification of vertical atmospheric optical clarity/quality. For example, if one considers a relative air mass of 2.0; the clear conditions have a direct irradiance of 850 w/m^2; the hazy conditions have a value of 780 w/m^2; and the very hazy conditions have a value of 660 w/m^2. It should be pointed out that the broadband, .3-2.8 μm, direct solar irradiance is also sensitive to attenuation by water vapor absorption in the near infrared region. However if one compares the results shown in Figure 36, it can be seen that both the broadband and narrowband results point out the significantly higher attenuation resulting from the hazy conditions on Aug. 6 and 7. The diffuse solar irradiance relative air mass results, Figure 60, show the significantly higher amounts of diffuse sky irradiance caused by the hazy conditions, especially at low values of relative air mass. For example, at a relative air mass of 1.15, the hazy conditions have a diffuse irradiance of about 105 w/m^2 whereas the clear conditions have values ranging from

64 to 80 w/m^2. The broadband total solar irradiance versus relative air mass, shown in Figure 61, results show a very well defined curve, with no separation of clear versus hazy conditions. This result is identical to the April results, again pointing out that the reduction of the direct solar beam is countered by an increase in diffuse irradiance. This results in the constant total solar irradiance versus relative air mass. The ratio of diffuse to total solar irradiance results, shown in Figure 62, also point out the differences between clear and hazy conditions. The average daily ratio of diffuse to total solar irradiance, shown in Figure 63, shows the relative clarity of the various days. The cloud present conditions have higher ratios of diffuse to total solar irradiance because of the large contribution of the clouds to the diffuse sky irradiance. The various ratios for cloudy days is an indicator of the amount of cloudiness, and not the amount of haze. For clear conditions, the relative clarity/haziness of the days is easily established. The days of July 16, 17, 23 and 26 were days having approximately the same clarity; whereas, Aug. 6 and 7 had much higher ratios indicating more haze. The average hourly broadband ratio of diffuse to total solar irradiance, shown in Figure 64, also shows the differences between clear and hazy conditions.

6.4 October Solar Irradiance - The October solar irradiance results are given in Figures 65, 66, 67, 68, 69 and 70. The month of October had a high occurrence of cirrus clouds, making the solar irradiance data very scattered and uncertain concerning the establishing of clear conditions. The broadband direct solar irradiance versus relative air mass results, shown in Figure 65, show a high degree of scattering of data points. The ground observers reported no apparent hazy conditions, as with the July data; however, they frequently reported high cirrus clouds. Therefore, the range of values shown in Figure 65 (and the remainder of the Oct. results) are most likely due to changing cirrus conditions. In order to establish the clear conditions one would have to assume that the highest values of direct irradiance represent clear conditions. The diffuse solar irradiance versus relative air mass results, shown in Figure 66, also show a high degree of scatter, probably caused by cirrus clouds. Again, the clear baseline is established by assuming no cirrus influence. The total broadband horizontal solar irradiance versus relative air mass results, Figure 67, again show a fairly constant relationship despite the influence of cirrus clouds. As pointed out previously, there seems to exist a natural mechanism where the total solar irradiance as a function of relative air mass is kept the same by increases in the diffuse sky irradiance whenever the direct is attenuated by thin clouds and/or haze. The ratio of diffuse to total solar irradiance versus relative air mass, Figure 68, showsa range of values due to probable cirrus influences. The clear baseline is assumed to be representative. The average daily ratio of diffuse to total solar irradiance results, Figure 69, show the relative clarity of the days. October 5 was the clearest day and October 29 was the least clear day. The influence of cirrus clouds is probable, but not known exactly. It is possible that October 5 represents a true clear day. The average hourly broadband ratio of diffuse to total solar irradiance results are shown in Figure 70.

6.5 January Solar Irradiance - The January solar irradiance results are shown in Figures 71, 72, 73, 74, 75 and 76. During January the ground was snow covered. Because snow has such a high albedo, it effects the diffuse sky irradiance by reflecting the direct solar irradiance, the reflected direct gets backscattered by the atmosphere. This results in higher values for the diffuse irradiance. The broadband direct solar irradiance versus relative air mass, Figure 71, shows the clear baseline and the influence of cirrus clouds. The diffuse solar irradiance versus relative air mass results, shown in Figure 72, show a marked difference between clear and haze/cirrus conditions. This difference is amplified by the ground snow cover, because of the strong backscatter of the reflected direct solar irradiance by the haze and/or cirrus clouds. The total solar irradiance versus relative air mass, Figure 73, also show the impact of cirrus clouds. For all the other months given previously, the total solar irradiance versus relative air mass has been a well defined relationship. The deviation for January is most likely caused by the combination of the high reflectance snow cover reflecting the direct solar beam up, then the thin cirrus clouds reflecting it back down toward the ground. This results in a very high value for the diffuse irradiance, as shown in Figure 72. The clear baseline shown in Figure 73, is assumed to be free of cirrus cloud influences. The ratio of diffuse to total solar irradiance versus relative air mass, Figure 74, also shows the influence of cirrus clouds. The average daily ratio of diffuse to total solar irradiance results, Figure 75, show the influences of haze, cirrus, and clear conditions. In particular, Jan. 17 was reported to be very hazy by the ground observer. The average hourly ratio of diffuse to total solar irradiance results, Figure 76, also show the cirrus versus clear influences.

6.6 Seasonal Solar Irradiance Comparisons - The seasonal comparisons of the solar irradiance results are shown in Figures 77, 78 and 79. The analysis shown in Figure 77 is the comparison of the direct solar irradiance versus relative air mass, for each of the seasonal months. For a given relative air mass, the seasonal month that has the highest level of direct solar irradiance has the lowest atmospheric attenuation. It is obvious that there exists a high degree of variation of atmospheric attenuation for the various seasons/months. The analysis shown in Figure 77, indicates that January had the lowest atmospheric attenuation, followed by October, July, and April. It should be pointed out that these curves, Figure 77, represent a sort of hypothetical best clear day for each season/month because (as previously shown in Figure 53, 59, 65 and 71) these clear baselines were derived from using the highest values of direct solar irradiance at given relative air masses for all days. Therefore, the curves (clear baselines) shown in Figure 77, represent a composite of the clearest conditions existing for the entire month. When these results are compared to the results for optical attenuation coefficients, shown in Figures 50 and 51, it can be seen that the ranking of the months is different. The optical attenuation coefficient results indicate that January was the clearest month, followed by October, April, and July. The reason for this is due to the fact that the optical attenuation results were obtained by averaging all values for clear day attenuation; whereas, the results shown in Figure 77 were obtained by the method described above. The results shown in Figure 77 simply indicate that the best case clear conditions in April were higher in attenuation than the best case clear conditions in July. The results shown in Figures 50 and 51 simply indicate that on the average the conditions during April had lower attenuation than July. Both sets of analyses are useful for establishing the clear day baseline attenuation; because one set of curves, Figure 77, represents the absolute clearest conditions observed over all days, and the other (Figures 50 and 51) represents the average clear conditions observed. Shown in Figure 78 is the composite of the seasonal months - total horizontal solar irradiance versus relative air mass. As previously discussed, the total solar irradiance versus relative air mass is a surprisingly consistent function despite the varying atmospheric conditions. The January results display a difference baseline because of the combination of snow cover and cirrus clouds. The monthly-seasonal diffuse to total ratio versus relative air mass analysis is shown in Figure 79. The ratio of diffuse to total solar irradiance is an indicator of overall atmospheric clarity because as the atmosphere becomes more turbid the diffuse sky irradiance will be altered and generally increased. Therefore, as the ratio increased the overall atmospheric clarity would be diminished. The general increase of the ratio with relative air mass is, as discussed previously, due to the total decreases and the diffuse increases because of sun angle effects. The diffuse to total ratio results shown in Figure 79 represent the hypothetical clearest conditions as discussed for the direct solar irradiance versus relative air mass results.

It should be recalled that the diffuse sky irradiance, and therefore the ratio of diffuse to total irradiance, is influenced by the ground albedo and any cloud cover present. Since the change in ground albedo for the various months - except January which was snow covered - is unknown, the actual magnitudes of the ratio versus relative air mass cannot be directly interpreted as an indicator of atmospheric clarity. The curves shown in Figure 79 represent the hypothetical clearest baseline for each of the seasonal months, with the ground albedo of that period of time. However, it is interesting to consider the slope of the ratio of diffuse to total versus relative air mass. This slope is somewhat indicative of the atmospheric optical attenuation coefficient. For example, a very clear atmosphere would have a low diffuse sky irradiance and high relative air masses (slant paths) would be required to substantially increase the diffuse sky irradiance. Hence, a very clear atmosphere would be associated with a low slope of the type of curves shown in Figure 79. A very turbid atmosphere would have a high slope because of the higher concentrations of aerosols causing much greater scattering as the direct solar beam path length (relative air mass) is increased. The actual level/magnitude of the line (diffuse to total ratio versus relative air mass) would be determined by the ground albedo. When the slopes of the curves shown in Figure 79 are calculated one obtains the following results.

Table 1. Comparison of seasonal slope of diffuse to total ratio versus relative air mass.

Month	Slope
April	.060
July	.048
Oct.	.038
Jan.	.026

As the results in Table 1 show, April was the most turbid month followed by July, October, and January was the clearest month. These results agree exactly with those obtained by comparing the direct solar irradiance versus relative air mass, Figure 77. The curve shown in Figure 80 verifies that the slope of the ratio of diffuse to total solar irradiance versus relative air mass is proportional to the atmospheric attenuation coefficient. The linear regression correlation coefficient for the plot shown in Figure 80 is 0.97, indicating a very good correlation. The optical attenuation coefficient, in Figure 80, was calculated by using the plots shown in Figure 77. As previously shown, the optical attenuation coefficient, τ, is given by

$$\tau = - \frac{\ln I/I_o}{m} \qquad (26)$$

where I is the direct solar irradiance at a given relative air mass, m, and I_o is the extraterrestrial solar irradiance. For each month, a value for I, at a relative air mass of 3.0, was taken from the dashed (corrected to mean sun-earth distance) lines shown in Figure 77. The value for the solar constant, I_o, was taken to be 1352 W/M^2. This resulted in a broadband optical attenuation coefficient for the hypothetical clearest day for each of the seasonal months, as plotted in Figure 80.

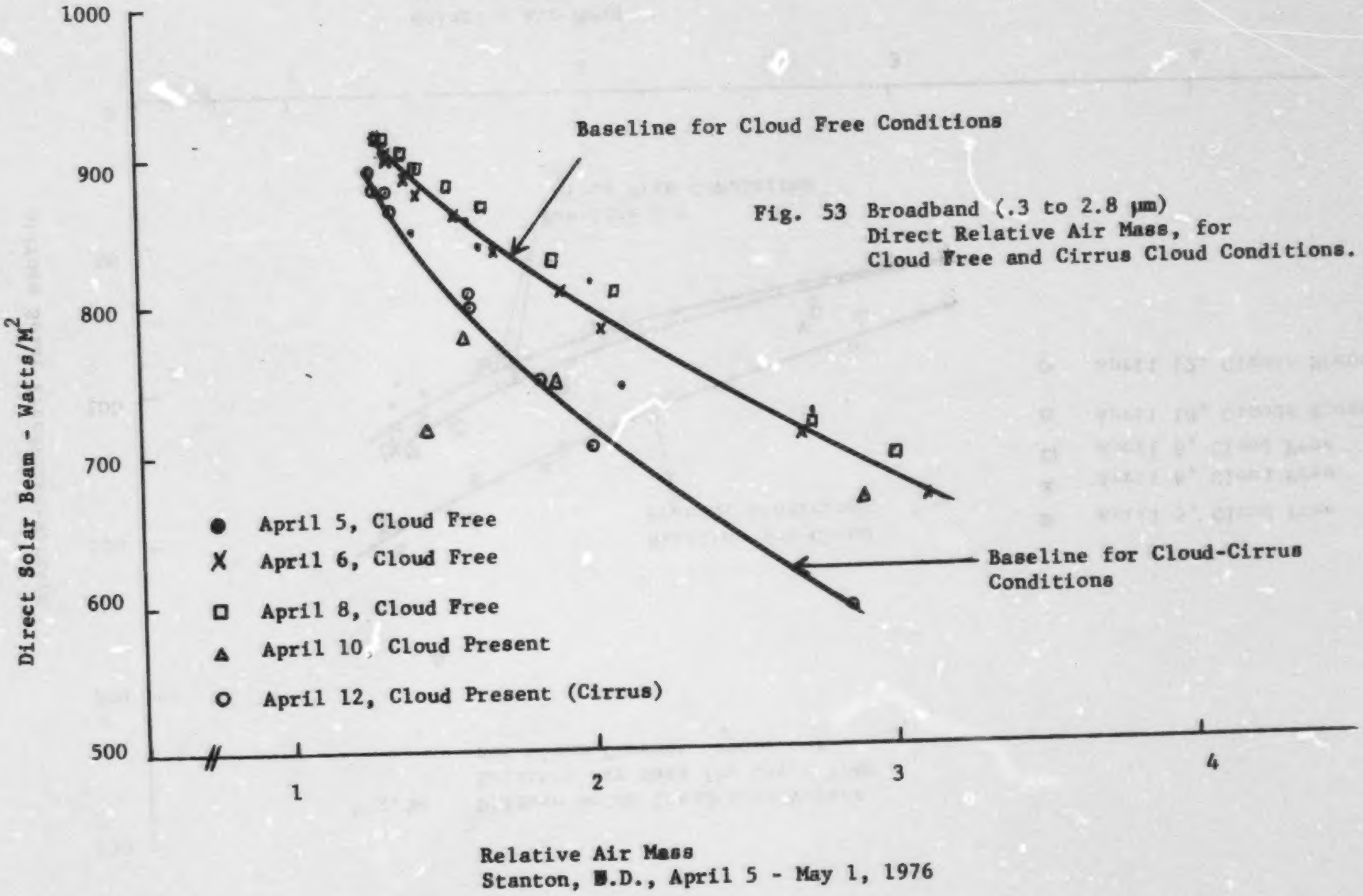

Fig. 53 Broadband (.3 to 2.8 μm) Direct Relative Air Mass, for Cloud Free and Cirrus Cloud Conditions.

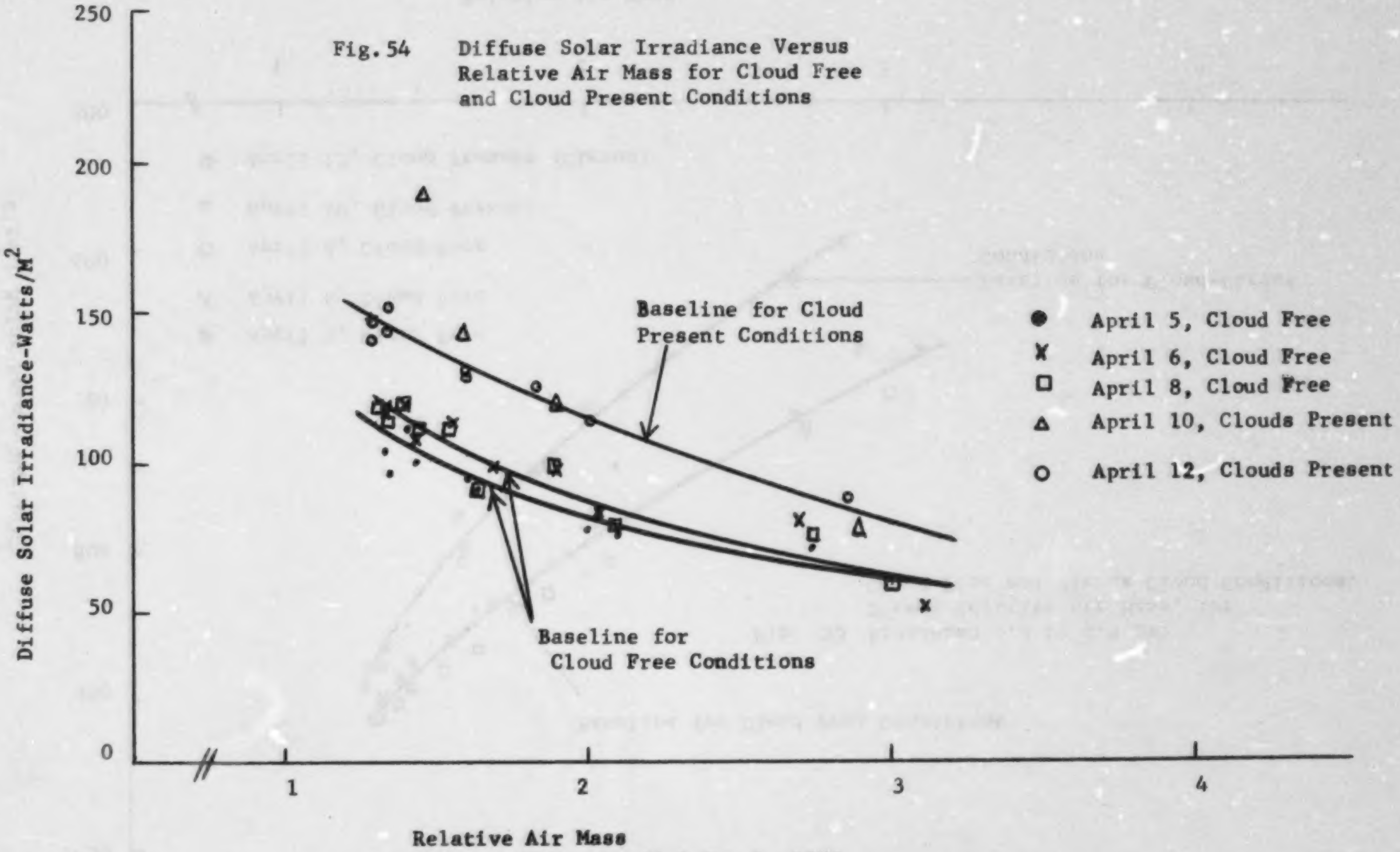

Fig. 54 Diffuse Solar Irradiance Versus Relative Air Mass for Cloud Free and Cloud Present Conditions

Stanton, N.D., April 5-May 1, 1976

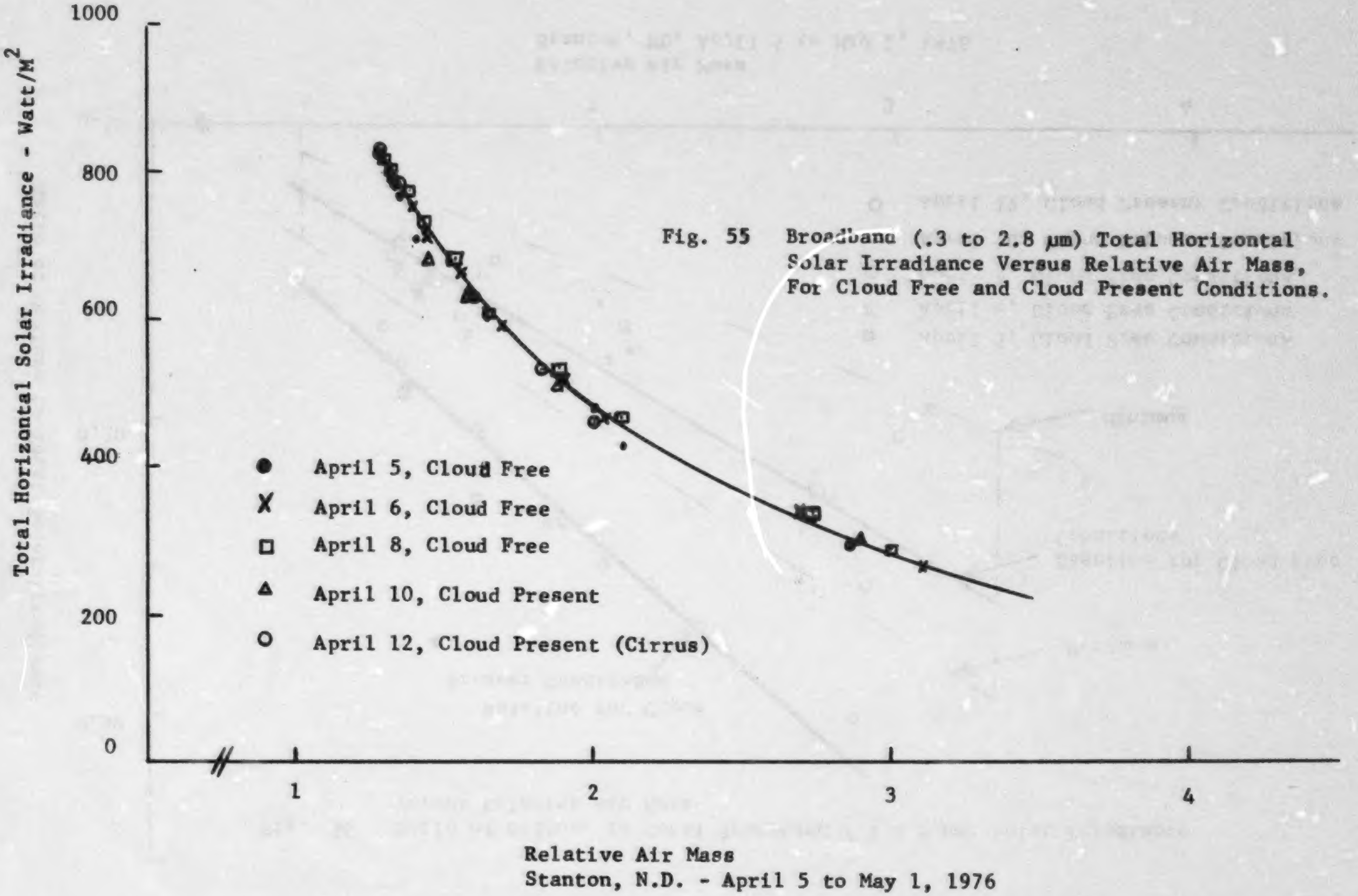

Fig. 55 Broadband (.3 to 2.8 µm) Total Horizontal Solar Irradiance Versus Relative Air Mass, For Cloud Free and Cloud Present Conditions.

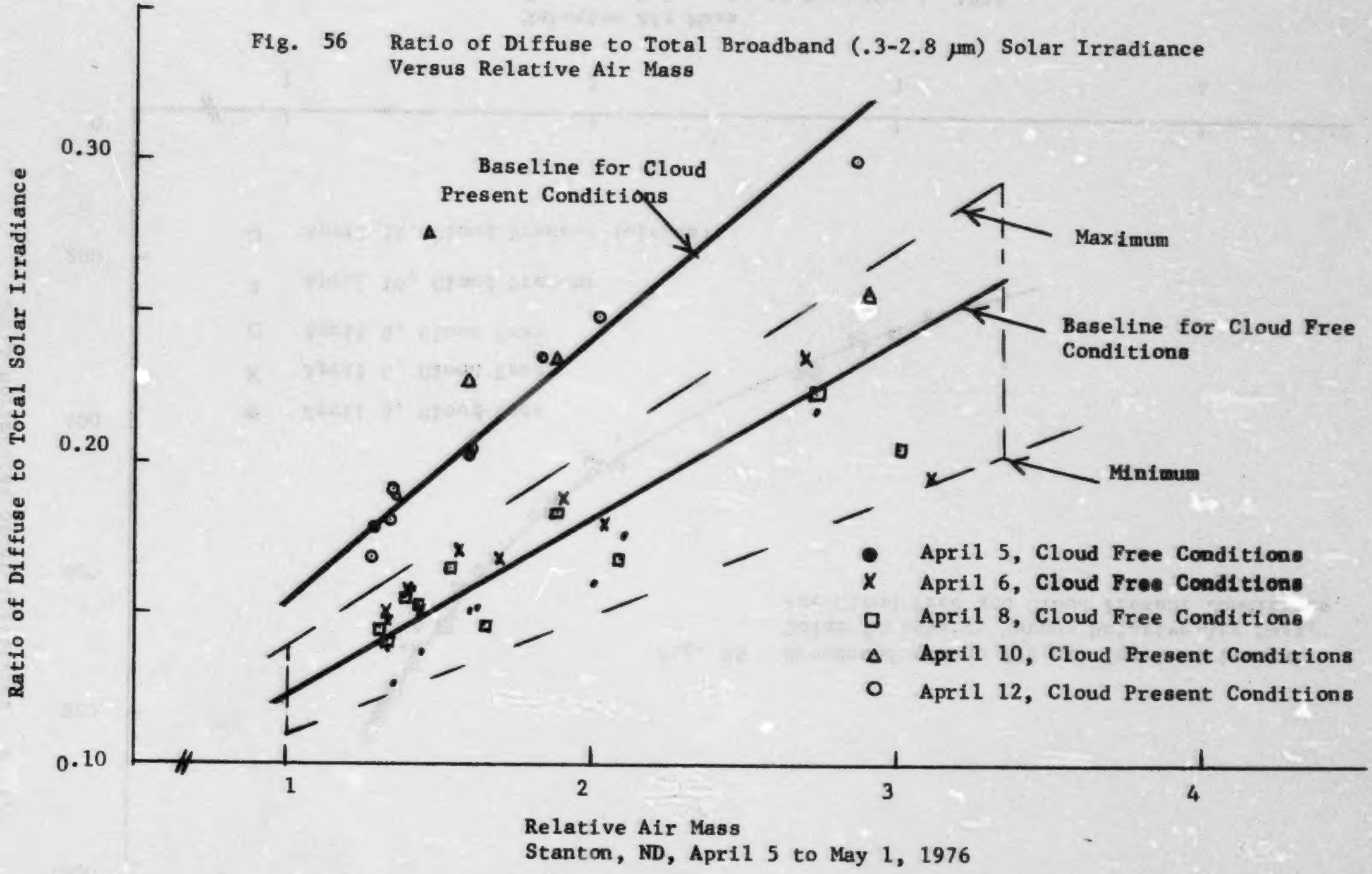

Fig. 56 Ratio of Diffuse to Total Broadband (.3-2.8 μm) Solar Irradiance Versus Relative Air Mass

Fig. 57 Average Daily Ratio of Diffuse To Total Solar Irradiance

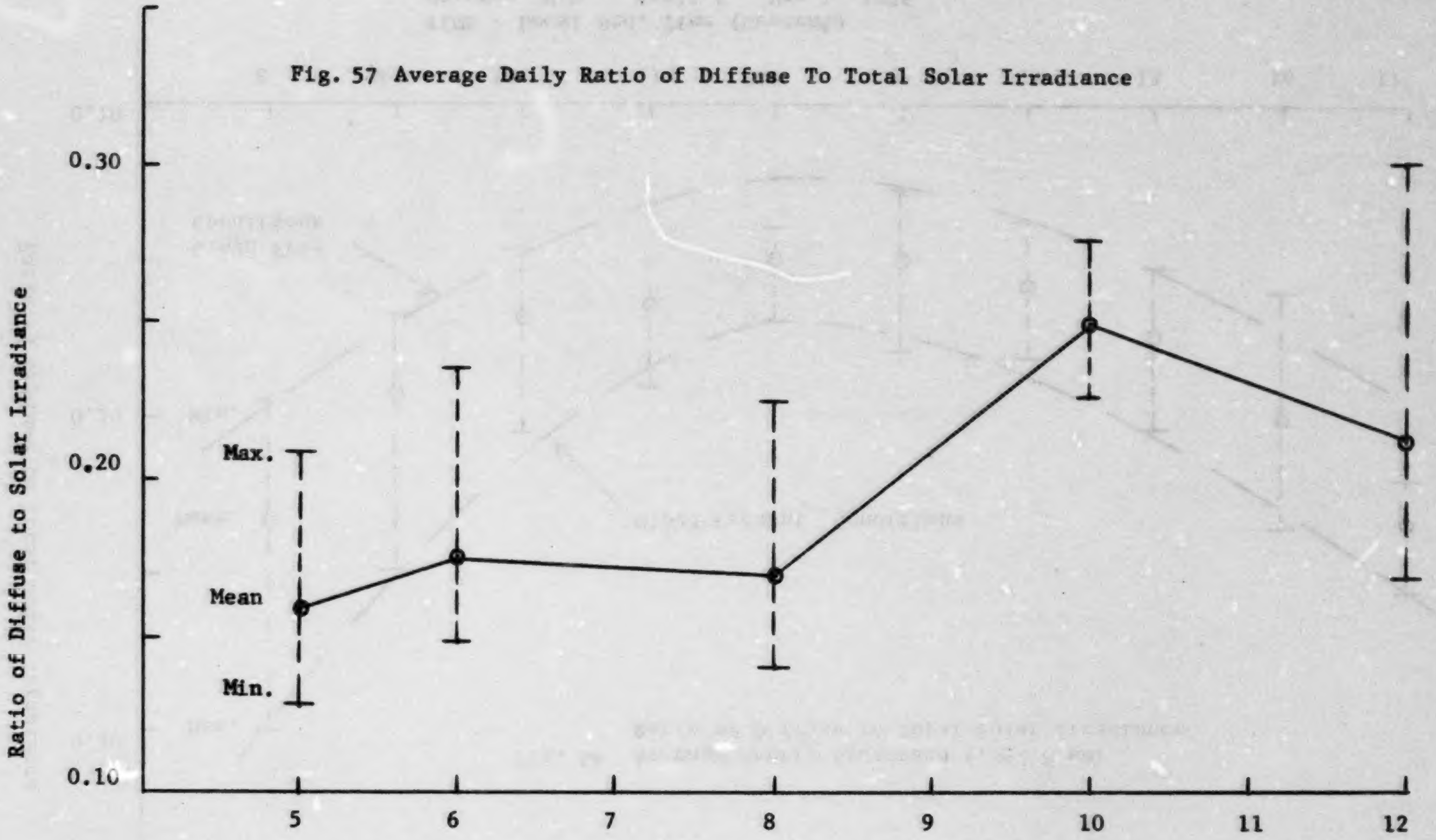

Date: April, 1976
Stanton, N.D.

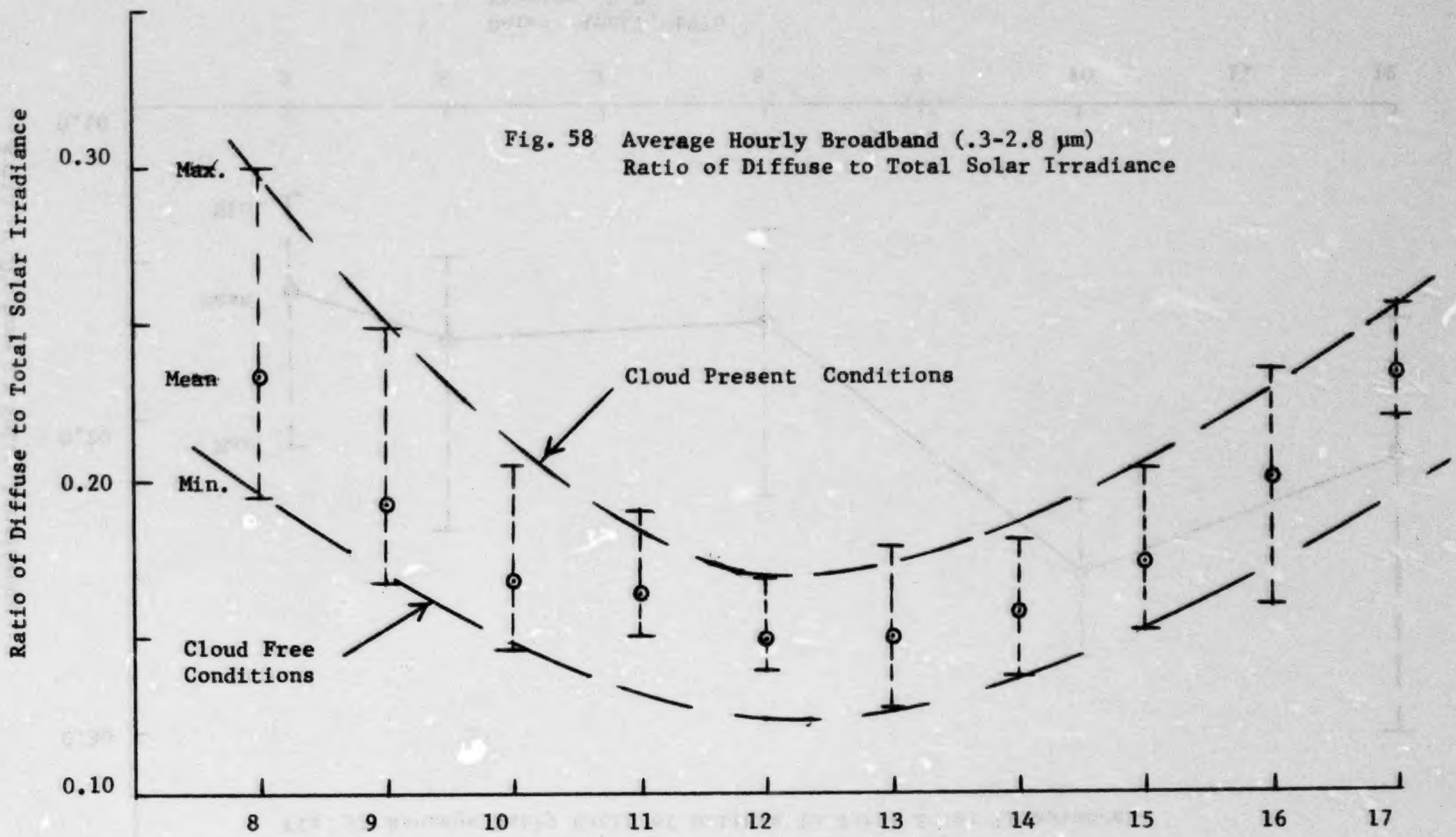

Fig. 58 Average Hourly Broadband (.3-2.8 µm) Ratio of Diffuse to Total Solar Irradiance

TIME - Local Std. Time (Central)
Stanton, N.D., April 5 - May 1, 1976

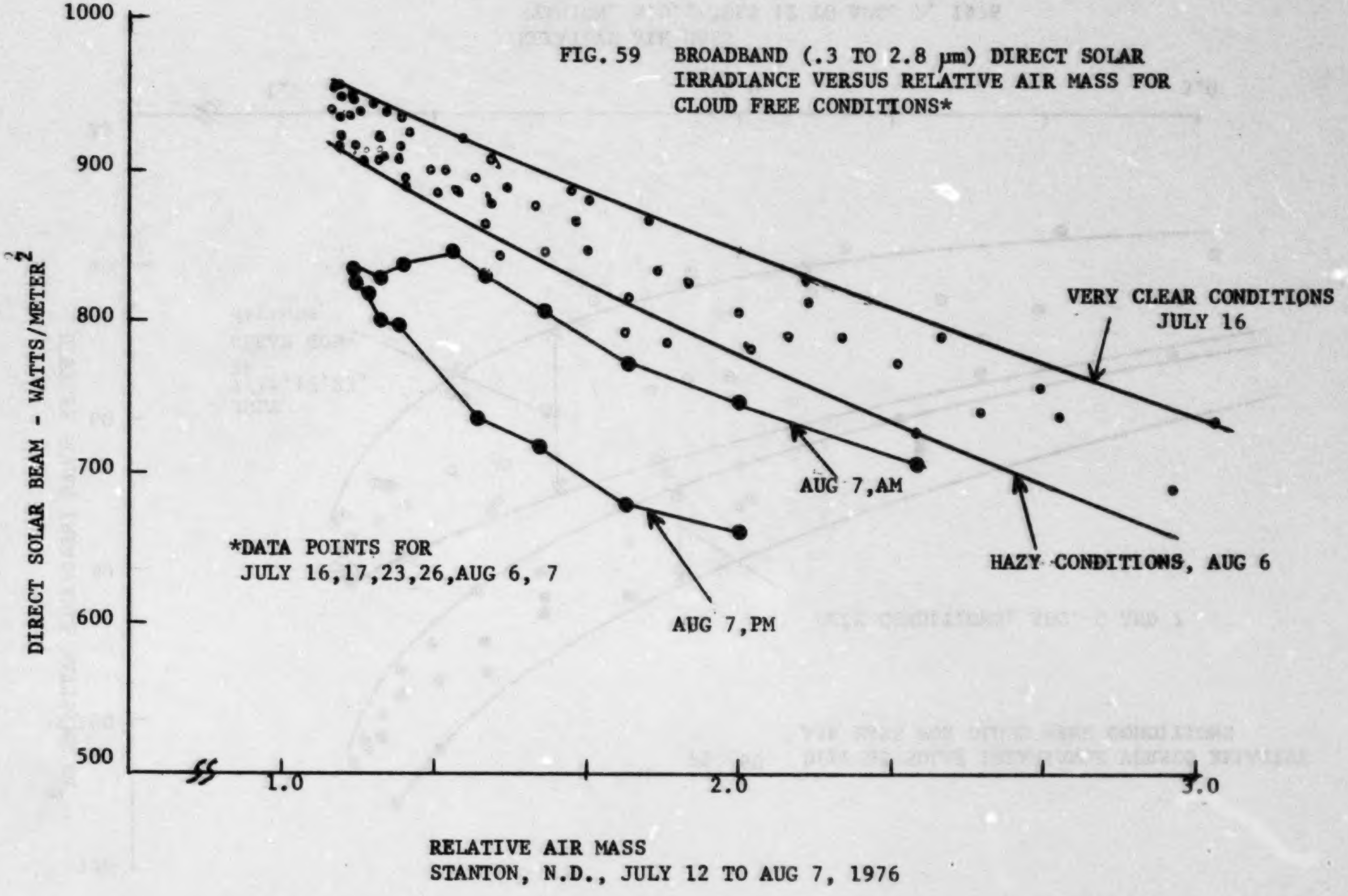

FIG. 59 BROADBAND (.3 TO 2.8 μm) DIRECT SOLAR IRRADIANCE VERSUS RELATIVE AIR MASS FOR CLOUD FREE CONDITIONS*

STANTON, N.D., JULY 12 TO AUG 7, 1976

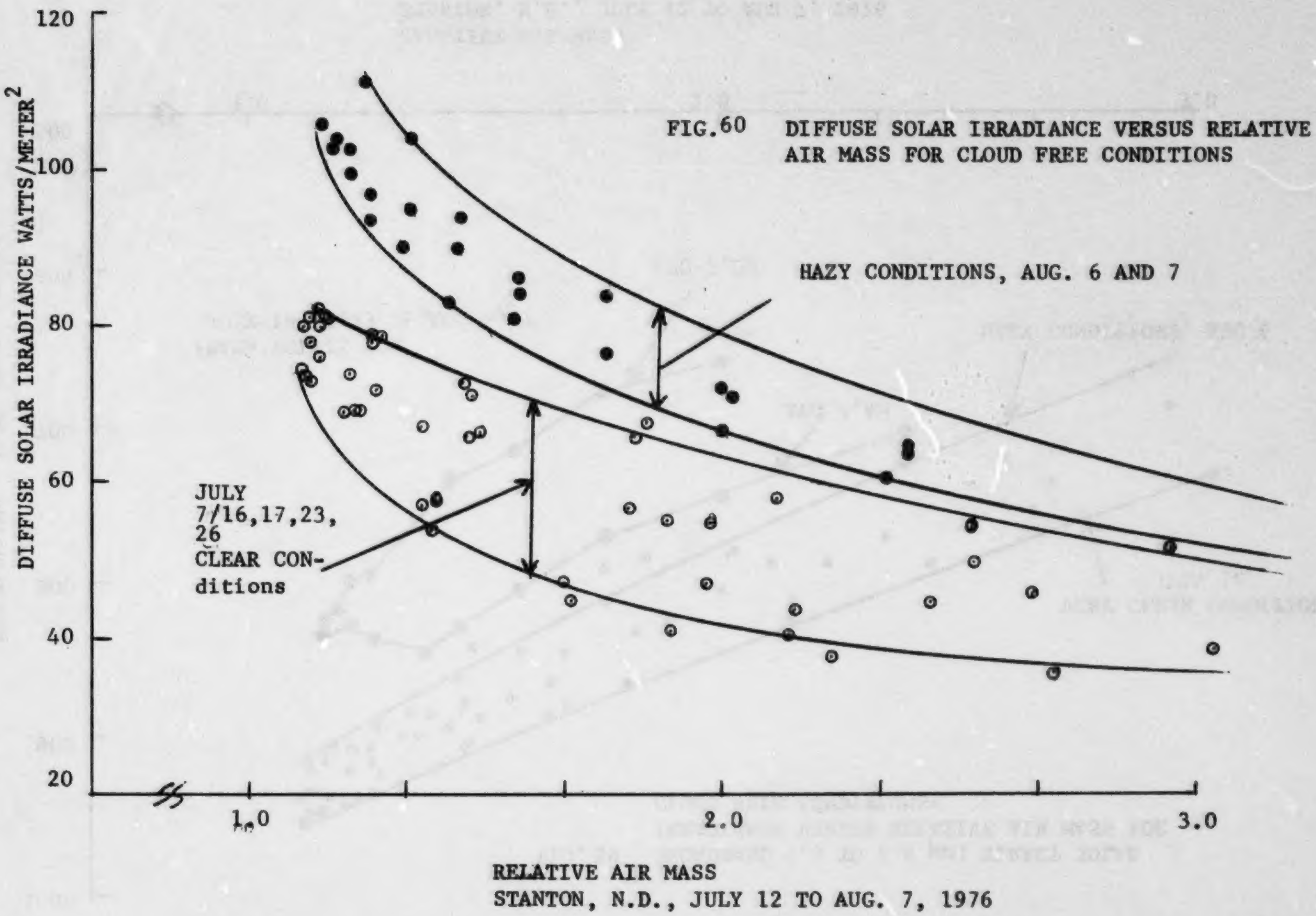

FIG. 60 DIFFUSE SOLAR IRRADIANCE VERSUS RELATIVE AIR MASS FOR CLOUD FREE CONDITIONS

STANTON, N.D., JULY 12 TO AUG. 7, 1976

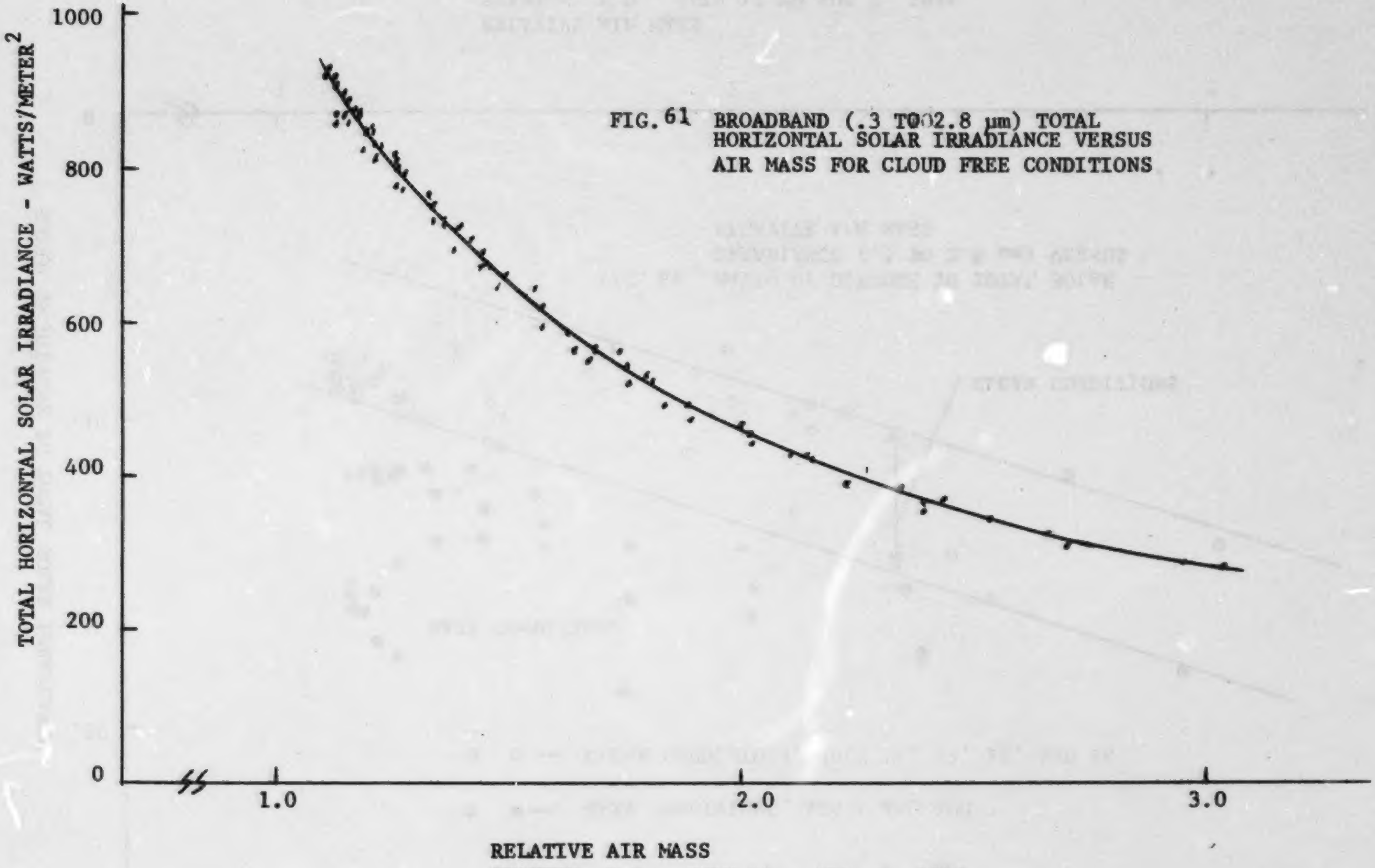

FIG. 61 BROADBAND (.3 TO 2.8 μm) TOTAL HORIZONTAL SOLAR IRRADIANCE VERSUS AIR MASS FOR CLOUD FREE CONDITIONS

STANTON, N.D., JULY 12 - AUG. 7, 1976

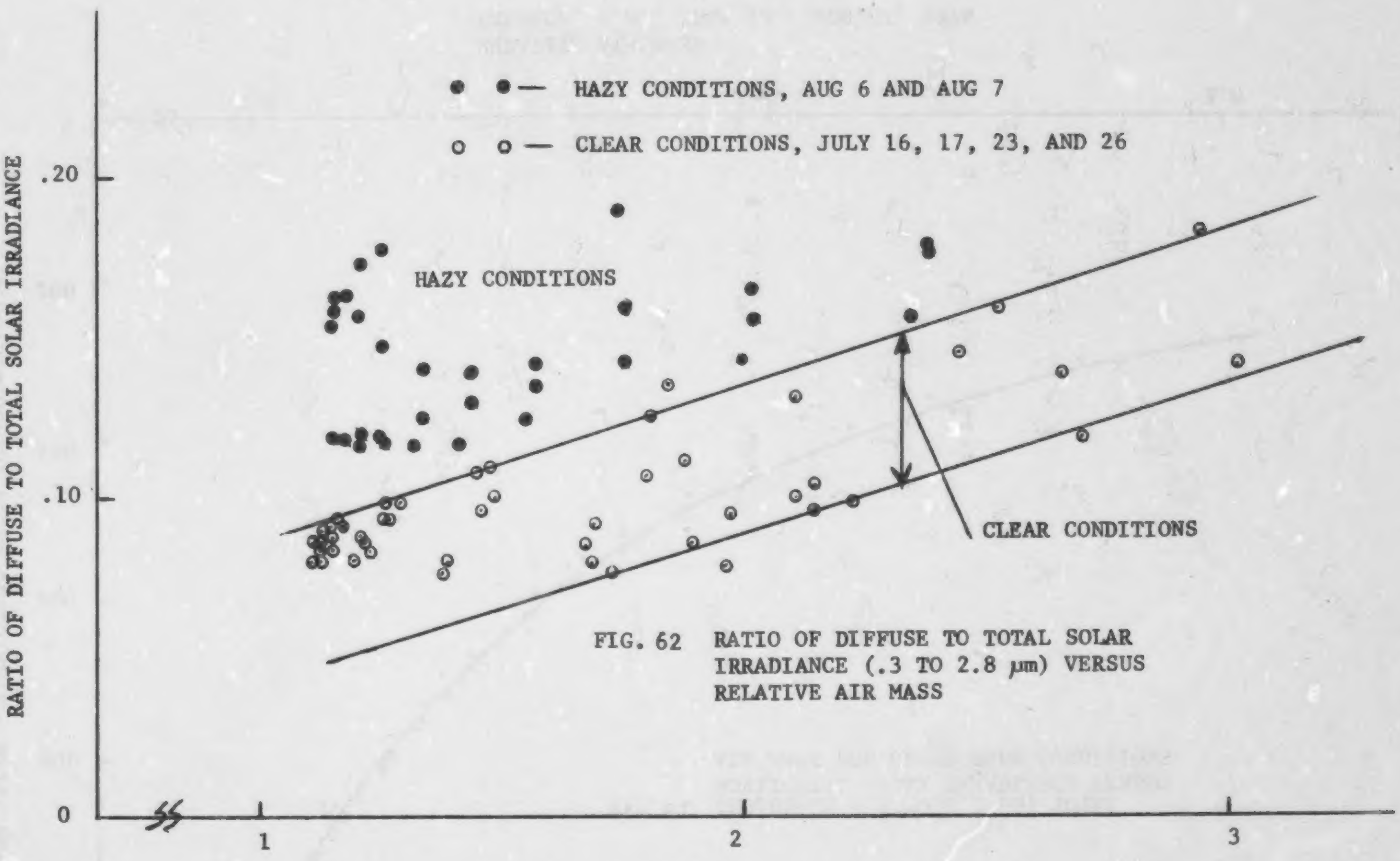

FIG. 62 RATIO OF DIFFUSE TO TOTAL SOLAR IRRADIANCE (.3 TO 2.8 μm) VERSUS RELATIVE AIR MASS

STANTON, N.D., JULY 12 TO AUG 7, 1976

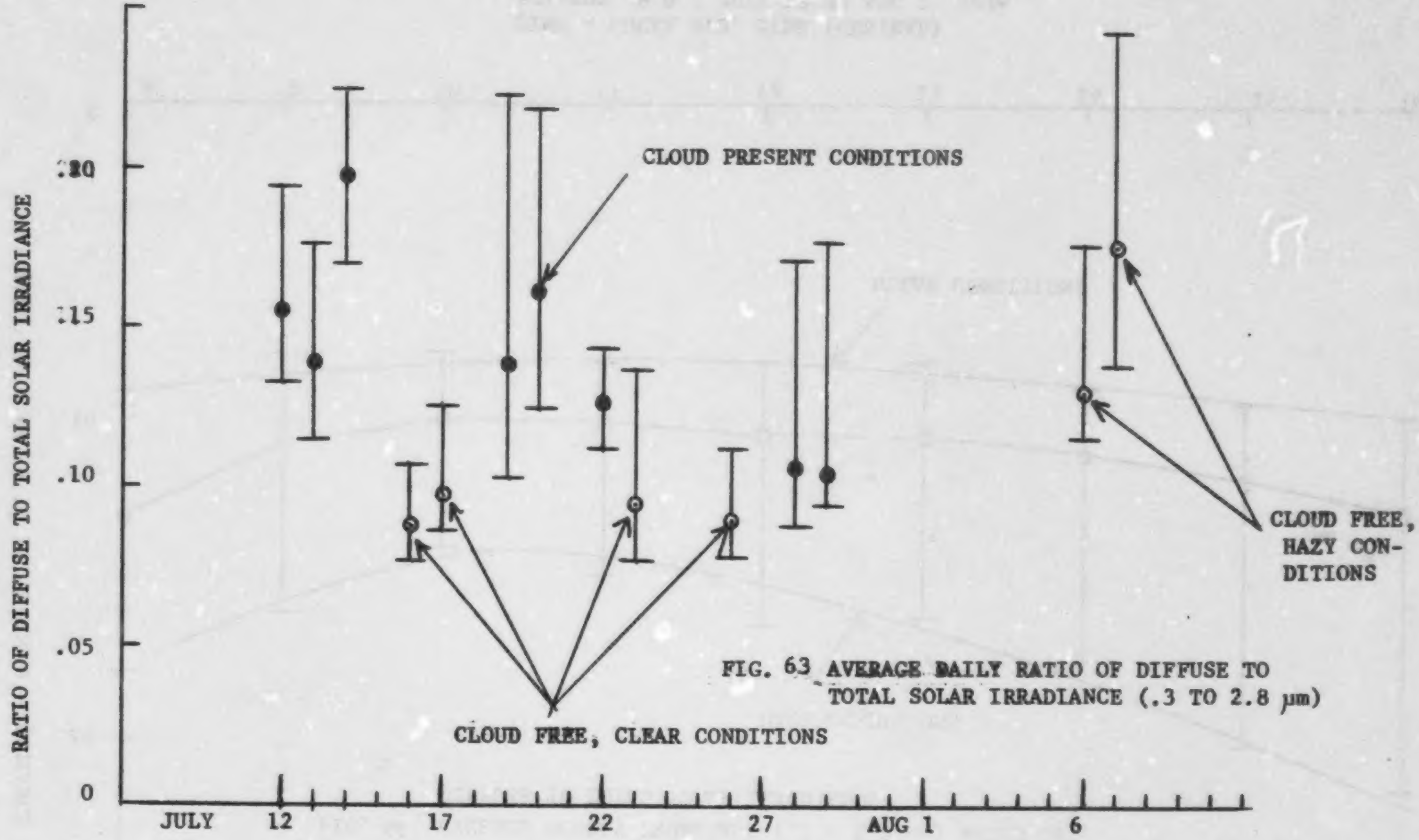

FIG. 63 AVERAGE DAILY RATIO OF DIFFUSE TO TOTAL SOLAR IRRADIANCE (.3 TO 2.8 μm)

DATE: JULY 12 TO AUG 7, 1976
STANTON, N.D.

FIG. 64 AVERAGE HOURLY BROADBAND (.3 - 2.8 μm) RATIO OF DIFFUSE TO TOTAL SOLAR IRRADIANCE

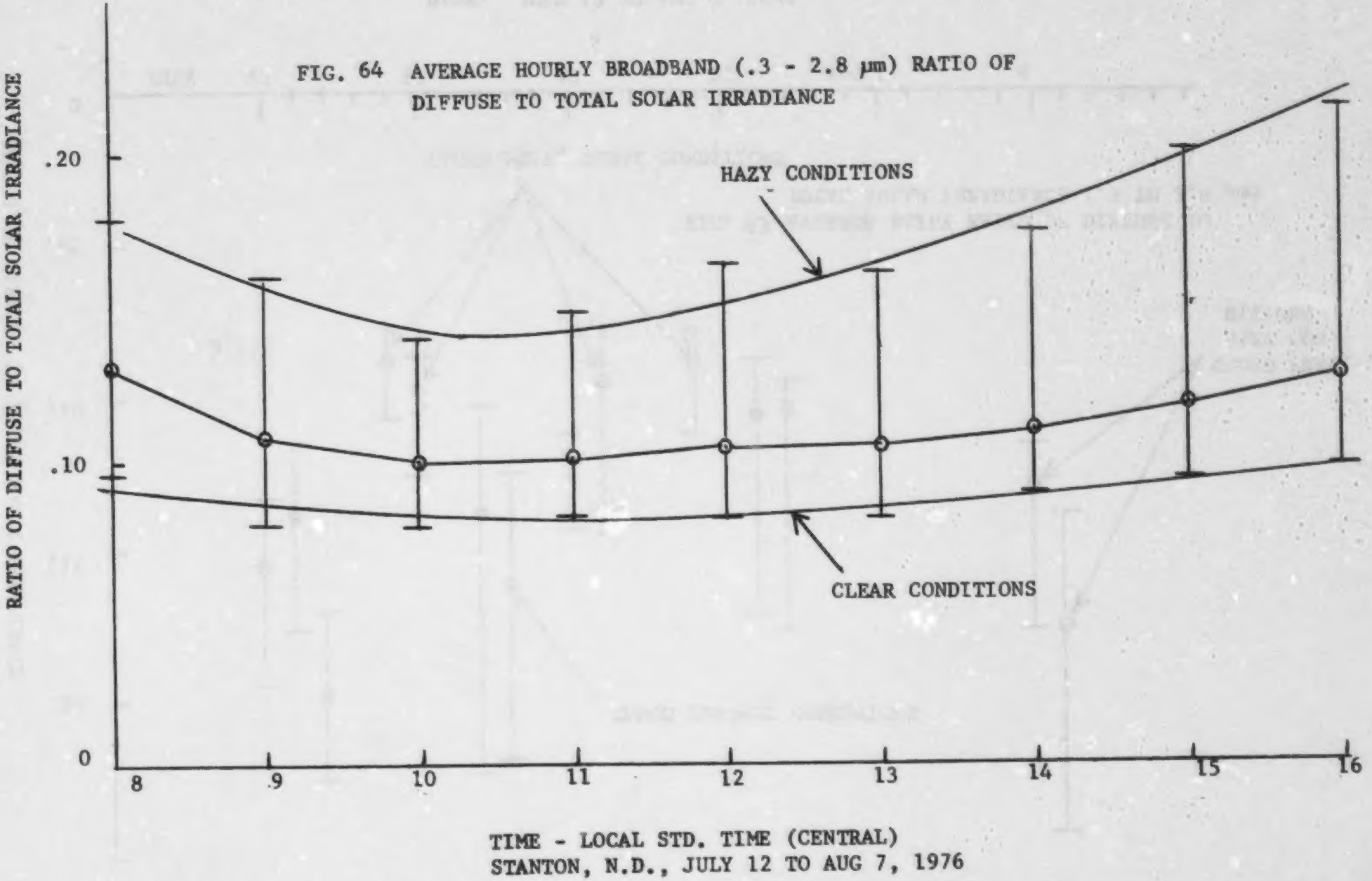

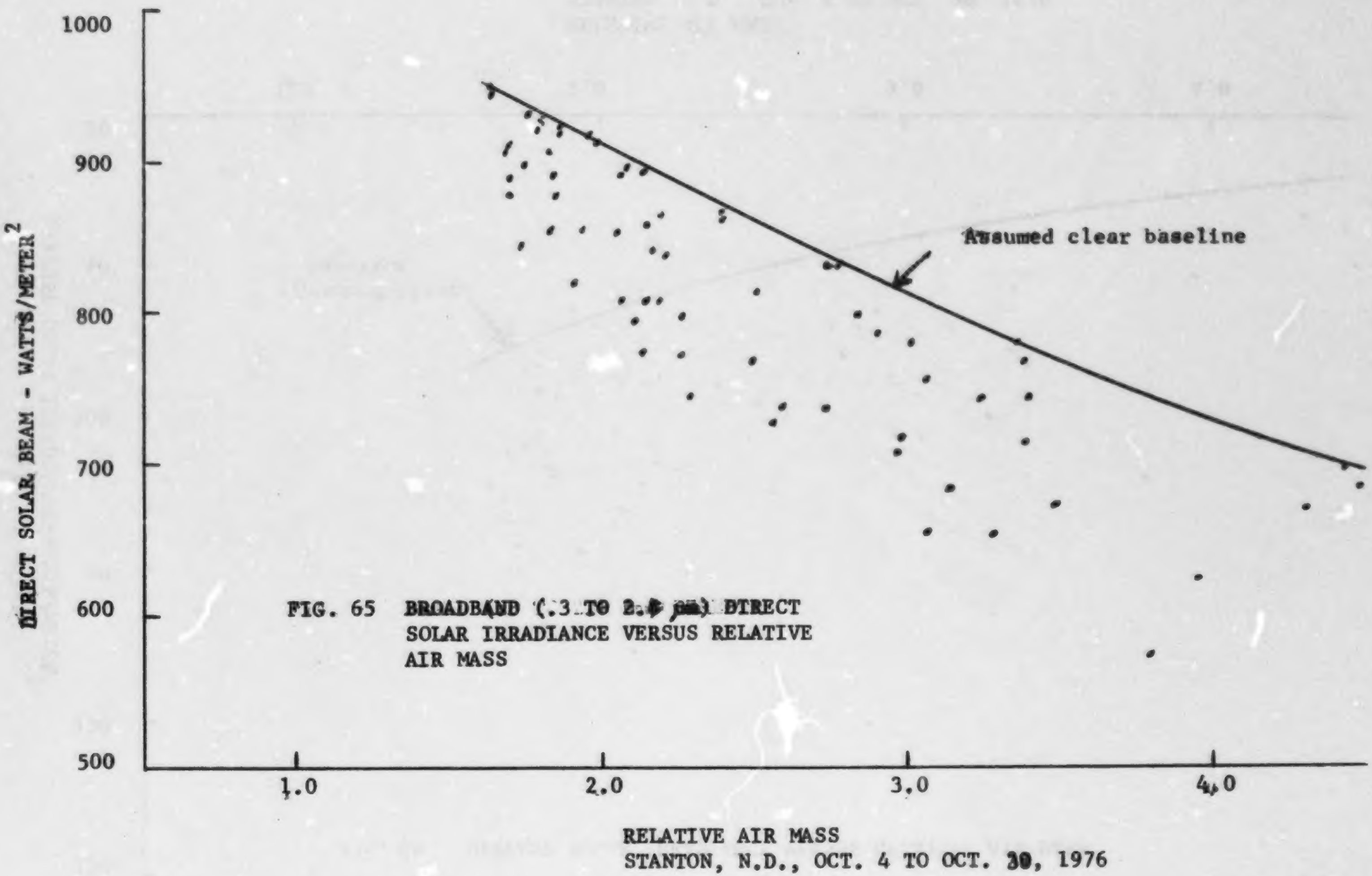

FIG. 65 BROADBAND (.3 TO 2.8 μm) DIRECT SOLAR IRRADIANCE VERSUS RELATIVE AIR MASS

FIG. 66 DIFFUSE SOLAR IRRADIANCE VERSUS RELATIVE AIR MASS

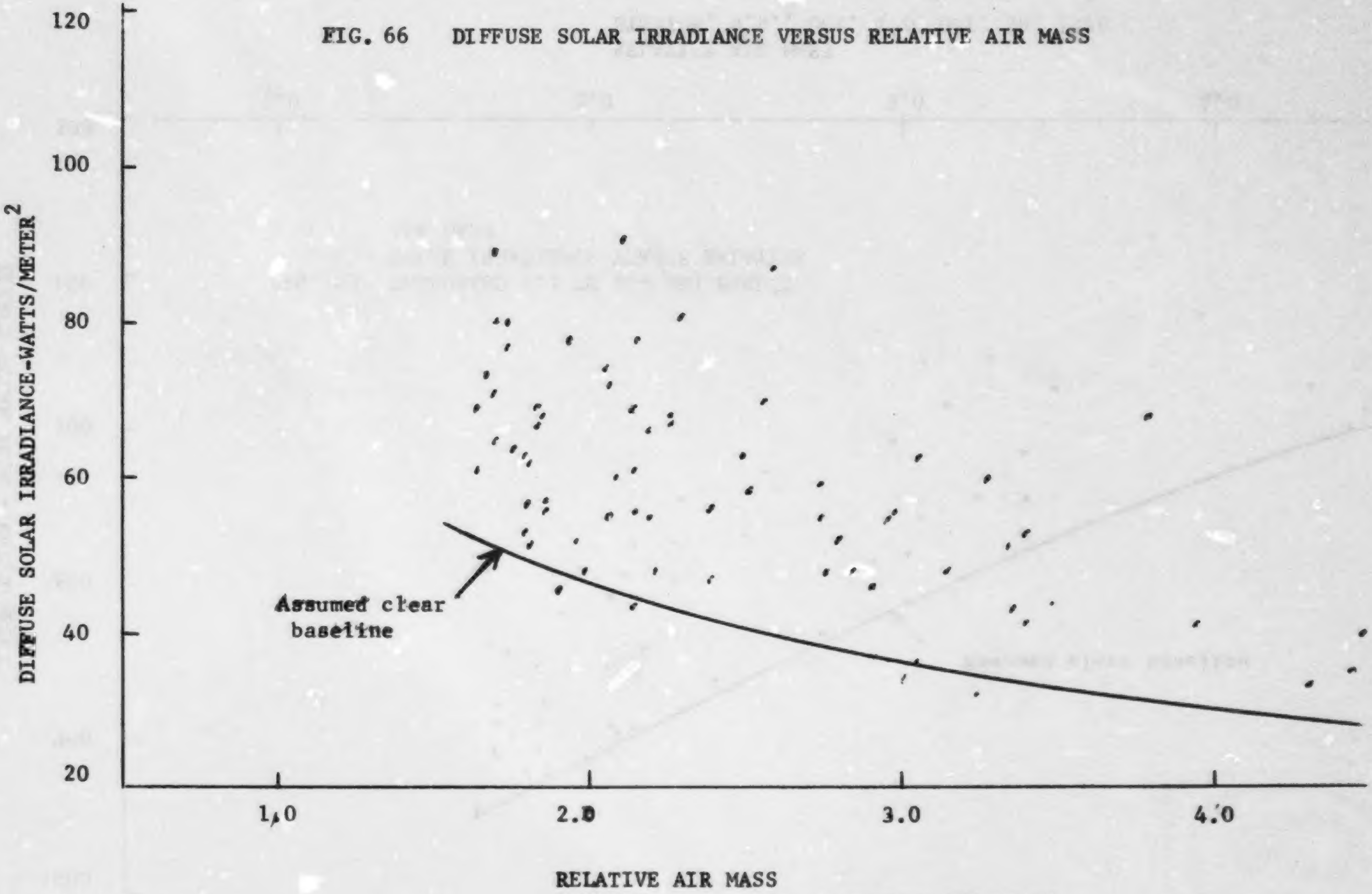

STANTON, N.D., OCT. 4 TO OCT. 30, 1976

FIG. 67 BROADBAND (.3 TO 2.8 μm) TOTAL HORIZONTAL SOLAR IRRADIANCE VERSUS AIR MASS

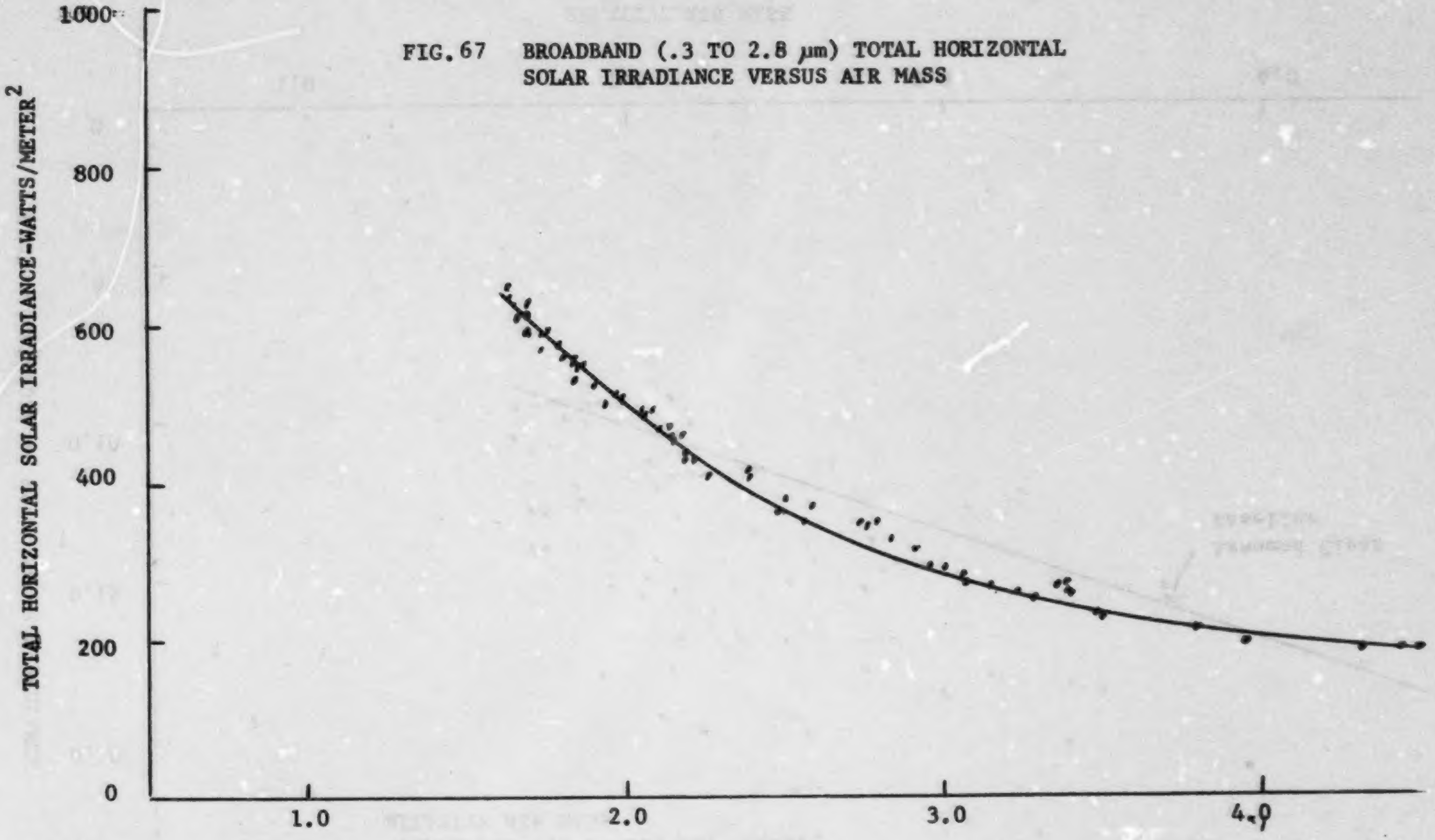

RELATIVE AIR MASS
STANTON, N.D., OCT. 4 TO OCT. 30, 1976

FIG. 68 RATIO OF DIFFUSE TO TOTAL SOLAR IRRADIANCE (.3 TO 2.8 μm) VERSUS, RELATIVE AIR MASS

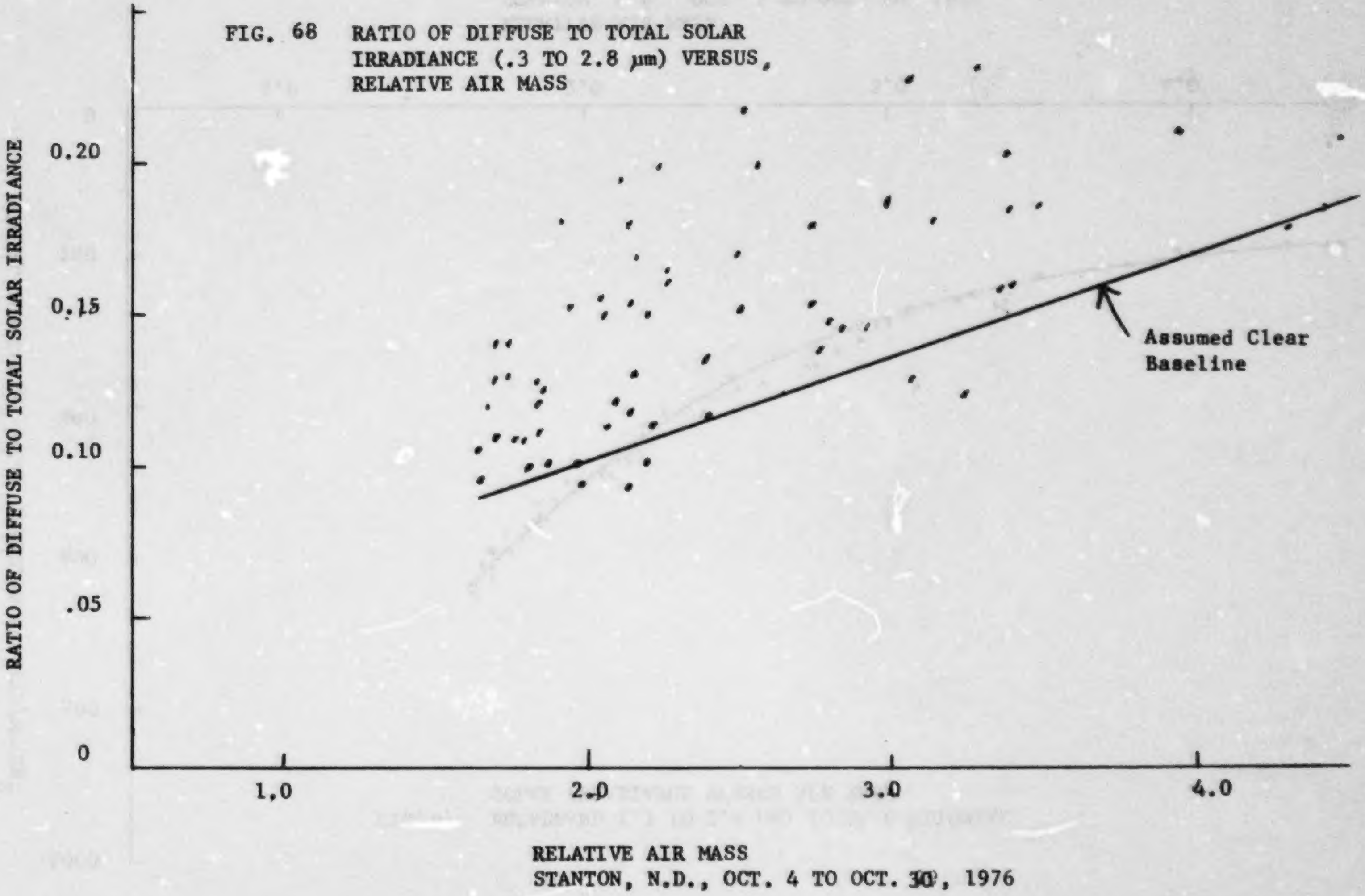

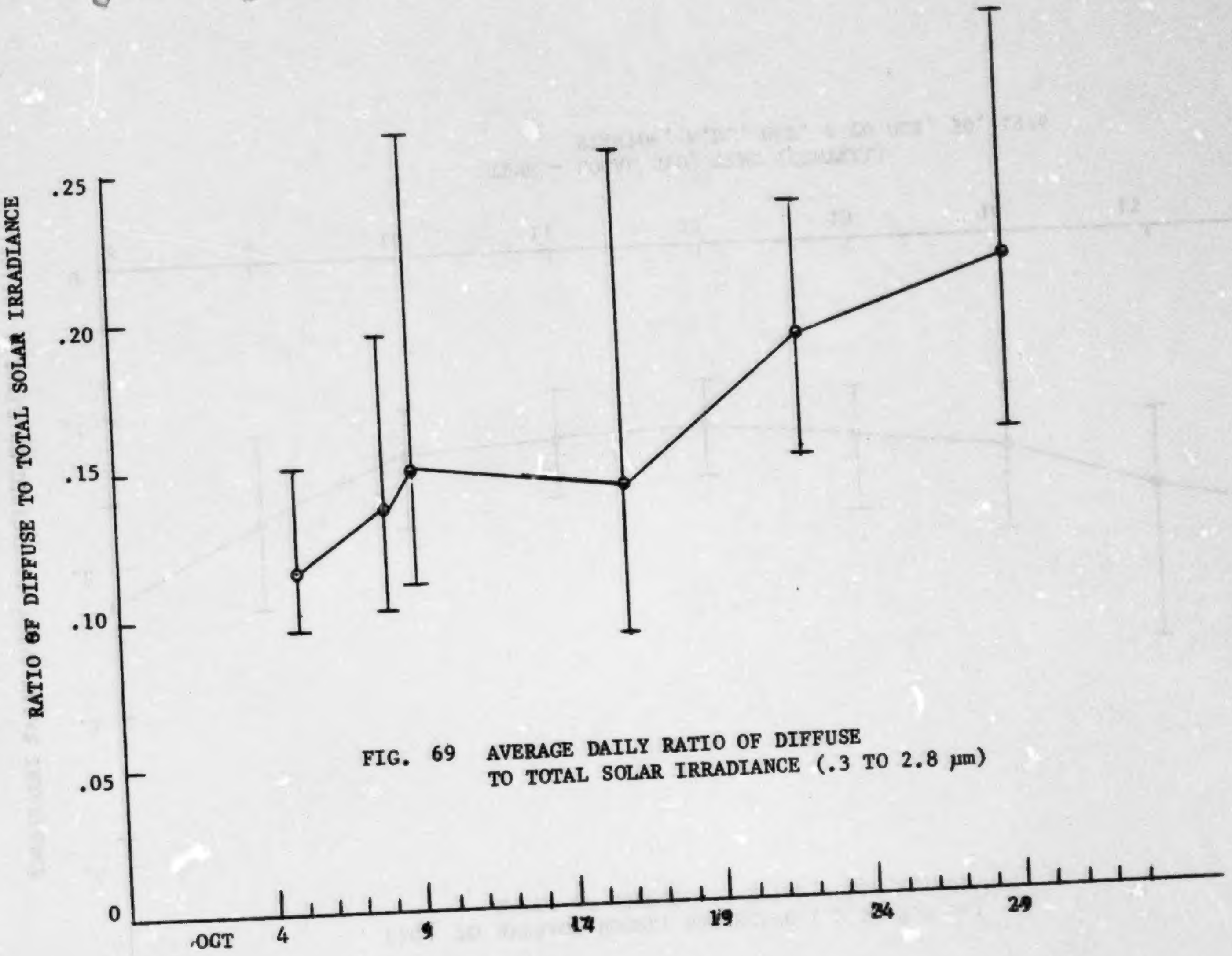

FIG. 69 AVERAGE DAILY RATIO OF DIFFUSE TO TOTAL SOLAR IRRADIANCE (.3 TO 2.8 µm)

DATE: OCT. 4 TO OCT. 30, 1976
STANTON, N.D.

FIG. 70 AVERAGE HOURLY BROADBAND (.3 TO 2.8 μm) RATIO OF DIFFUSE TO TOTAL SOLAR IRRADIANCE

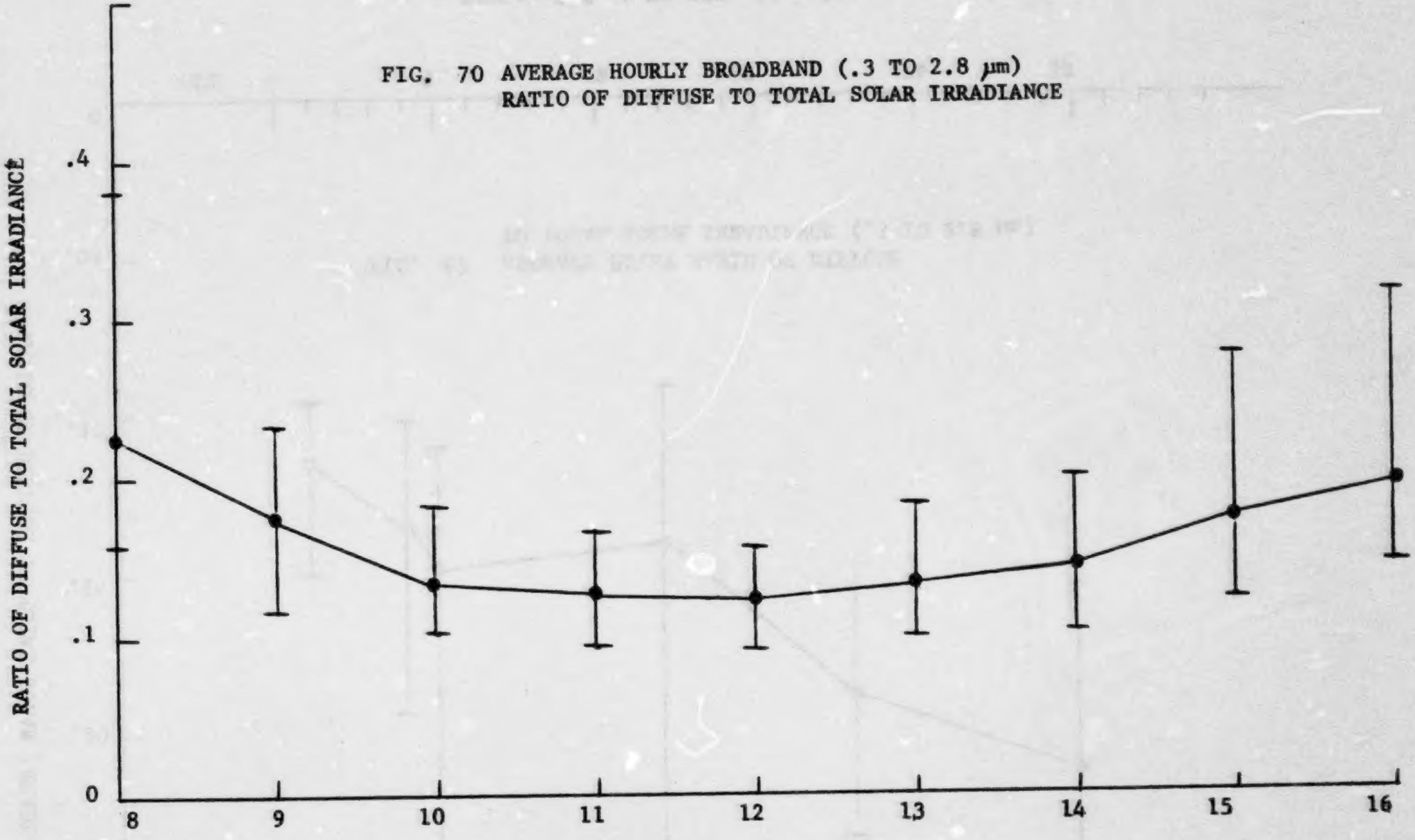

TIME - LOCAL STD. TIME (CENTRAL)
STANTON, N.D., OCT. 4 TO OCT. 30, 1976

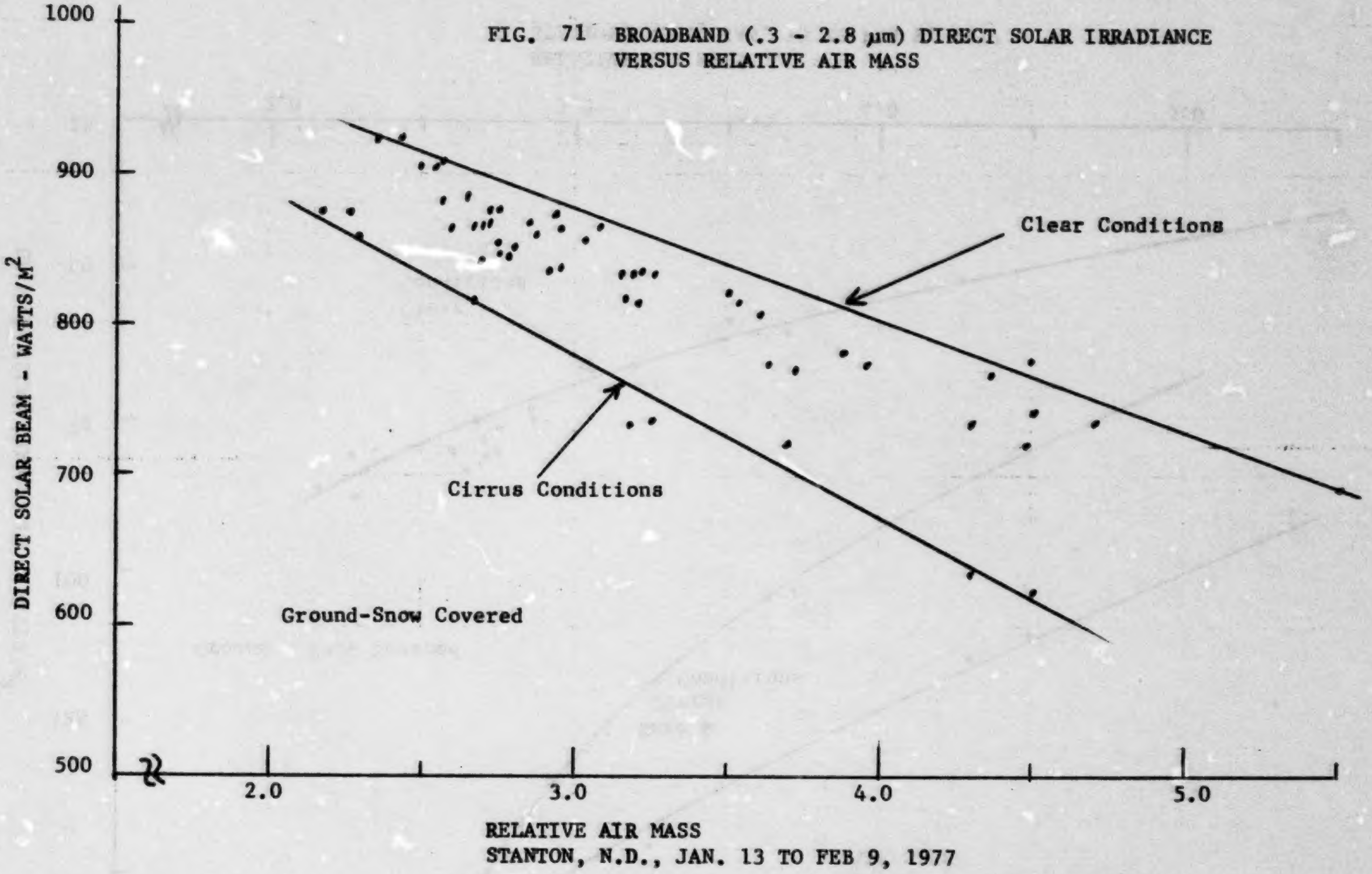

FIG. 71 BROADBAND (.3 - 2.8 μm) DIRECT SOLAR IRRADIANCE VERSUS RELATIVE AIR MASS

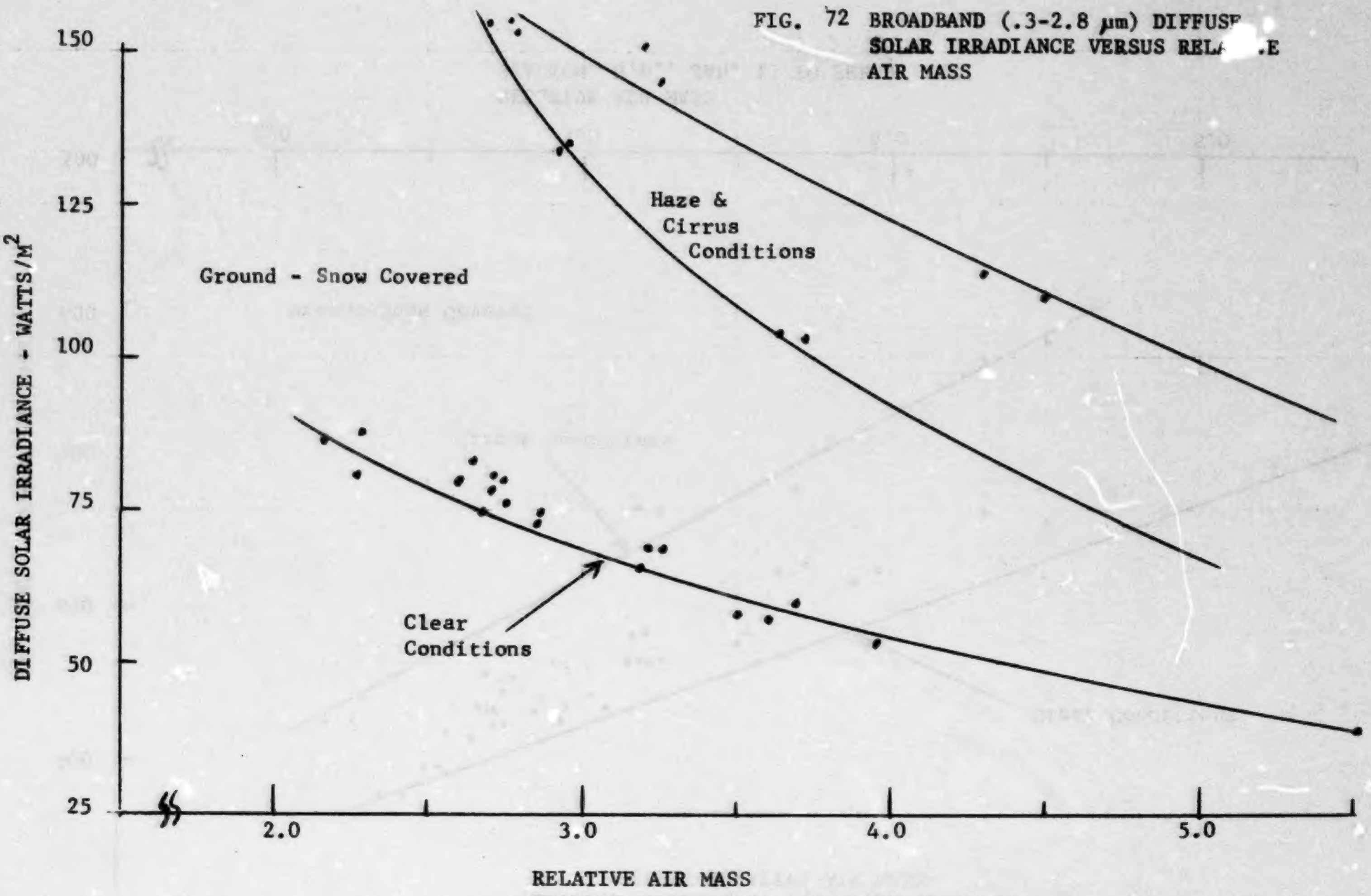

FIG. 72 BROADBAND (.3-2.8 μm) DIFFUSE SOLAR IRRADIANCE VERSUS RELA[illegible]E AIR MASS

STANTON, N.D., JAN. 13 TO FEB 9, 1977

FIGURE 73 BROADBAND (.3-2.8 μm) TOTAL HORIZONTAL SOLAR IRRADIANCE VERSUS RELATIVE AIR MASS

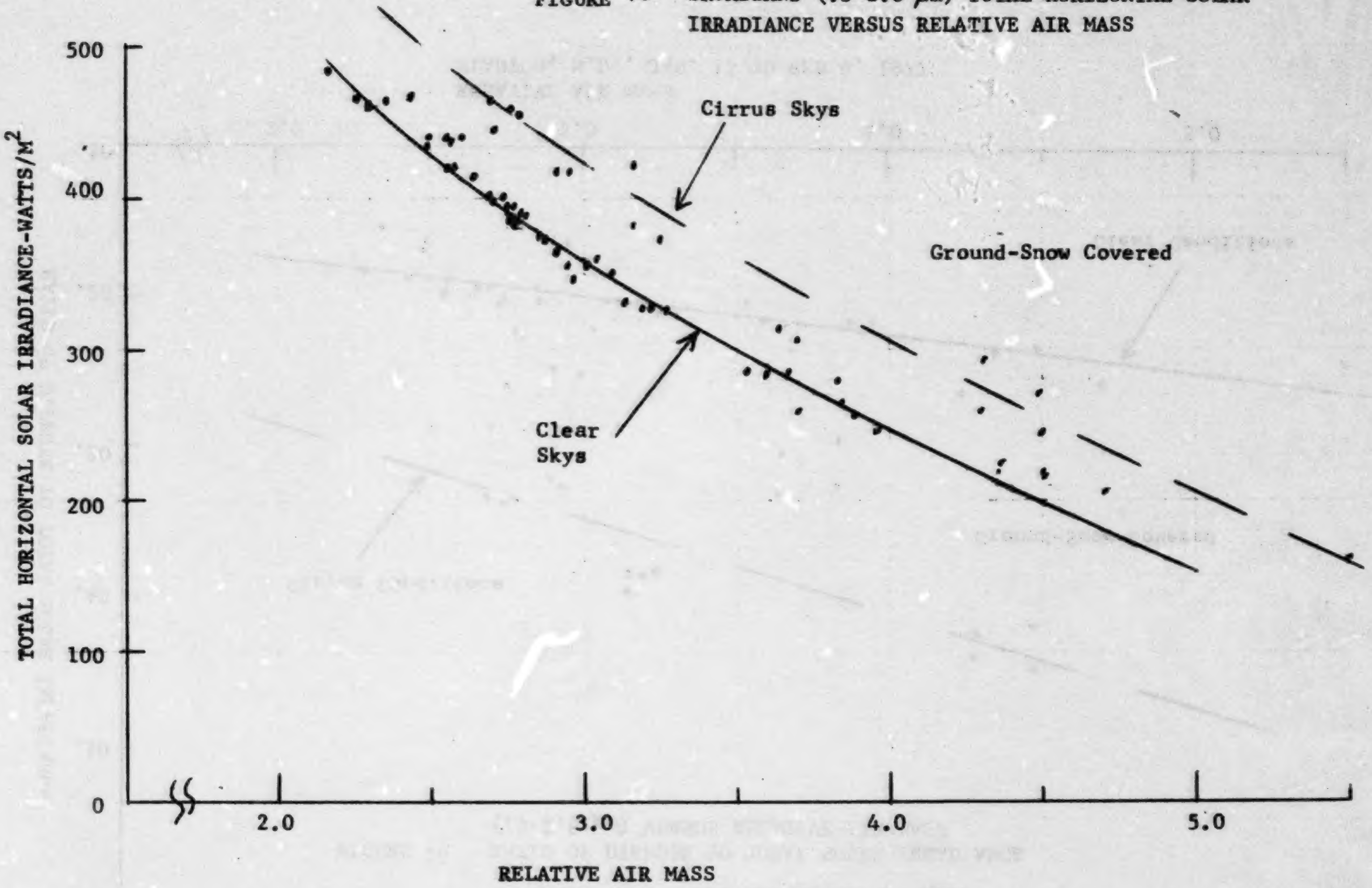

STANTON, N.D., JAN. 13 TO FEB 9, 1977

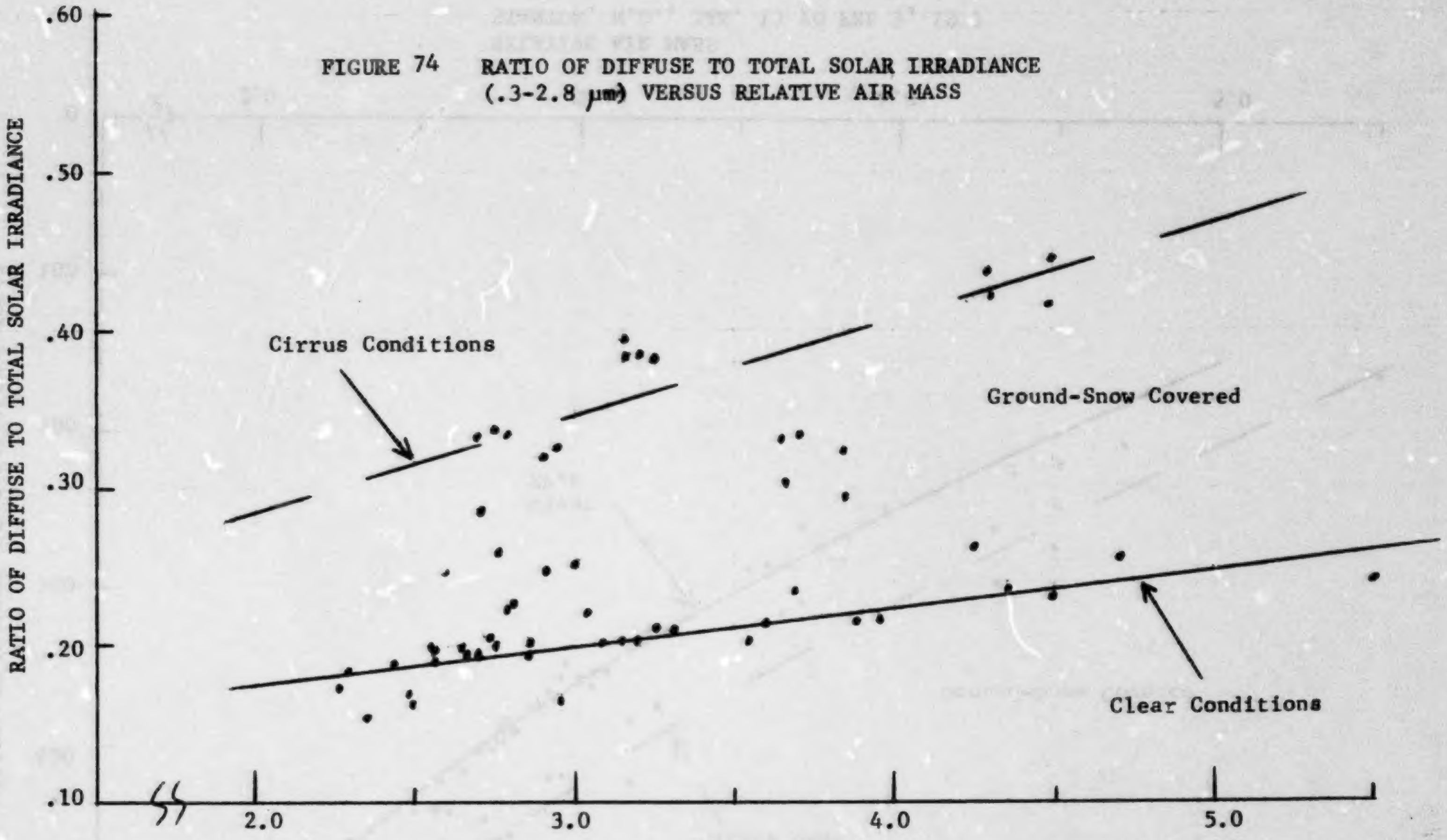

FIGURE 74 RATIO OF DIFFUSE TO TOTAL SOLAR IRRADIANCE
(.3-2.8 μm) VERSUS RELATIVE AIR MASS

STANTON, N.D., JAN. 13 TO FEB 9, 1977

FIGURE 75 AVERAGE DAILY RATIO OF DIFFUSE TO TOTAL SOLAR IRRADIANCE (.33TO 2.8 μm)

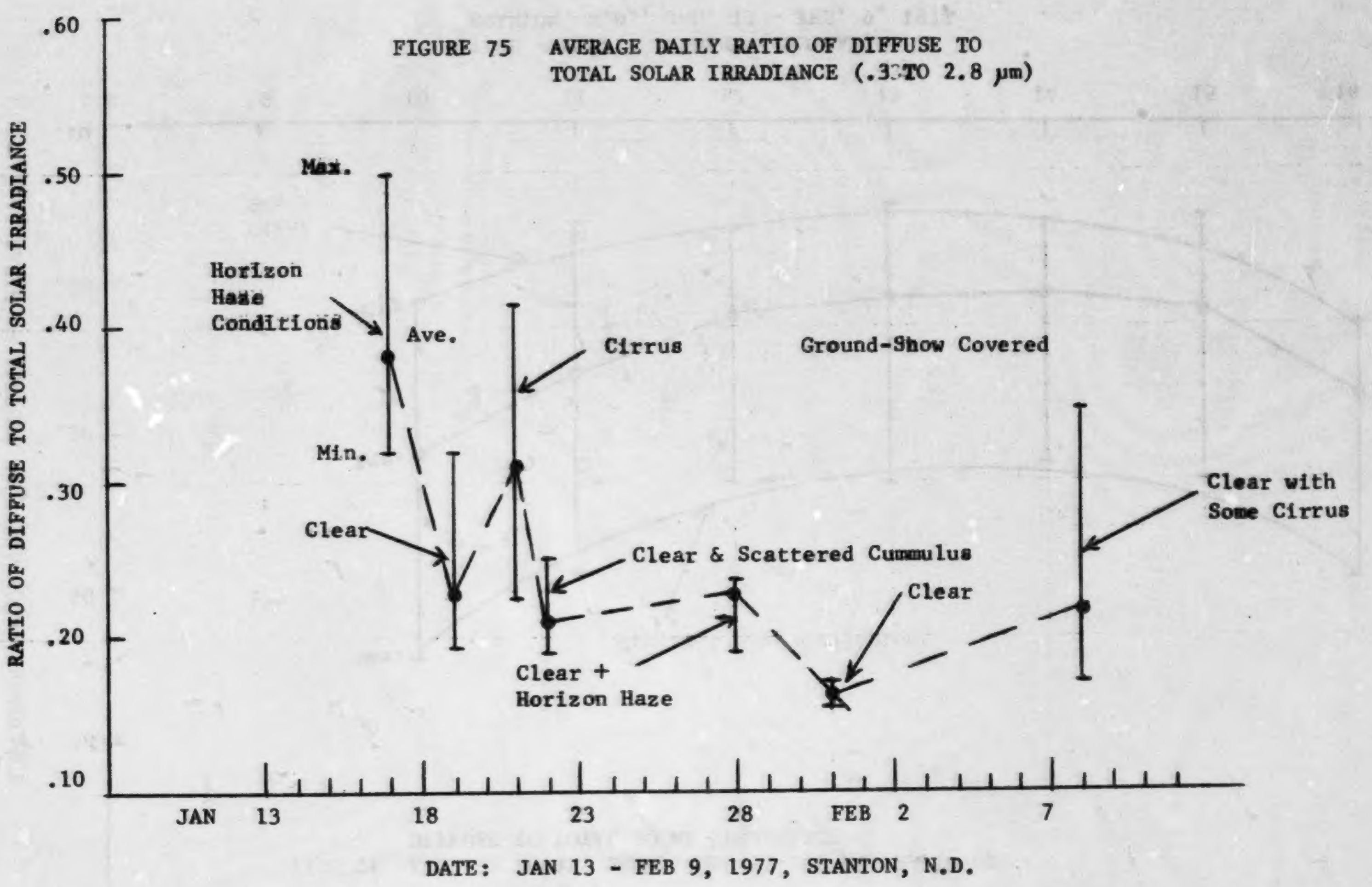

FIG. 76 AVERAGE HOURLY BROADBAND (.3-2.8 μm) RATIO OF DIFFUSE TO TOTAL SOLAR IRRADIANCE

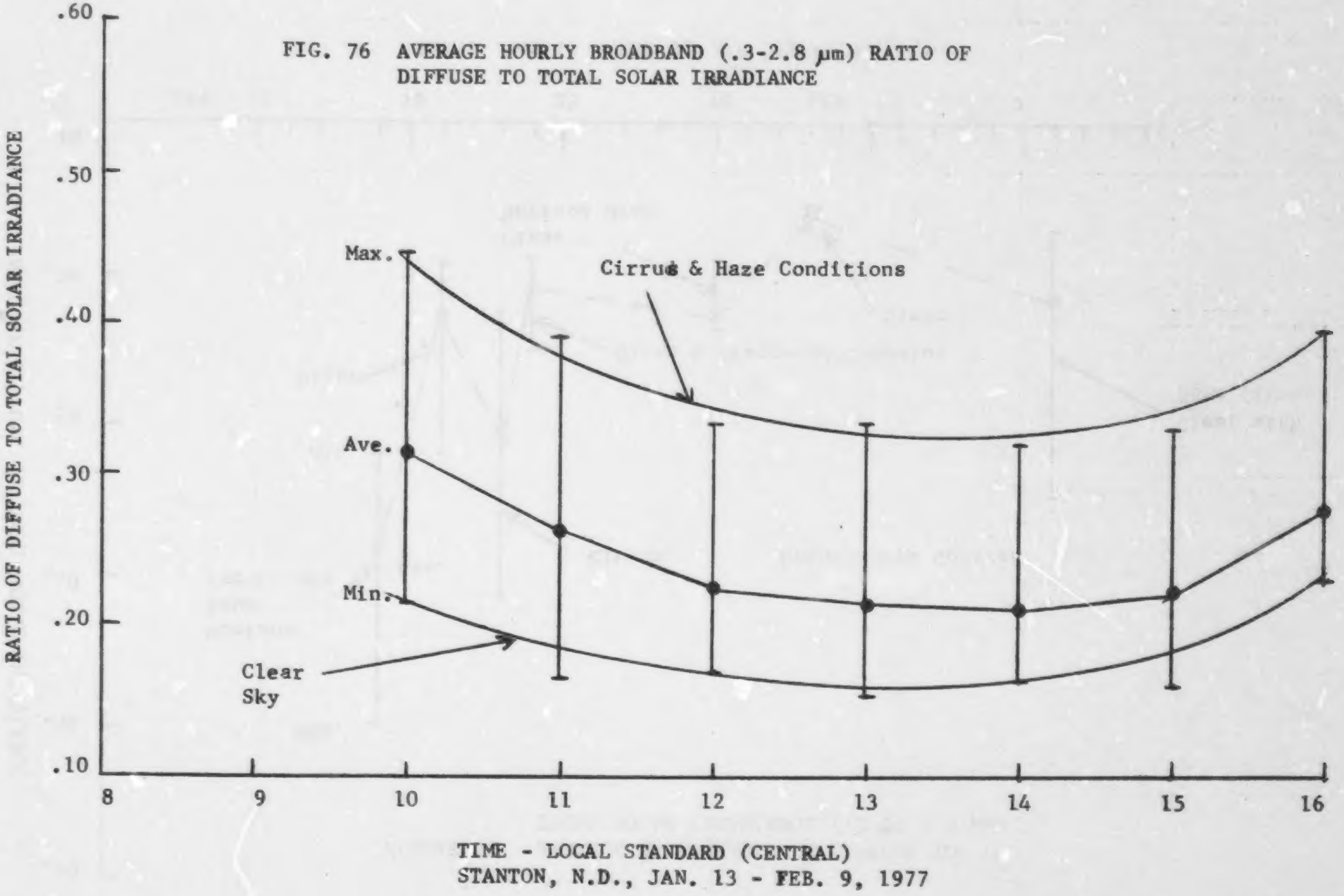

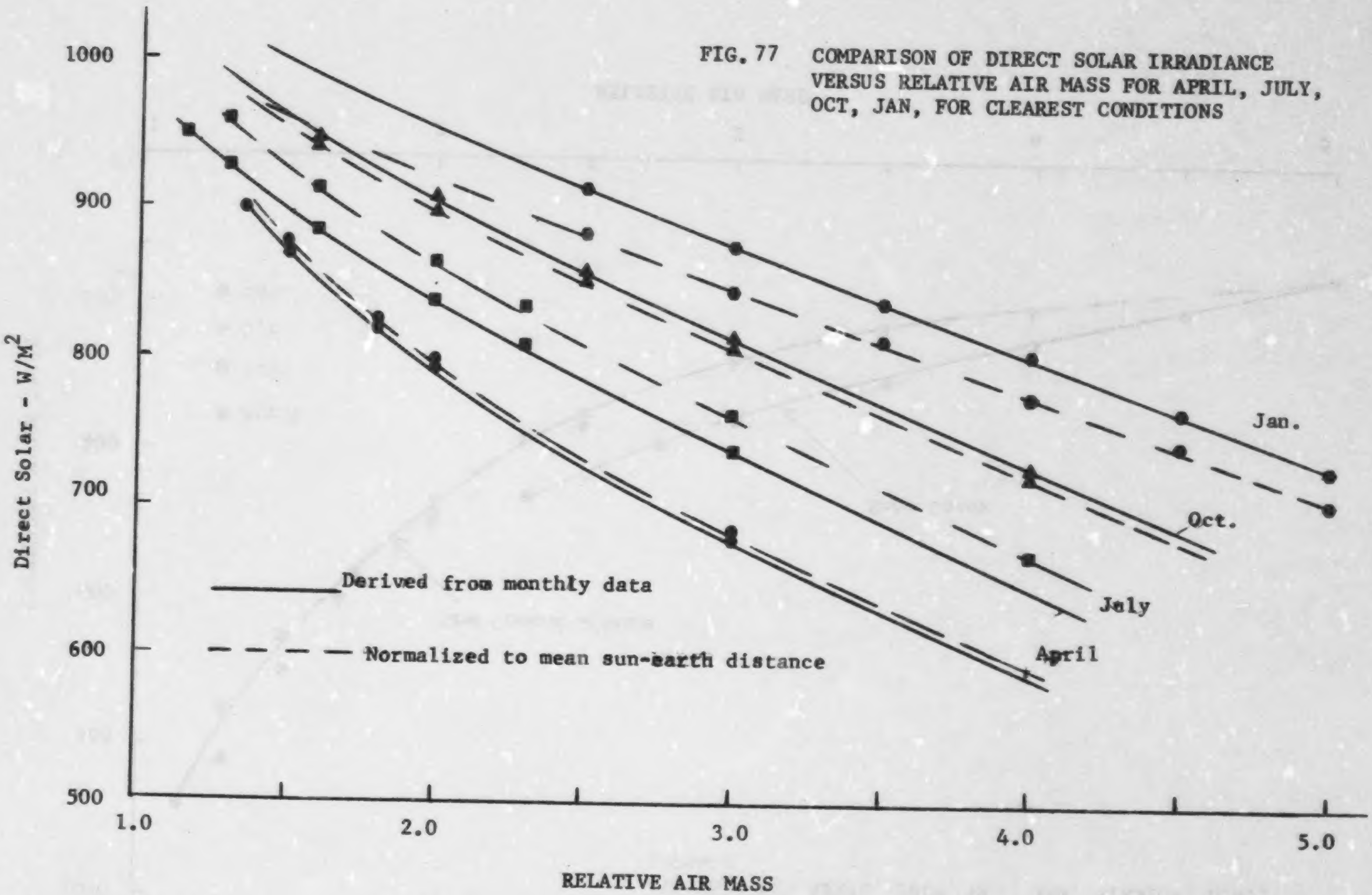
FIG. 77 COMPARISON OF DIRECT SOLAR IRRADIANCE VERSUS RELATIVE AIR MASS FOR APRIL, JULY, OCT, JAN, FOR CLEAREST CONDITIONS

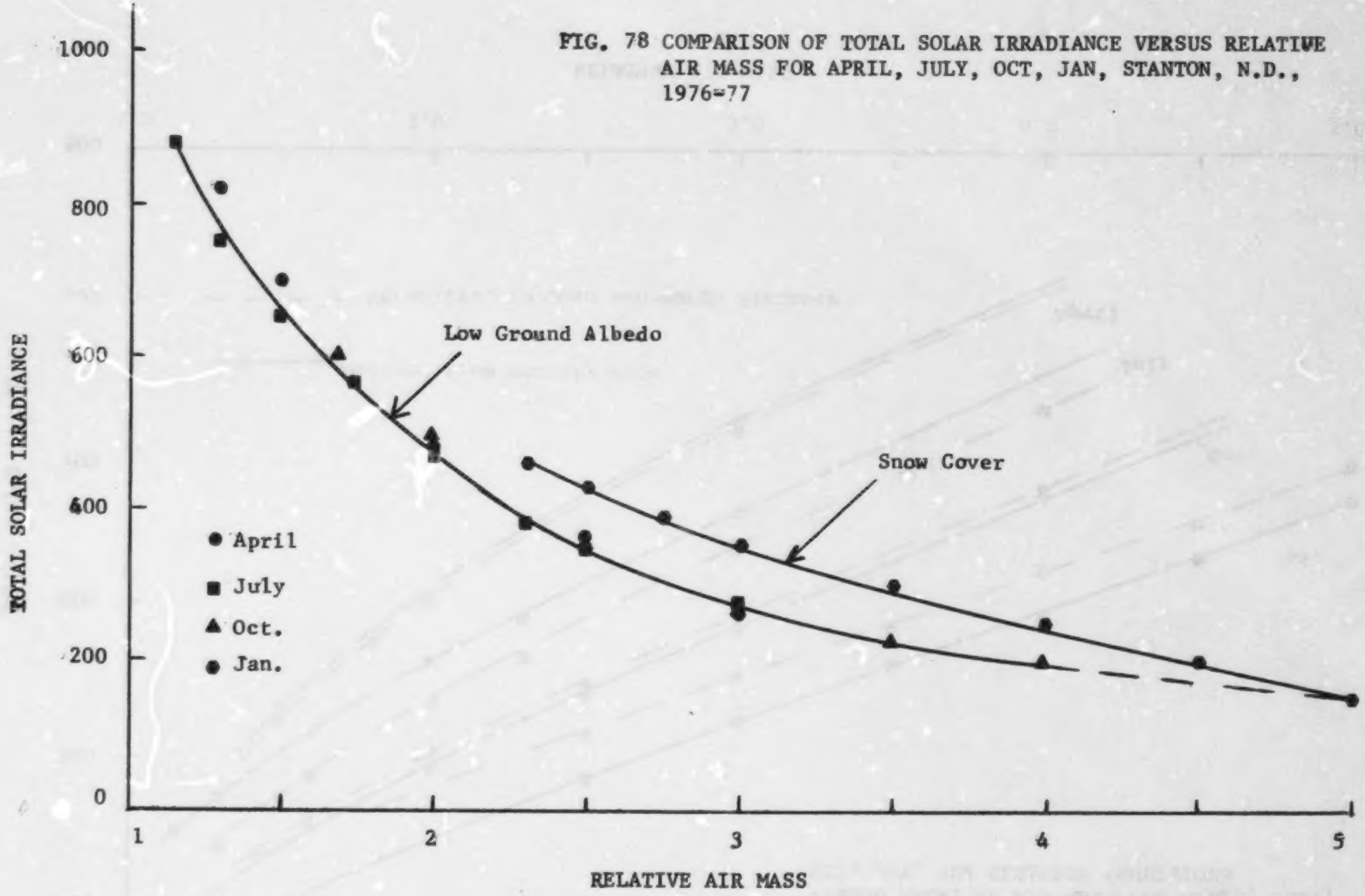

FIG. 78 COMPARISON OF TOTAL SOLAR IRRADIANCE VERSUS RELATIVE AIR MASS FOR APRIL, JULY, OCT, JAN, STANTON, N.D., 1976-77

FIGURE 79: COMPARISON OF THE RATIO OF DIFFUSE TO TOTAL SOLAR IRRADIANCE VERSUS AIR MASS FOR APRIL, JULY, OCT, JAN, STANTON, N.D. 1976-77

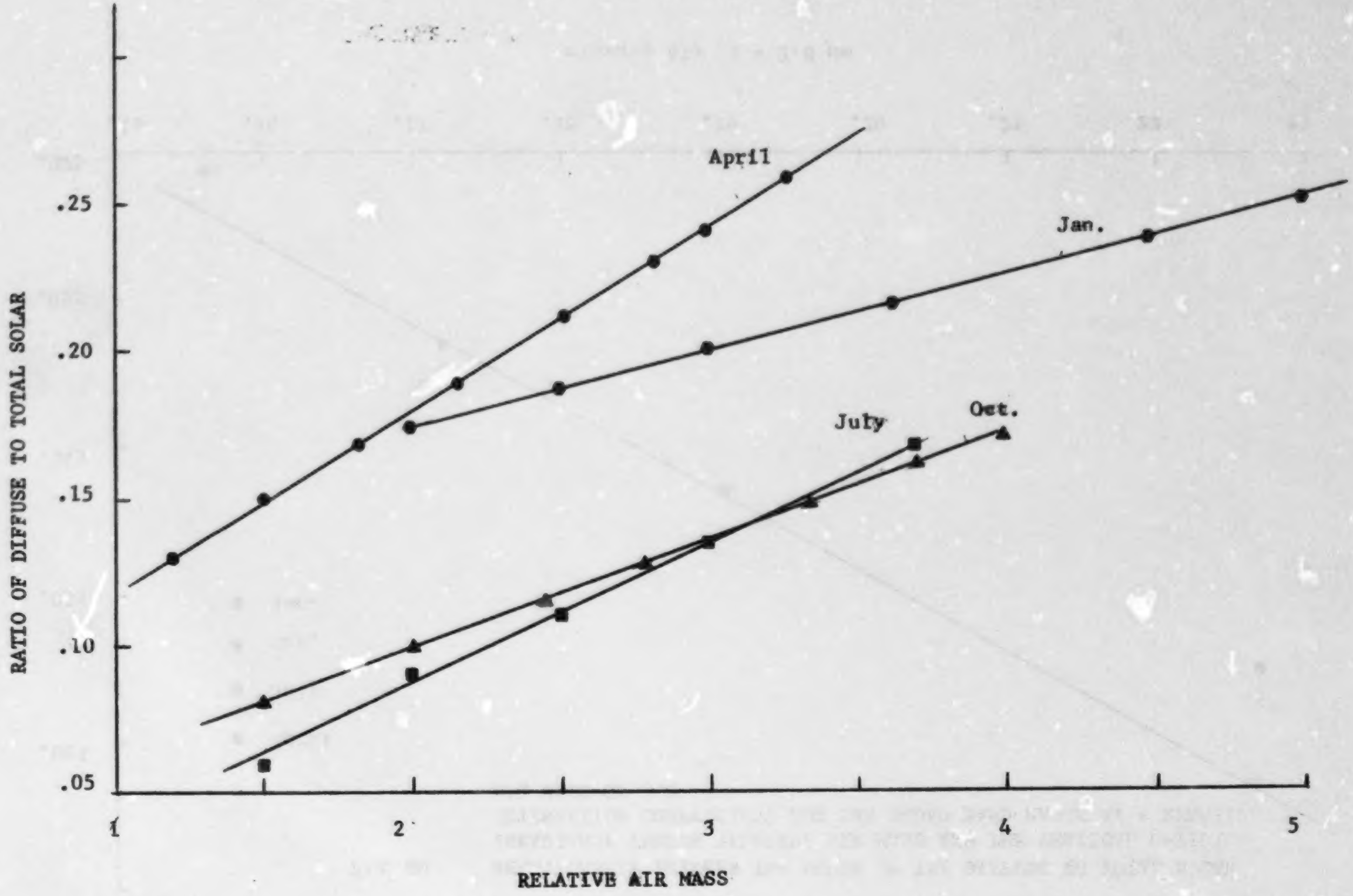

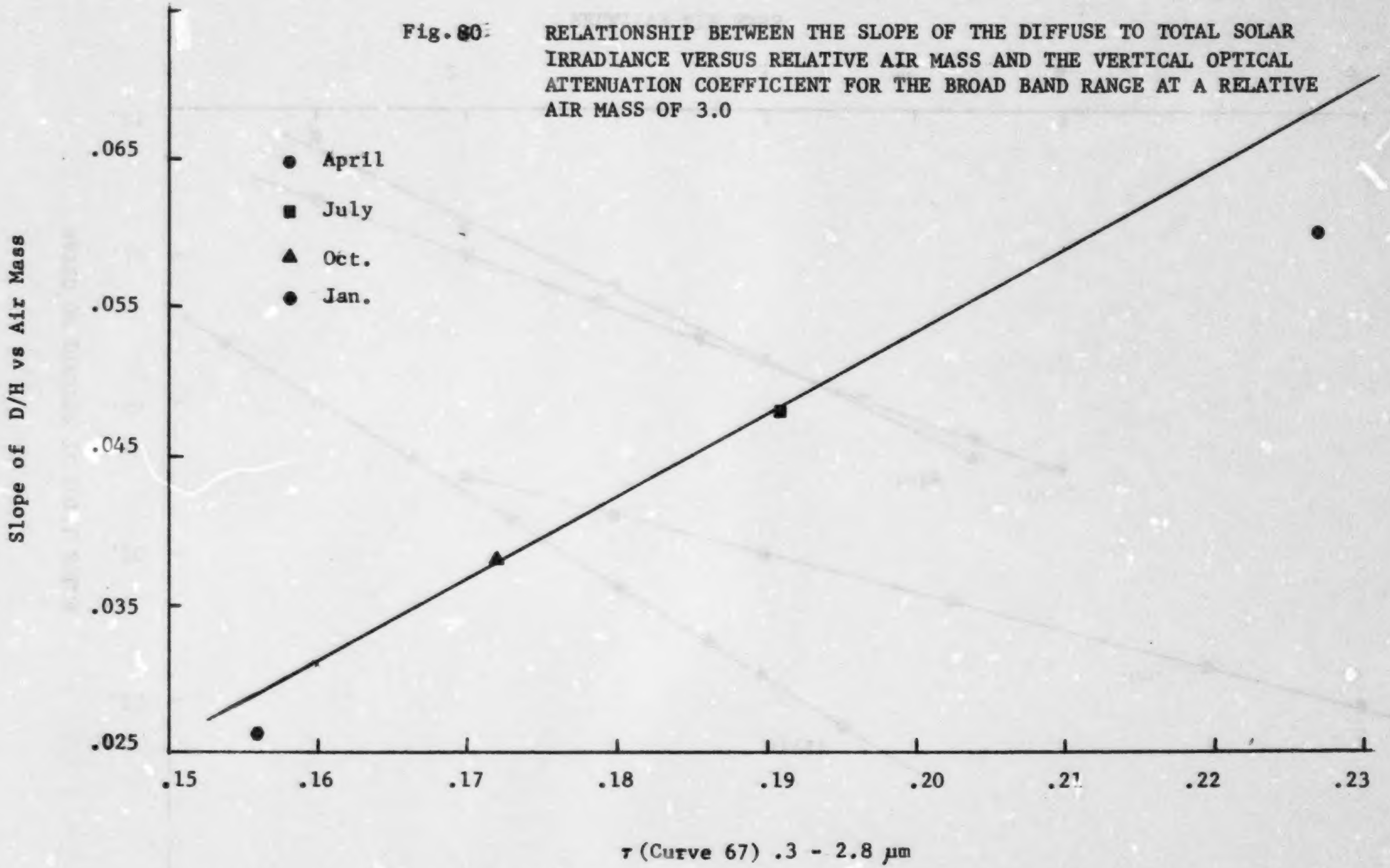

Fig. 80 RELATIONSHIP BETWEEN THE SLOPE OF THE DIFFUSE TO TOTAL SOLAR IRRADIANCE VERSUS RELATIVE AIR MASS AND THE VERTICAL OPTICAL ATTENUATION COEFFICIENT FOR THE BROAD BAND RANGE AT A RELATIVE AIR MASS OF 3.0

7. SKY APPEARANCE

7.1 Techniques/Instrumentation Used - The general sky appearance, in the horizontal direction, was documented (hourly from 0800 to 1600 LST) with Kodak Kodachrome color film (35 mm slides) and a Honeywell Pentax Spotmatic camera equipped with a 200 mm lens. Hourly photographs were taken for each of four views, see Figure 1. Each of the four views, as seen through the 200 mm lens, are shown in Figures 81 through 84.

7.2 April Sky Appearance - Due to weather conditions, only 18 of the possible 24 days of observation were documented in terms of sky appearance. Of the 18 observation days, 4 days were visibly hazy, and a very noticeable smog layer was observed on 2 days. The 4 hazy days were April 5, 12, 13 and 19. The two days having noticeable smog layer, which was located to the north-northwest of the site, were April 27, and the 28th.

7.3 July Sky Appearance - Of the 24 possible days of observation, 24 days were documented in terms of sky appearance. Of the 24 observation days, 4 days were visibly hazy, and a very noticeable smog layer occurred on 5 days. Days having a slightly noticeable haze were July 12, 19 and the 26th. A medium haze was evident on Aug. 6. On July 24 a smog layer existed to the northeast. On Aug. 2, smog was evident east to west. On Aug. 3, smog was evident to the north. On Aug. 4 smog was evident to the north and west. On Aug. 7 a very heavy haze/smog was evident in all directions.

7.4 October Sky Appearance - Out of the 24 possible days of operation, 24 days were documented in terms of sky appearance. Of the 24 observation days, 4 days were visibly hazy and a noticeable smog layer occurred on one day. These days were Oct. 19, 21, 22, and 29. On Oct. 11 a smog layer existed existed to the north.

7.5 January Sky Appearance - Of the 24 possible days of observation, 21 days were documented in terms of sky appearance. Hazy conditions

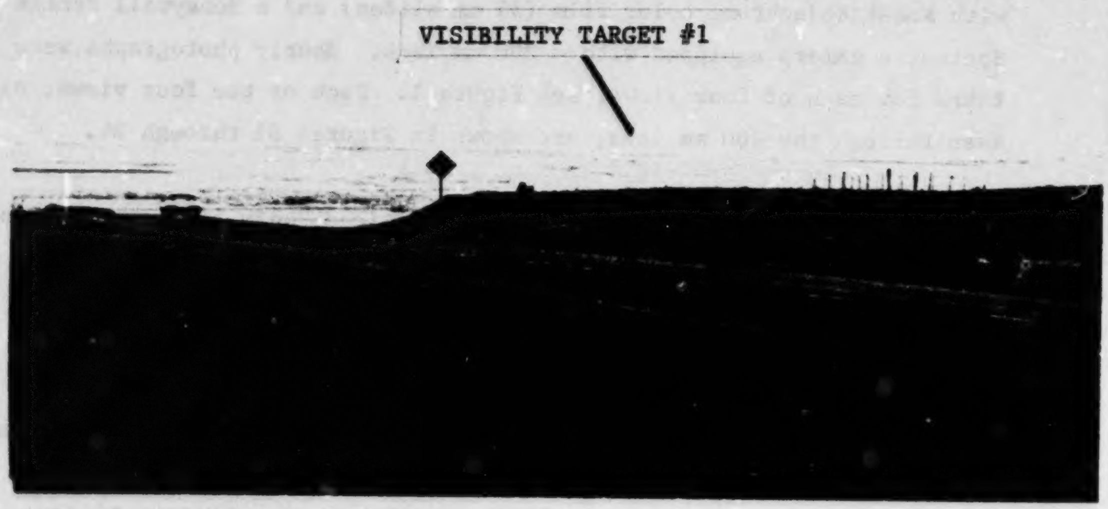
VISIBILITY TARGET #1

Figure 81 View #1 - 200 mm Lens

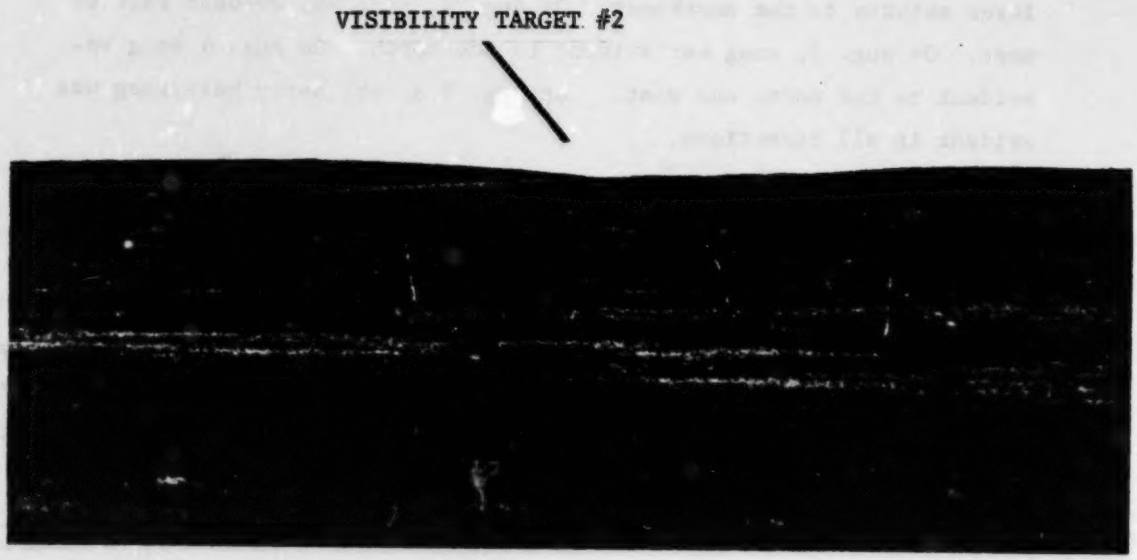
VISIBILITY TARGET #2

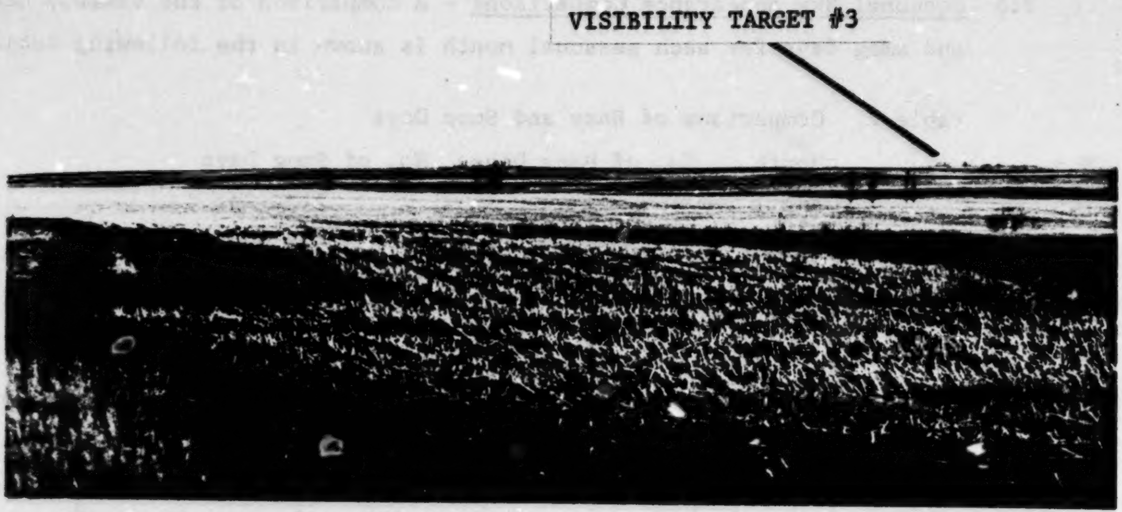
VISIBILITY TARGET #3

Figure 83 View #3 - 200 mm Lens

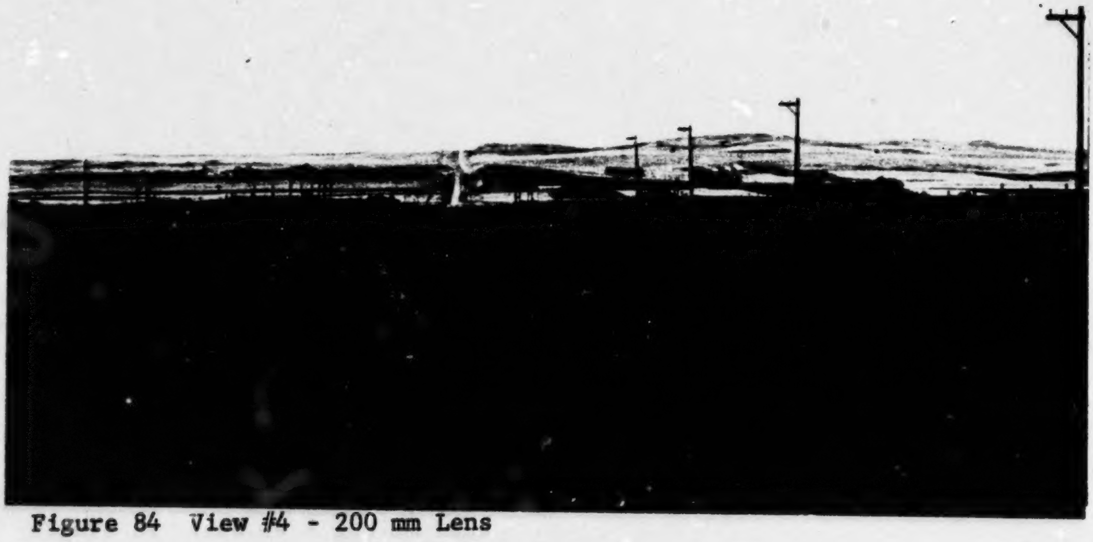

Figure 84 View #4 - 200 mm Lens

existed on January 13, 17, 21 and February 7. On January 28 and February 1, smog was evident to the north and east.

7.6 Seasonal Sky Appearance Comparisons - A comparison of the visibly hazy and smog days for each seasonal month is shown in the following table.

Table 2. Comparison of Hazy and Smog Days

Month	No. of Hazy Days	No. of Smog Days
April	4	2
July	4	5
Oct.	4	1
Jan.	4	2

As shown in the above table, each month had four days where a haze was visibly noticeable. These four days represents about 17% of the total number of observed days. Considering the days where smog was noticed, July had by far the greatest smog occurrence, a total of 5 days. The other months had about 2 days of smog occurrence. The document direction of this smog was reported to be the north, northeast, and northwest.

8. Meteorology

8.1 **Techniques/Instrumentation Used** - The meteorological parameters measured consisted of the temperature, pressure, relative humidity, wind direction, wind speed, dust concentration, and total precipitable water vapor.

The temperature and relative humidity were measured using a sling psychometer to determine dry and wet bulb temperatures. The pressure was measured with an aneroid-type engineer barometer. The wind speed was measured using a hand-held cup anemometer. The wind direction was measured with a precision Brunton compass and a directional flag. The relative dust concentration was measured with an integrating, 90° scattering angle nephelometer, manufactured by Weather Measure Corporation (Digital Dust Meter). This nephelometer is an electro-optical instrument that provides an indication of atmospheric dust concentrations in the range from 0.01 to 500 mg/m^3 of air. Light scattered by dust, as it aspirates past a fixed intensity lightbeam, is measured by a photomultiplier tube yielding a count rate directly proportional to dust concentration. The size of dust particles sampled are determined by an optical maze that screens out all particles greater than 20 microns and accepts approximately 60% of 10 micron particles and 100% of 5 micron or smaller particles. An estimate of dust concentration in mg/m^3 of air is made by

$$C = (R-D)K \tag{27}$$

where:

C = dust concentration in mg/m^3 in air

R = counts per minute

D = background counts (known)

K = mg/m^3 of dust per count (known)

The absolute accuracy of the nephelometer is subject to errors associated with difficulties of calibrating the instrument with a known aerosol that closely approximates the aerosol measured on site. However, the counts per minute will give an accurate indication of relative dust concentration. For this reason only the counts per minute are reported because of a lack of calibration (after repair) of the instrument.

The amount of precipitable water vapor was measured with the Volz 5 channel photometer. The basic method involves the measurement of direct solar beam intensity in an absorption band of water vapor, 0.940 μm, and the measurement of intensity in an adjacent "window" or region of no absorption, 0.880 μm. The ratio of these measurements is sensitive to the amount of water vapor present in the atmosphere. The relationship used is

$$P.W. = K/m \left[\log (q_o/q)\right]^2 \qquad (28)$$

where K and q_o are constants, m is the relative air mass, and q is the ratio of the 0.940 and 0.880 solar photometer meter readings.

The baseline meteorological parameters were established for the hours from 0800 to 1600 L.S.T., on the hour; they were as follows:

(1) Average daily temperature
(2) Average daily pressure
(3) Average daily relative humidity
(4) Average daily wind velocity
(5) Average daily wind direction
(6) Average daily relative dust concentration
(7) Average daily vertical precipitable water vapor
(8) Average hourly vertical precipitable water vapor

8.2 April Meteorology - The results for the April meteorological measurements are shown in Figure 85 - average daily temperature, 86 - average daily pressure, 87 - average daily relative humidity, 88 - average daily wind velocity, 89 - average daily wind direction, 90 - average daily relative dust concentration, 91 - average daily precipitable water vapor, and 92 - average hourly precipitable water vapor. The mean temperature for April (for 0800 to 1700 LST) was 12.7°C. The mean relative humidity was 47.7%. As shown in Figure 89, the prevailing wind direction would fall from south to east. The average precipitable water vapor, for those days when measurements were possible, was approximately 0.55 cm.

8.3 July Meteorology - The July meteorological measurement results are shown in Figure 93 - temperature, Figure 94 - pressure, Figure 95 - relative humidity, Figure 96 - wind velocity, Figure 97 - wind direction, Figure 98 - relative dust concentration, Figure 99 - daily precipitable water vapor, and Figure 100 - hourly preciptable water vapor. The mean temperature (0800 to 1700 LST) was 25.7°C. The mean relative humidity was 38.6%. As shown in Figure 97, the wind direction was quite variable. The average precipitable water vapor, as derived from Figure 100, was approximately 1.35 cm.

8.4 October Meteorology - The October meteorological results are shown in Figure 101 - temperature, Figure 102 - pressure, Figure 103 - relative humidity, Figure 104 - wind velocity, Figure 105 - wind direction, Figure 106 - relative dust concentration, Figure 107 - daily precipitable water vapor, and Figure 108 - hourly precipitable water vapor. The mean temperature (0800 to 1700 OST) was 5.8°C, and the mean relative humidity was 53.1%. As shown in Figure 105, the general revailing wind direction was from the northwest to south. The average precipitable water vapor, as derived from Figure 108, was approximately 0.65 cm.

8.5 January Meteorology - The January meteorological results are shown in Figure 109 - temperature, Figure 110 - pressure, Figure 111 - relative humidity, Figure 112 - wind direction, Figure 113 - wind velocity, Figure 114 - relative dust concentration, Figure 115 - daily precipitable water vapor, and Figure 116 - hourly precipitable water vapor. The mean temperature (0800 to 1700 LST) was -9.6°C, and the mean relative humidity was 78.9%. As shown in Figure 112, the general prevailing wind direction was from the northwest to west. The average precipitable water vapor, as derived from Figure 116, was approximately 0.35 cm.

8.6 Seasonal Comparisons - A comparisons of the various meteorological parameters is shown in Table 3.

Table 3 Comparison of Meteorological Results

Month	T-C°	R.H.	P.W.-cm	W.D.	Vis-Miles
April	12.7	47.7	0.55	S-E	34.0
July	25.7	38.6	1.35	Varibale	39.9
Oct.	5.8	53.1	0.65	NE-S	32.2
Jan.	-9.6	78.9	0.35	NW-W	27.2

$\bar{T}$ - mean temperature;
R.H. - mean relative humidity;
P.W. - mean precipitable water vapor;
W.D. - wind direction;
Vis - mean daily visibility, overall view.

As can be seen, January had very cold temperatures, high relative humidity, low precipitable water vapor, and the lowest visibility. Whereas, July had the high temperatures, low relative humidity, high precipitable water vapor, and the highest visibility. April and October were somewhat similar in all parameters.

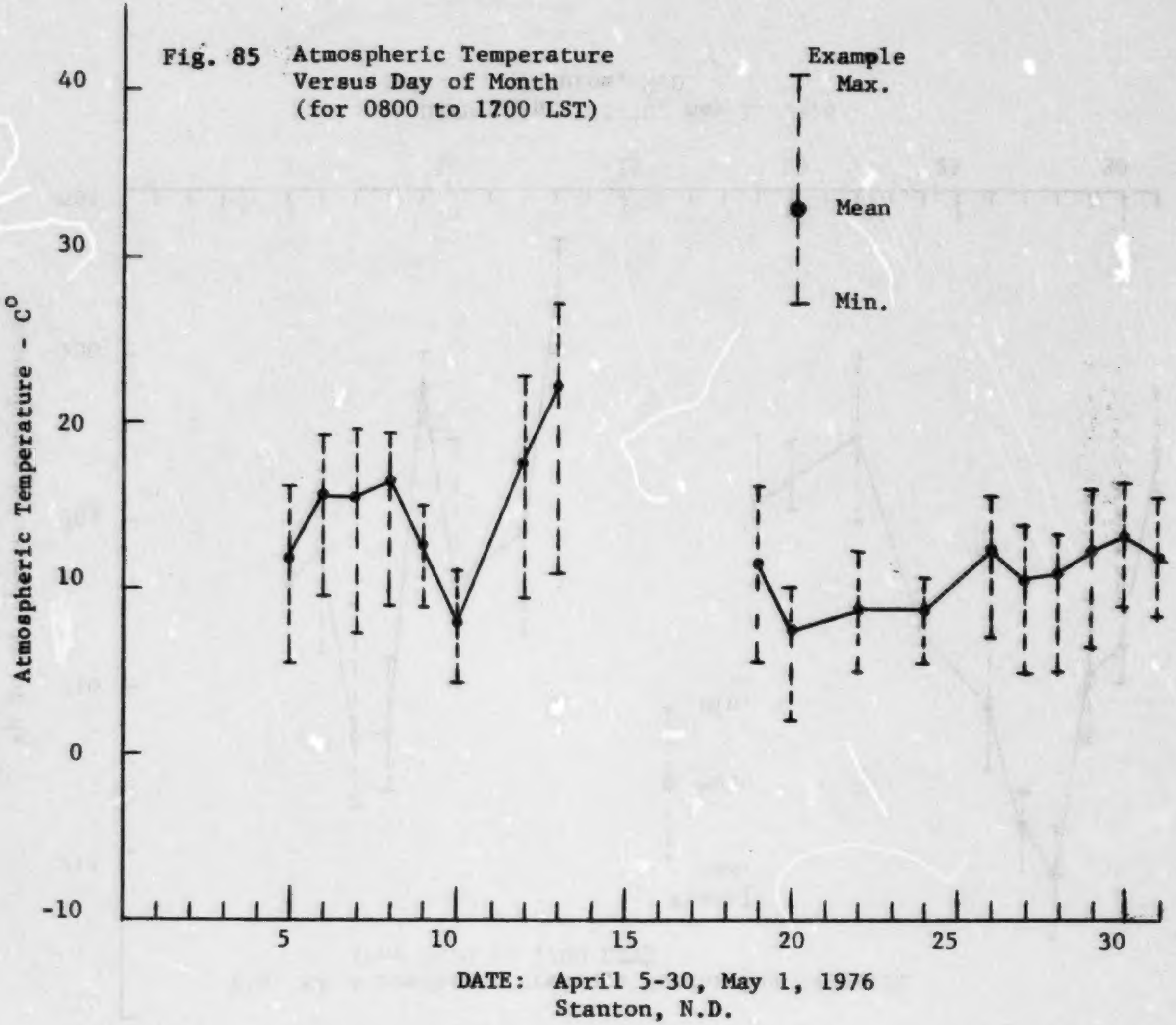

Fig. 85 Atmospheric Temperature Versus Day of Month (for 0800 to 1700 LST)

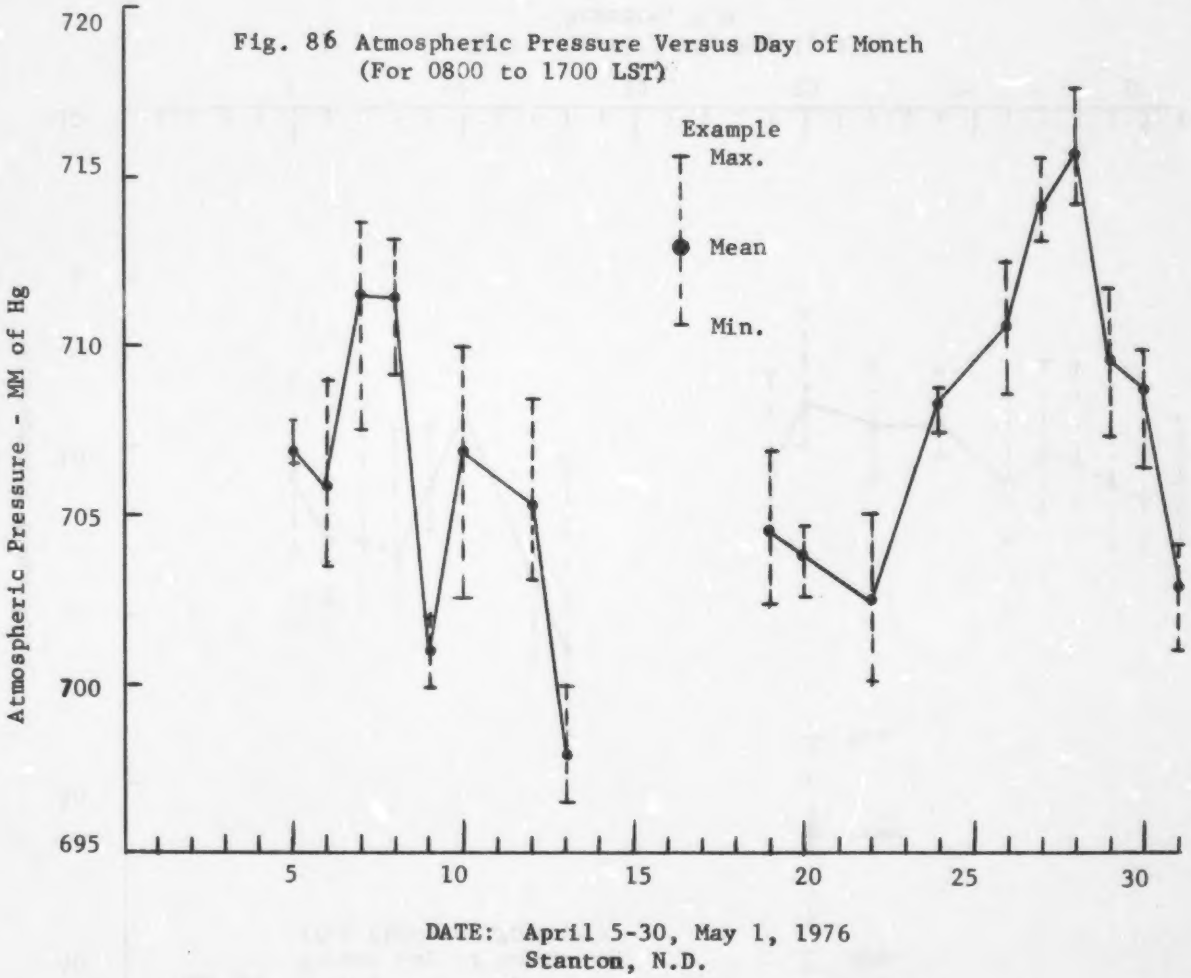

Fig. 86 Atmospheric Pressure Versus Day of Month
(For 0800 to 1700 LST)

Fig. 87 Atmospheric Relative Humidity Versus Day of Month
(For 0800 to 1700 LST)

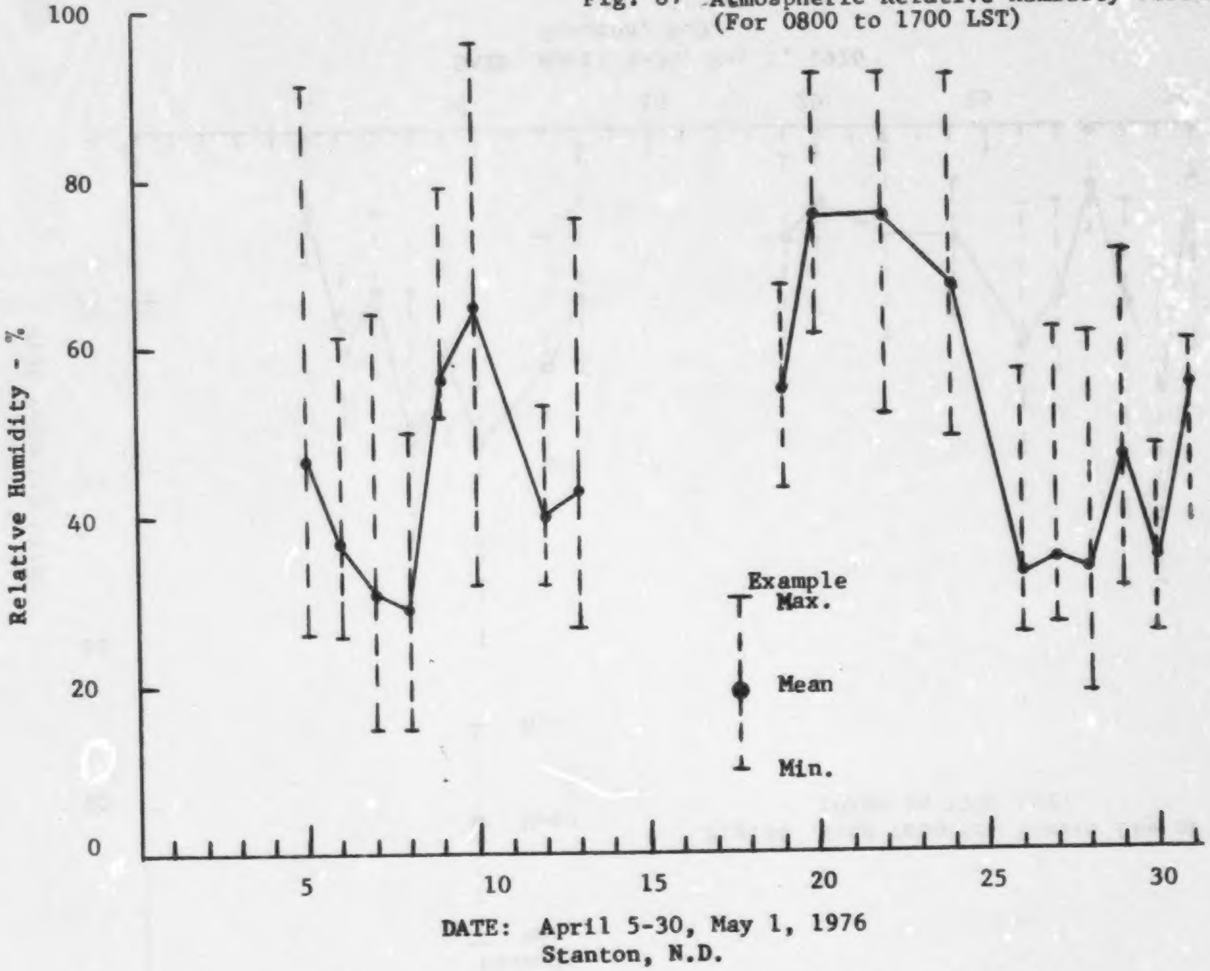

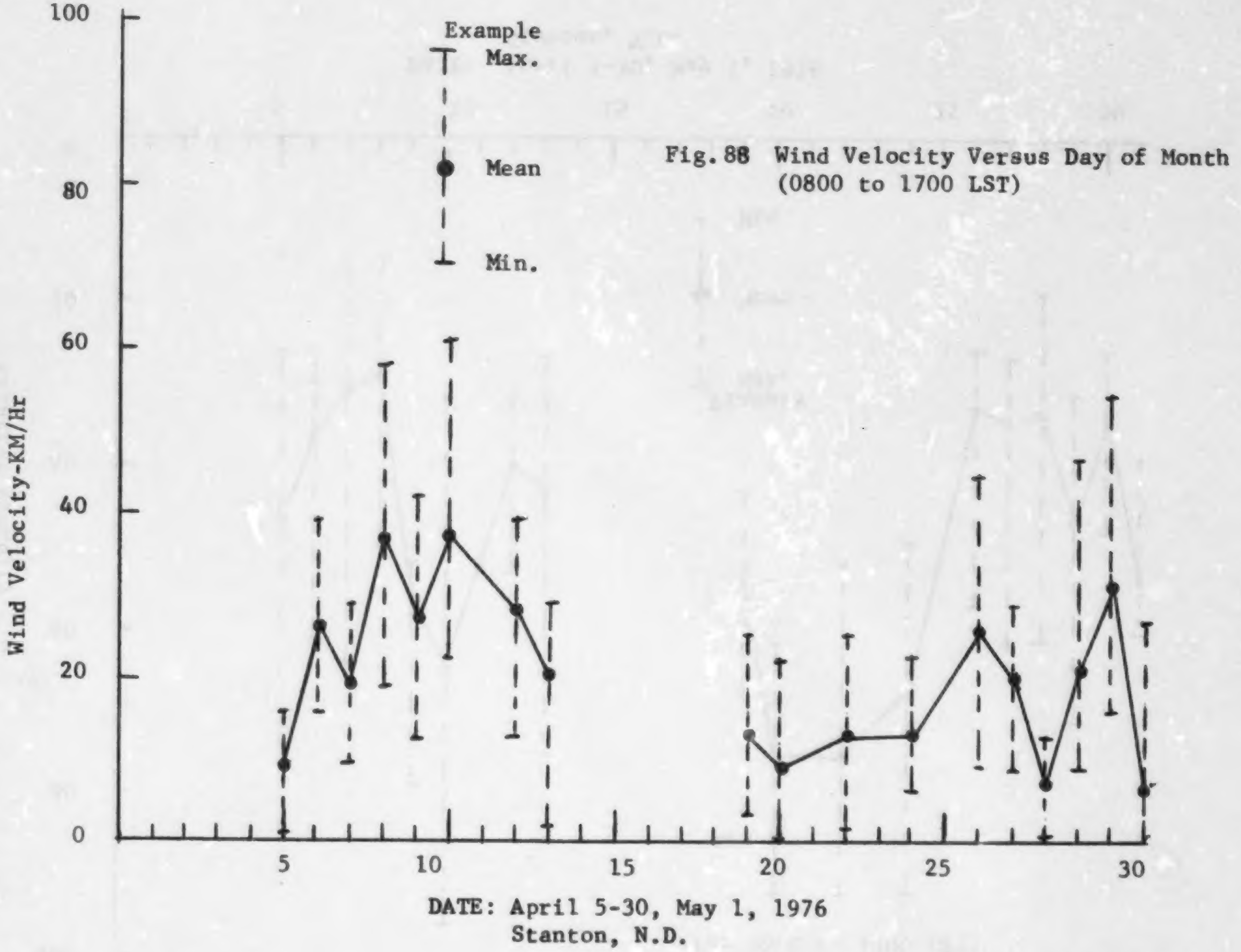

Fig. 88 Wind Velocity Versus Day of Month (0800 to 1700 LST)

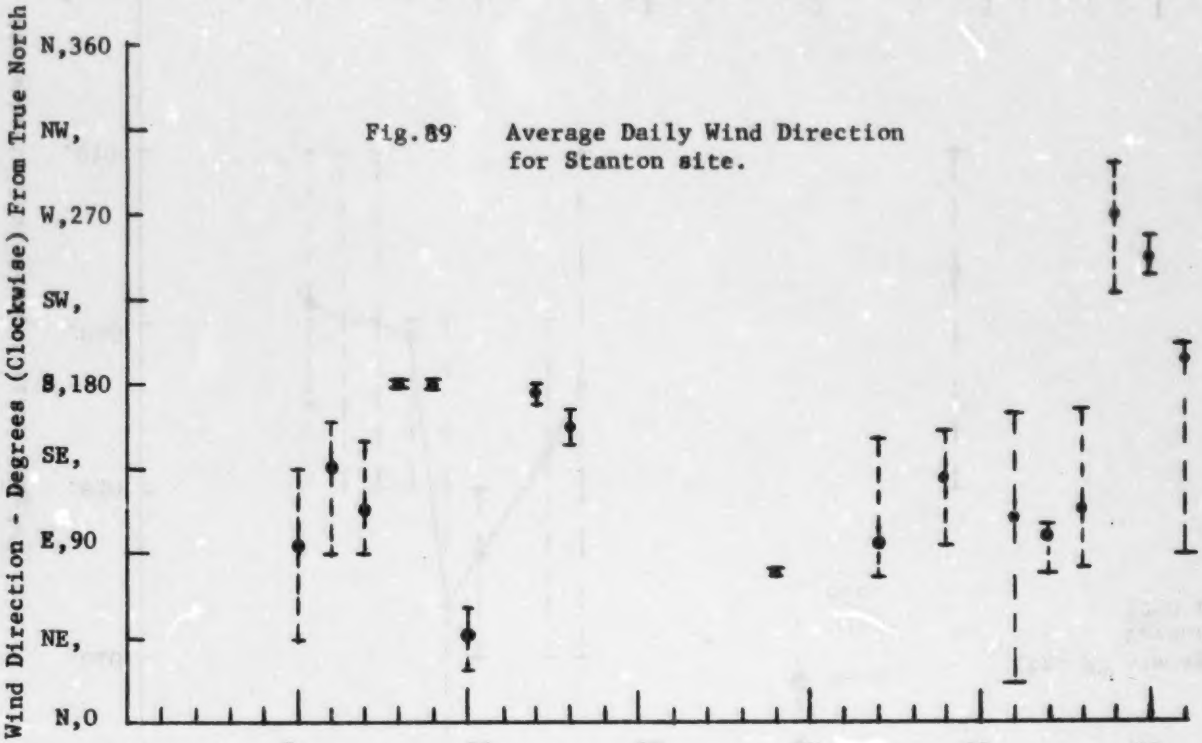

Fig. 89 Average Daily Wind Direction for Stanton site.

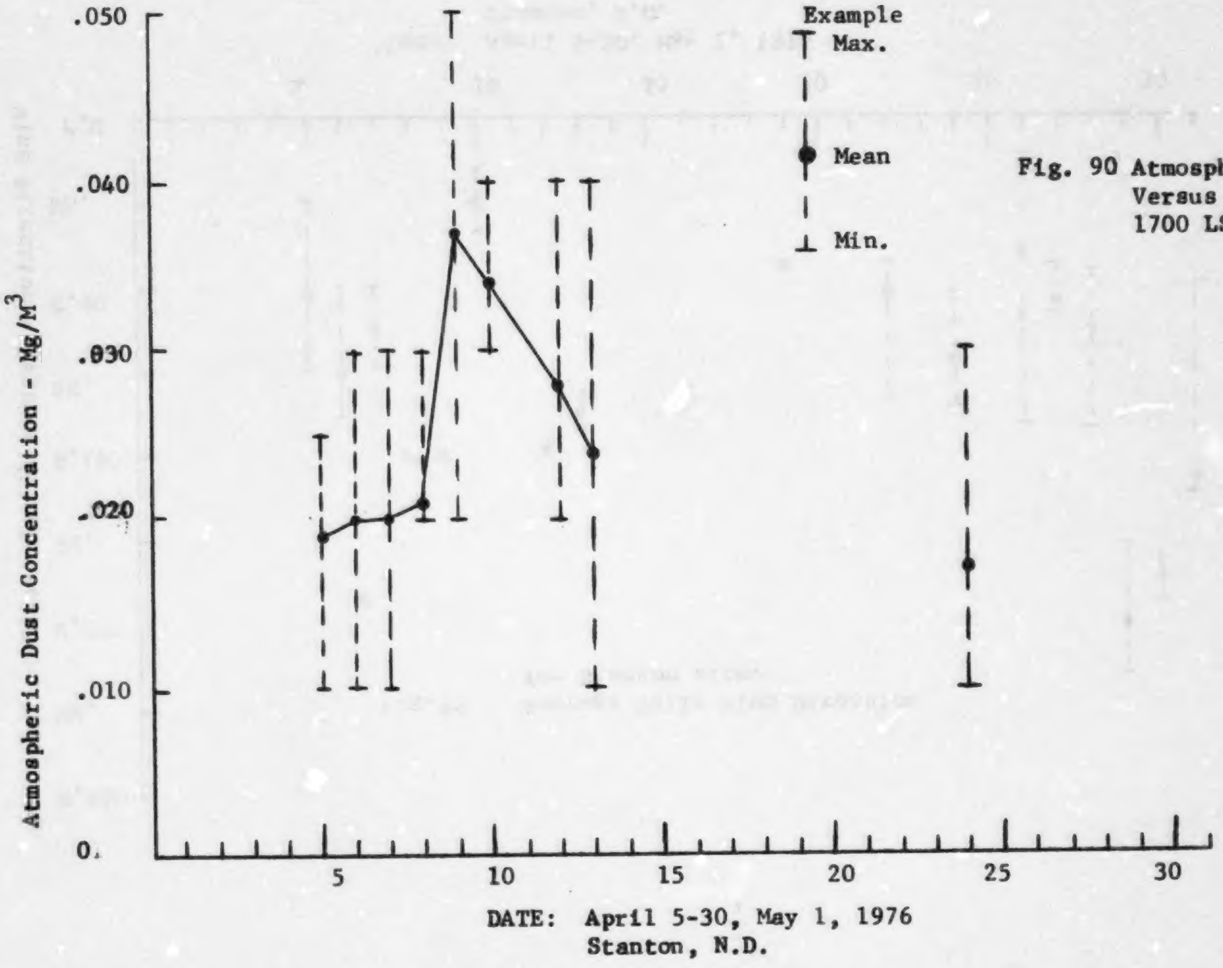

Fig. 90 Atmospheric Dust Concentration Versus Day of Month (0800 to 1700 LST)

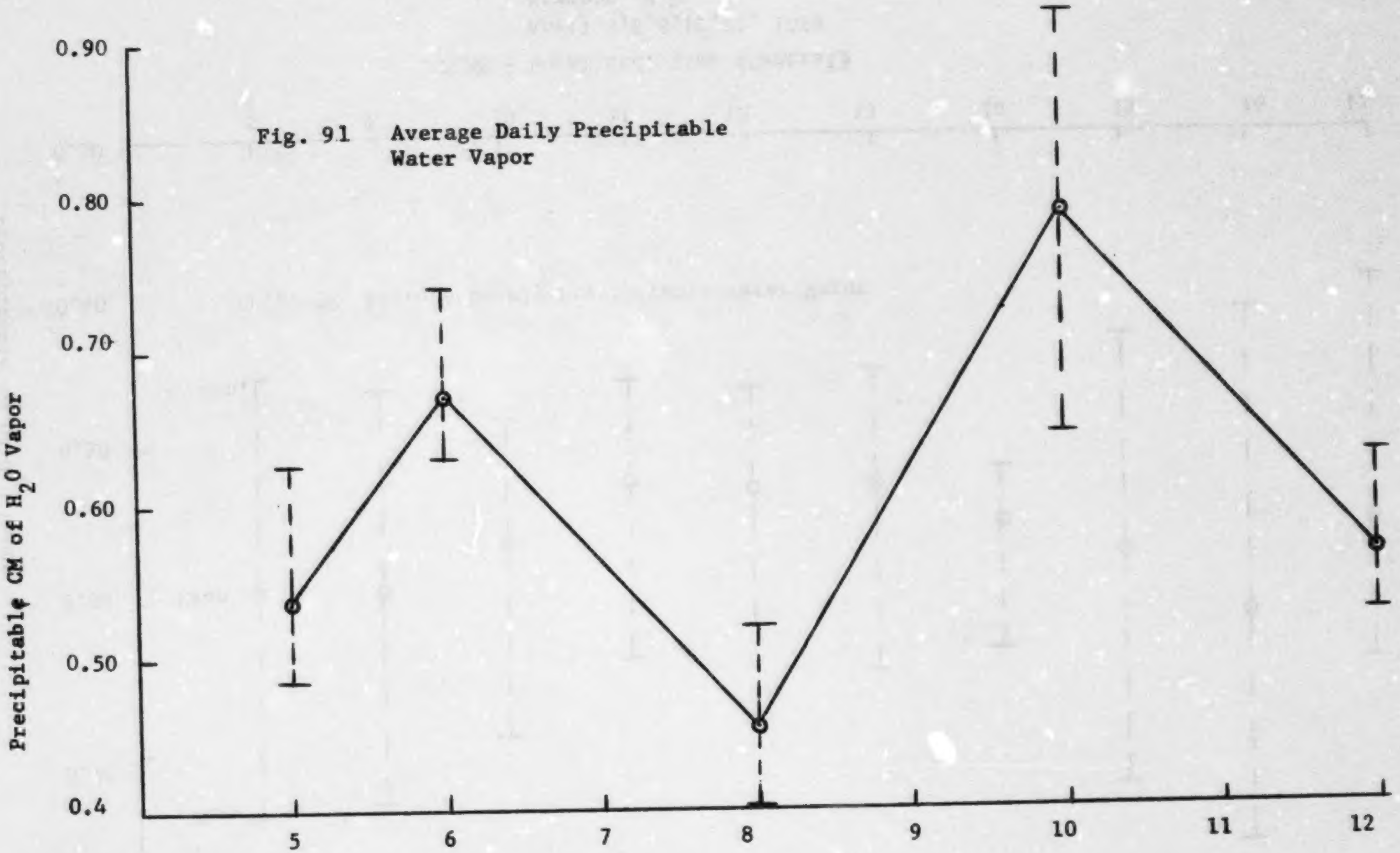

Fig. 91 Average Daily Precipitable Water Vapor

Date: April 1976
Stanton, N.D.

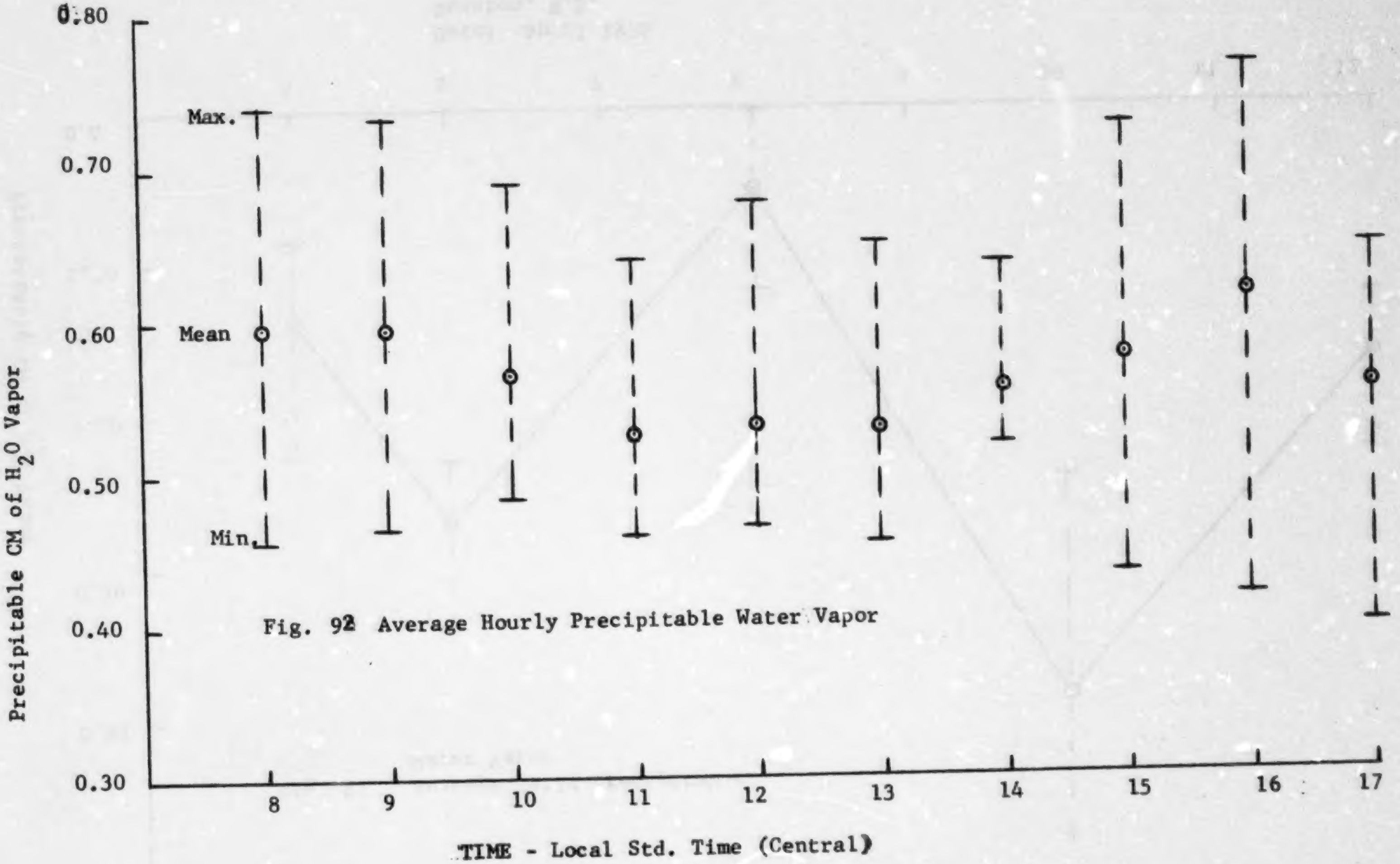

Fig. 92 Average Hourly Precipitable Water Vapor

April 5,6,8,10,12, 1976
Stanton, N.D.

FIG. 93 ATMOSPHERIC TEMPERATURE VERSUS DAY OF MONTH (FOR 0800 TO 1700 LST_

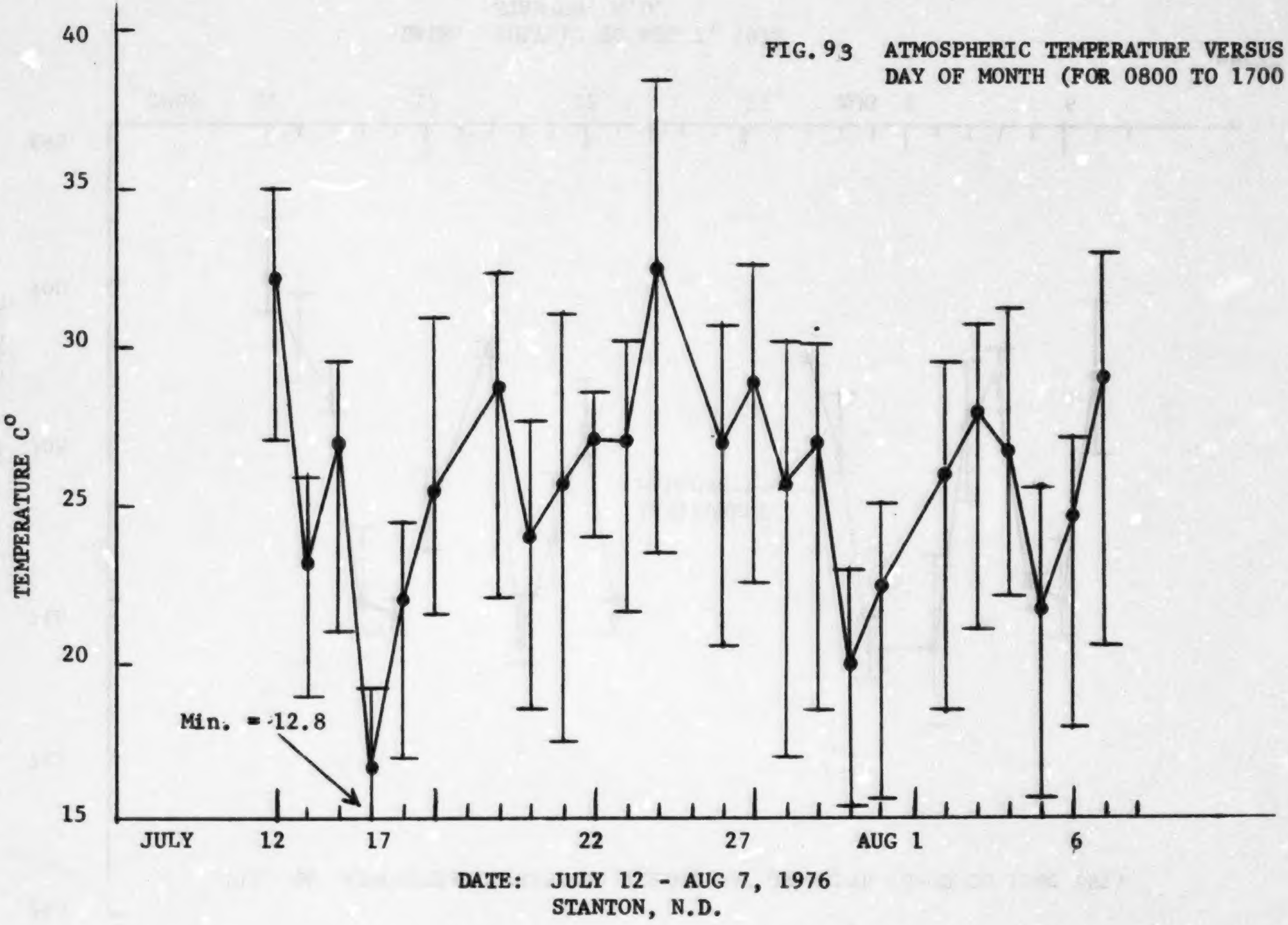

FIG. 94 ATMOSPHERIC PRESSURE VERSUS DAY OF MONTH (0800 TO 1700 LST)

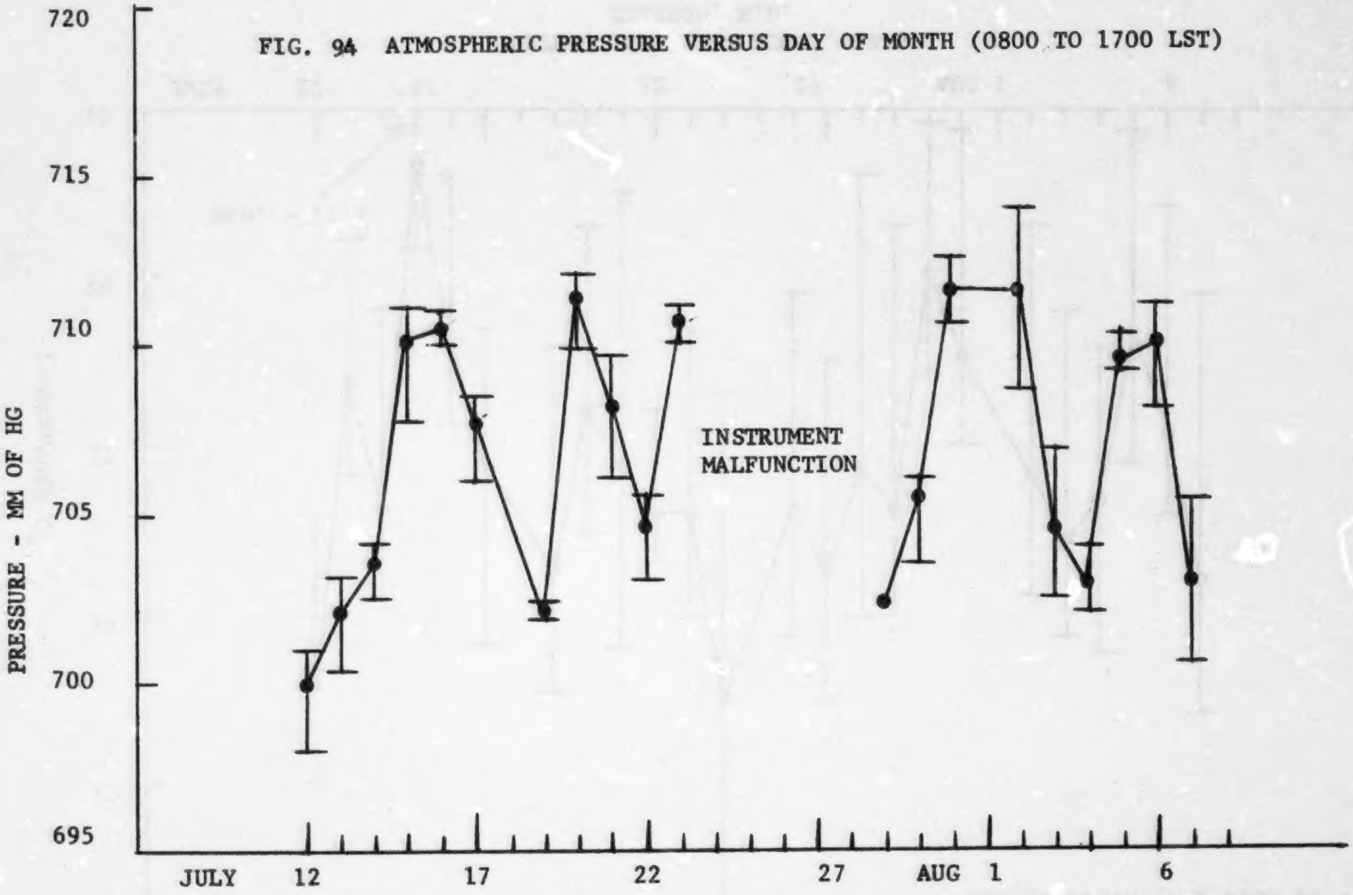

DATE: JULY 12 TO AUG 7, 1976
STANTON, N.D.

FIG. 95 ATMOSPHERIC RELATIVE HUMIDITY VERSUS DAY OF THE MONTH (0800 TO 1700 LST)

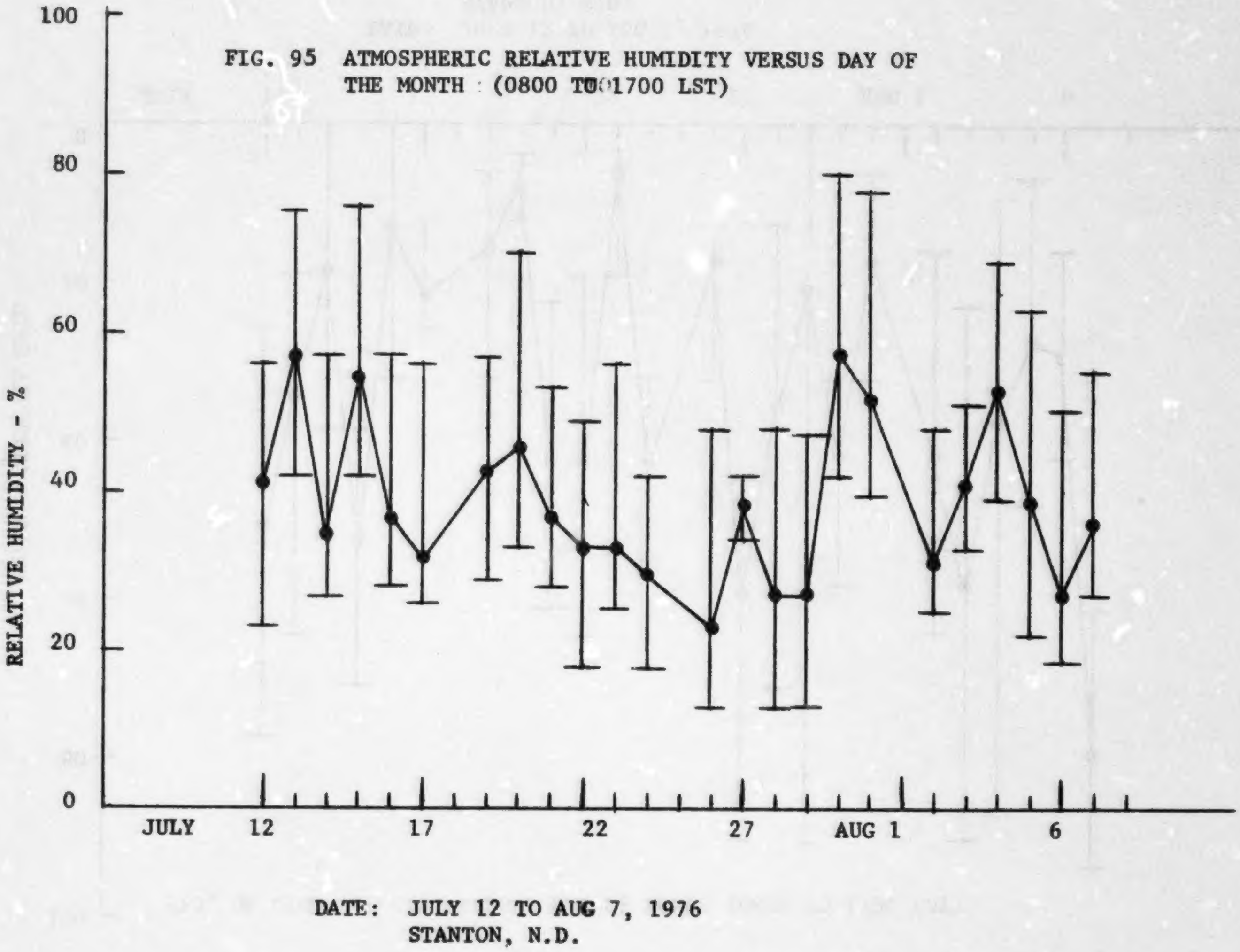

FIG. 96. WIND VELOCITY VERSUS DAY OF MONTH (0800 TO 1700 LST)

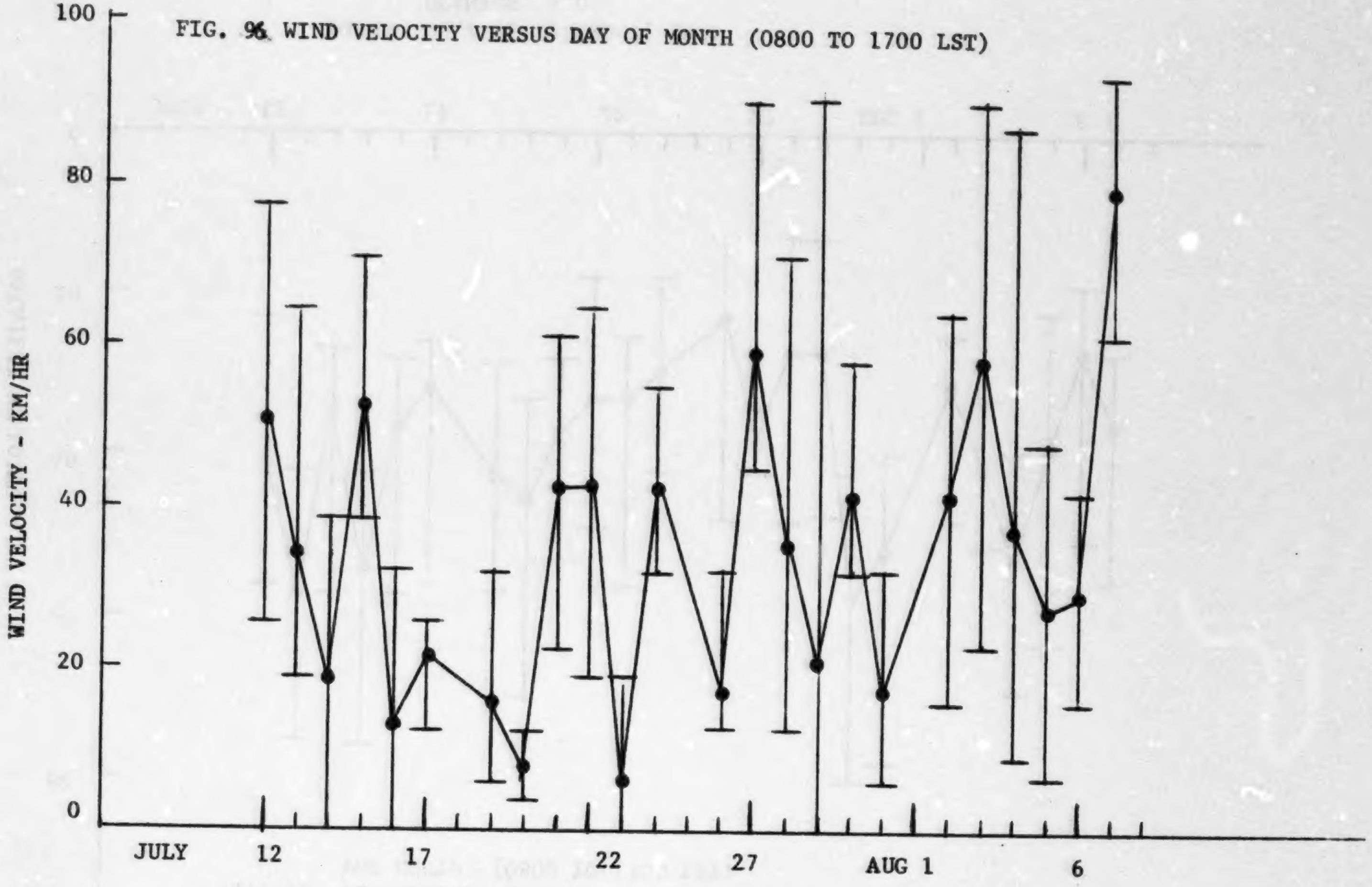

DATE: JULY 12 TO AUG 7, 1976
STANTON, N.D.

FIG.97 AVERAGE WIND DIRECTION FOR STANTON SITE

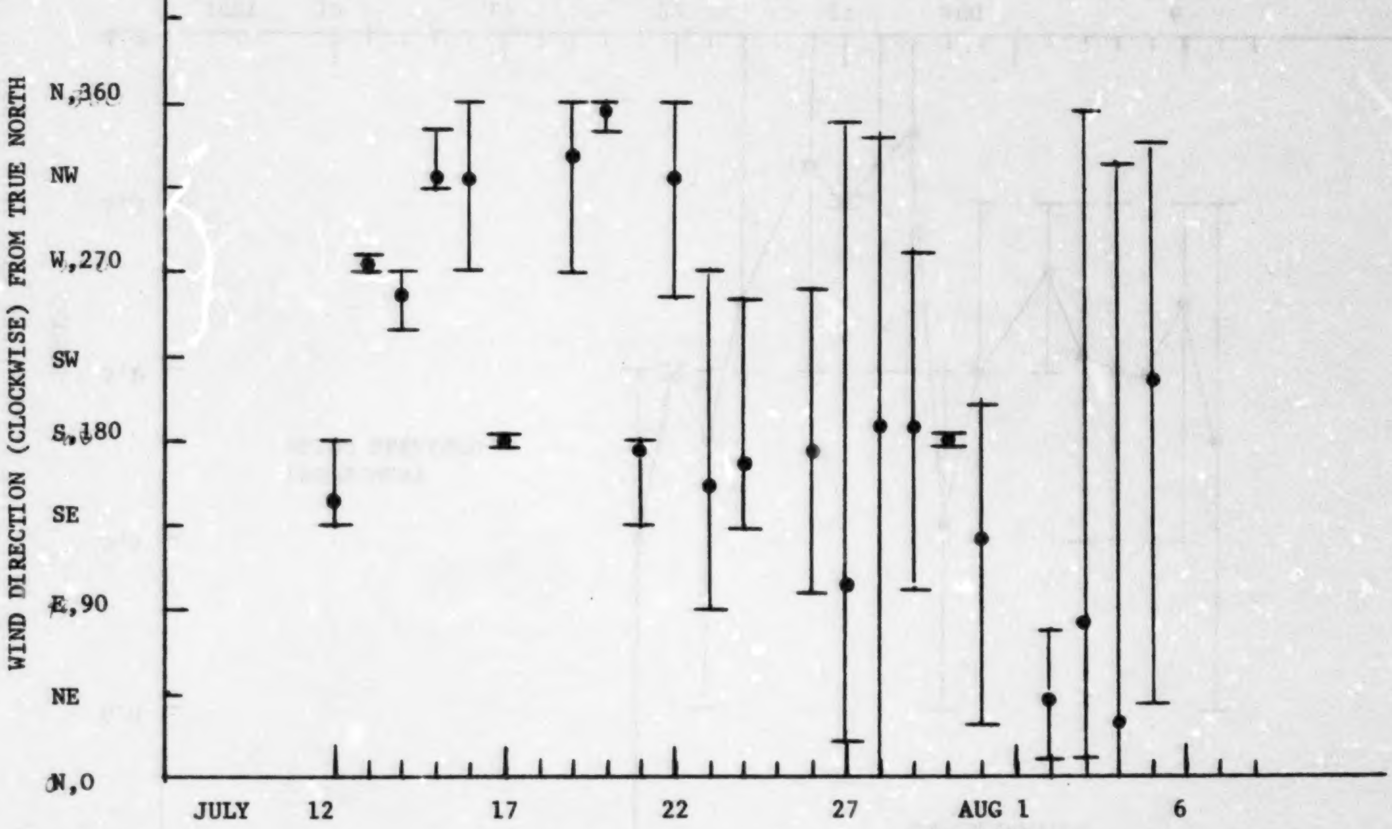

DATE: JULY 12 TO AUG 7, 1976
STANTON, N.D.

FIG. 98 RELATIVE ATMOSPHERIC DUST CONCENTRATION

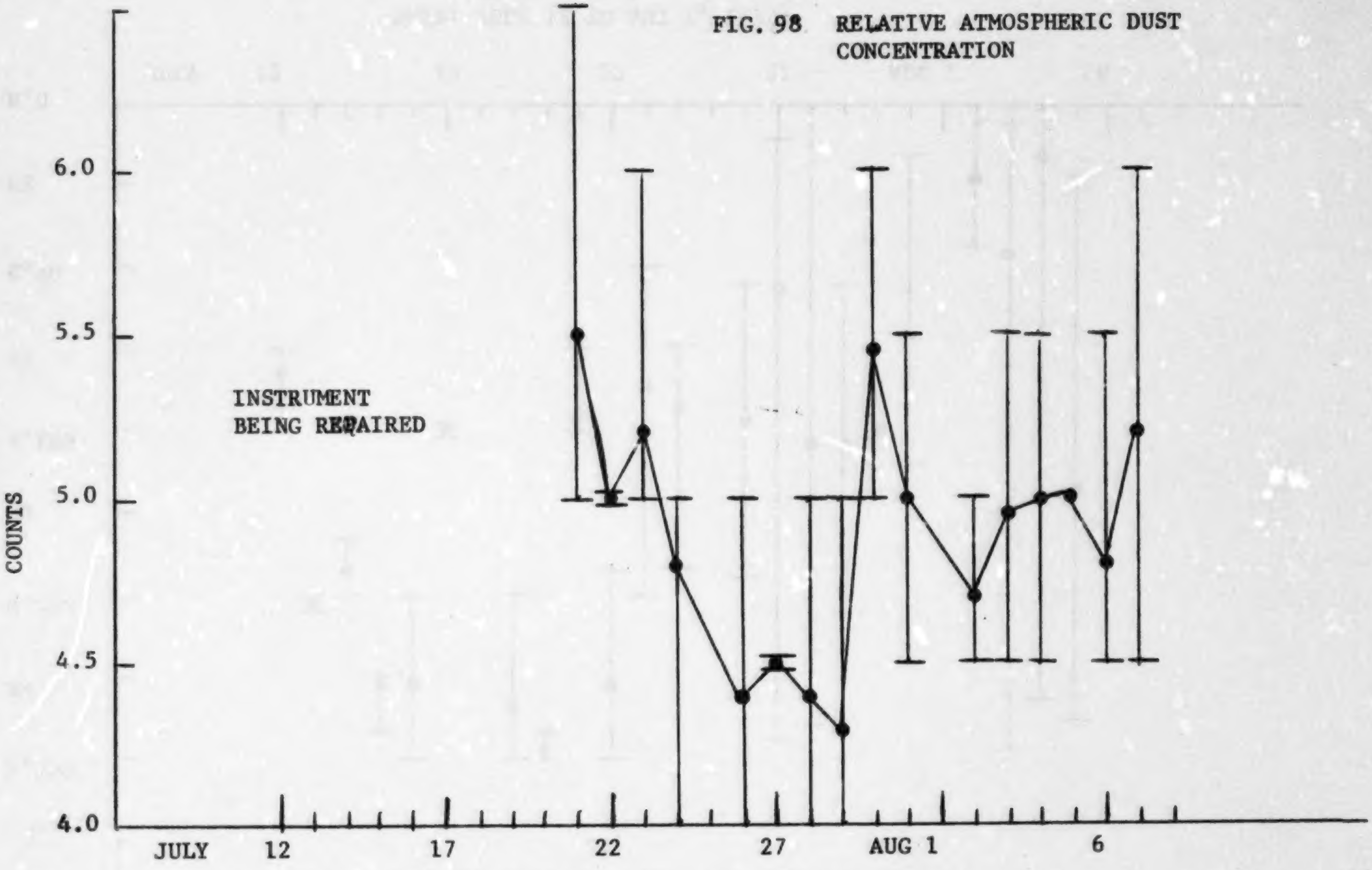

DATE: JULY 12 TO AUG 7, 1976
STANTON, N.D.

FIG. 99 · AVERAGE DAILY PRECIPITABLE WATER VAPOR

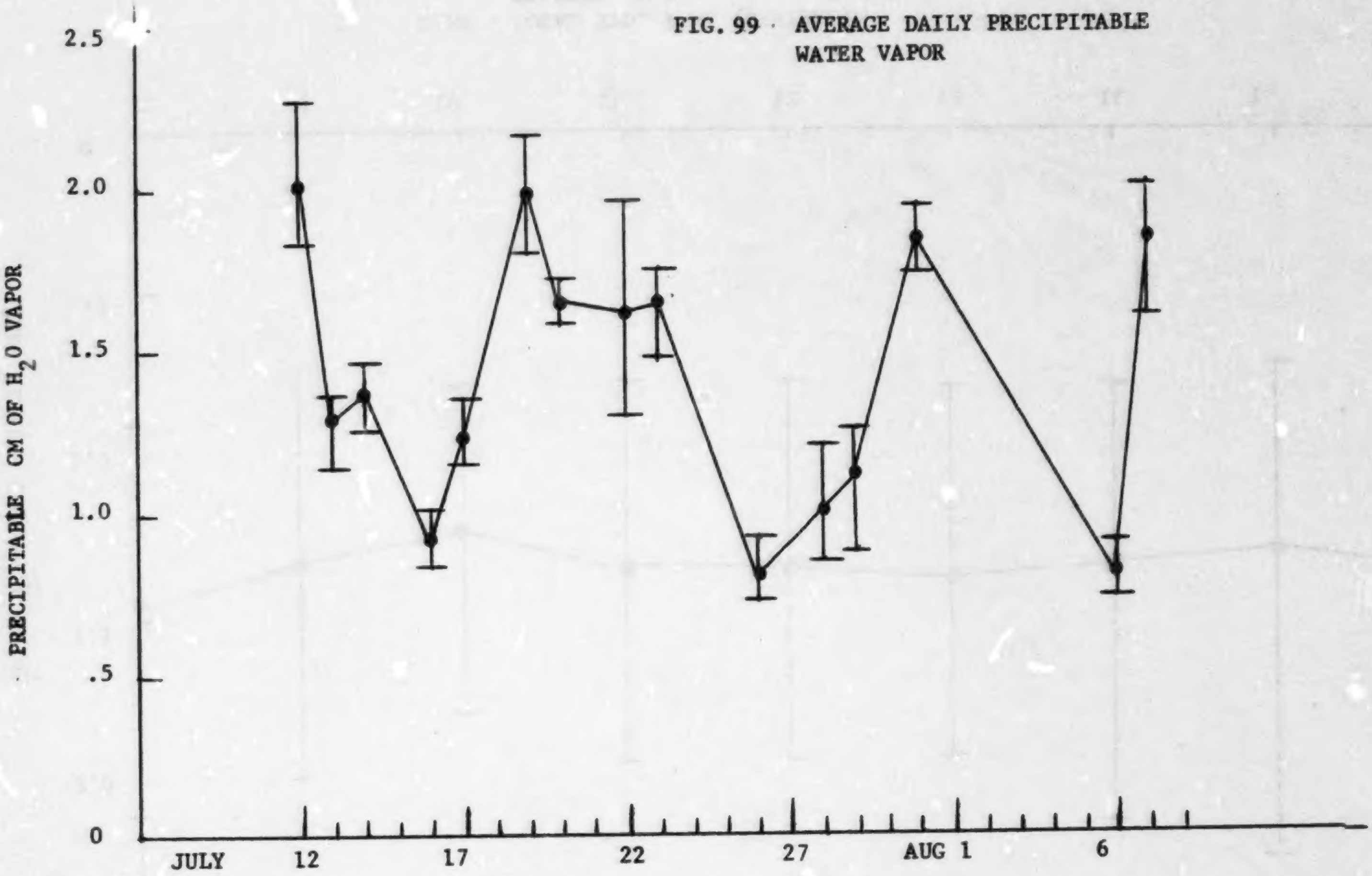

DATE: JULY 12 TO AUG 7, 1976
STANTON, N.D.

FIG. 100 AVERAGE HOURLY PRECIPITABLE WATER VAPOR (CM)

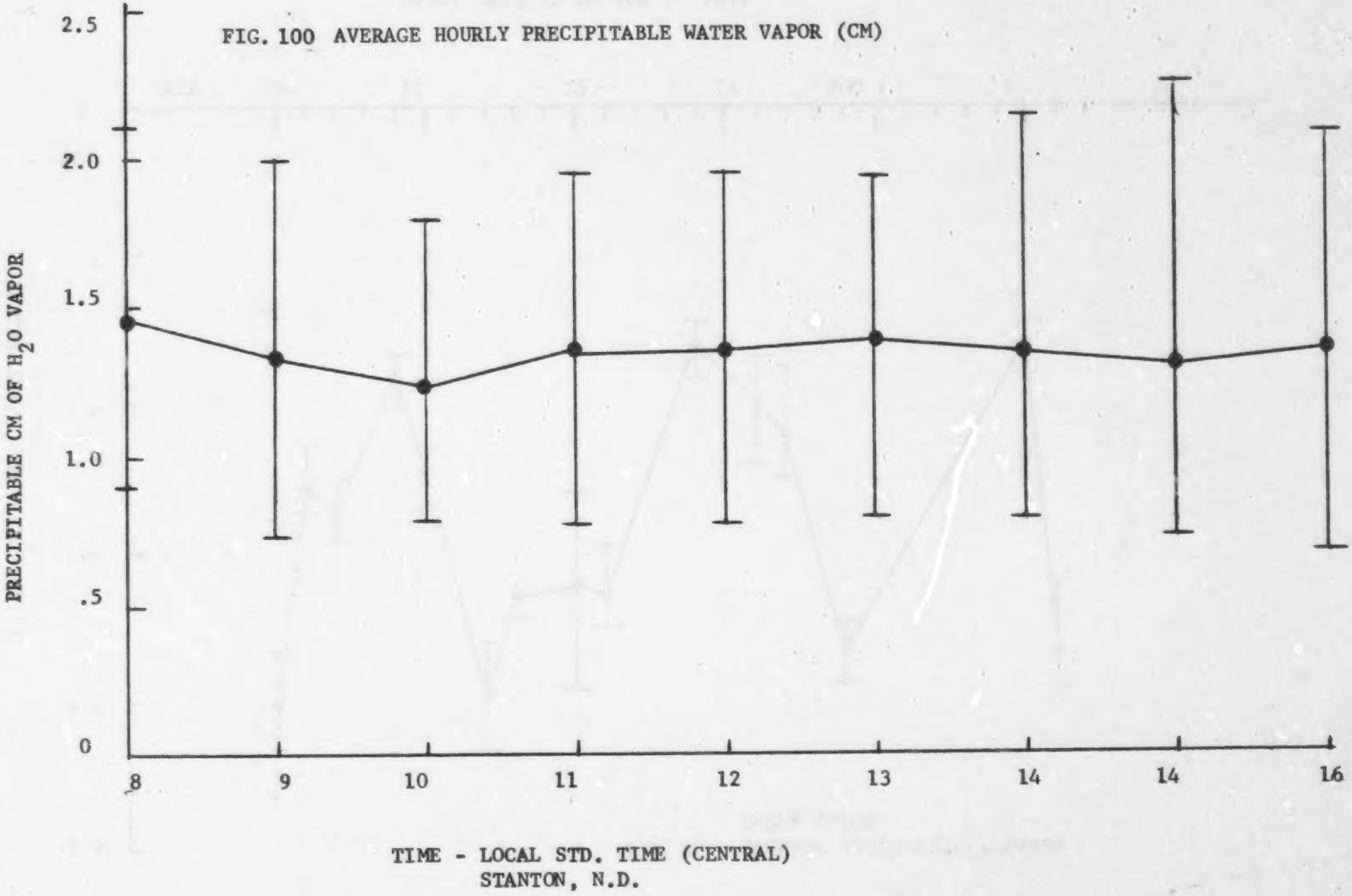

FIG. 101 ATMOSPHERIC TEMPERATURE VERSUS DAY OF THE MONTH (FOR 0800 TO 1700 LST)

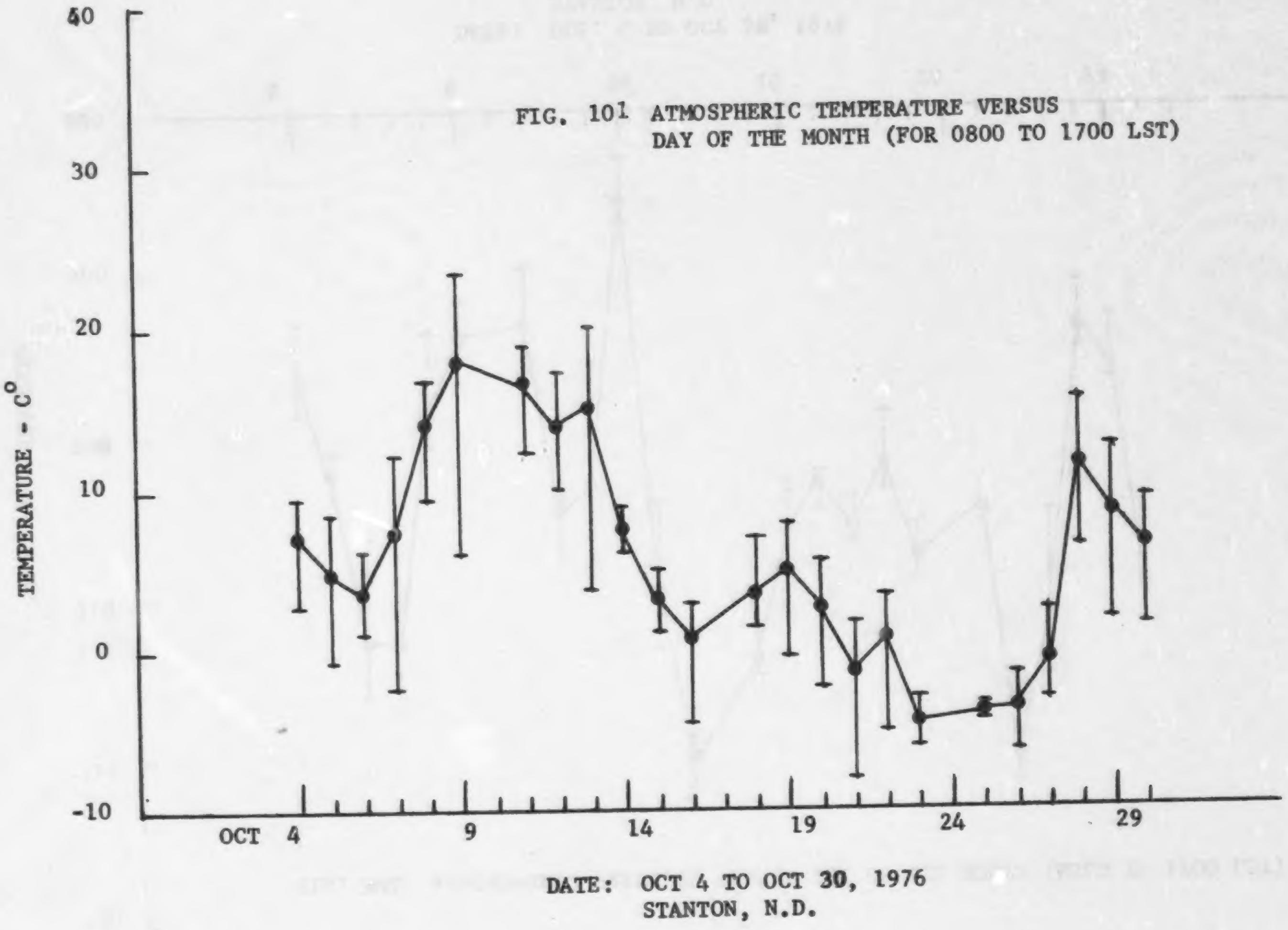

FIG. 102 ATMOSPHERIC PRESSURE VERSUS DAY OF THE MONTH (0800 TO 1700 LST)

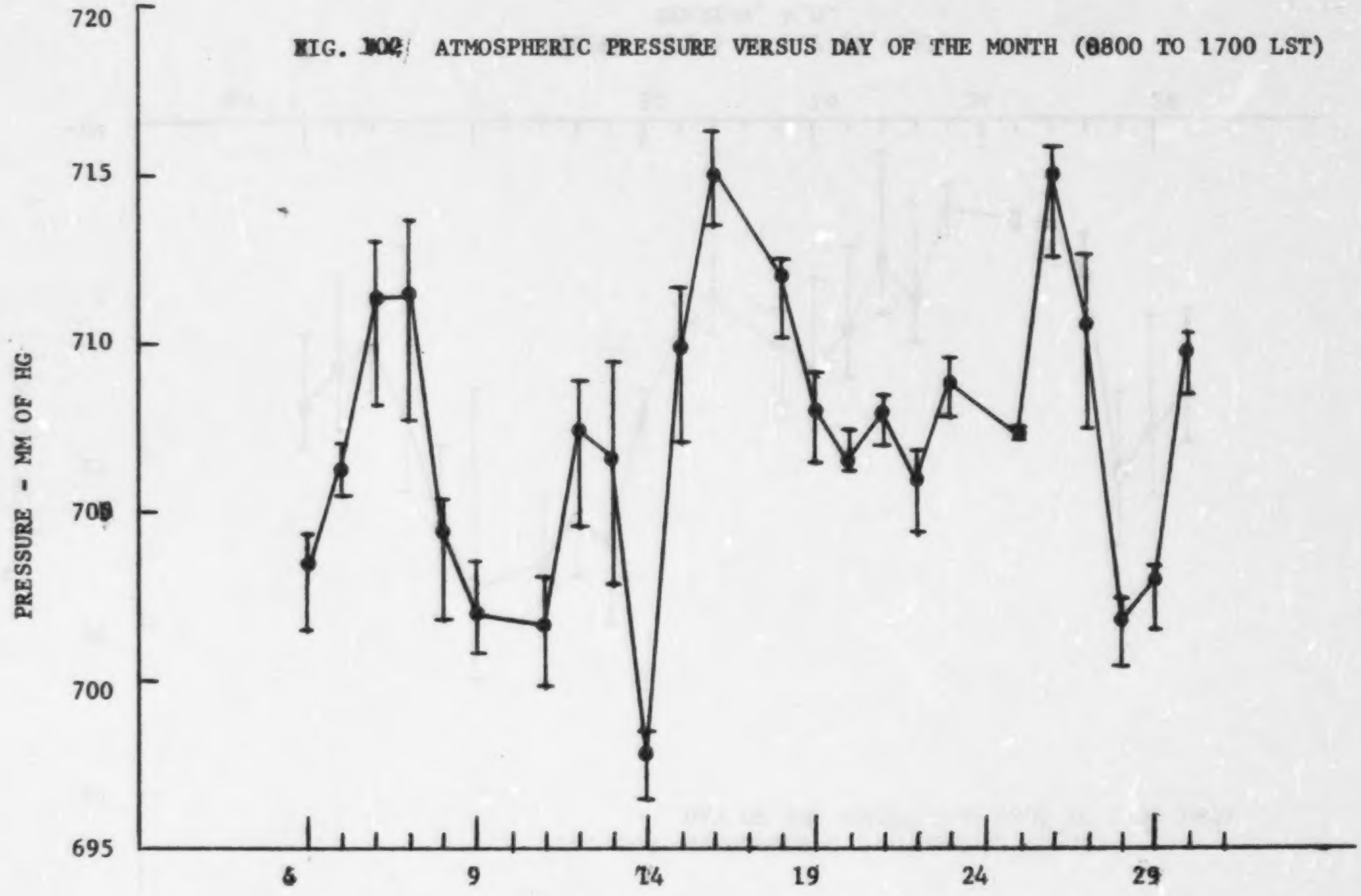

DATE: OCT. 4 TO OCT 30, 1976
STANTON, N.D.

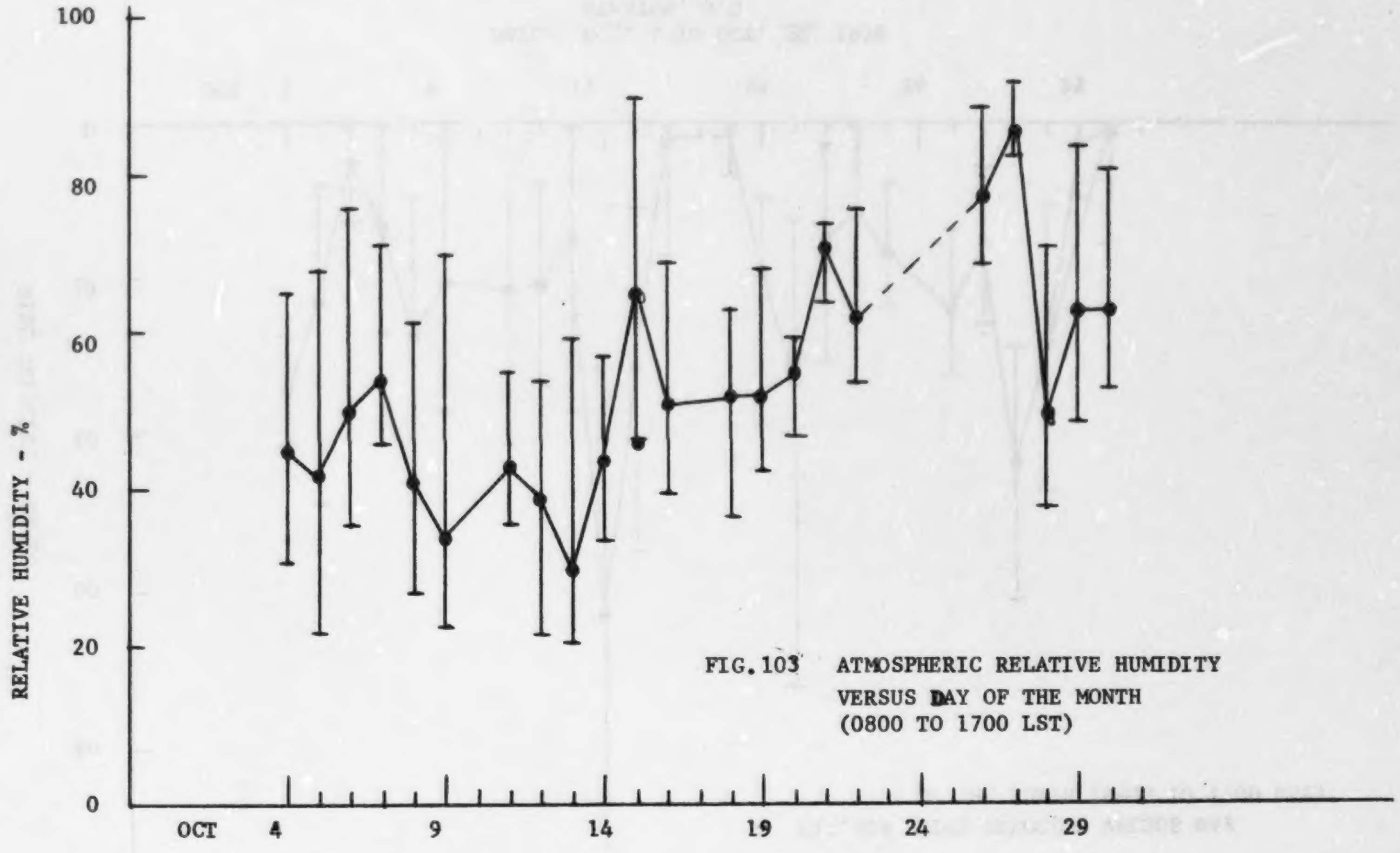

FIG. 103 ATMOSPHERIC RELATIVE HUMIDITY VERSUS DAY OF THE MONTH (0800 TO 1700 LST)

DATE: OCT. 4 TO OCT. 30, 1976
STANTON, N.D.

FIG. 104 WIND VELOCITY VERSUS DAY OF THE MONTH (0800 TO 1700 LST)

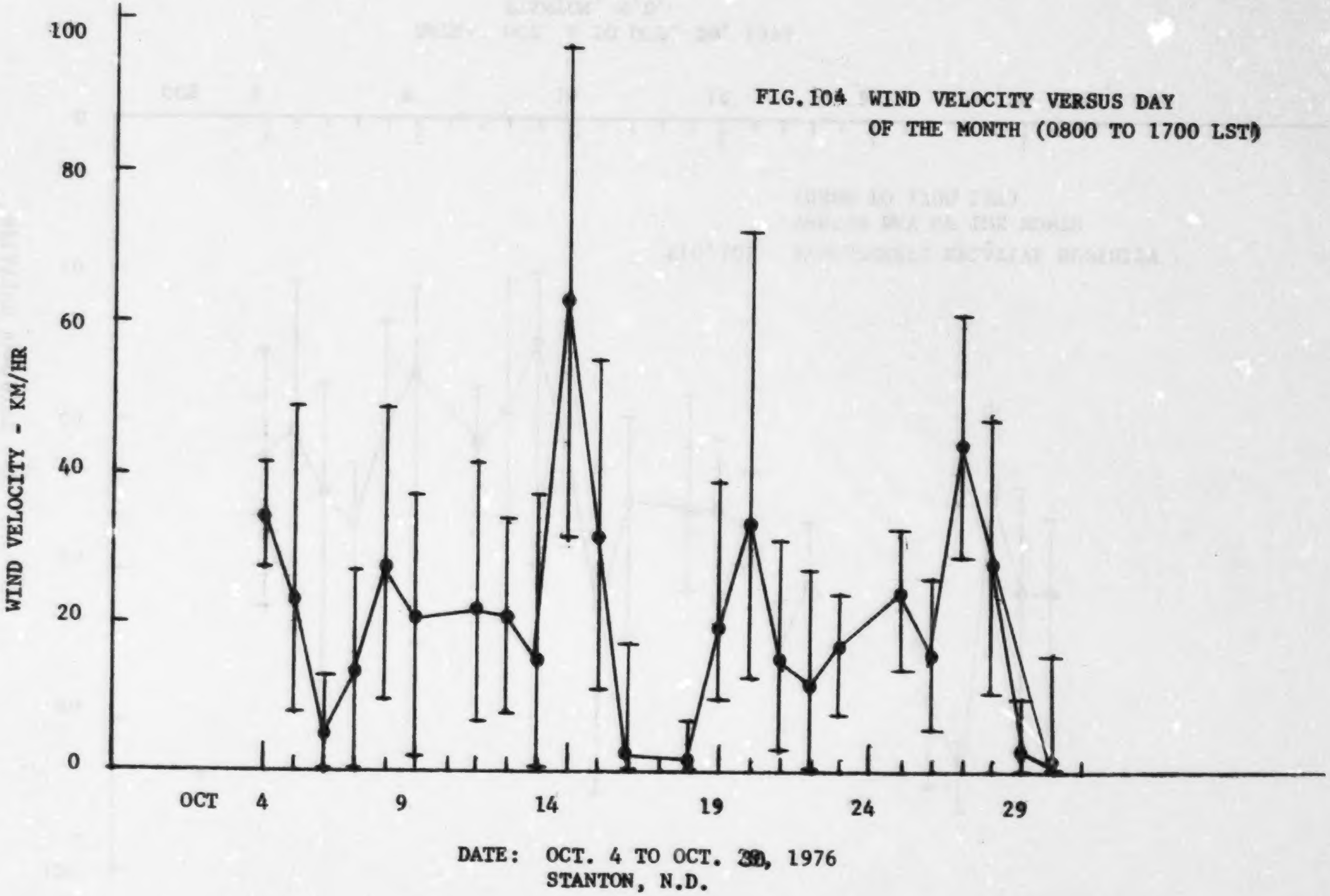

FIG. 105 AVERAGE WIND DIRECTION FOR STANTON SITE

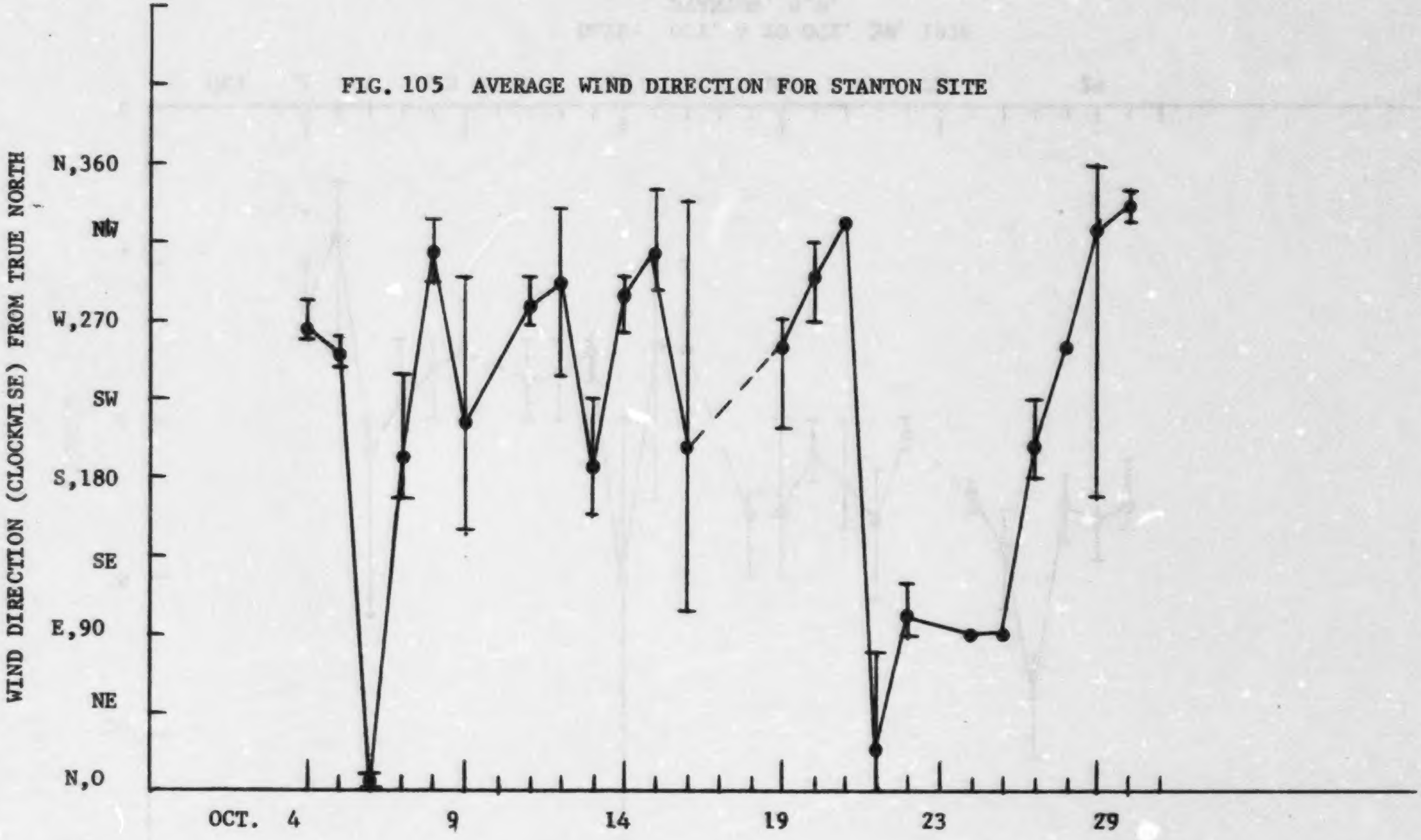

DATA: OCT. 4 TO OCT. 30, 1976
STANTON, N.D.

FIG. 106 RELATIVE ATMOSPHERIC DUST CONCENTRATION

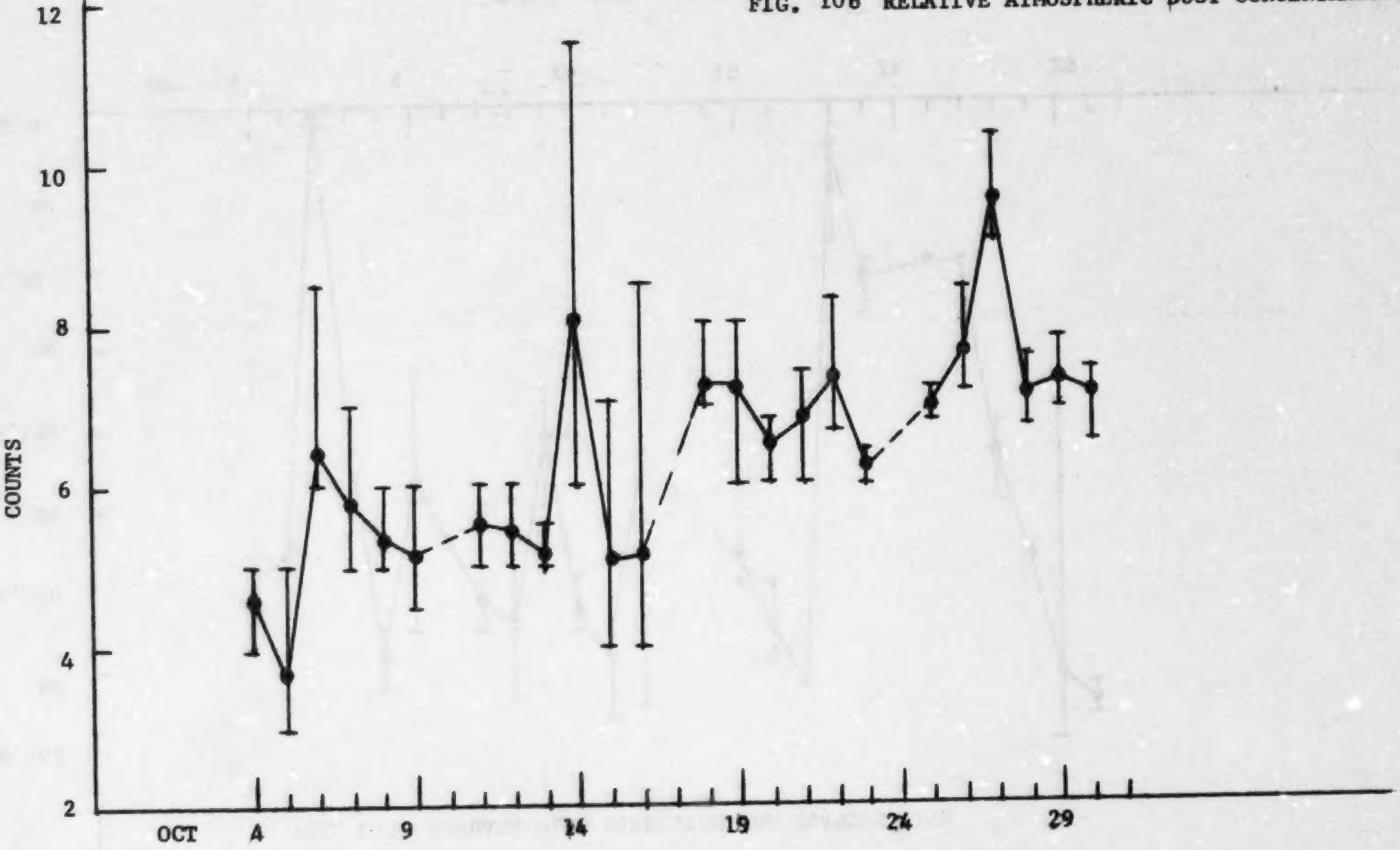

DATE: OCT. 4 TO OCT. 30, 1976
STANTON, N.D.

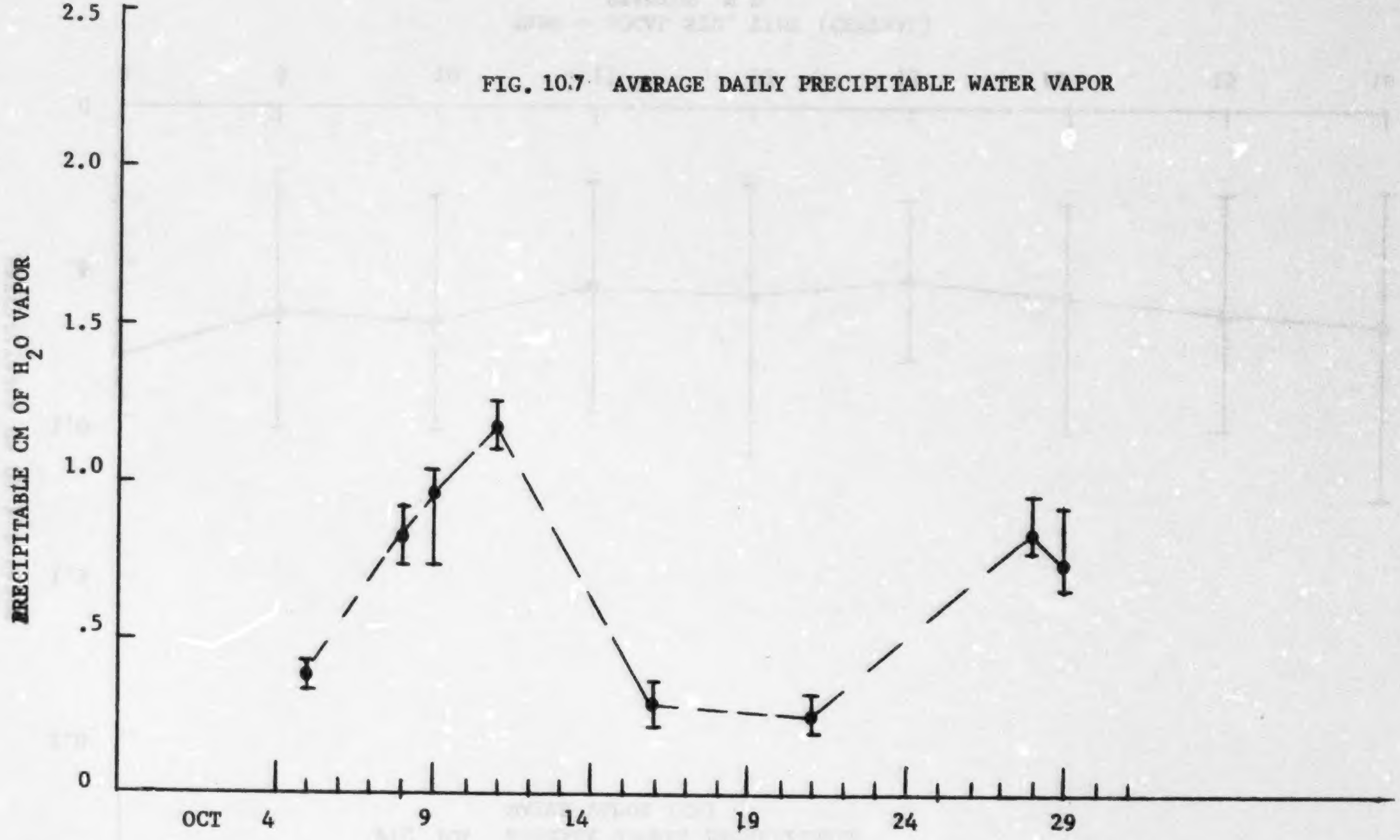

FIG. 10.7 AVERAGE DAILY PRECIPITABLE WATER VAPOR

DATE: OCT. 4 TO OCT. 30, 1976
STANTON, N.D.

FIG. 108 AVERAGE HOURLY PRECIPITABLE WATER VAPOR (CM)

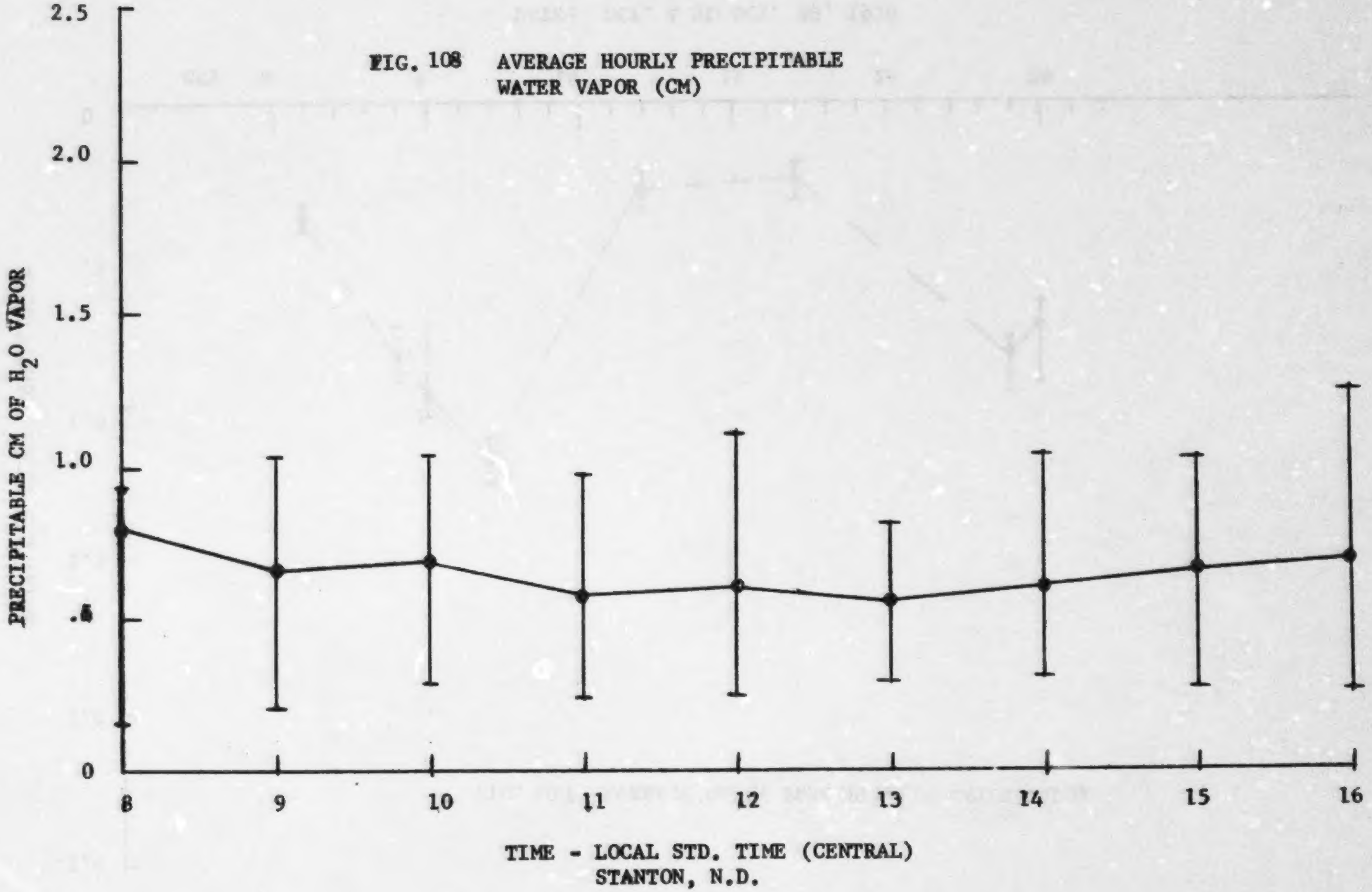

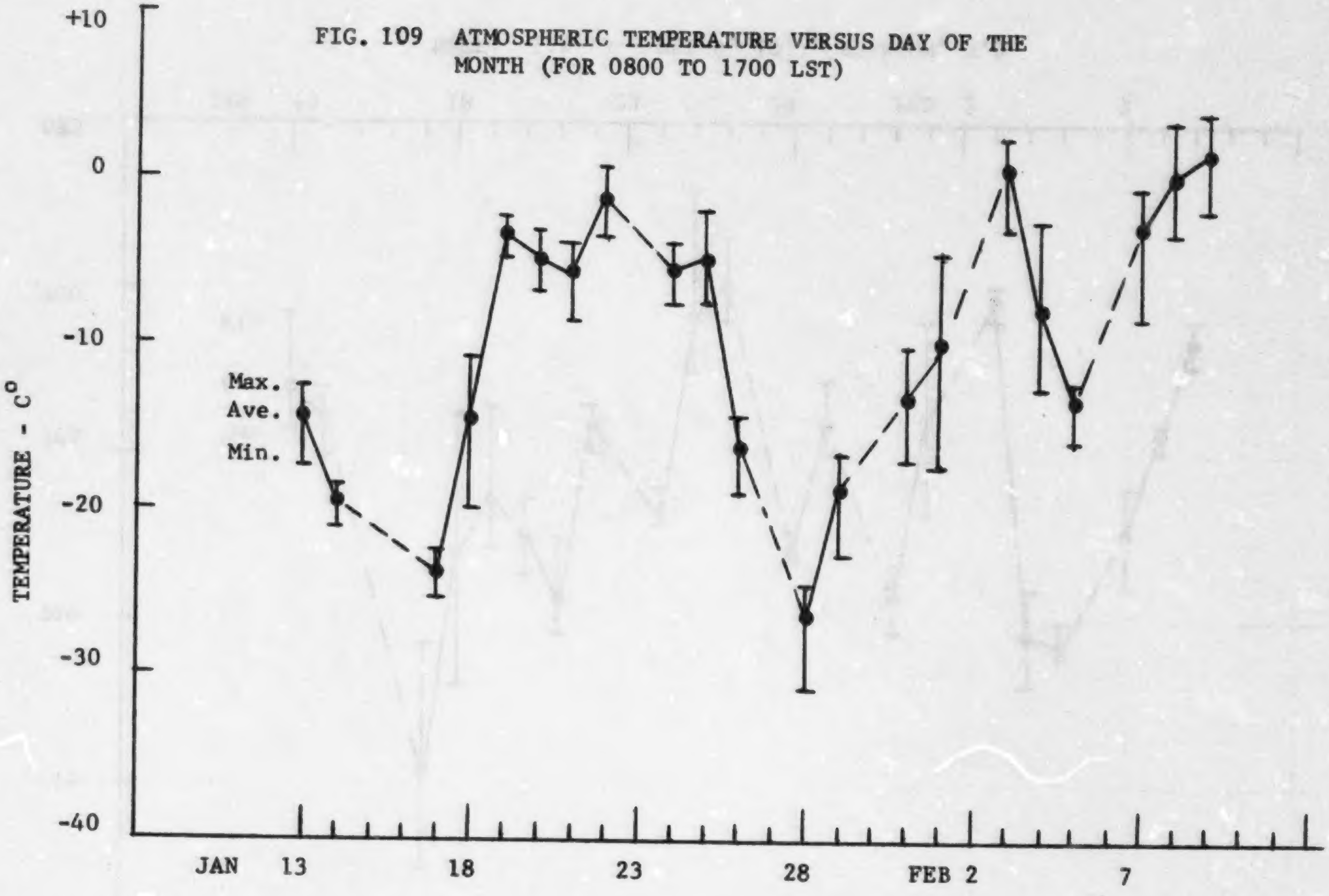

FIG. 109 ATMOSPHERIC TEMPERATURE VERSUS DAY OF THE MONTH (FOR 0800 TO 1700 LST)

DATE: JAN. 13 - FEB 9, 1977, STANTON, N.D.

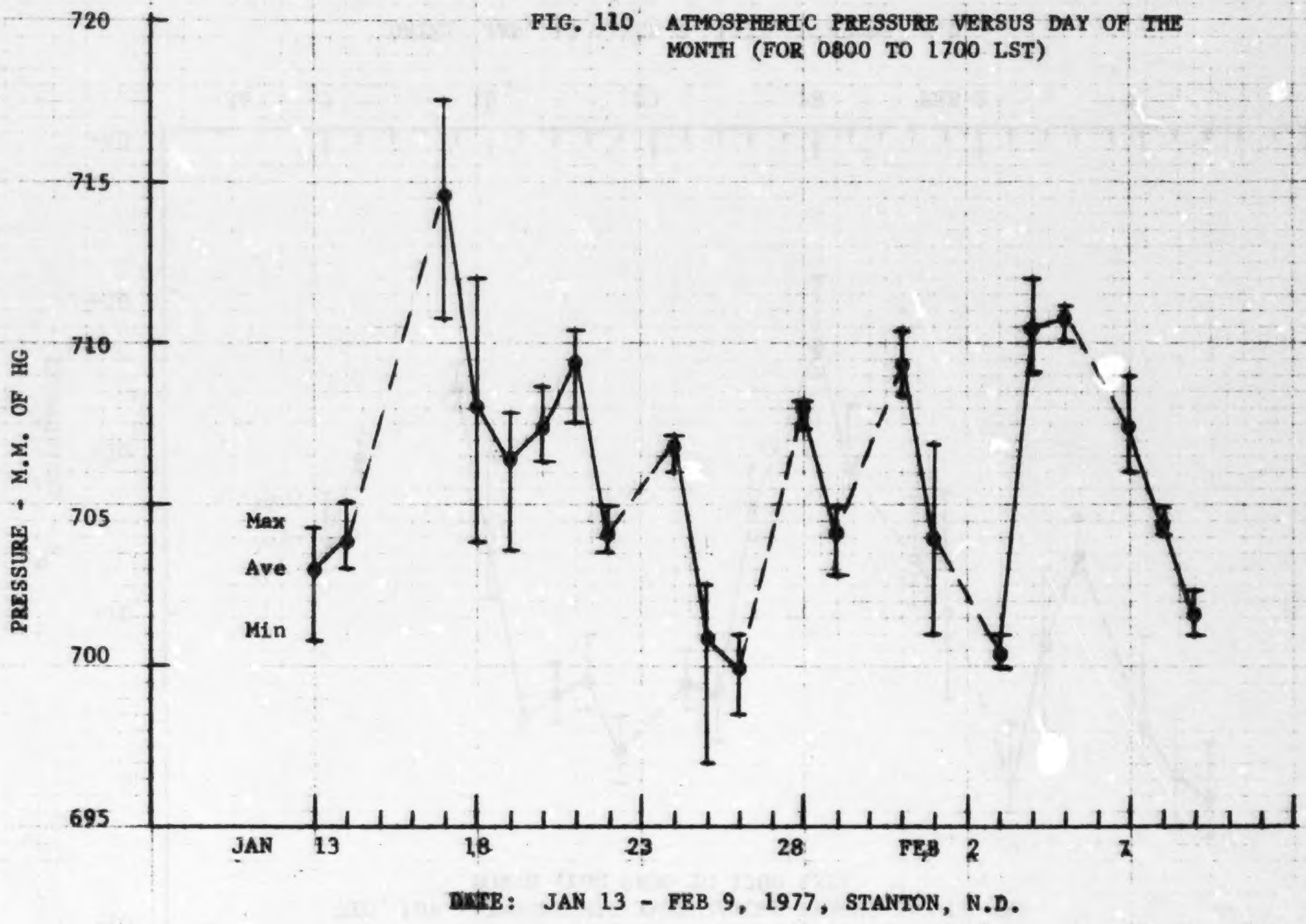

FIG. 110 ATMOSPHERIC PRESSURE VERSUS DAY OF THE MONTH (FOR 0800 TO 1700 LST)

PRINTED ON CLEARPRINT 1000H

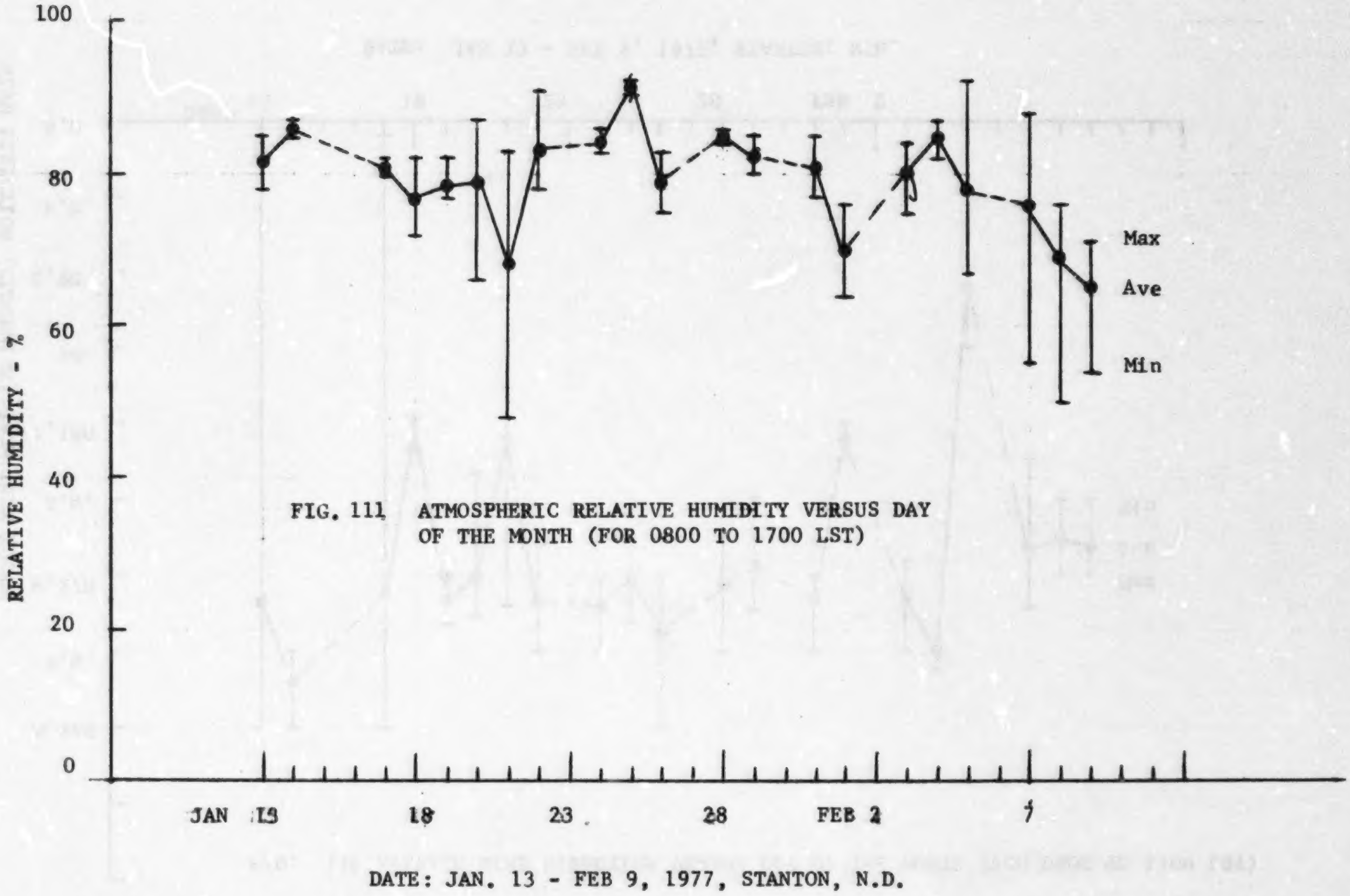

FIG. 111 ATMOSPHERIC RELATIVE HUMIDITY VERSUS DAY OF THE MONTH (FOR 0800 TO 1700 LST)

FIG. 112 AVERAGE WIND DIRECTION VERSUS DAY OF THE MONTH (FOR 0800 TO 1700 LST)

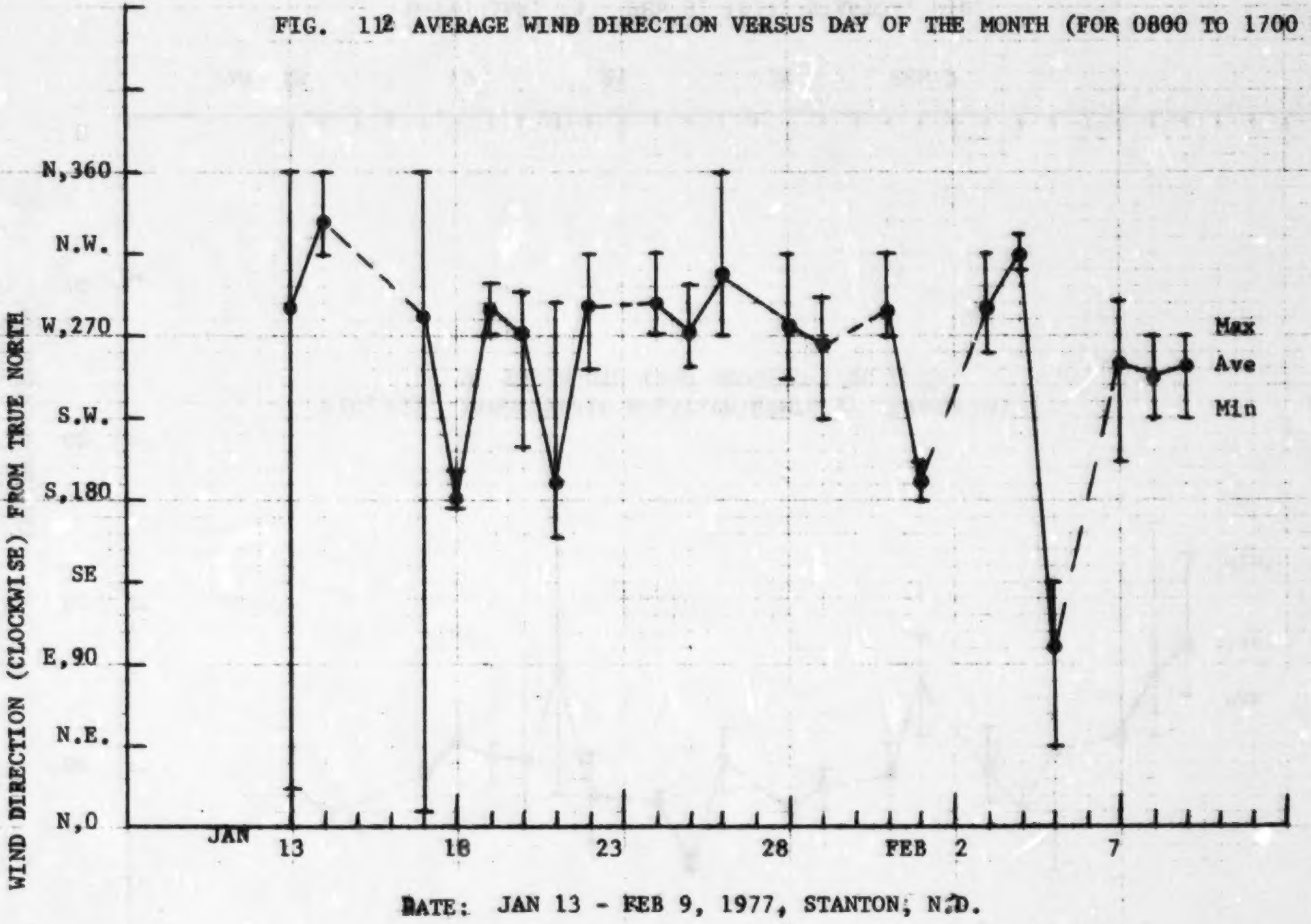

PRINTED ON CLEARPRINT 1000H

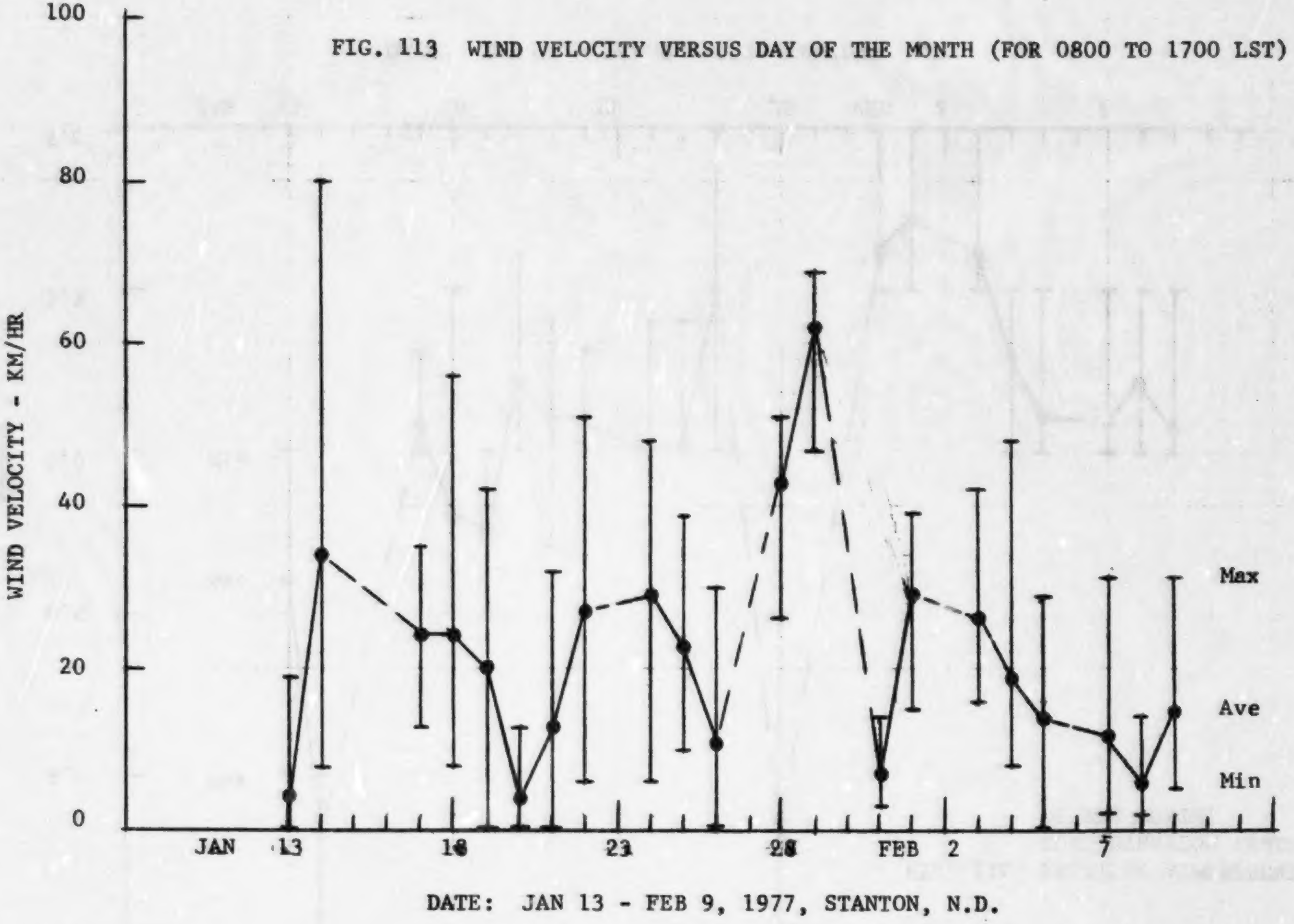

FIG. 113 WIND VELOCITY VERSUS DAY OF THE MONTH (FOR 0800 TO 1700 LST)

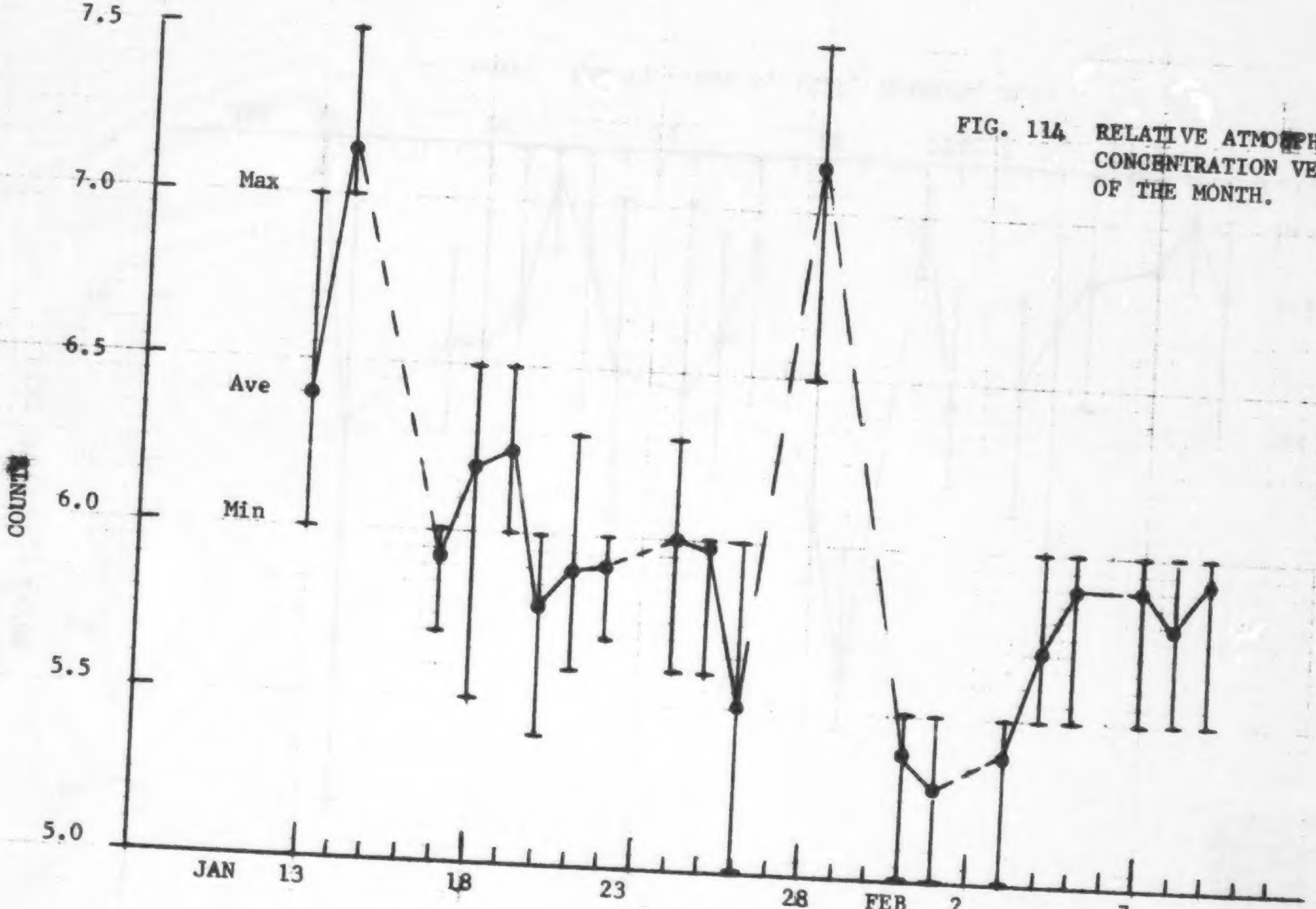

FIG. 114 RELATIVE ATMOSPHERIC DUST CONCENTRATION VERSUS DAY OF THE MONTH.

DATE: JAN 13 - FEB 9, 1977, STANTON, N.D.

FIG. 115 AVERAGE DAILY PRECIPITABLE WATER VAPOR VERSUS DAY OF THE MONTH

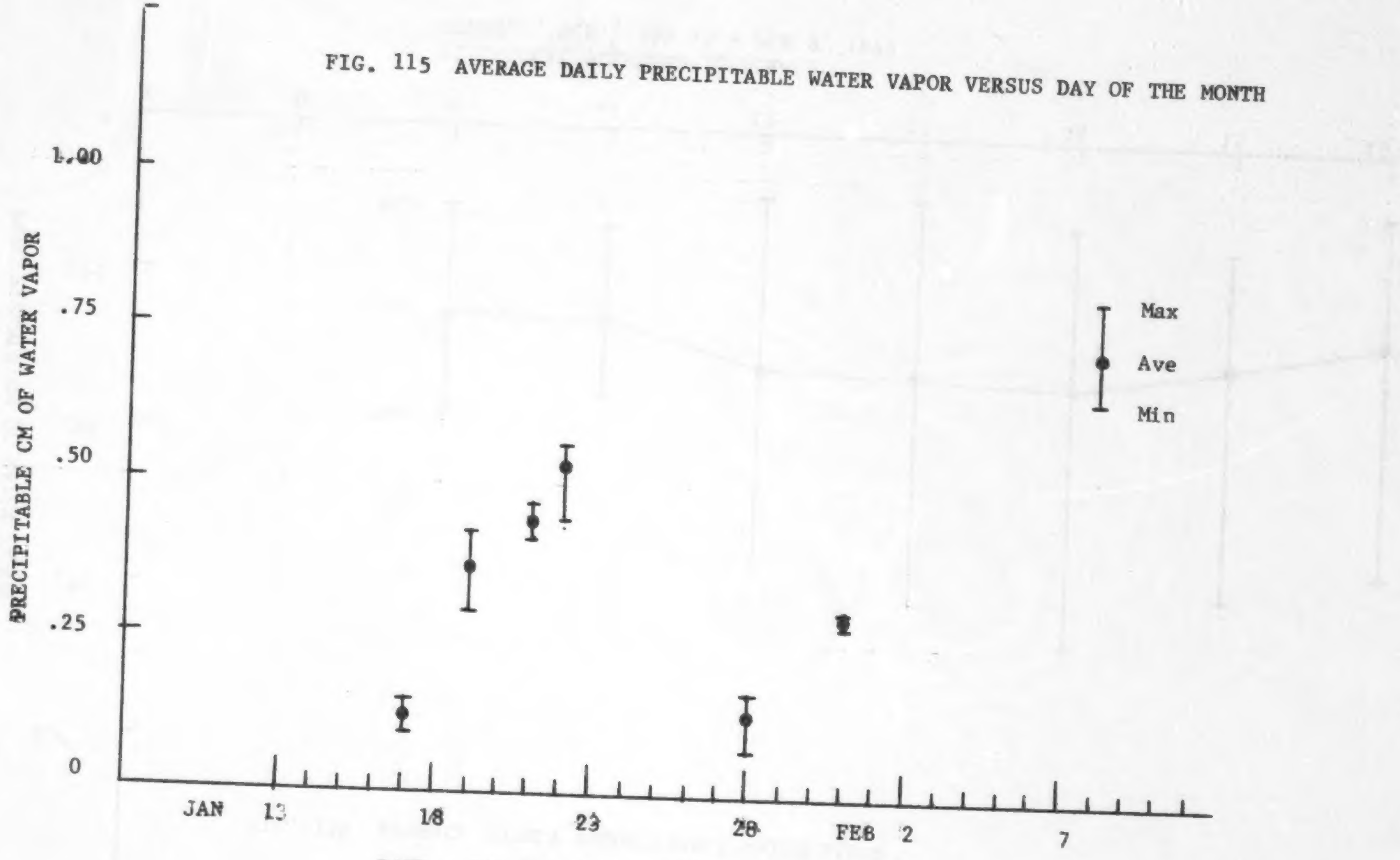

DATE: JAN 13 - FEB 9, 1977, STANTON, N.D.

FIG. 116 AVERAGE HOURLY PRECIPITABLE WATER VAPOR

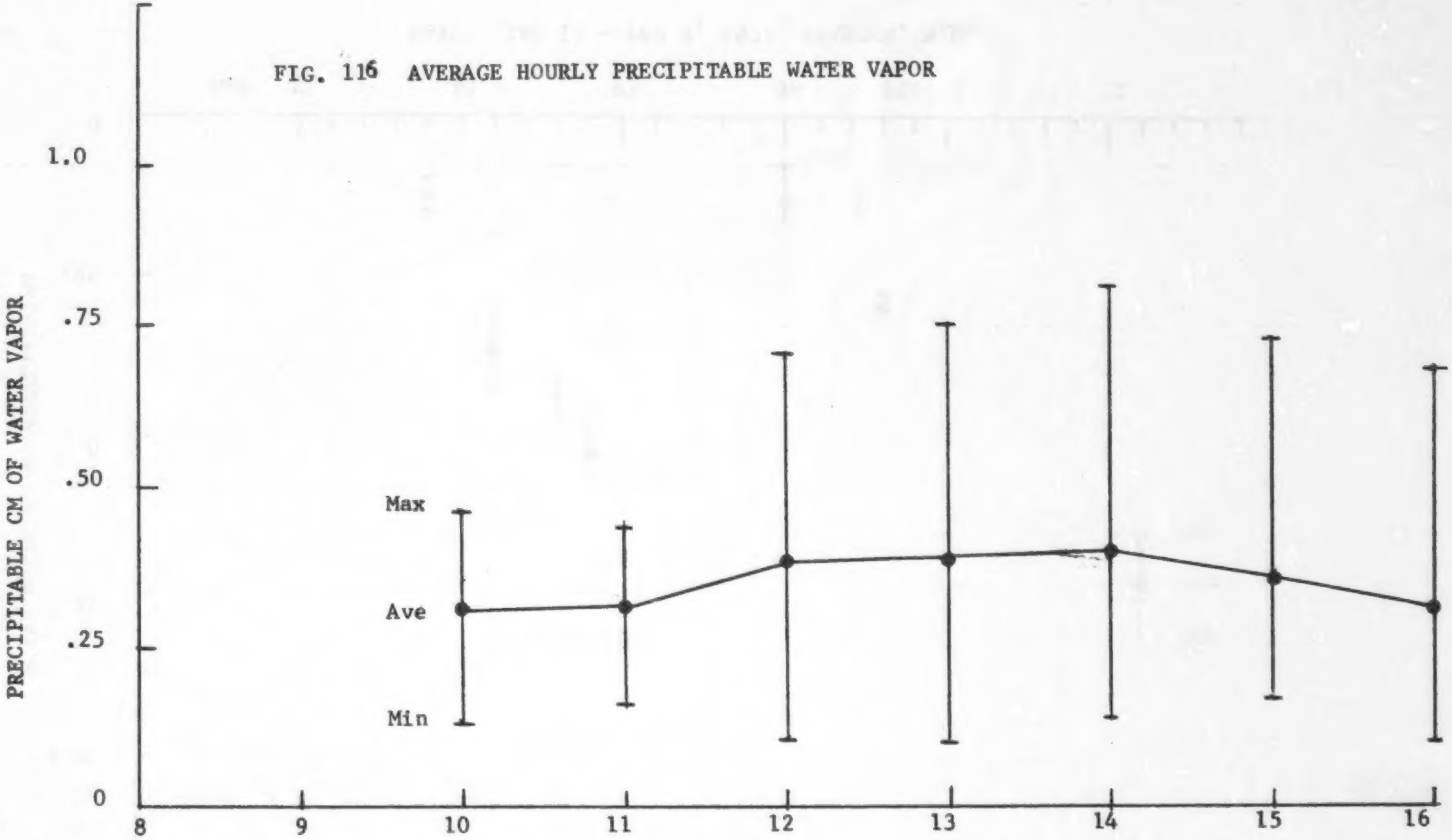

STANTON, N.D., JAN 13 - FEB 9, 1977

9. SATELLITE IMAGERY

9.1 **Techniques/Instrumentation Used** - The instrumentation used consists of the LANDSAT satellite systems. These systems image a 100 x 100 mile surface area, every 18 days, in four spectral bands (.5 to .6, .6 to .7, .7 to .8 and .8 to 1.1 micrometers). This satellite imagery that was used consists of 9 x 9 in. positive, black and white, transparencies, ordered directly from the EROS data center. Two bands were considered, the .5 to .6 and .7 to .8 µm bands. These positive transparencies were enlarged by a factor of approximately 7X to give the maximum spatial resolution possible, as shown in Figure 117. The technique used was to simply photointerpret the images to detect any smoke plumes or pollution clouds, and determine their source, size, and opacity. The opacity of the smoke plume can be qualitatively estimated by comparison of the .5 to .6 µm and .7 to .8 um images. For example, a thin plume will exhibit a different appearance in the shorter .5 to .6 µm wavelengths than the longer .7 to .8 um wavelengths, because of the greater opacity in the shorter wavelengths. An opaque/dense plume will exhibit a similar appearance in both the short and long wavelengths because of its high opacity.

9.2 **April Satellite Imagery** - Imagery was obtained for April 3 & 12 inspection of this imagery, in the .5 to .6 µm and .7 to .8 µm bands, revealed no detectable plumes and/or pollution clouds.

9.3 **July Satellite Imagery** - Imagery was obtained for Aug. 7. No detectable plumes were present.

9.4 **October Satellite Imagery** - Imagery was obtained for October 9. No detectable plumes were present.

9.5 January Satellite Imagery - Imagery was obtained for January 17. As shown in Figure 117, a very noticeable smoke plume was detected. Although Figure 117 is for the 0.5 to 0.6 um band, the 0.7 to 0.8 band displayed the same opacity, indicating that the plume was fairly dense. The plume is approximately 7 miles long, 0.4 miles wide, and is at an altitude of approximately 850 ft. above terrain. The altitude of the plume is easily determined by a knowledge of the sun angle and the length of the plume shadow. The time of the LANDSAT overpass is approximately 10:30 AM LST.

9.6 Seasonal Satellite Imagery Comparisons - Because the LANDSAT satellite passes over a given site so infrequently, it is difficult to make any seasonal comparisons.

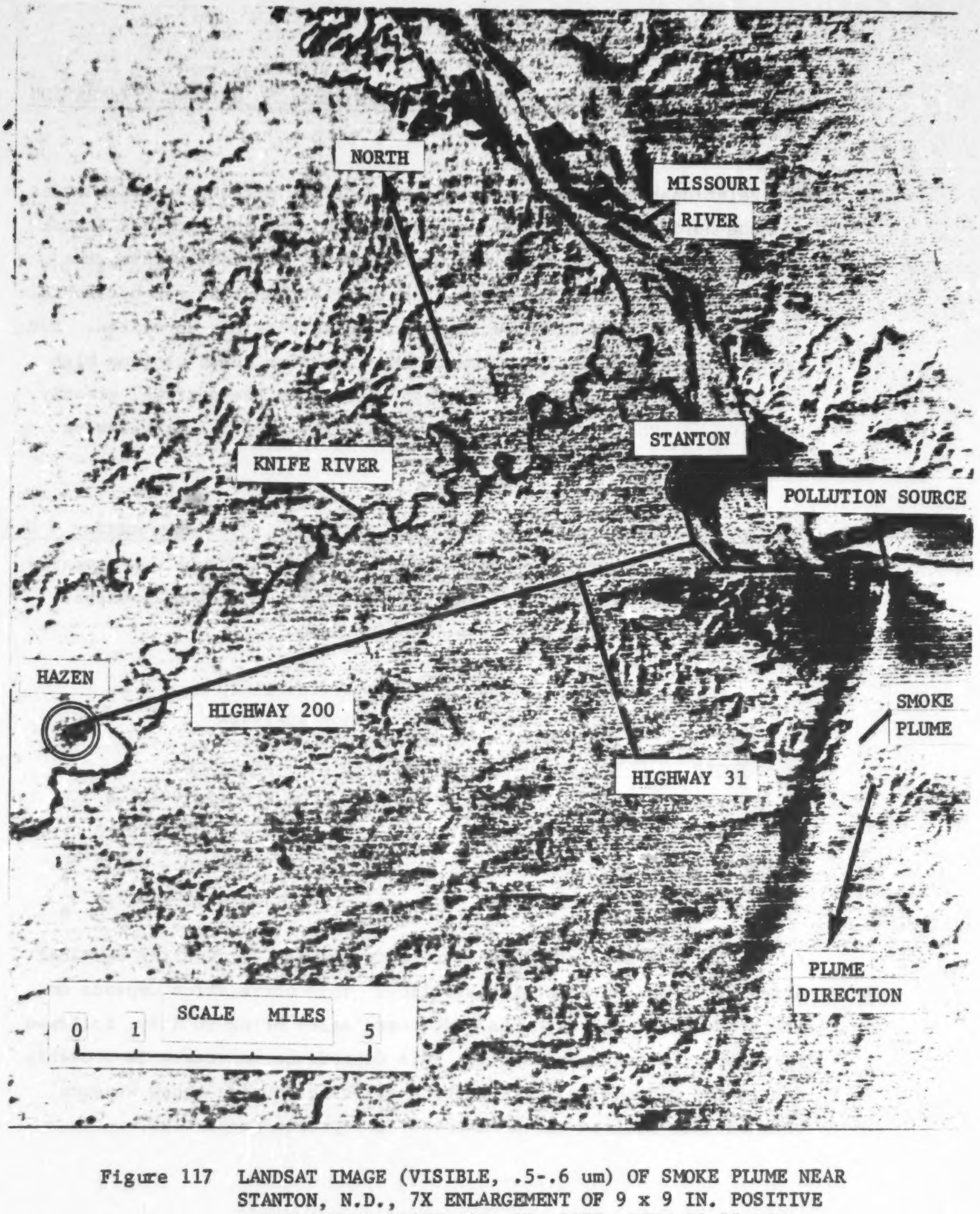
NORTH
MISSOURI
RIVER
STANTON
KNIFE RIVER
POLLUTION SOURCE
HAZEN
HIGHWAY 200
SMOKE
PLUME
HIGHWAY 31
PLUME
DIRECTION
SCALE MILES
0
1
5

Figure 117 LANDSAT IMAGE (VISIBLE, .5-.6 um) OF SMOKE PLUME NEAR STANTON, N.D., 7X ENLARGEMENT OF 9 x 9 IN. POSITIVE TRANSPARENCY, DATE-JAN. 17, 1977; TIME-10:30 LST

10. COMPARISON OF HORIZONTAL VISIBILITY WITH VERTICAL OPTICAL ATTENUATION AND SOLAR IRRADIANCE

The relationships between the vertical optical attenuation properties and the horizontal visibility are dependent upon the vertical atmospheric profiles of aerosols and water vapor. Because of this, the relationships between the vertical optical attenuation and horizontal visibility could be quite variable and quite possibly unrelated. For example, a strong, shallow temperature inversion could confine high concentrations of aerosols and water vapor near the surface, greatly reducing horizontal visibility. Whereas, the vertical attenuation would not be affected nearly as much.

10.1 Horizontal Visibility Versus Vertical Optical Aerosol Attenuation @ 0.5 um

The vertical aerosol attenuation coefficient at 0.500 μm was compared to the overall horizontal visibility for the four seasonal months. The results of such an analysis is shown below:

Table 4 τ_a(.500 μm) versus Visibility
Linear Correlation Analysis

Month	Correlation Coefficients (r^2)	Equation
April	0.38	$V = 45.3 - 71.8\ \tau_a$
July	0.56	$V = 68.0 - 193.6\ \tau_a$
Oct.	0.51	$V = 52.0 - 181.3\ \tau_a$
Jan.	0.45	$V = 36.9 - 212.5\ \tau_a$

As can be seen a fairly good correlation exists between the vertical attenuation and horizontal visibility. This correlation depends on the seasonal month, with the best correlation being in July, followed by October, January and April. This dependence on season is probably due to the particular relationships existing, during those seasons, between the vertical and horizontal atmospheric properties.

10.2 Horizontal Visibility Versus Ratio of Diffuse to Total Solar Irradiance

As previously mentioned, the ratio of diffuse to total solar irradiance is one indicator of atmospheric clarity because it indicates the scattered diffuse skylight, which is determined by the amount of a aerosols and relative air mass. A linear correlation analysis was performed for the visibility versus ratio of diffuse to total solar irradiance. The results of this analysis are shown below.

Total 5 Correlation Between Visibility & Diffuse to Total Solar Irradiation Ratio

Month	Correlation Coefficient	Equation
April	0.27	$V = 50.38 - 83.5 (D/H)$
July	0.24	$V = 61.5 - 178.4 (D/H)$
Oct.	0.82	$V = 78.3 - 25.3 (D/H)$
Jan.	0.81	$V = 57.9 - 110.7 (D/H)$

In general, all months of data show that visibility is inversely proportional to the ratio of diffuse to total solar irradiance. For the seasonal months of April and July this correlation coefficient of 0.27 and 0.24, respectively. However, for the months of October and January, the correlation is extremely good, correlation coefficients of 0.82 and 0.81, respectively. This wide variation in the correlation coefficient verifies the fact that, as pointed out previously, the relationship between the vertical atmospheric optical air quality and the horizontal visibility may or may not be directly correlated because of the variable vertical structure of the atmosphere.

APPENDIX A

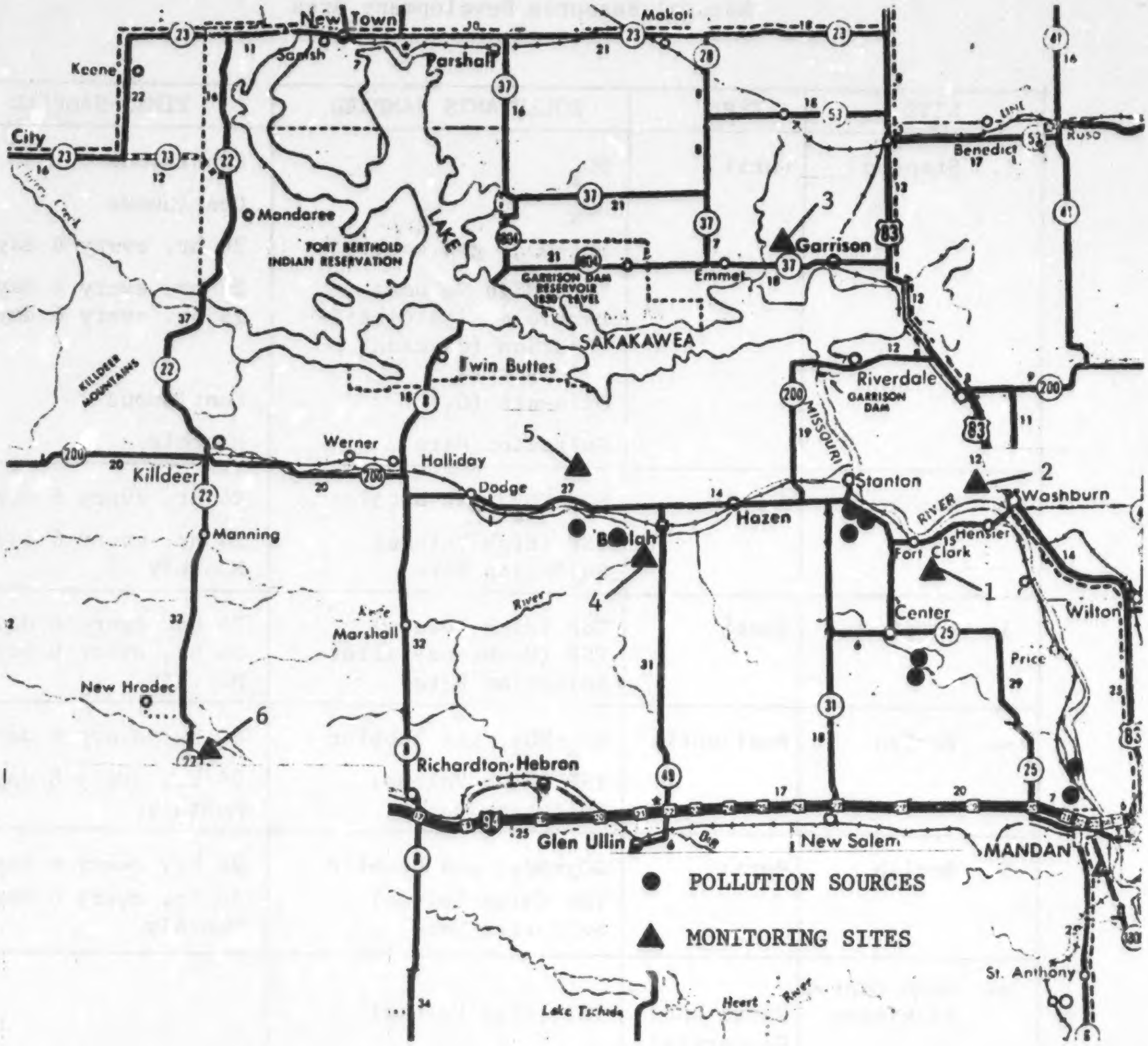

New Town
Sanish
Parshall
Makoti
Keene
City
Mandaree
FORT BERTHOLD INDIAN RESERVATION
LAKE
SAKAKAWEA
GARRISON DAM RESERVOIR
Emmet
Garrison
3
Benedict
Ruso
Riverdale
GARRISON DAM
MISSOURI
RIVER
KILLDEER MOUNTAINS
Twin Buttes
Werner
Halliday
Killdeer
Dodge
5
Hazen
Stanton
2
Washburn
Beulah
4
Fort Clark
Hensler
1
Manning
Knife River
Marshall
Center
Wilton
Price
New Hradec
6
Richardton
Hebron
Glen Ullin
New Salem
MANDAN
St. Anthony
Lake Tschida
Heart River
● POLLUTION SOURCES
▲ MONITORING SITES

Figure A-1 Location of Pollution Sources and North Dakota Department of Health Monitoring Sites

North Dakota Air Quality Monitoring Sites

Natural Resource Development Area

SITE	TYPE	POLLUTANTS SAMPLED	TIMES-SAMPLED
1. Stanton	Rural	SO_2 NO_x SO_2-NO_2, gas bubbler TSP (High Volume) Particle size distribution (cascade impactor) Oxidants (O_3) Sulfation Rate	Continuous Continuous 24 hr. every 6 days 24 hr. every 6 days 24 hr. every 6 days Continuous Monthly
2. Washburn	Rural	SO_2-NO_2, gas bubbler TSP (High Volume) Sulfation Rate	24 hr. every 6 days 24 hr. every 6 days Monthly
3. Garrison	Rural	TSP (High Volume) TSP (Membrane-filter Sulfation Rate)	24 hr. every 6 days 24 hr. every 6 days Monthly
4.. Beulah	Residential	SO_2-NO_2, gas bubbler TSP (High Volume) Sulfation Rate	24 hr. every 6 days 24 hr. every 6 days Monthly
5. Beulah	Rural	SO2-NO_2, gas bubbler TSP (High Volume) Sulfation Rate	24 hr. every 6 days 24 hr. every 6 days Monthly
6. Dunn Center Dickinson	Rural and Commercial	TSP (High Volume)	